

Modelling of nitrogen transport and turnover during soil and groundwater passage in a small lowland catchment of Northern Germany

Dissertation
zur Erlangung des akademischen Grades
"doctor rerum naturalium"
(Dr. rer. nat.)
in der Wissenschaftsdisziplin „Geoökologie“

eingereicht an der
Mathematisch-Naturwissenschaftlichen Fakultät
der Universität Potsdam

von
Gunter Wriedt

Gutachter:

1. Prof. Dr. Axel Bronstert
2. Prof. Dr. Helmut Geistlinger
3. Dr. Michael Rode

Tag der wissenschaftlichen Aussprache: 27.05.2004

Table of Contents

LIST OF TABLES	iv
LIST OF FIGURES	v
ABBREVIATIONS	ix
ACKNOWLEDGEMENTS.....	xi
ABSTRACT	xiii
KURZFASSUNG.....	xv
1 INTRODUCTION.....	1
1.1 GENERAL INTRODUCTION	1
1.2 OBJECTIVES	2
1.3 METHODOLOGICAL APPROACH	2
2 THEORETICAL BACKGROUND.....	3
2.1 HYDROLOGICAL CHARACTERISTICS OF LOWLAND CATCHMENT SYSTEMS.....	3
2.2 TRANSPORT AND TURNOVER OF NITROGEN IN SOIL AND VADOSE ZONE	3
2.3 TRANSPORT AND TURNOVER OF NITROGEN IN GROUNDWATER	4
2.3.1 <i>Groundwater flow and transport</i>	4
2.3.2 <i>Groundwater nitrogen dynamics</i>	5
2.4 ORGANIC MATTER AS SUBSTRATE FOR DENITRIFICATION.....	6
2.5 RECENT MODELLING STUDIES	7
3 MODELS AND MODELLING STRATEGY.....	9
3.1 OUTLINE OF THE INTEGRATIVE MODELLING CONCEPT.....	9
3.2 MODELLING OF WATER AND NITROGEN IN SOILS AND VADOSE ZONE	10
3.2.1 <i>Model choice</i>	10
3.2.2 <i>Soil-nitrogen dynamics</i>	10
3.2.3 <i>Soil water dynamics</i>	11
3.2.4 <i>Soil temperature</i>	12
3.2.5 <i>The mRISK-N-Model</i>	12
3.2.6 <i>Preprocessor RISKNREGIO</i>	12
3.3 DEVELOPMENT OF A GROUNDWATER-REACTION-MODULE FOR THE SIMULATION OF GROUNDWATER NITROGEN TURNOVER	13
3.3.1 <i>Definition of the chemical system</i>	13
3.3.2 <i>Mathematical implementation</i>	14
3.3.2.1 General formulation	14
3.3.2.2 Temperature dependency	15
3.3.2.3 Mineral update	15
3.3.2.4 Implementation of equilibrium reactions – calcite dissolution and pH	16
3.3.2.5 SOM release control function	16
3.3.2.6 Rate expressions	16
3.3.3 <i>Run-scheme of the reaction-module</i>	19
3.3.4 <i>Parameterisation of the reaction-module</i>	20
3.3.5 <i>Algorithm verification</i>	22
3.3.6 <i>Effect of cell-size on the behaviour of rate expressions</i>	23
3.3.6.1 Introduction.....	23
3.3.6.2 General considerations.....	24
3.3.6.3 Behaviour of a first-order reaction term.....	25
3.3.6.4 Behaviour of a zero-order reaction term	25
3.3.6.5 Behaviour of a Monod reaction term	26
3.3.6.6 Behaviour of the Monod-half term	27
3.3.6.7 Behaviour of the inhibition term	28
3.3.6.8 Discussion.....	28

4	MATERIALS AND METHODS	30
4.1	STUDY AREA	30
4.2	DATA SOURCES	33
4.3	SOIL WATER AND NITROGEN MODELLING WITH LYSIMETER DATA	33
4.3.1	<i>Input data</i>	33
4.3.2	<i>Sensitivity analysis</i>	34
4.3.3	<i>Calibration and validation procedure</i>	36
4.4	SENSITIVITY ANALYSIS OF THE GROUNDWATER-REACTION-MODULE	36
4.5	SIMULATION OF A FIELD SCALE TRACER EXPERIMENT	37
4.5.1	<i>Description of the tracer experiment</i>	37
4.5.2	<i>Evaluation of the tracer experiment</i>	38
4.5.3	<i>Model setup and flow simulation</i>	39
4.5.4	<i>Calibration of the transport model</i>	40
4.5.5	<i>Simulation of reactive nitrate transport</i>	40
4.6	SIMULATION OF NITROGEN TRANSPORT AND TURNOVER AT THE TRANSECT SCALE	41
4.6.1	<i>Model setup</i>	41
4.6.2	<i>Definition of flow simulations</i>	42
4.6.3	<i>Reference reaction scenario</i>	43
4.6.4	<i>Definition of transport simulations</i>	43
4.7	SIMULATION OF WATER AND NITROGEN FLUXES AT THE CATCHMENT SCALE	44
4.7.1	<i>Outline of the modelling procedure</i>	44
4.7.2	<i>Simulation of groundwater recharge and nitrogen leaching at the catchment scale</i>	45
4.7.2.1	Climatic data	45
4.7.2.2	Soil data	45
4.7.2.3	Landuse data and management practices	46
4.7.2.4	Atmospheric deposition	47
4.7.2.5	Initial conditions	47
4.7.2.6	Setup of model runs	47
4.7.3	<i>Regional groundwater flow modelling</i>	48
4.7.3.1	Model Setup	48
4.7.3.2	Sensitivity analysis of the regional flow model	49
4.7.3.3	Calibration of the regional flow model	50
4.7.3.4	Delineation of the Schaugraben catchment	51
4.7.4	<i>Groundwater modelling on catchment and subcatchment scale</i>	51
4.7.4.1	Model setup and flow simulation	51
4.7.4.2	Transport scenarios	52
4.7.4.3	Data Analysis	54
5	RESULTS AND DISCUSSION	55
5.1	SOIL WATER AND NITROGEN MODELLING WITH LYSIMETER DATA	55
5.1.1	<i>Results of lysimeter sensitivity analysis</i>	55
5.1.2	<i>Calibration and validation of the mRISK-N model using lysimeter data</i>	59
5.1.3	<i>Uncertainty of input data</i>	64
5.1.4	<i>Discussion</i>	66
5.2	SENSITIVITY ANALYSIS OF THE GROUNDWATER-REACTION-MODULE	68
5.3	SIMULATION OF A FIELD SCALE TRACER EXPERIMENT	70
5.3.1	<i>Evaluation of experimental results</i>	70
5.3.2	<i>Calibration results</i>	72
5.3.3	<i>Nitrate transport simulation results</i>	73
5.3.4	<i>Discussion</i>	75
5.4	SIMULATION OF NITROGEN TRANSPORT AT THE TRANSECT SCALE	77
5.4.1	<i>Flow simulation results</i>	77
5.4.2	<i>Chemical interactions</i>	78
5.4.3	<i>Investigation of controlling factors</i>	83
5.4.4	<i>Discussion</i>	87
5.5	SIMULATION OF NITROGEN TRANSPORT IN THE SCHAUGRABEN CATCHMENT	88
5.5.1	<i>Distributed soil nitrogen modelling of the Schaugraben catchment</i>	88
5.5.2	<i>Regional flow model</i>	92
5.5.2.1	Results of the sensitivity analysis	92
5.5.2.2	Model calibration results	93
5.5.2.3	Delineation of the P5 catchment boundary	94

5.5.3	<i>Modelling of groundwater nitrogen transport in the Schaugraben catchment P5</i>	95
5.5.3.1	Results of the P5 catchment simulation	95
5.5.3.2	Results of the subcatchment simulation	105
5.5.3.3	Discussion	106
6	DISCUSSION	109
6.1	TRANSPORT AND TURNOVER OF NITROGEN IN LOWLAND CATCHMENTS	109
6.2	PRACTICAL CONSEQUENCES FOR MANAGING NITROGEN POLLUTION	110
6.3	CHARACTERISTICS OF THE MODELLING SYSTEM	111
6.4	TRANSFER OF THE MODELLING APPROACH AND SIMULATION RESULTS	112
6.5	PROBLEMS OF MODEL IDENTIFICATION	114
6.6	RELATION BETWEEN MODELLING EFFORT AND PROGRESS IN STUDYING CATCHMENT PROCESSES... ..	114
6.7	RECOMMENDATIONS FOR MODEL IMPROVEMENT AND FUTURE RESEARCH.....	115
7	REFERENCES	117

APPENDIX

CURRICULUM VITAE

EIDESSTATTLICHE ERKLÄRUNG

List of Tables

Table 1: Selected applications of soil-nitrogen-models on a catchment scale	7
Table 2: Definition of the chemical system	14
Table 3: Rate expressions used in reaction-module A.....	18
Table 4: Rate expressions changed in reaction-module B.....	19
Table 5: Default parameter set of the reaction-module	21
Table 6: Initial component concentrations of the batch reaction problem	22
Table 7: Simulation runs and parameter ranges used in sensitivity analysis.....	35
Table 8: Initial soil parameters used in sensitivity analysis	36
Table 9: Parameter values used for sensitivity analysis of the groundwater-reaction-module	37
Table 10: Model runs and parameter settings for tracer transport simulations	41
Table 11: Definition of flow simulations	42
Table 12: Definition of simulation runs for the artificial transect model.	44
Table 13: Definition of distributed soil simulations for the P5 catchment model	48
Table 14: Calculation of reference discharge fluxes.....	50
Table 15: Simulation runs defined for catchment and subcatchment scale transport simulations... 53	
Table 16: Model performance measures for groundwater recharge	60
Table 17: Model performance measures for nitrate leaching	60
Table 18: Model parameters (field capacity FC, reduction point RP and denitrification rate constant kden) for initial model run (Initial), for PEST-assisted calibration (C-1) and for manual calibration (C-2), $AWC = FC - RP$	61
Table 19: Effect of temporal displacement on model performance measures	67
Table 20: Results of the tracer experiment, based on analysis of temporal moments.....	70
Table 21: Result of bromide transport calibration.....	72
Table 22: Results of flow simulations: Seepage fluxes and travel times.....	78
Table 23: Input data for the P5 catchment simulation, groundwater recharge and N-leaching are given as total averages and averages by landuse type, based on simulation 3	91
Table 24: Input data for the subcatchment simulation, as total averages and averages by landuse type	91
Table 25: Summary of regional flow model calibration.....	94
Table 26: Water balance of P5 catchment simulations	96

List of Figures

Figure 1: Nitrogen cycle of an arable soil.....	3
Figure 2: General modelling approach – Submodels and modelling software	9
Figure 3: Structure of the RISK-N model	11
Figure 4: Structure of the soil water submodel	12
Figure 5: Spatial relation between distributed soil simulation and groundwater model.....	13
Figure 6: First-order rate expression adapted to observed Nitrate concentration vs. groundwater age	17
Figure 7: Adaption of a zero-order rate expression (linear regression) to the data from Figure 6. ...	17
Figure 8: Run scheme of the RT3D reaction-module	19
Figure 9: Concentrations vs. time for selected components calculated with the RT3D reaction-module and Min3P in batch mode.	22
Figure 10: Concentrations vs. time for H, Ca and CO ₃ calculated with the RT3D reaction-module and Min3P in batch mode.	23
Figure 11: One-dimensional transport problem	24
Figure 12: Example of a one dimensional model domain with different discretisations	24
Figure 13: Map of the (extended) Schaugraben study area near Osterburg (Altmark).....	31
Figure 14: Mean monthly climatic data of UFZ Lysimeter station in Falkenberg.....	32
Figure 15: Distribution of landuse classes in the study area	32
Figure 16: Experimental layout of the tracer experiment.....	38
Figure 17: Observed breakthrough-curves of bromide and nitrate-N after a travel distance of 3, 8 and 15 m	38
Figure 18: Model setup for simulation of the tracer experiment.....	39
Figure 19: Model layout for artificial transect simulations.....	42
Figure 20: Nested modelling domains	45
Figure 21: Data inheritance between the nested modelling domains.....	45
Figure 22: Derivation of the hydrogeological model	49
Figure 23: Regional flow model – Boundary conditions and model grid.....	50
Figure 24: Boundary conditions and model grid of P5 catchment model	51
Figure 25: Subcatchment model - Boundary conditions and model grid	52
Figure 26: Local sensitivity of annual evapotranspiration to selected parameters	55
Figure 27: Local sensitivity of annual groundwater recharge to selected parameters	55
Figure 28: Local sensitivity of annual N-leaching to selected parameters.....	56
Figure 29: Local sensitivity of annual nitrification to selected parameters.....	56
Figure 30: Local sensitivity of annual mineralisation to selected parameters.....	56
Figure 31: Local sensitivity of annual denitrification to selected parameters.....	57
Figure 32: Model response to ground-water depth, Lysimeter 05	57

Figure 33: Model response to infiltration storage capacity, Lysimeter 05	57
Figure 34: Model response to saturated hydraulic conductivity, Lysimeter 05.....	58
Figure 35: Model response to field capacity, Lysimeter 05	58
Figure 36: Model response to slow mineralisation constant, Lysimeter 05	58
Figure 37: Model response to rapid mineralisation constant, Lysimeter 05	58
Figure 38: Model response to denitrification rate constant, Lysimeter 05	58
Figure 39: Model response to leaf storage capacity, Lysimeter 05	58
Figure 40: Cumulative groundwater recharge for Lysimeter 03 – observed, PEST-assisted calibration and manual calibration	59
Figure 41: Annual groundwater recharge and N-Leaching of Lysimeter 03.....	62
Figure 42: Cumulative annual groundwater recharge and N-Leaching of Lysimeter 03	62
Figure 43: Annual groundwater recharge and N-Leaching of Lysimeter 05.....	63
Figure 44: Cumulative annual groundwater recharge and N-Leaching of Lysimeter 05	63
Figure 45: Annual groundwater recharge and N-Leaching of Lysimeter 53.....	63
Figure 46: Cumulative annual groundwater recharge and N-Leaching of Lysimeter 53	64
Figure 47: Monthly groundwater recharge of Lysimeter 03.....	64
Figure 48: Average crop yields and comparison of crop specific N-Uptake rates, taken from Lysimeter data and calculated according to data taken from fertilizing directives	65
Figure 49: N-fixation of lysimeter 05 and 07 as postulated from the N-budget and calculated.....	66
Figure 50: Calculated total N-Fixation in relation to plant N-uptake for the Lysimeters 05 and 07 ..	66
Figure 51: Model response to initial oxygen concentration	69
Figure 52: Model response for different rate constants of autotrophic denitrification.....	69
Figure 53: Model response to initial content of SOM.....	69
Figure 54: Model response to different SOM-release coefficients	69
Figure 55: Model response to initial nitrate concentration.....	69
Figure 56: Model response to different temperatures.....	69
Figure 57: Model response to initial nitrate concentration using the full Monod reaction-module ...	69
Figure 58: Model response to temperature, using the full Monod reaction-module	69
Figure 59: Processing of Bromide BTC's: observed, analytical equivalent and scaled reference BTC's.	71
Figure 60: Evaluation of Nitrate BTC's: observed, analytical equivalent and scaled reference BTC's.	72
Figure 61: Bromide-breakthrough curves – scaled reference BTC and simulated BTC (best fit)	73
Figure 62: Effect of different SOM-release coefficients on Nitrate and DOM-concentrations observed after a travel distance of 3m (BTC 1).....	73
Figure 63: Effect of different DOM sorption coefficients K_d on DOM and Nitrate concentrations observed after a travel distance of 3m (BTC 1).....	74
Figure 64: Calibration of denitrification rate constant – simulated and reference nitrate	

breakthrough-curves	74
Figure 65: Nitrate breakthrough curves –scaled reference BTC and simulated BTC (best fit)	75
Figure 66: Flow simulations – hydraulic heads and pathlines	77
Figure 67: Distribution of nitrate (conservative transport) after 4, 8, 13 and 23 years.	79
Figure 68: Distribution of nitrate (reactive transport) after 4, 23 and 75 years.	80
Figure 69: Distribution of pyrite and sulphate after 23 and 75 years	81
Figure 70: Distribution of DOM, hydrogensulfide, nitrogen and inorganic carbon after 23 years.....	82
Figure 71: Nitrate concentrations in seepage water – effect of different flow systems	83
Figure 72: Nitrate concentrations in seepage water at different hydraulic gradients.....	84
Figure 73: Nitrate concentrations in seepage water at different temperatures (5°, 10° and 15°C) ..	84
Figure 74: Nitrate concentrations in seepage water at different porosities.....	85
Figure 75: Nitrate concentrations in seepage water with contaminated and uncontaminated lower aquifer	85
Figure 76: Nitrate concentrations in seepage water using different reactive pools	86
Figure 77: Nitrate concentrations in seepage water under different N-loads	86
Figure 78: Nitrate concentrations in seepage water – effect of different buffer areas.....	87
Figure 79: Comparison of distributed soil simulation runs 1-4.....	89
Figure 80: Simulated mean annual groundwater recharge.....	89
Figure 81: Simulated mean annual denitrification.....	90
Figure 82: Simulated mean annual N-leaching.....	90
Figure 83: Simulated annual water balances.....	91
Figure 84: Simulated annual N-budgets	91
Figure 85: Sensitivity of groundwater level to saturated conductivity of upper sand.....	93
Figure 86: Sensitivity of groundwater level to saturated conductivity of glacial till	93
Figure 87: Sensitivity of groundwater level to saturated conductivity of deep sand	93
Figure 88: Sensitivity of groundwater level to drain-bed conductivity.....	93
Figure 89: Sensitivity of seepage flux to substrate conductivity	93
Figure 90: Relative change of seepage flux to drainbed conductivity	93
Figure 91: Simulated hydraulic head distribution (interval = 0.5m).....	94
Figure 92: Observed and simulated groundwater heads.....	94
Figure 93: Pathlines of regional groundwater flow.....	95
Figure 94: Calculated groundwater heads of the P5 catchment model.....	96
Figure 95: Development of mean seepage concentrations (conservative transport).....	97
Figure 96: Development of mean seepage concentrations (reactive transport).....	97
Figure 97: P5 catchment model runs – Nitrate concentrations of seepage water vs. time for conservative transport.....	98

Figure 98: P5 catchment model runs – Nitrate concentrations in seepage water vs. time for reactive transport.....	98
Figure 99: P5 catchment model runs – Change of Nitrate concentrations in seepage water vs. time for conservative transport	98
Figure 100: P5 catchment model runs – Change of nitrate concentrations in seepage water vs. time for reactive transport.....	98
Figure 101: Seepage flux, nitrate concentrations and nitrate loads after 50 years	99
Figure 102: Distribution of Nitrate in upper and deep groundwater after 50 years	100
Figure 103: Distribution of nitrate along a cross-section of the model domain (conservative transport) after 50, 100 and 200 years.	101
Figure 104: Distribution of nitrate along a cross-section of the model domain (reactive transport) after 50, 100 and 200 years.....	102
Figure 105: Distribution of sulfate and pyrite along a cross-section of the model domain after 50 and 200 years.	103
Figure 106: Distribution of rOM and hydrogensulfide along a cross-section of the model domain after 50 and 200 years.....	104
Figure 107: Simulated groundwater heads of the subcatchment model	105
Figure 108: Subcatchment model runs – Mean nitrate concentrations in seepage water vs. time for conservative transport	106
Figure 109: Subcatchment model runs – Mean nitrate concentrations in seepage water vs. time for reactive transport	106
Figure 110: Subcatchment model runs – Change of mean nitrate concentrations in seepage water vs. time for conservative transport.....	106
Figure 111: Subcatchment model runs – Change of mean nitrate concentrations in seepage water vs. time for reactive transport	106

Abbreviations

DM	Dry matter
DOM	Dissolved organic matter
DOC	Dissolved organic carbon
DVO-SA	Düngerverordnung Sachsen-Anhalt (Fertilizer guidelines Saxony-Anhalt)
EU-WFD	European Water Framework Directive
FD	Finite Difference
GLA-SA	Geologisches Landesamt Sachsen-Anhalt (Geological Survey Saxony-Anhalt)
IVZ	Intermediate vadose zone
LRZ	Lower root zone
MOC	Method of Characteristics – Algorithm
OM	Organic matter
rOM	„Reactive“ organic matter
SOM	Sedimentary organic matter
STATLA-SA	Statistisches Landesamt Sachsen-Anhalt (Bureau of Statistics Saxony-Anhalt)
STAU	Staatliches Amt für Umweltschutz Sachsen-Anhalt (Environmental Protection Agency Saxony-Anhalt)
TVD	Total Variation Diminishing – Algorithm
UFZ	Umweltforschungszentrum Leipzig-Halle GmbH = Centre for Environmental Research Leipzig-Halle GmbH
URZ	Upper root zone
TIC	Total inorganic carbon

Mathematical symbols are explained directly with the corresponding equations.

Acknowledgements

First of all, I want to thank Sibylle Aben for her companionship and patience during the period that I was working on this dissertation. I thank Prof. Dr. Axel Bronstert, Dr. Michael Rode and Prof. Helmut Geistlinger for taking the work of supervising and examining this thesis. I thank all the scientists involved in the DFG research project for their cooperation and assistance: Prof. Dr. Ralph Meissner, Dr. Gerhard Strauch, Benjamin Blank, Dirk Möller, Juliane Seeger, Dr. Horst Behrend and Dr. Rosemarie Pöthig. Special thanks to Benjamin Blank and Rosemarie Pöthig, who were responsible for all the field work of the project. I am very grateful to my colleagues from the UFZ Department of Hydrology, for all the discussions, reading some drafts, providing computational capacities and their support: Dierk Wagenschein, Nadine Borges, Kathrin Poser, Irina Kistner, Fred Hesser, Dr. Kirsten Hennrich, Dr. Gregor Ollesch, Dr. Karl-Erich Lindenschmidt. I am indebted to Prof. Geistlinger for assisting me with the development of the reaction-module. Burkhard Kuehn and Olaf Buettner helped me with many technical problems. Special thanks to Janna Wriedt and Jardena de Leve for reviewing grammar and orthography.

The study was funded by the German Research Foundation DFG, which is gratefully acknowledged.

Abstract

Diffuse nitrogen pollution is a threat for ground and surface waters. Observed nitrogen loads in surface waters often do not reflect the actual input situation. This apparent retention of nitrogen can be explained by various chemical transformations and hydrological processes in soil and groundwater. The quantification of these processes in the field is difficult and models are needed to evaluate the interaction of these processes in space and time. The objectives of this work are

1. to develop a specific modelling approach by combining selected modelling tools allowing for simulation of N-transport and turnover in soils and groundwater of lowland catchments on various spatial scales (lysimeter, transect and catchment).
2. to study interactions between catchment characteristics (such as landuse distribution, geochemistry, channel and river system) and nitrogen transport. Special attention is paid to potential N-loads to surface waters.

The modelling approach combines various submodels for water flow and solute transport in soil and groundwater: The soil-water- and nitrogen-model mRISK-N is used to calculate groundwater recharge and nitrate leaching as input data for subsequent groundwater modelling. Groundwater flow is simulated using MODFLOW, groundwater solute transport is simulated using RT3D. A reaction-module was developed to simulate various chemical processes in groundwater, such as degradation of organic matter by oxygen, nitrate, sulphate or pyrite oxidation by oxygen and nitrate. The reaction-module is implemented as a user-defined reaction-module of the RT3D code.

Various simulation studies were carried out in order to assess model behaviour and to demonstrate the interactions between physical and chemical properties and nitrate export from the model domain. The modelling studies were based on data from the Schaugraben catchment, which is located close to Osterburg, Altmark in the north of Saxony Anhalt. The study catchment is a pleistocene lowland catchment typical for Northern Germany.

A first application of the groundwater-reaction-module was the simulation of a tracer experiment on nitrate transport in shallow groundwater, in order to quantify denitrification rates in the study area. A second application focuses on investigation of basic interactions between chemical and physical aquifer properties and nitrate turnover, using an artificial transect representing selected flow situations typical for lowland catchments.

Lysimeter data were used for a sensitivity analysis and a calibration study of the soil model mRISK-N, in order to test model suitability. A distributed soil simulation was carried out for the study area to provide groundwater recharge and nitrate leaching as input data for subsequent groundwater simulations on catchment and subcatchment scale.

The subsequent groundwater simulations followed a nested modelling approach, starting from a regional flow model to a catchment scale and a sub-catchment scale model. The regional flow model served as a base for delineation of the Schaugraben catchment boundaries and provided necessary boundary conditions needed for the subsequent groundwater flow simulations. The catchment model covers the catchment area of the Schaugraben related to the central gauging station P5. Distributed input from the soil and conservative as well as reactive groundwater nitrogen transport simulations were combined at this scale, focussing on interactions between spatial distribution of N-sources and N-discharge into the surface water system. Further simulations were carried out for a cut-out of the catchment area. These subcatchment scale simulations were basically identical to catchment scale simulations, using the same input data and definitions of model runs, but a finer grid resolution.

The field scale tracer experiment could be simulated reasonably well using a 2D-groundwater model with the reaction-module. However, experimental data did not allow a complete description of the system. Thus, various assumptions were necessary to allow simulation of the experiment. The observed decay of nitrate is the result of interacting factors, such as denitrification and release of organic matter. Therefore, the model does not provide a unique solution and a similar behaviour can be reproduced by using different parameter settings, giving different weight to individual processes.

The artificial transect simulation and the regional simulations clearly show the interaction of substrate properties and solute transport. Under conservative transport, the distribution of solutes

in the aquifer and the development of mean seepage concentrations are directly related to the distribution of source areas and the travel time distribution. Under reactive transport conditions, the distribution of solutes within the aquifer and breakthrough to surface waters is affected by the reaction rate constants and the distribution of reaction partners. Changes of hydraulic properties also affect total turnover and seepage concentrations. As chemical reactions are kinetically controlled, residence time in the aquifer also defines the possible reaction time.

The soil submodel mRISK-N reflects soil water balances and nitrogen turnover processes reasonably well in lysimeter studies. However, it was found that uncertainties inherent to input data are possibly higher than the observed fluxes of nitrate. A calibration of the mRISK-N model to lysimeter data did not lead to an improvement of model results compared to initial parameterisation, due to parameter equifinality and uncertainties of input data.

The 3-dimensional catchment and subcatchment simulations show the spatial and temporal development of substance concentrations in the model domain and allow the identification of impact-relevant areas. Basic results taken from the simulation runs are i) the distribution and turnover of solutes (e.g. nitrate, sulphate, DOM) and immobile components (pyrite, SOM) in space and time, ii) the development of average seepage concentrations as a measure for baseflow contribution to surface water loads, and iii) the spatial distribution of seepage and seepage concentrations within the channel system. The distribution of nitrate in the catchment strongly depends on the distribution of inputs, sediment transport properties (and the resulting flow paths and travel times), and the distribution of reactive substances involved in nitrogen turnover. Seepage loads into the surface water system are spatially distributed. A reduction of spatial information of nitrate loads to the groundwater system did not affect average seepage loads substantially. However, spatial information is lost and the possibility to identify "hot spots" of nitrogen pollution is reduced. A comparison to observed nitrate concentrations in the Schaugraben drain channel suggests that groundwater contribution can not be the only source of nitrate to the surface water system, even for the conservative transport case. A significant contribution of other sources, such as drain flow and direct inputs of nitrate through fertilization, needs to be taken into account in order to explain elevated nitrate concentrations during winter.

The modelling approach is capable of simulating the fate of nitrogen compounds in lowland catchment systems. The distributed approach and the implementation of a full reactive groundwater transport model facilitated the study of spatial and geochemical interactions. The modelling system is well suited for a variety of tasks, for example i) the identification of source and sink areas of nitrate pollution, allowing targeted measures for ground- and surface water protection and design of experimental studies, ii) investigation of system response to management measures or landuse changes using scenario simulations and iii) it is an aid in interpretation of observed data, as it allows to integrate local observations into a spatial and temporal framework. The prognostic value of the model strongly depends on the possible spatial resolution and the quality of input data. In this study it was shown how various processes interact at different scales, but uncertainties of input data need to be taken into account when interpreting model results for the specific study area. However, model results allow to improve and to target field studies and monitoring, which in turn allow improvement of input data and enhance the prognostic value of the model. Not all potential sources of nitrate relevant for surface water pollution are yet included in the modelling system. Suggested model extensions are the consideration of drain flow and of surface water and hyporheic zone processes. Further simulations should focus more closely on the investigation of interactions between the spatial distribution of N-loads, reactive compounds and flow paths. More research is necessary to quantify the various chemical processes in the field. These investigations can not be confined to nitrogen species, but all elements and compounds taking part in turnover reactions have to be taken into account as well.

Kurzfassung

Diffuse Stickstoffbelastungen stellen eine Gefahr für Grund- und Oberflächengewässer dar. Gemessene Stickstofffrachten in Oberflächengewässern spiegeln oft die aktuelle Eintragungssituation nicht wieder. Diese Retention kann auf das Wirken verschiedener chemischer und hydrologischer Prozesse zurückgeführt werden. Eine Quantifizierung dieser Prozesse durch Feldmessungen ist nur bedingt möglich und mit großen Schwierigkeiten verbunden. Die Wechselwirkungen dieser Prozesse in Raum und Zeit können mit Hilfe von Modellen untersucht werden. Ziele dieser Arbeit sind:

1. die Entwicklung eines speziellen Modellansatzes auf Grundlage ausgewählter Modelle zur Simulation von N-Transport und -umsatz im Boden und Grundwasser auf verschiedenen Skalenbereichen (Lysimeter, Transekt und Einzugsgebiet) in kleinen Tieflandeinzugsgebieten,
2. die Untersuchung von Wechselwirkungen zwischen Gebietseigenschaften (Landnutzung, Geochemie, Gewässersystem) und Stickstofftransport, unter besonderer Berücksichtigung der potentiellen N-Einträge in die Oberflächengewässer.

Der Modellansatz beruht auf der Kombination verschiedener Teilmodelle zur Beschreibung von Wasserfluss und Stofftransport im Boden und Grundwasser: Grundwasserneubildung und Stickstoffauswaschung wurden mit dem Bodenwasser- und -stickstoffmodell mRISK-N berechnet. Sie dienen als Eingangsdaten für die nachfolgenden Grundwassersimulationen. Der Grundwasserfluss wird mit MODFLOW berechnet, die Stofftransportsimulation erfolgt mit dem Programm RT3D. Zur Simulation verschiedener chemischer Prozesse im Grundwasser, wie zum Beispiel die Oxidation organischer Substanzen durch Sauerstoff, Stickstoff und Sulphat oder die Pyritoxidation durch Sauerstoff und Stickstoff wurde ein spezielles Reaktionsmodul entwickelt. Dieses Reaktionsmodul wurde als benutzerdefiniertes Reaktionsmodul für RT3D implementiert.

Mit Hilfe verschiedener Modellstudien wurden das Modellverhalten untersucht und Wechselwirkungen zwischen den physikalischen und chemischen Gebietseigenschaften mit dem Stickstoffexport aus dem Modellgebiet untersucht. Den Modellstudien wurden Daten aus dem Einzugsgebiet des Schaugrabens bei Osterburg in der Altmark, im Norden von Sachsen-Anhalt, zugrundegelegt. Es repräsentiert ein typisches Kleineinzugsgebiet im pleistozänen Tiefland Norddeutschlands.

Eine erste Anwendung des Reaktionsmoduls erfolgte bei der Simulation eines Tracerexperimentes zur Untersuchung von Stickstofftransport und -umsatz im oberflächennahen Grundwasser, mit dem Ziel, Denitrifikationsraten im Untersuchungsgebiet zu quantifizieren. In einer zweiten Anwendung wurden die Wechselwirkungen zwischen physikalischen und chemischen Substrateigenschaften und Nitratauswaschung am Beispiel eines künstlichen Transektes untersucht. An diesem Transekt wurden typische Fließsituationen in Tieflandeinzugsgebieten nachgestellt.

Ein Test des Bodenmodells hinsichtlich seiner Eignung für das Modellvorhaben wurde auf Basis von Lysimeterdaten durchgeführt. Dazu wurden Sensitivitätsanalysen und eine Untersuchung zur Modellkalibrierung durchgeführt. Aufbauend auf den Ergebnissen der Lysimetersimulation wurde eine regionale Bodensimulation für das Untersuchungsgebiet durchgeführt. Diese Simulation diente der Bereitstellung von flächendifferenzierten Daten der Grundwasserneubildung und Nitratauswaschung für die nachfolgenden Grundwassersimulationen im Einzugsgebiet und in einem Teileinzugsgebiet.

Die Grundwassersimulationen folgen einem genesteten Modellansatz, beginnend mit einem regionalem Grundwasserflussmodell, aus dem Teilgebiete (Einzugsgebiet und Teileinzugsgebiet) für die Transportsimulation abgeleitet wurden. Das regionale Grundwasserflussmodell diente der Abgrenzung des Schaugraben-Einzugsgebietes und stellt die notwendigen Randbedingungen für die nachfolgenden hydraulischen Teilmodelle bereit. Dem Einzugsgebietsmodell wurde das Einzugsgebiet des Schaugrabens bezogen auf die zentralen Abfluss- und Gütemessstelle P5 zugrundegelegt. Auf diesem Maßstab wurden der flächendifferenzierte Eintrag aus der Bodenzone sowie konservativer und reaktiver Transport im Grundwasser kombiniert und die Wechselwirkung zwischen der räumlichen Verteilung der Einträge in das Grundwasser und der Austräge in die Oberflächengewässer untersucht. Weitere Simulationen wurden an einem Teileinzugsgebiet durchgeführt. Die Datengrundlagen und Simulationsläufe waren identisch mit der

Einzugsgebietssimulation, es wurde lediglich ein kleineres Gebiet mit einer feineren Zellauflösung betrachtet.

Das Tracerexperiment konnte mit einem 2D-Grundwassermodell und dem Reaktionsmodul in befriedigender Weise simuliert werden. Die experimentellen Daten liefern jedoch nur eine unvollständige Beschreibung des Systems, so dass die Simulation nur auf Grundlage verschiedener Annahmen durchgeführt werden konnte. Der beobachtete Nitratabbau resultiert aus verschiedenen Faktoren, wie Denitrifikation oder die Verfügbarkeit organischer Substanz. Daher ist das Modell nicht eindeutig, ein ähnliches Verhalten kann mit unterschiedlicher Parameterisierung und Gewichtung der einzelnen Prozesse reproduziert werden.

Die Simulation am künstlichen Transekt zeigt deutlich die Wechselwirkungen zwischen Substrateigenschaften und Stofftransport. Unter konservativen Transportbedingungen ergibt sich die Verteilung im Grundwasserleiter und der Austrag in das Grabensystem direkt aus der Verteilung der Stoffeinträge und der Fließzeitverteilung. Bei reaktivem Stofftransport wird die Verteilung gelöster Stoffe im Aquifer sowie der Durchbruch in die Oberflächengewässer deutlich von den Umsatzraten und der Verteilung der Reaktionspartner beeinflusst. Die Änderung der hydraulischen Substrateigenschaften hat ebenfalls einen deutlichen Einfluss auf den Stoffumsatz und die Stoffausträge. Da die chemischen Reaktionen kinetisch kontrolliert sind, bestimmt die Verweilzeit im Untergrund auch die mögliche Reaktionszeit.

Im Vergleich zu beobachteten Lysimeterdaten können Bodenwasserhaushalt und Stickstoffumsätze mit dem Bodenmodell mRISK-N gut dargestellt werden. Es zeigte sich jedoch, dass die Unsicherheiten in den Eingangsdaten möglicherweise größer sind als die beobachteten Stoffflüsse. Eine Kalibrierung des Modells anhand der Lysimeterdaten führte aufgrund der Datenunsicherheiten und der Prozesswechselwirkungen nicht zu einer weiteren Verbesserung der Modellergebnisse.

Die 3-dimensionalen Simulationen auf Einzugs- und Teileinzugsgebietsebene zeigen die zeitliche und räumliche Entwicklung der Stoffkonzentrationen im Modellgebiet. Dadurch können belastungsrelevante Teilflächen identifiziert werden. Wichtige Ergebnisse aus den Simulationen sind i) die Verteilung und der Umsatz von gelösten Stoffen (z.B. Nitrat, Sulfat, DOM) und immobilisierbaren Stoffen (Pyrit, SOM) in Raum und Zeit, ii) die Entwicklung der mittleren Konzentrationen im Grundwasserzustrom zu den Oberflächengewässern als ein Maß für den Beitrag des Basisabflusses zur Gewässerbelastung und iii) die räumliche Verteilung von Grundwasserzuströmen und Konzentrationen im Zustrom innerhalb des Gewässersystems. Die Verteilung von Nitrat im Einzugsgebiet wird bestimmt von der Verteilung der Einträge in das Grundwasser, den Transporteigenschaften des Sediments (und den resultierenden Fließpfaden und Verweilzeiten) und der Verteilung der reaktiven Substanzen, die am Nitratumsatz beteiligt sind. Die Einträge in die Oberflächengewässer über den Grundwasserzustrom zeigen eine deutliche räumliche Verteilung. Eine Reduktion der räumlichen Verteilung der Grundwassereinträge führt nicht zu einer wesentlichen Änderung der mittleren Austräge in die Oberflächengewässer. Jedoch kommt es zu einem Verlust an räumlicher Information und die Möglichkeit der Identifikation belastungsrelevanter "hot spots" ist deutlich verringert. Ein Vergleich mit beobachteten Nitratkonzentrationen zeigt, dass der Nitratedeintrag über den Grundwasserzustrom selbst unter konservativen Transportbedingungen nicht als alleinige Belastungsquelle in Frage kommt. Vor allem im Winter muss ein bedeutender Eintrag aus anderen Quellen, wie zum Beispiel Dränzuflüssen oder direkten Einträgen von Nitrat über die Düngung berücksichtigt werden, um die hohen Nitratkonzentrationen zu erklären.

Der Modellansatz eignet sich zur Simulation des Stickstofftransports in Tieflandeinzugsgebieten. Der flächendifferenzierte Ansatz und die Berücksichtigung eines reaktiven Grundwassertransportmodells ermöglicht die Untersuchung räumlicher und geochemischer Wechselwirkungen. Das Modellsystem erlaubt i) die Identifizierung von Quellen und Senken von Stickstoffbelastungen, wodurch gezielte Maßnahmen für den Schutz von Grund- und Oberflächengewässern getroffen oder weitergehende experimentelle Untersuchungen geplant werden können, ii) die Untersuchung der Auswirkungen von Maßnahmen oder Landnutzungsänderungen mit Hilfe von Szenariosimulationen und iii) bietet eine wertvolle Hilfe bei der Interpretation von Felddaten, welche in der Regel als lokale Messungen vorliegen und durch die Simulation in einen räumlichen und zeitlichen Zusammenhang gestellt werden. Die Prognosefähigkeit des Modells hängt jedoch stark von der verfügbaren Dichte und Qualität der

Eingangsdaten ab. In dieser Studie wurde gezeigt, wie verschiedene Prozesse auf unterschiedlichen Maßstabsebenen miteinander interagieren. Die Datenunsicherheiten müssen jedoch bei der Interpretation der Ergebnisse für das Untersuchungsgebiet unbedingt berücksichtigt werden.

Die Modellergebnisse erlauben eine gezielte Verbesserung von Felduntersuchungen. Diese können im Gegenzug zu einer verbesserten Datengrundlage führen und so die Prognosefähigkeit des Modells erhöhen. Es konnten noch nicht alle für Oberflächengewässer relevanten Nitratquellen im Modellsystem erfasst werden. Als mögliche Modellerweiterung ist die Implementierung von Drainageabflüssen und von Prozessen im Fließgewässer (inklusive der hyporheischen Zone) beabsichtigt. Zukünftige Simulationen sollen die räumlichen Wechselwirkungen von Nitratreinträgen, der Verteilung reaktiver Stoffe und der Fließpfade stärker berücksichtigen. Weitere Forschung ist notwendig, um die Umsatzprozesse zu quantifizieren und zu parametrisieren. Diese Untersuchungen dürfen sich nicht nur auf Stickstoffkomponenten beschränken, sondern müssen alle Stoffe, die an den Umsatzreaktionen beteiligt sind, berücksichtigen.

1 Introduction

1.1 General introduction

Diffuse nitrogen pollution is a threat for ground and surface waters. On the one hand, nitrate poses a health risk in drinking water, on the other hand, nitrate is a major nutrient, favouring plant and algae growth and leading to eutrophication of water bodies. Groundwater nitrogen turnover may subsequently cause an increase in sulphate or iron concentrations, also posing drinking water quality problems.

Nitrogen loads in surface water often do not reflect the actual input situation. A variety of studies has shown that output fluxes of nitrogen are much lower than to be expected from actual input loads (Meissner, 2000; Behrend, 1996; Werner and Wodsack, 1994; Reiche, 1994). This retention of nitrogen can be explained by chemical transformations and hydrological factors in soil and groundwater, such as:

- Soil nitrogen turnover
- Denitrification in groundwater
- Groundwater travel times of years to decades causing temporal delay of system response
- Dilution due to mixing of water bodies of different pollution
- Incomplete knowledge of flow paths

The relative contribution of these processes strongly depends on geological, topographical and geochemical patterns within the catchment areas. Such factors are, e.g. the distribution of N-input, distribution and availability of reactive substances favouring denitrification, distribution and heterogeneity of geological units and density of the drainage network.

According to the EU-Water Framework Directive (EU-WFD) (European Communities, 2000, Art. 4), all member states shall implement measures, which are necessary to prevent deterioration of the status of water resources, to reverse significant upward trends in the concentration of pollutants and progressively reduce the pollution of ground- and surface waters. A good ecological and chemical status of surface waters is to be achieved until 2015. In the case of nitrogen pollution, ground- and surface waters in lowland areas respond slowly over years and decades to a given input situation. Thus it is necessary to assess future developments and system response in order to define the priority of measures and to target measures effectively.

Transport and turnover processes are complex and difficult to observe and quantify in field. On the one hand, processes can not clearly be separated by chemical data and on the other hand, spatial and temporal characteristics of N-transport phenomena are difficult to resolve with the available experimental methods. Kersebaum (1999) points out, that models are a useful help for the estimation of diffuse pollution of groundwater resources. They are essential for the spatial and temporal inter- and extrapolation of point measurements and snap-shots as for the assessment of scenarios e.g. of management alternatives.

Considerable progress has been made in the field of soil nitrogen modelling and reactive groundwater transport modelling. Coupling of soil and groundwater modelling is a straightforward approach to investigate the interactions between various processes related to the N-problem. However, although various integrated hydrological models have been developed, modelling approaches implementing coupled N-transport and turnover in soils and groundwaters of lowland watersheds are still missing.

This study is part of the DFG-research project *“Stickstofftransport und –umsatz während der Boden- und Grundwasserpassage und seine Modellierung im pleistozänen Tiefland des Elbegebietes (Nitrogen transport and turnover during soil and groundwater pasage and its modelling in the pleistocene lowlands of the Elbe-area)”*, which was carried out in cooperation of the UFZ Centre for Environmental Research Leipzig-Halle (Department of Hydrological Modelling, Department of Soil Science, Department of Hydrogeology) and the Leibniz-Institute of Freshwater Ecology and Inland Fisheries in Berlin.

1.2 Objectives

The main objectives of this study are:

- Investigation of the space-time behaviour of N-transport and turnover during soil and groundwater passage until output into the surface water system in typical catchment areas of the North German Lowlands.
- Development of a specific modelling approach by combination of selected modelling tools allowing for simulation of N-transport and turnover in soils and groundwater of lowland catchments on various spatial scales (lysimeter, transect and catchment).
- The study shall reveal interactions between catchment characteristics (such as landuse distribution, geochemistry, channel and river system) and nitrogen loads. Special attention is paid to the potential N-load exfiltrating to surface waters with base flow.

The investigations shall focus on the question, whether the spatial distribution of nitrate input has an influence on surface water loads and how catchment characteristics influence the distribution and seepage of nitrate.

1.3 Methodological approach

Appropriate models were selected and combined in an integrative modelling concept to cope with the problem of nitrate transport in lowland catchments. For simulation of soil water and nitrogen processes, the soil-water-model SIMPEL (Hörmann, 1998) and the soil-nitrogen-model RISK-N (Gusman and Marino, 1999) were chosen and modified in order to serve the special needs of coupling to groundwater models (mRISK-N model). A sensitivity analysis and a calibration study against lysimeter data were carried out in order to assess model suitability. Groundwater flow and multi-species transport were based on the well-known models MODFLOW (McDonald and Harbaugh, 1988) and RT3D (Clement, 1997). To simulate chemical reactions of nitrate in groundwater, a reaction-module was developed, which can be used with the RT3D groundwater transport model. A sensitivity analysis was carried out for a batch-reaction, in order to evaluate the behaviour of the reaction-module.

A first application of the groundwater-reaction-module was the simulation of a field-scale tracer experiment on groundwater nitrate transport in order to quantify reaction rates of nitrate turnover on a selected plot within the study area. A second application focused on the investigation of basic interactions between chemical and physical aquifer properties and nitrate turnover, using an artificial transect representing a typical lowland catchment flow situation.

A distributed soil simulation was carried out for the study area to provide groundwater recharge and nitrate leaching as input data for the subsequent groundwater simulations. The subsequent groundwater simulations followed a nested modelling approach, starting from a regional flow model to a catchment scale and a sub-catchment scale model.

1. Regional flow model: The regional flow model covered an extended study area defined by the surrounding river systems, which were used as boundary conditions. The regional flow model served as a basis for delineation of the Schaugraben catchment boundaries and provided necessary boundary conditions (constant head boundaries) needed for subsequent models.
2. Schaugraben P5 catchment: The catchment model covers the catchment area of the Schaugraben related to the gauging station P5. Distributed input from the soil and conservative and reactive nitrogen transport were combined at this scale, focussing on interactions between spatial distribution of N-sources and N-discharge into the surface water system.
3. Subcatchment of the Schaugraben P5 catchment: Simulations on this scale are identical with the catchment simulations. However, a finer grid resolution was used.

The work was carried out in close cooperation with the UFZ Lysimeter station in Falkenberg, which did an intensive survey of the Schaugraben area, including collection of data on landuse and management, climatic data and measurement of discharge and loads in the Schaugraben drain. They also carried out experimental studies in the Schaugraben, including the tracer experiment on nitrate transport. The reaction-module was developed in cooperation with the UFZ Department of Hydrogeology.

2 Theoretical background

2.1 Hydrological characteristics of lowland catchment systems

Pleistocene landscapes are characterized by a mosaic of upland areas and depressions. Height differences are low compared to mountainous areas and lie in the range of metres and dekametres. Wetlands and semi-terrestrial soils cover wide areas. An intensive drainage is necessary and a more or less dense network of natural and artificial drains can be found.

The sedimentary cover is made up of pleistocene and holocene sediments (glacial sand, till and loam, glaciofluvial deposits, cover sands, peat, alluvial deposits). The aquifer system in pleistocene lowlands is organized in more or less continuous different groundwater floors forming local and regional flow systems. Correspondingly, solute transport includes short and long distance components with transit times of years to decades.

The total discharge can be subdivided into the following flow components:

- Surface runoff of water not infiltrating into the soil, with a residence time of a few hours
- Interflow, resulting from infiltrating water, running on impermeable layers above the groundwater surface, with a residence time of one to several days.
- Baseflow or groundwater flow resulting from water percolating down to the groundwater, following the hydraulic head gradient to the discharge system. Residence times of up to several decades are possible.
- Drainage systems also produce a drain flow, contributing to total discharge especially during the drain period from November to April/May.

In semi-terrestrial locations (wetlands), capillary rise from the groundwater can play an important role, leading to a decrease in net groundwater recharge or even cause net groundwater consumption. At these locations, leaching of substances can also be partly reversed.

According to Kunkel and Wendland (1998), total discharge originates almost completely from baseflow in areas characterized by loose sediments and deep groundwater tables. However, the fraction of baseflow is reduced, if soils become saturated due to high groundwater tables or water logging. In this case, direct runoff components increasingly contribute to total runoff.

2.2 Transport and turnover of nitrogen in soil and vadose zone

Soil and vadose zone modelling of soil nitrogen dynamics requires the integration of various biochemical and physico-chemical processes as well as soil water and vegetation dynamics.

The soil nitrogen cycle is an assembly of input and output fluxes, N-pools and internal fluxes. The main components and processes of an arable soil are summarized in Figure 1.

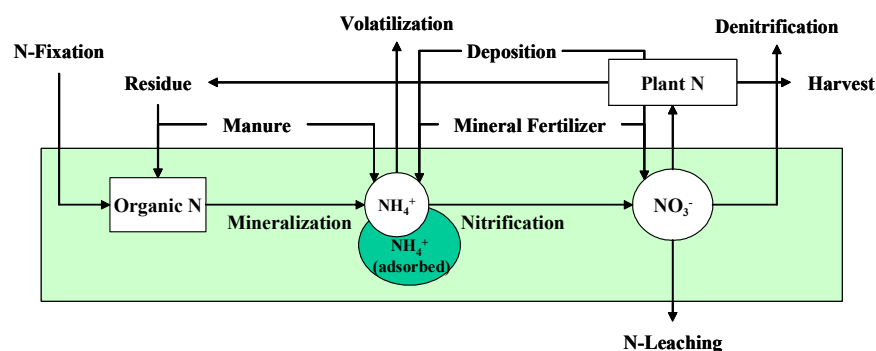


Figure 1: Nitrogen cycle of an arable soil

The main sources of nitrogen are i) input of organic and mineral fertilizer from agriculture, ii) incorporation of plant residues into soil organic matter, iii) fixation of atmospheric nitrogen by specialized symbiotic bacteria and fungi, and iv) atmospheric deposition. The various inputs are incorporated into the soil as soil organic matter (organic N), ammonium-N, and nitrate-N.

Mineralisation, nitrification and denitrification processes control the transformation of nitrogen between the various pools. An effective removal of nitrogen from the soil takes place by i) plant uptake and relocation by harvest, ii) leaching of nitrate to groundwater due to percolation and iii) denitrification, causing a transformation into gaseous nitrogen (N₂). For a detailed discussion of soil nitrogen processes see standard literature of soil science, e.g. Scheffer and Schachtschabel (1998) and Miller and Donahue (1995).

In the last decades, numerous soil-nitrogen-models of different complexity were developed, e.g. WASMOD/STOMOD (Reiche, 1991), HERMES (Kersebaum, 1995), CANDY (Franko et al. 1995), WHNSIM (Huwe, 1992), ANIMO (Groenendijk and Kroes, 1997), EPIC (Sharpley and Williams, 1990), RISK-N (Gusman and Marino, 1999). A short review on the current state of soil nitrogen modelling approaches is also given by Kersebaum (1999).

Soil-nitrogen-models are an assembly of various submodels, describing soil water dynamics, source and sink-fluxes, and transformation processes. A soil water simulation is a precondition for the simulation of advective transport and of various biochemical transformations (Kersebaum, 1999), where soil water content is considered as a controlling factor. Soil water dynamics are simulated using the Richards-equation or storage approaches. The transport of nitrate is simulated using the one-dimensional convection-dispersion-equation (1D-CDE) or by mixing-cell models, considering convective transport only. Generally, first-order reaction kinetics are used to simulate the mineralisation process. The use of first-order kinetics follows the concept of a potential mineralisable N-pool (Stanford, Smith (1972) cited in Kersebaum, 1999), which becomes depleted, if no further addition of organic matter occurs in specific intervals. The organic N-pool generally is divided into two or more N-pools of different mineralisation velocity. For practical simulations, two mineralisable N-pools are considered to be sufficient (Kersebaum, 1999; Scheffer and Schachtschabel, 1998). Correction functions account for soil temperature and soil water content. Rodrigo et al. (1997), cited in Kersebaum, 1999, found considerable differences applying various correction functions for the calculation of mineralisation rates up to a factor of five. Various models couple N-mineralisation to soil carbon dynamics. Mineralisation and immobilisation of soil nitrogen are then controlled by soil carbon dynamics and CN-ratio. Denitrification is generally described by zero or first-order kinetics, modified by correction functions to account for soil temperature, soil saturation (as an indirect measure of oxygen partial pressure) and organic carbon. A comparison of varying denitrification functions is provided by Marchetti et al. (1997).

Modelling approaches of plant uptake range from logistic uptake functions to complex plant sub-models. The use of plant sub-models is restricted by the availability of reliable model parameters, logistic uptake functions can not account for site specific stress factors, such as drought or N-depletion, as total N-uptake is provided as input data.

Soil-nitrogen-models are generally confined to the root zone, as they were developed to serve agricultural needs and to quantify soil losses. However, transport and turnover in the vadose zone are principally based on the same physical and chemical processes as in the root-zone. Nitrogen turnover can be simplified to denitrification only, as complex soil-plant interactions are missing in this zone. Denitrification is mainly driven by organic matter leaching from the root zone. It is generally assumed, that the vadose zone is of low importance for nutrient turnover and denitrification due to the low availability of organic matter (Walther et al., 2001). Intensive turnover, however, is possible if a carbon source is available.

2.3 Transport and turnover of nitrogen in groundwater

2.3.1 Groundwater flow and transport

Saturated groundwater flow is generally described through the application of Darcy's Law and the principle of mass conservation. According to Zheng (1990) the flow equation can be written as

$$S_s \frac{\partial h}{\partial t} = \nabla \cdot (K_{ij} \nabla h) + q_s$$

with S_s = storage [m³], h = hydraulic head [m], t = time [d], K_{ij} = saturated conductivity [m/d], q_s = source and sink flux [m³/d].

The flow equation is solved by various solution schemes implemented in groundwater modelling

software such as MODFLOW McDonald and Harbaugh, 1988) and FEFLOW (Diersch, 1998).

Transport velocities are given by the equation

$$v_i = -\frac{K_{ij}}{\Phi} \nabla h$$

with v_i =transport velocity [m/d], K_{ij} =saturated conductivity [m/d], Φ =porosity [m^3/m^3], h =hydraulic head [m].

The general macroscopic equations describing the fate and transport of aqueous- and solid-phase species in multi-dimensional saturated porous media can be written as in the equations

$$\frac{\partial C_k}{\partial t} = \nabla(D_{ij} \nabla C_k) - \nabla(v_i C_k) + \frac{q_s}{\Phi} C_{s_k} + r_c, \text{ where } k = 1, 2, \dots, m$$

and

$$\frac{\partial C_{im}}{\partial t} = r_c, \text{ where } im = 1, 2, \dots, n - m$$

with C_k = concentration of mobile component k [mg/l], C_{im} =concentration of immobile component im [mg/l], D_{ij} =dispersion [m], v_i =transport velocity [m/d], Φ =porosity [m^3/m^3], q_s = source/sink- flux [m^3/d], C_{s_k} = source/sink concentration of component k [mg/l], r_c =reaction rate for component [mg/l/s] (internal source/sink), m = number of mobile components, n = number of components.

RT3D solves the transport equation with an operator split strategy, where advection, dispersion and reactions are solved in separate, subsequent steps.

Solution algorithms used to solve the transport equation are the pure finite-difference method, the TVD (Total variation diminishing) scheme and Eulerian-Lagrangian methods such as the Method of Characteristics (MOC), which implement particle tracking methods in order to minimize numerical dispersion (Chiang et al., 2002; Zheng, 1990). Common modelling software such as MT3D or RT3D allow to choose between various solution algorithms according to the specific requirements of the modelling task. The choice of a specific solution algorithm always depends on the problem under consideration. MOC minimizes the effect of numerical dispersion, but is not entirely mass conserving and therefore not suited for reactive transport modelling. FD and TVD-schemes can both be used for reactive transport modelling, but higher numerical dispersion (FD) or higher computational demand (TVD) have to be taken into account (Chiang et al., 2002).

2.3.2 Groundwater nitrogen dynamics

Denitrification can be considered as the most important nitrogen turnover reaction in the groundwater. A review of denitrification in groundwater is given by Korom (1992). The general requirements for denitrification are in principle the same as in soils: lack of oxygen, presence of denitrifying bacteria and suitable electron donors. According to various authors cited by Wendland and Kunkel (1999), oxygen concentrations limiting the denitrification in groundwater range between 1 to 5 mg/l. The most important denitrification pathways are i) organo-heterotrophic denitrification, where organic substances serve as electron donor, and ii) litho-autotrophic denitrification, where reduced iron (Fe(II)) or reduced sulphur compounds act as electron donor. Pyrite (FeS₂) is the most typical source of reduced sulphur. Other possible electron donors are manganese and iron ions of a low oxidation stage (Mn(II), Mn(III), Fe(II)).

Organo-heterotrophic and litho-autotrophic denitrification are linked with two other important reaction pathways, the decay or mineralisation of organic matter and pyrite oxidation. A variety of substances may act as electron acceptor. O₂, NO₃⁻, Mn(IV), Fe(III), and SO₄²⁻ are possible electron acceptors used for oxidation of organic matter, being reduced to H₂O, N₂, N_xO_y, Mn(II), Fe(II) and HS⁻. The electron acceptors are utilised in a more or less defined sequence according to their energy yield, expressed as redox potential. The pyrite oxidation reaction utilises O₂ and NO₃⁻ as electron acceptors. In this reaction, Fe²⁺ is released, which also acts as an electron donor for the reduction of nitrate. The utilisation of oxygen is always preferred to the utilisation of nitrate, thus

aerobic conditions limit the denitrification reaction.

The sequential oxidation of pyrite and organic matter combined with the groundwater flow leads to a distinct zonation of hydrogeochemical conditions within the aquifer: After the consumption of oxygen nitrate will be used as electron acceptor. If pyrite is present, the pyrite oxidation leads to a distinct production of sulfate. After the consumption of nitrate, sulfate will be used as electron acceptor for the oxidation of organic matter (Desulfurication), leading to a production of hydrogen sulfide. As discussed by Postma et al. (1991), this zonation is more or less well expressed in the field, depending on reaction rates, amounts of reactive substances and flow characteristics.

It was also found that the autotrophic denitrification is strongly preferred to the heterotrophic denitrification if pyrite is present Kölle (1999), due to the high ratio of non-degradable fractions of sedimentary organic matter. There are only few studies available, providing field measurements of reaction kinetics. Frind et al. (1990) found a NO_3^- -half-life constant for autotrophic denitrification of 1.0-2.3 years and for the desulfurication reaction a SO_4^{2-} -half-life constant of 70-100 years assuming a first-order unlimited decay. In contrast, Molenat and Gascuel-Oudoux (2002) reported half life constants for autotrophic denitrification of 2.1-7.9 days and complete heterotrophic denitrification within a few hours, based on investigations in pyrite-rich schist aquifers of the Kervidy catchment, Brittany. Pättsch et al. (2003) reported half life for denitrification between 1.3-3.4 years, in a pleistocene aquifer near Thülsfeld, Lower Saxony. These discrepancies show that denitrification rates have to be considered as specific to the aquifer.

Another reaction pathway observed in groundwater systems might be the dissimilatory nitrate reduction to ammonium (DNRA). In contrast to the denitrification reactions, the DNRA preserves nitrogen in the aquifer as NH_4^+ . The NH_4^+ can be converted back to NO_3^- if anaerobic conditions are encountered. There are only few studies dealing with the DNRA-reaction in aquifers (e.g. Tiedje et al. (1982), cited in Korom, 1992) and no reliable data on the DNRA-reaction is available.

2.4 Organic matter as substrate for denitrification

In soil systems, organic matter is the most important electron donor, and consequently denitrification rates are correlated to the content of organic matter. This relation has become an integral part of many denitrification models (Marchetti et al., 1997). The pool of soil organic matter is constantly regenerated by net plant production and decomposition of plant residues. Therefore, soil denitrification might be limited by available carbon, but the denitrification capacity is sustained.

Subsoil denitrification is mainly driven by leaching of organic carbon from the topsoil. Brye et al. (2001) found in lysimeter studies, that the subsoil denitrification potential in an agroecosystem was limited by the supply of DOC, whereas in the grassland nitrate was the limiting factor. At the same time DOC-concentrations were higher in the agroecosystem than in the grassland (prairie) ecosystem, indicating different reactivity of DOC in both ecosystems (In the upper soil, denitrifying conditions were not observed).

As shown by Richards and Webster (1999), Springob and Böttcher (1999) and Walther et al. (2001), subsoil and vadose zone denitrification is negligible in many locations, as the low availability of organic carbon strongly limits denitrification processes.

During the transition of the vadose zone, DOM undergoes considerable adsorption and chemical transformation. Chemical transformation causes a decrease in organic matter concentrations and chemical alteration of the remaining organic substances into more stable compounds (Oswald et al., 1999; Kalbitz et al., 2000; Kalbitz et al., 2003; Kalbitz and Geyer, 2003; Marschner and Kalbitz, 2003; Neff and Asner, 2001). The concentration of DOM and its reactivity can be considered to decrease with the vadose zone residence time and the depth of the groundwater table (Siemens, 2003; Oswald et al., 1999). In semiterrestrial locations the DOM-load to groundwater generally is higher than in terrestrial locations, due to shorter percolation distance and residence time (Oswald et al., 1999). As shown by Becker (1999), soil organic matter becomes available for groundwater denitrification processes, if the groundwater table is at least periodically located within the root zone.

In the groundwater domain, two potential sources of organic matter have to be considered: dissolved organic matter (DOM) leached from the soil and sedimentary organic matter (SOM).

The contribution of DOM for groundwater denitrification still is unclear. Siemens (2003) found no

evidence for dissolved organic carbon acting as a substrate for groundwater denitrification in groundwaters which are overlain by a vadose zone of several metres. He found a strong decrease in dissolved organic carbon concentrations while passing the vadose zone, which can mainly be referred to sorption processes. Incubation experiments were carried out with groundwater samples to quantify denitrification processes. It was found that denitrification did not take place with the original DOM and addition of easily decomposable carbon compounds was necessary to induce denitrification. In contrast, Well et al. (2001) could derive good correlations between the content of total organic carbon and groundwater denitrification rates in semiterrestrial locations for various groundwater influenced soils in Northern Germany. These studies, however, are not contradictory. In semiterrestrial locations, groundwater is in close contact with the root zone and soil organic matter, allowing intensive denitrification to take place. In contrast, after the transition of a vadose zone the organic matter reaching the groundwater is chemically strongly altered or quantities are too low to maintain considerable denitrification.

According to Korom (1992), thermodynamic considerations show that over geologic time scales the organic matter remaining in the sediment is not very labile, as the more labile forms of SOM tend to be oxidized first, leading to a relative enrichment of stable fractions. Thus, heterotrophic denitrification processes are slow compared to autotrophic denitrification (Kölle, 1990; Kölle, 1999, see also chapter 2.3). Recent studies by Buckau et al. (2000) and Artinger et al. (2000) show that sedimentary carbon is a possible source of dissolved organic matter: in-situ generation of DOM occurs in conjunction with the microbially mediated mineralisation of SOM. The mineralisation process is based on reduction of sulphate (desulfurication) or fermentation processes and can release considerable amounts of humic substances. In-situ generated DOM may then also be involved in subsequent reactions.

Whereas in surface-near groundwaters (e.g. in wetlands) the groundwater denitrification capacity may be sustained by leaching of DOC from the soil, the denitrification capacity of deeper groundwaters is based on the pools of sedimentary electron donors only. These pools (sedimentary organic matter and pyrite) are limited, thus denitrification processes inevitably decrease the denitrification potential of the aquifer (Kölle, 1990; Kölle, 1999).

2.5 Recent modelling studies

Modelling studies concerning the fate of nitrogen in catchment systems are widespread in literature. Many studies confine to either soil nitrogen turnover or groundwater nitrogen transport. In the last years, there was a clear trend to combine soil and groundwater models and also to include reactive groundwater transport.

The suitability of soil-nitrogen-models (CANDY, DYNAMIT, MESO-N, Expert-N, Hermes, Minerva, SIMULAT, SWIM, WASMOD) for the simulation of N-dynamics in mesoscale areas is discussed by Projektgruppe Elbe-Ökologie (1997). Most of the models under consideration were originally designed for field scale applications, but they were applied to catchment studies as well. In general, the models show comparable results. Main limitations of model application are: i) the limited capabilities to consider lateral flow and transport (interflow or groundwater flow), ii) the scaling problem (choice of an appropriate model complexity and upscaling of model parameters) and iii) availability and accuracy of input data. A lot of expert knowledge is needed to cope with model peculiarities. Some examples for the application of soil-nitrogen-models in small catchment areas are given in Table 1.

Table 1: Selected applications of soil-nitrogen-models on a catchment scale

Catchment	Size	Compartments considered	Model	Author
Schaugraben	25 km ²	Soil	CANDY	UFZ (unpublished)
Bruchsal water works		Soil	WHNSIM	Huwe and Totsche (1995)
Lake Belau	4.5 km ²	Soil	WASMOD/STOMOD	Reiche (1994)
Gelliehausen	3.90 km ²	Soil	WASMOD/STOMOD	Kenkel (1999)
Thülsfeld water works catchment	27 km ²	Soil, Groundwater	HERMES	Pätsch (2003)
...				

During the last 15 years various modelling approaches have been published focussing on modelling of groundwater nitrate transport or biogeochemistry of subsurface environments. Widdowson et al. (1988), Kinzelbach et al. (1991), MacQuarrie and Sudicky (2001) present reaction models based on sequential degradation of organic matter using Monod-type reaction kinetics including growth and transport of microorganisms. Böttcher et al. (1989) and Frind et al. (1990) implement autotrophic denitrification and desulfurification as reaction pathways using first-order kinetics based on investigations in the Fuhrberger Feld, Lower Saxony. These studies concentrate on a few selected processes, as i) reactive transport models for solving the reaction systems had to be developed as well and ii) computational possibilities were limited. More complex reaction systems are presented by Van Capellen et al. (1996) and Hunter et al. (1998). Degradation of organic matter by various electron acceptors and secondary redox reactions as well as mineral precipitation and dilution are included in their models emphasizing the “strong coupling between subsurface heterotrophic activity and an extensive network of secondary reactions (Hunter et al., 1998, p.53)”. They implement first-order reaction kinetics and equilibrium reactions. All these works include case studies or model demonstrations of different complexity. None of the models has been applied to small catchments or three dimensional problems. Recently a variety of reactive transport models has emerged, allowing flexible implementation of reaction systems, such as RT3D (Clement, 1997), PHT3D (Prommer, 2002) and TBC (Schäfer et al., 1998). They couple geochemical modelling approaches with conventional transport codes. However, applications on catchment scale are rare. TBC was applied to the Torgau basin (Saxony) by Herlitzius et al. (2003) for the simulation of three-dimensional reactive sulphate transport in groundwaters near Torgau water works.

A methodology for the assessment of nitrate pollution in large catchment systems was presented by Kunkel and Wendland (1998), Kunkel and Wendland (1999) and Wendland and Kunkel (1999) and applied in the Elbe-catchment. This methodology does not provide site-specific information, but gives a valuable overview of large scale patterns.

Combining soil and groundwater models would be a straightforward approach allowing the investigation of spatial patterns of nitrogen distribution in small catchment systems. Still there are only a few studies following this approach to simulate nitrogen transport in small catchments. Molenat and Gascuel-Oudou (2002) investigated nitrate transport in a pyrite rich shist aquifer in the Kervidy catchment (5 km²) in Brittany. MT3D was used to describe groundwater transport of nitrate. Denitrification is included as first-order decay of nitrate. Recent studies within the framework of the 4th INCO-COPERNICUS EU-Framework programme aimed at the development of software tools for the simulation of changes in agricultural soil use and their effect on groundwater for small catchment areas (Pätsch et al., 2003). This modelling approach is based on the soil-water- and nitrogen-models HERMES (Kersebaum, 1995), SWAP/ANIMO (Van Dam et al., 1997; Groenendijk and Kroes, 1997) and WAVE (Vanclouster et al., 1994) for the simulation of soil and vadose zone processes. Groundwater processes are simulated using MODFLOW and MT3D, including first-order nitrate decay due to autotrophic and heterotrophic denitrification. Applications of these modelling tools are given by Pätsch et al. (2003) for a Pleistocene catchment in Thülsfelde, Lower Saxony, and by Diankov et al. (2003) for a study site of 4 ha in Chelopechene, Bulgaria. All of these studies consider nitrate turnover as a first-order decay reaction, using the widespread MT3D-code. Heterotrophic and autotrophic denitrification are not considered as separate processes and denitrification is described by one parameter (first-order decay constant). The implicit assumption is made that reactive pools are not depleted and do not limit turnover rates within the simulation period, as this approach does not account for consumption and availability of reaction partners. The decay constant can be assigned as distributed value as well as a constant for the model. As reported by the authors, major problems were i) availability of suitable input data and ii) heterogeneity of physico-chemical parameters in unsaturated and saturated zone (Pätsch et al., 2003).

For the investigation of interactions between physical and chemical catchment properties in heterogeneous catchments, these approaches are unsuited. In order to study spatial, temporal and geochemical interactions, a distributed, full reactive transport model is needed, which can account for the fate of reaction partners as well. The application of such approaches, however, is restricted, as the increased demand for model parameters and input data also adds a lot of uncertainty.

3 Models and modelling strategy

3.1 Outline of the integrative modelling concept

In catchment modelling, a variety of different ecosystem compartments and their specific processes need to be combined. Compartments and related processes are not only characterized by spatial heterogeneity, but by specific time scales as well (e.g. residence times). A straightforward modelling strategy was chosen, simulating different ecosystem compartments and processes separately using appropriate modelling approaches. These separate submodels are linked by one-way coupling, i.e. model output serves as input for subsequent models. Interactions between submodels, for example dynamic groundwater levels and subsequent relocation of matter are neglected.

Major compartments are vegetation, soil and vadose zone, groundwater and surface water. The processes under consideration can roughly be separated into water fluxes, solute transport and reactions. Based on this separation, existing models and modelling approaches were chosen to simulate soil and groundwater processes, as given in Figure 2.

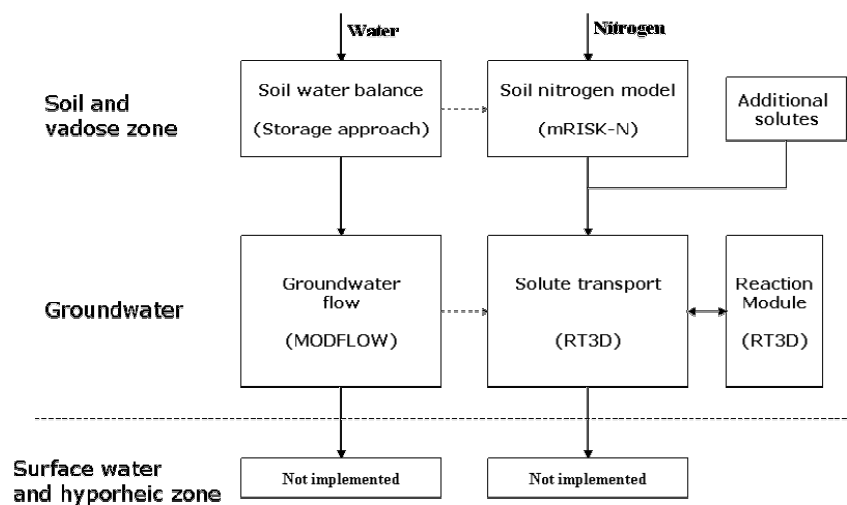


Figure 2: General modelling approach – Submodels and modelling software

Soil processes are based on the mRISK-N model, which combines modified versions of the soil-water-model SIMPEL (Hörmann, 1998) and the analytical soil-nitrogen-model RISK-N (Gusman and Marino, 1999). The RISK-N model considers the entire vadose zone from soil surface to groundwater table and does not require the development of a separate vadose zone transport module, as it would be necessary for other models. Water flow is calculated using a storage approach based on three subsequent soil water storages representing upper and lower root zone and intermediate vadose zone (until groundwater surface). Transport is considered as advective transport, applying the complete mixing assumption to any storage. A separate vegetation model to simulate plant growth was not included. Soil-plant interactions are confined to nitrogen uptake and residue incorporation, which have to be supplied as input parameters. The soil model mRISK-N is discussed in more detail in chapter 3.2.

The three-dimensional finite difference code MODFLOW (McDonald and Harbaugh, 1988) was used for the simulation of groundwater flow. As discussed by Schöniger (1998), Modflow was originally designed for confined groundwater flow problems and therefore, the free groundwater surface is approximated by a straightforward solution (Exact solution schemes, considering the free groundwater surface as a boundary condition, are implemented e.g. in the groundwater software FEFLOW (Diersch, 1998), which is only available at high costs and currently does not offer extensions to integrate full reactive transport). Nevertheless, MODFLOW has been used for the simulation of free surface problems as well. Using MODFLOW offers various advantages compared to other models: i) the flexible design allowing to consider various processes (ground- and surface water interaction and evaporation from groundwater) needed in catchment scale modelling and ii) the compatibility with groundwater transport models, including full reactive models.

Based on the MODFLOW code, various solute transport models have been developed such as MT3D (Zheng, 1990; RT3D (Clement, 1997) and PHT3D (Prommer, 2002). MT3D is a multi species solute transport model, RT3D and PHT3D are extensions of MT3D for full reactive transport simulation, allowing for implementation of complex geochemical systems. Whereas RT3D allows the implementation of rate-limited reaction systems, PHT3D is a full implementation of the geochemical software PHREEQC (Parkhurst and Appelo, 1999) into a groundwater transport model. In this study, groundwater transport and turnover processes were based on the RT3D code. Turnover processes were implemented as a user-defined reaction-module, running with the RT3D code. The implementation of the reaction-module was carried out in close cooperation with the UFZ Department of Hydrogeology and is described more detailed in chapter 3.3.

The modelling concept presented here is considered as a tool box providing a variety of modelling capabilities. Their selection and combination strongly depends on the specific requirements of the modelling task.

3.2 Modelling of water and nitrogen in soils and vadose zone

3.2.1 Model choice

A suitable soil-nitrogen-model has to meet technical as well as scientific requirements. From a technical point of view, a free source code is needed, as automatic data transfer from the soil model to the groundwater model requires modification of output routines or development of specific postprocessing software. For this reason, output files should also allow direct access regardless of specific software environments. Distributed soil-nitrogen-models are generally based on elementary areas or response units, defined in vector format (as polygons). Considering a vadose zone of varying depth would require further subdivision of these response units or a raster based simulation, leading to a large number of elementary simulations and high computation times. The soil-nitrogen-model should consider all relevant turnover processes. This was the case for all models under consideration. Also, the model should not be confined to the root zone but also consider transport through the vadose zone to the groundwater table. Otherwise, a development of a separate vadose zone transport model would be necessary. Generally, increasing model complexity decreases applicability for practical purposes, due to an increased demand for input data and model parameters (Kersebaum, 1999). For catchment scale simulations, input data and model parameters are often defined via transfer functions or taken from existing data sets, often provided by public authorities. Therefore, an increased demand for input data is opposed by a decrease in data quality.

To overcome these limitations, a low complexity soil-water- and nitrogen-model mRISK-N was developed, which is basically a combination of the soil water storage model SIMPEL (Hörmann, 1998) and the analytical soil-nitrogen-model RISK-N (Gusman and Marino, 1999). From a technical point of view, this approach has considerable advantages. The nitrogen-model solves the model equations analytically, and no time-consuming iterative solution algorithm is needed to solve transport equations. Model input- and output-structure could be organized according to the specific requirements of this study, distributed simulations are not bound to a grid based or polygon based structure. From a scientific point of view, all relevant processes can be considered. Although on a very simple stage, even transport and turnover in the intermediate vadose zone is implemented and no separate model is necessary. The cost is limited model accuracy. Field conditions can only be approximated due to the simplification of spatial and temporal resolution and model structure. However, this does not affect the model's capability of scenario simulations. A detailed documentation of the mRISK-N model is given in Appendix B.

3.2.2 Soil-nitrogen dynamics

The soil-nitrogen submodel is presented first, as the concept of the RISK-N model was also used as a basis for the development of the soil water submodel.

Included nitrogen related processes are mineralisation, ammonium immobilisation, ammonium adsorption, ammonia volatilisation, nitrification, denitrification, plant uptake, and leaching. Input of nitrogen takes place in the form of mineral fertilizer, manure, crop residue and atmospheric deposition. The unsaturated soil column is separated into the upper root zone (URZ), lower root zone (LRZ) and intermediate vadose zone (IVZ) (Figure 3). Most transformation processes are limited to the upper root zone. In the LRZ, plant uptake and denitrification are the only

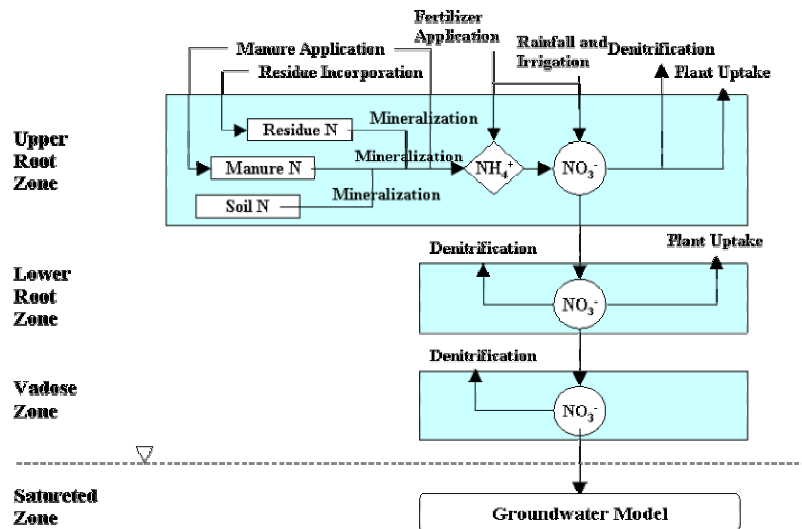


Figure 3: Structure of the RISK-N model (modified, Gusman and Marino, 1999)

transformation processes taken into account. In the IVZ, only denitrification is considered.

Transport is considered as advective flux assuming complete mixing within each compartment. Ammonia-volatilisation is considered as constant fraction of fertilizer application. Mineralisation is simulated by first-order reaction kinetics according to Kersebaum and Richter (1991). However, in contrast to the original model, mineralisation constants can be defined arbitrarily. Nitrification is simulated by first-order reaction kinetics as well. Adsorption of ammonium is implemented using a linear isotherm. Denitrification is simulated using first-order reaction kinetics. A detailed description of the model including model equations is given in Gusman and Marino (1999).

Temporal resolution is based on free defined stress periods ("seasons"), during which all boundary fluxes are kept constant. This simplification allows solving model equations analytically instead of using time-consuming iterative solution algorithms. The length of stress periods can be defined arbitrarily. In this study, stress periods were defined on a monthly basis, and all input data for the nitrogen-model were also given as monthly data. The model does not implement a model of plant growth and dynamic N-uptake. Plant uptake and residue have to be provided as input data. Consequently, it is possible that plant N-uptake exceeds the content of N available for plant uptake. In order to maintain the correct N-budget in this case, the amount of residue input is reduced by the difference between postulated N-uptake and available N. The thickness of the first two soil layers is defined by crop characteristics and covers a depth of 1-2m. The extent of the last horizon, however, is fixed by groundwater depth. Groundwater depth is kept constant over time, a dynamic exchange between groundwater and soil can not be considered. For model equations, see appendix B.

3.2.3 Soil water dynamics

The basic concept for the soil-water-model is taken from the SIMPEL-Model (Hörmann, 1998), which was modified according to the specific demands of the nitrogen-model RISK-N. The model describes water flux through a series of different storages (Figure 4): a leaf interception storage, an infiltration storage and one or more soil water storages. Input variables of the soil-water-model are precipitation, potential evapotranspiration and leaf area index. Model parameters are basic soil-physical parameters (pore size distribution and saturated conductivities) and storage capacities for leaf interception storage and infiltration storage. The original model runs with daily data and is distributed as an EXCEL-worksheet.

In accordance with the RISK-N model, the soil column is represented by three capacity storages, equivalent to the URZ, LRZ and IVZ. The thickness of the IVZ is variable and depends on the average groundwater depth. The original equation for storage depletion and percolation was based on the model of Glugla (1969). This approach was exchanged with the percolation equation used in the EPIC-model (Sharpley and Williams, 1990). This was done in order to substitute the empirical leaching parameter with a formulation directly related to soil physical parameters (Conductivity and

porosity), which can be derived from pedotransfer functions. Time steps can be defined independent from the RISK-N model. In this study, the soil model runs with daily data. After running the water balance model, the results are aggregated according to the stress periods used in the RISK-N model. For model equations, see appendix B.

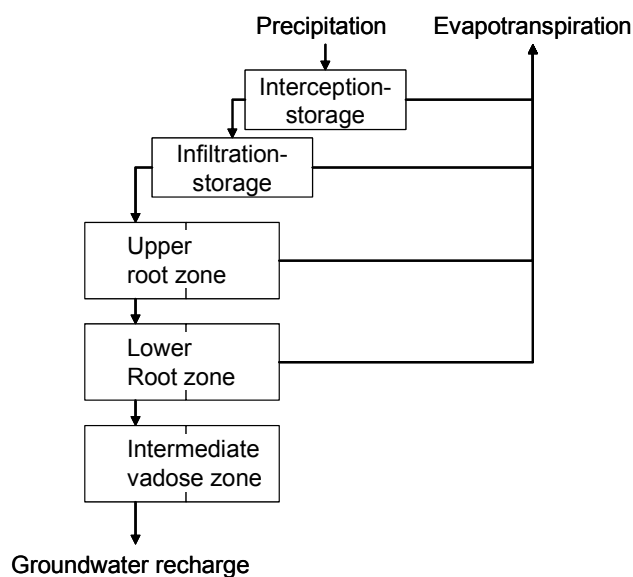


Figure 4: Structure of the soil water submodel

3.2.4 Soil temperature

The models do not contain a submodel for heat transport to calculate soil temperature dynamics. However, temperature is a boundary condition for mineralisation and denitrification processes. Due to the division of the soil column in three layers and the seasonal nature of stress periods of the nitrogen-model, no temperature model was implemented but soil temperature was set according to simple rules as follows:

- Soil temperature in the first layer was set equal to the average temperature of the preceding three days.
- Soil temperature in the intermediate vadose zone was set to the mean annual temperature if the depth of groundwater level was below 3m, otherwise to the mean temperature of the preceding two months.
- Soil temperature of the lower root zone was interpolated between upper root zone and intermediate vadose zone temperature.

3.2.5 The mRISK-N-Model

The modified RISK-N model (mRISK-N) is a software application, which was written by the author to integrate the soil water and the soil nitrogen submodels in an executable code and to add specific routines for the input of simulation data and the output of simulation results. The program was written in Visual Basic.

The mRISK-N model can handle multiple simulations. A set of elementary simulations is defined in a simulation list, which is part of the input files. These elementary simulations are defined by a combination of soil type, management scenario (patch) and groundwater depth.

Results are printed as annual data or based on stress periods (months in this study). The soil-water-model runs with daily data, but the results are internally aggregated, based on the nitrogen-model stress periods.

1.1.1 Preprocessor RISKNREGIO

The mRISK-N model can be used for local and distributed or regional simulations. The mRISK-N model can handle multiple simulations being defined in a simulation list. A distributed simulation

basically is a set of multiple simulations, with each elementary simulation being referenced to a specific spatial object using a simulation identifier. This can be a polygon as well as a grid cell.

The setup of a distributed mRISK-N-simulation is supported by the program RISKNREGIO (written in Visual Basic), which was also developed by the author. The code reads grid based data on soil type, management scenario and groundwater depth and identifies elementary simulations as unique combinations of these data. The elementary simulations are added to the simulation list and the corresponding simulation identifiers are written into a grid defining the spatial distribution of the elementary simulations. The mRISK-N simulation is started and after completion the annual totals and total averages of the water balance and nitrogen balance are extracted as grid data.

In order to link simulation results to a groundwater model, the data grids have to be identical with the finite difference groundwater model grid (Figure 5).

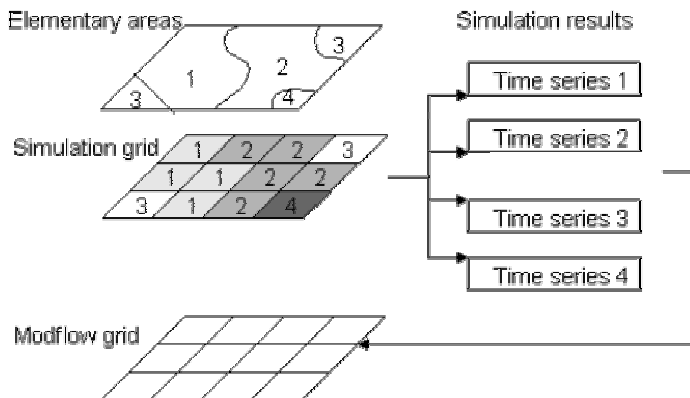


Figure 5: Spatial relation between distributed soil simulation and groundwater model

3.3 Development of a groundwater-reaction-module for the simulation of groundwater nitrogen turnover

3.3.1 Definition of the chemical system

Autotrophic denitrification and heterotrophic denitrification are the most important nitrogen turnover reactions in groundwater. Autotrophic denitrification is based on the oxidation of reduced sulphur compounds, heterotrophic denitrification is based on the oxidation of organic matter. These reactions take place in a geochemical context of sequential redox-reactions and secondary reactions.

The reaction system is based on the oxidation of organic matter (OM) by O_2 , NO_3^- and SO_4^{2-} and on the oxidation of Pyrite (FeS_2) by O_2 and NO_3^- . Oxidation of organic matter by Iron(III) and Manganese(IV) is not considered for simplification purposes. Additionally, the carbonate equilibrium is considered as a major buffer reaction in pleistocene aquifers. Nitrification was included following a proposal of the UFZ Department of Hydrology for the study of coupled nitrification-denitrification treatment of waste waters.

Organic matter is a heterogeneous substance class, involving a variety of chemically different substances. Thus the implementation of organic matter as a component is based on a conceptual model rather than on chemical processes: A pool of "reactive" organic matter (rOM) was defined, which is available for various chemical reactions and covers a dissolved as well as a sorbed phase. This pool is fed from two sources, i) a reactive fraction of organic matter leaching from the soil by recharge water and ii) a slowly degradable pool of sedimentary organic matter (SOM) (in-situ generation of DOM). Degradation of the SOM-Pool is implemented using a transfer function between the SOM-pool and the rOM-pool (OM-release control function). The SOM transfer rate depends on the total SOM-content allowing to represent substrate limitation in sediments with low contents of organic matter and to allow for increased rOM-availability in sediments rich of organic matter (e.g. peat, wetlands). The advantage of this approach is to refer all chemical reactions to one pool of OM. Otherwise the same reactions had to be defined for SOM and rOM, adding more complexity to the model. The disadvantage of this approach is that identification of transfer parameters and quantification of pools can not be based on chemical observations, but on

expected or observed phenomenological behaviour only. Strictly speaking, rOM is not equivalent to DOM, as reactive fractions may be found in both, DOM and SOM. DOM also contains chemically inert fractions, not taking part in chemical reactions (see 2.4). Although a quantitative separation of these fractions is not possible, the term rOM is introduced to account for the conceptual difference of DOM, SOM and the pools of OM involved in reactive processes.

The reaction equations implemented in the reaction-module are summarized in Table 2.

Table 2: Definition of the chemical system (stoichiometry relative to unit electron donor)

Degradation of dissolved organic matter	
1) $\text{CH}_2\text{O} + \text{O}_2 \rightarrow 2 \text{H}^+ + \text{CO}_3^{2-}$	Mineralisation
2) $\text{CH}_2\text{O} + 0.8 \text{NO}_3^- \rightarrow 1.2 \text{H}^+ + \text{CO}_3^{2-} + 0.4 \text{N}_2(\text{aq}) + 0.4 \text{H}_2\text{O}$	Heterotrophic Denitrification
3) $\text{CH}_2\text{O} + 0.5 \text{SO}_4^{2-} + 2.5 \text{H}^+ \rightarrow \text{CO}_3^{2-} + 0.5 \text{HS}^- + 2 \text{H}_2\text{O}$	Desulfurication
rOM release from SOM-pool	
4) $\text{CH}_2\text{O}(\text{s}) \leftrightarrow \text{CH}_2\text{O}(\text{dissolved+sorbed}) \equiv \text{SOM} \leftrightarrow \text{rOM}$	SOM release
Pyrite oxidation and related oxidation of Fe(II)	
5) $\text{FeS}_2 + 3.5 \text{O}_2 \rightarrow \text{Fe}^{+2} + 2 \text{SO}_4^{2-} + 2 \text{H}^+$	Pyrite oxidation
6) $\text{FeS}_2 + 2.8 \text{NO}_3^- + 0.8 \text{H}^+ \rightarrow \text{Fe}^{+2} + 2 \text{SO}_4^{2-} + 1.4 \text{N}_2(\text{aq}) + 0.4 \text{H}_2\text{O}$	Autotrophic denitrification
7) $\text{Fe}^{+2} + 0.25 \text{O}_2 + 2.5 \text{H}_2\text{O} \rightarrow \text{Fe}(\text{OH})_3(\text{s}) + 2 \text{H}^+$	
8) $\text{Fe}^{+2} + 0.2 \text{NO}_3^- + 2.4 \text{H}_2\text{O} \rightarrow \text{Fe}(\text{OH})_3(\text{s}) + 0.1 \text{N}_2(\text{aq}) + 1.8 \text{H}^+$	
Nitrification	
9) $\text{NH}_4^+ + 2 \text{O}_2(\text{aq}) \rightarrow \text{NO}_3^- + 2 \text{H}^+ + \text{H}_2\text{O}$	Nitrification
Buffer system	
10) $\text{CaCO}_3 \leftrightarrow \text{Ca}^{+2} + \text{CO}_3^{2-}$	Calcite dissolution
11) $\text{CO}_3^{2-} + 2 \text{H}^+ \leftrightarrow \text{H}_2\text{CO}_3$	Carbonate equilibrium I
12) $\text{CO}_3^{2-} + \text{H}^+ \leftrightarrow \text{HCO}_3^-$	Carbonate equilibrium II
13) $\text{H}_2\text{O} \leftrightarrow \text{OH}^- + \text{H}^+$	Dissociation of water

3.3.2 Mathematical implementation

3.3.2.1 General formulation

RT3D solves the 3D-convection-dispersion equation for solute transport in porous media. Solute turnover is implemented as an internal source/sink-term r_c . This reaction term provides the change in component concentration per time increment, according to the equation

$$r_c = \frac{dC}{dt}$$

with r_c = reaction rate [mg/m³/d], C = Concentration [mg/l], t = Time [d].

The reaction-module provides a set of reaction terms r_c for each species or component c under consideration. The concentration change of each component is defined by the reaction rates and stoichiometric relations of the specific reactions the component is involved in:

$$\frac{dC_i}{dt} = \sum_{j=1}^n y_{ij} r_j$$

with C_i = Concentration of component i [mol/l], t = Time [d], y_{ij} = stoichiometric coefficient for component i in reaction j [mol/mol], r_j = reaction rate of reaction j [mol/l/s].

The reaction system defined in the previous section, can be solved straightforward by combining species and rate expressions, as proposed in Clement (1997). This approach may cause numerical problems, as concentrations of the various species range across several orders of magnitude. Extremely low concentrations (e.g. Fe^{3+} or H^+) may cause problems of numerical accuracy. Thus, the reaction system was solved for total component concentrations rather than species concentrations, following approaches presented in Lichtner (1996): The chemical species are first split into primary and secondary components (=species), so that secondary components can be defined by a combination of primary components (e.g. the secondary components HCO_3^- , H_2CO_3 , CO_3^{2-} , H^+ as a combination of the primary components H and CO_3). Then the reaction system can be rewritten as canonical matrix. This yields a set of total concentrations of the primary components, which is defined as the sum of the primary components over all secondary components multiplied with their stoichiometric factor. Total component concentrations can be subdivided into mobile and immobile component concentrations, which are defined as sum over all aqueous and mineral species concentrations. The mobile component concentrations are only affected by reactions among primary components and thus simplify the overall reaction rate expressions considerably. Finally, for each primary component a total reaction rate r_c is obtained, which is returned to the transport model. The formal delineation of the total reaction rates for each component is given in appendix C. This approach allows the implementation of equilibrium reactions into the reaction system. Using the specific laws of mass action, species concentrations and pH can be resolved from total component concentrations.

3.3.2.2 Temperature dependency

Reaction rates tend to increase with increasing temperature. This relation can be described by the law of Arrhenius, which is based on the laws of thermodynamics or specific empirical relations of temperature dependency. In the case of biochemical reactions, the empirical Van t'Hoff equation can be applied according to the equation

$$k_{\text{eff}} = k^0 \cdot 2.1 \cdot e^{25-T}$$

with k_{eff} = effective rate constant [1/s], k^0 = standard rate constant [1/s], T = Temperature [$^{\circ}\text{C}$].

Roughly spoken, Van t'Hoff's equation states an increase in reaction rates by a factor of 2 for an increase in temperature by 10° . The Van't Hoff equation was implemented into the model in order to define temperature relationship. The RT3D transport model does not simulate heat transport. Thus, the groundwater temperature has to be considered constant during each simulation run. For long term simulations or deep groundwater bodies, the assumption of constant temperatures may be sufficient, annual temperature cycles in shallow groundwater, however, can not be resolved by the model. Thus, a simple temperature function can be considered as sufficient to compare the behaviour of simulation runs at different temperatures.

3.3.2.3 Mineral update

If mineral phases are involved in chemical reactions, reaction rates also depend on the reactive surface area and the state of crystallisation. With ongoing reactions, poorly crystallised parts are consumed first, leading to a relative increase in well crystallized and less reactive parts.

The consequence of mineral consumption is a decrease in reaction rates. This effect is considered for SOM and pyrite, using an update-function (Mayer, 2000) according to the equation:

$$k_{\text{eff}} = k_0 \cdot \left(\frac{\varphi}{\varphi_0} \right)^{\frac{2}{3}} = k_0 \cdot \left(\frac{C}{C_0} \right)^{\frac{2}{3}}$$

with k_{eff} = effective rate constant [$\text{mol l}^{-1} \text{s}^{-1}$], k_0 = specific rate constant [$\text{mol l}^{-1} \text{s}^{-1}$], φ = mineral volume fraction [m^3 mineral / m^3 soil], φ_0 = initial mineral volume fraction [m^3 mineral / m^3 soil], C = mineral concentration [mg/l^3 solution], C_0 = initial mineral concentration [mg/l^3 solution].

3.3.2.4 Implementation of equilibrium reactions – calcite dissolution and pH

Calcite dissolution and carbonate reactions are defined as equilibrium reactions. In order to calculate carbonate dissolution pH and carbonate species concentrations have to be calculated from the total H- and CO₃-concentrations. Starting from the mobile component concentrations for H and CO₃, which are defined as sum over all secondary species of H and CO₃, species concentrations are substituted by the corresponding equilibrium expressions. Rearranging the equations for CO₃ yields two equations for CO₃, f₁(H⁺) and f₂(H⁺), which depend on the concentration of H⁺ only. The equations are set equal and rearranged for H⁺, providing a quadratic function which is solved by an iterative algorithm. Ion activities are approximated using the Debye-Hückel-equation. The approximated activities are then used for an iterative calculation of pH. See appendix C for detailed calculations. It was found that the iterative solution algorithm was considerably time-consuming, which made it impossible to run this reaction-module even for field scale problems. Thus, the calculation of pH and carbonate species concentrations was included in a developer's version of the reaction-module only and omitted in the working versions of the reaction-module. As the rate expressions used in the reaction-module do not contain feedbacks to pH and carbonate species, this simplification has no effect on the behaviour of the reaction system.

3.3.2.5 SOM release control function

The SOM release control function defines the transfer rate of organic matter from the SOM-pool to the rOM-pool using the equation

$$R^4 = k_0^4 \cdot (rOM_{MAX} - [rOM]) \cdot [SOM]$$

R^4 = reaction rate [mol/l/s], k_0^4 = effective rate constant [mol⁻¹ l¹ s⁻¹], rOM_{MAX} = threshold concentration [mg/l].

The first multiplier ($rOM_{MAX} - [rOM]$) defines a concentration dependent transfer rate until a maximum concentration rOM_{MAX} is reached, where the transfer rate becomes zero. This term prevents a constant transfer of organic matter leading to a constantly growing rOM-pool. The second multiplier $[SOM]$ implements a first-order dependency of the transfer rate to the SOM-pool (see also Table 5). This approach allows to consider a wide range of organic matter contents ranging from histic soils (>20 Mass-% OM) to virtually OM free sediments (<0.1 Mass-%), assuming enhanced availability of organic matter, if the SOM-pool increases. A similar formulation can be found in the PHT3D database (Prommer, 2002).

3.3.2.6 Rate expressions

The general form of a kinetic rate expression can be written utilising mixed order terms, Monod-terms and inhibition terms, as in the equation

$$R_j = k_{eff}^j \cdot \prod_{i=1}^m (C_i)^{a_i} \cdot \prod_{i=1}^m \left(\frac{C_i}{K_i + C_i} \right)^{b_i} \cdot \prod_{i=1}^m \left(\frac{I_i}{I_i + C_i} \right)^{c_i}$$

with R_j = Reaction rate for reaction j [Mol l⁻¹ s⁻¹], k_{eff}^j = rate constant for reaction j [Mol l⁻¹ s⁻¹], C_i = Concentration of component i [Mol l⁻¹], M_i = Half rate constant [Mol l⁻¹], I_i = Inhibition constant [Mol l⁻¹], T_i = Threshold constant [Mol l⁻¹], n = number of components

Mixed order reaction terms (**second product**) assume an exponential relation between the component concentration and reaction rate. Monod-type rate expressions (**third product**) assume a constant reaction rate (**reaction of zero-order**), if sufficient reactands are available. Significant limitation occurs if the concentrations of the reactands approach the half concentration values or fall below. The fourth product describes an inhibition term, which acts inversely to a Monod-term, reducing reaction rates with increasing concentration of the inhibiting species.

There is no general agreement about which kinetic expressions and parameters represent the specific reactions most accurately. For example, for simulating heterotrophic denitrification, Hunter et al. (1998) applied a first-order reaction kinetic, whereas Kinzelbach et al. (1991) and also MacQuarrie and Sudicky (2001) used Monod-type reaction kinetics.

The choice of a suitable rate expression to describe a chemical process is a difficult task. A mathematical model for chemical processes can be derived from laboratory studies on the one hand and from field observations on the other hand. Whereas laboratory data may not represent field processes adequately, field observations often are uncertain and ambiguous. Thus, the selection of the kinetic approaches is partly arbitrary and should be considered as a conceptualisation of reaction behaviour and species interactions rather than a chemical law. In many cases, a rate expression is chosen in advance and then fitted to the observed data. For example, Böttcher et al. (1989) describe autotrophic denitrification by fitting observed nitrate concentrations to a first-order rate expression (Figure 6). However, the same data would also justify the application of a zero-order rate expression (Figure 7).

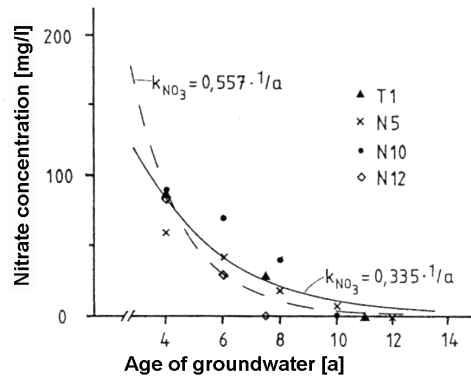


Figure 6: First-order rate expression adapted to observed Nitrate concentration vs. groundwater age, taken from Böttcher et al. (1989).

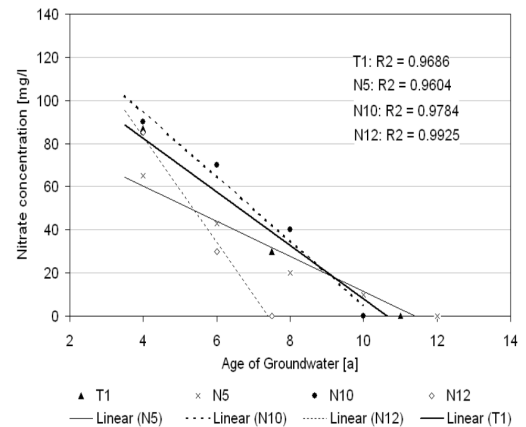


Figure 7: Adaption of a zero-order rate expression (linear regression) to the data from Figure 6.

Two separate reaction-modules were developed. The first one (A) was entirely based on Monod-type rate expressions, whereas in the second module (B), the slow reactions (degradation of organic matter and pyrite oxidation) were described by first-order rate expressions.

For the reaction-module A, Monod-type rate expressions were used for all rate expressions according to the equation:

$$R_j = k_{eff}^j \cdot \prod_{i=1}^n \frac{C_i}{M_i + C_i} \cdot \prod_{i=1}^n \frac{I_i}{I_i + C_i} \cdot \prod_{i=1}^n \left(\frac{C_i}{T_i + C_i} \right)^2$$

with R_j = Reaction rate of reaction j , [$\text{Mol l}^{-1} \text{s}^{-1}$], k_{eff}^j = rate constant for reaction j [$\text{Mol l}^{-1} \text{s}^{-1}$], C_i = Concentration of component i [Mol l^{-1}], M_i = Half rate constant [Mol l^{-1}], I_i = Inhibition constant [Mol l^{-1}], T_i = Threshold constant [Mol l^{-1}], n = number of components.

The Monod-expression approximates a constant reaction rate above a limiting concentration (half concentration) and a decrease in reaction rates if reactand concentrations approach the Half-concentration or fall below. A threshold term (4th product) was applied to each reactand. Threshold terms have no chemical meaning, but are used to reduce reaction rates to zero and stop the reaction if one of the reactands becomes depleted. If not applied, the full reaction rate is applied to concentrations of zero, resulting in negative concentration values and numerical errors. The single rate expressions for the individual chemical reactions are defined in Table 3.

Table 3: Rate expressions used in reaction-module A (indizes correspond to the chemical reactions defined in Table 2).

$$\begin{aligned}
 R_1 &= k_{eff}^1 \cdot \frac{[DOM]}{K_m^1 + [DOM]} \cdot \frac{[O_2]}{K_m^2 + [O_2]} \cdot \left(\frac{[DOM]}{T + [DOM]} \right)^2 \cdot \left(\frac{[O_2]}{T + [O_2]} \right)^2 \\
 R_2 &= k_{eff}^2 \cdot \frac{[DOM]}{K_m^1 + [DOM]} \cdot \frac{[NO_3^-]}{K_m^3 + [NO_3^-]} \cdot \frac{I_2}{I_2 + [O_2]} \cdot \left(\frac{[DOM]}{T + [DOM]} \right)^2 \cdot \left(\frac{[NO_3^-]}{T + [NO_3^-]} \right)^2 \\
 R_3 &= k_{eff}^3 \cdot \frac{[DOM]}{K_m^1 + [DOM]} \cdot \frac{[SO_4^{2-}]}{K_m^3 + [SO_4^{2-}]} \cdot \frac{I_2}{I_2 + [O_2]} \cdot \frac{I_2}{I_2 + [NO_3^-]} \cdot \left(\frac{[DOM]}{T + [DOM]} \right)^2 \cdot \left(\frac{[NO_3^-]}{T + [NO_3^-]} \right)^2 \\
 R_4 &= k_{eff}^4 \cdot ([rOM]_{max} - [rOM]) \cdot [SOM] \\
 R_5 &= k_{eff}^5 \cdot [O_2] \cdot \left(\frac{[O_2]}{T + [O_2]} \right)^2 \cdot \left(\frac{[FeS_2]}{T + [FeS_2]} \right)^2 \\
 R_6 &= k_{eff}^6 \cdot \frac{[NO_3^-]}{K_m^3 + [NO_3^-]} \cdot \frac{I_2}{I_2 + [O_2]} \cdot \left(\frac{[NO_3^-]}{T + [NO_3^-]} \right)^2 \cdot \left(\frac{[FeS_2]}{T + [FeS_2]} \right)^2 \\
 R_7 &= k_{eff}^7 \cdot \frac{[Fe^{2+}]}{K_m^1 + [Fe^{2+}]} \cdot \frac{[O_2]}{K_m^2 + [O_2]} \cdot \left(\frac{[Fe^{2+}]}{T + [Fe^{2+}]} \right)^2 \cdot \left(\frac{[O_2]}{T + [O_2]} \right)^2 \\
 R_8 &= k_{eff}^8 \cdot \frac{[Fe^{2+}]}{K_m^1 + [Fe^{2+}]} \cdot \frac{[NO_3^-]}{K_m^2 + [NO_3^-]} \cdot \left(\frac{[Fe^{2+}]}{T + [Fe^{2+}]} \right)^2 \cdot \left(\frac{[NO_3^-]}{T + [NO_3^-]} \right)^2 \\
 R_9 &= k_{eff}^9 \cdot \frac{[NH_4^+]}{K_m^1 + [NH_4^+]} \cdot \frac{[O_2]}{K_m^2 + [O_2]} \cdot \left(\frac{[NH_4^+]}{T + [NH_4^+]} \right)^2 \cdot \left(\frac{[O_2]}{T + [O_2]} \right)^2
 \end{aligned}$$

In the reaction-module B, slow reactions (degradation of organic matter and pyrite oxidation) were implemented using first-order rate expressions. Table 4 gives an overview of rate expressions which were formulated as first-order rate expressions replacing the Monod-expressions of the first reaction-module. The other reactions were implemented as Monod-type rate expressions, as in reaction-module A. These expressions were directly parameterized from literature data and they can be considered as fast reactions, so that complete turnover within cell residence times can be assumed and an over- or underestimation of reaction rates will not affect the simulation results. Threshold terms were applied as in reaction-module A for all reactions.

Table 4: Rate expressions changed in reaction-module B (indizes correspond to numbers of chemical reactions defined in Table 2).

$$R_1 = k_{eff}^1 \cdot [DOM] \cdot [O_2] \cdot \left(\frac{[DOM]}{T + [DOM]} \right)^2 \cdot \left(\frac{[O_2]}{T + [O_2]} \right)^2$$

$$R_2 = k_{eff}^2 \cdot [DOM] \cdot [NO_3^-] \cdot \frac{I_2}{I_2 + [O_2]} \cdot \left(\frac{[DOM]}{T + [DOM]} \right)^2 \cdot \left(\frac{[NO_3^-]}{T + [NO_3^-]} \right)^2$$

$$R_3 = k_{eff}^3 \cdot [DOM] \cdot [SO_4^{2-}] \cdot \frac{I_2}{I_2 + [O_2]} \cdot \frac{I_2}{I_2 + [NO_3^-]} \cdot \left(\frac{[DOM]}{T + [DOM]} \right)^2 \cdot \left(\frac{[NO_3^-]}{T + [NO_3^-]} \right)^2$$

$$R_5 = k_{eff}^5 \cdot [O_2] \cdot \left(\frac{[O_2]}{T + [O_2]} \right)^2$$

$$R_6 = k_{eff}^6 \cdot [NO_3^-] \cdot \frac{I_2}{I_2 + [O_2]} \cdot \left(\frac{[NO_3^-]}{T + [NO_3^-]} \right)^2 \cdot \left(\frac{[FeS_2]}{T + [FeS_2]} \right)^2$$

3.3.3 Run-scheme of the reaction-module

RT3D provides a template code for a user-defined reaction-module. This template is written in Fortran and defines the interface between RT3D and the reaction system. The code is completed by the addition of all reaction parameters and equations and can be addressed by RT3D after compilation into a dynamic link library (DLL).

In groundwater models, concentrations are usually given in mg/l. However, for chemical calculations the use of moles/l is more convenient, as stoichiometric relations can directly be taken from the reaction equations. Therefore, all calculations of the reaction-modules are based on moles/l and the concentrations are converted from mg/l to mol/l and back before and after reaction calculations. All internal reaction parameters are defined in a data module. Seven parameters can be defined as external parameters which are given to the reaction-module via the model's input files. These parameters are: three rate constants for the oxidation of organic matter by oxygen, nitrate and sulfate, the release rate of OM from the SOM-Pool, the maximum OM-concentration controlling SOM-release, the rate constants for the oxidation of pyrite by nitrogen, and temperature. Then the reaction rates are calculated and subsequently the component reaction rates, as the sum over all reaction rates weighed by the stoichiometric coefficient for the component under consideration. If calcite dissolution is to be included into the reaction-module, ion activities, carbonate species concentrations and pH have to be calculated before the reaction rates. A run scheme of the reaction-module is given in Figure 8.

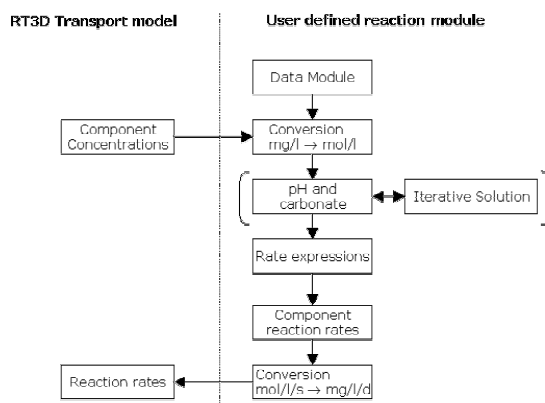


Figure 8: Run scheme of the RT3D reaction-module

3.3.4 Parameterisation of the reaction-module

Rate expressions determine a stoichiometric dependency of reactands and introduce a time dependency of the process. However, in spatially distributed modelling, they do not identify a chemical process, but describe a phenomenological behaviour. If a reaction is fast with respect to the residence time within the cell, i.e. if complete turnover can be expected within the residence time, the choice of the rate expression and its parameterisation is arbitrary, as long as this observed behaviour is maintained. The chemical process itself can not be resolved by the model in this case. For slow reactions, however, rate expressions and parameters have to be chosen carefully.

Reaction parameters were derived as follows: A first-order rate constant for autotrophic denitrification was determined by Böttcher et al. (1989), using data of nitrate concentrations vs. groundwater age. The observed half life times ranged between 1.1-3.4 years. A half life of 2 years was assumed for the first-order approach (Reaction-module B), the rate constant used in the Monod approach of reaction-module A was derived by fitting a linear function to the data given by Böttcher et al. (1989), see also chapter 3.3.2.6. For desulfurication, Böttcher et al. (1989) derived a first-order rate expression with half-life times between 76-100 years. In this case, the Monod rate expression was defined as linear decay between a sulphate concentration of 100 mg/l at $t=0$ and the resulting concentration at $t=50$ years, assuming a half-life of 100 years. The degradation of organic matter by nitrate was parameterized according to the results of the tracer experiment simulation (see chapter 5.2). No data was available to determine the degradation of organic matter by oxygen. It was assumed that the degradation by oxygen was slightly faster than the degradation by nitrate. In the case of oxygen inhibiting denitrification reactions, different threshold concentrations are reported in literature (e.g. Wendland and Kunkel (1999)), ranging between 5 and 0 mg/l. No values were found given for the inhibition of desulfurication by nitrate. It was assumed that a depletion of the inhibitor is necessary to allow for full turnover rates. For oxygen, the inhibition constant was set to 0.2 mg O_2 /l. The inhibition effect then declines for oxygen concentrations between 2 and 0.02 mg/l (at 0.2 mg/l, turnover rate = 0.5 maximum turnover rate). The nitrate inhibition constant was set to 0.1 mg NO_3^- /l, with a decreasing inhibition effect in the range of 1 - 0.01 mg/l. All other reaction parameters were taken from literature data and databases of the geochemical codes Min3P and PHREEQC. A summary of the reaction parameters used as default values is given in Table 5. The reaction parameters were converted from different notations and units, thus the given values may not be identical to the values reported in literature. Threshold constants were set to $1.0e-7$ mol/l as default. The absolute value of the threshold constant is not of interest for the reactions, as long as the order of magnitude is well below the concentration range of interest.

Table 5: Default parameter set of the reaction-module

	Parameter	Reaction module A	Reaction module B	Reference A [B]
A. Mineralisation of dissolved organic matter				
1	K_{eff}^1	4.0e-9	1.92e-1	1) [10)]
	M_{Dom}	3.35e-5 (=1mg/l)	[-]	1)
	M_{O_2}	3.125e-5 (=0.1 mg/l)	[-]	1)
2	K_{eff}^2	3.0e-9	1.12e-1	9) [10)]
	M_{Dom}	3.35e-5	[-]	1)
	M_{NO_3}	8e-5 (=0.1 mg/l)	[-]	1)
	I_{O_2}	6.25e-6 (=0.2 mg/l)	6.25e-6	1)
3	K_{eff}^3	4.56e-13	2.64e-6	10) [4)]
	M_{Dom}	3.35e-5	[-]	1)
	M_{SO_4}	3.0e-4 (=30mg/l)	[-]	10)
	I_{NO_3}	1.6e-5 (=0.1 mg/l)	1.6e-5	1)
B. Transfer of SOM to rOM				
4	K_{eff}^4	6.0e-9		7)
	DOM_{max}	0.00067 (=20 mg/l)		7)
C. Oxidation of Pyrite (FeS₂)				
5	K_{eff}^5	10e-5.3		6)
	RSA	2.69e-1 [m ² /I _{bulk}]		6)
6	K_{eff}^6	1.8e-12	3.925e-12	10) [4)]
	M_{NO_3}	8e-5	-	1)
	I_{O_2}	6.25e-6 (=0.2 mg/l)	6.25e-6	1)
D. Oxidation of Fe²⁺ by O₂ and NO₃⁻				
7	K_{eff}^7	5e-9		5)
	M_{Fe}	1e-5		8)
	M_{O_2}	3.125e-5		8)
8	K_{eff}^8	5e-9		5)
	M_{Fe}	1e-5		8)
	M_{NO_3}	8e-5		8)
	I_{O_2}	3.125e-6 (=0.1 mg/l)		1)
E. Nitrification				
9	K_{eff}^9	1.16e-5		3)
	M_{NH_4}	6.25e-6 (=0.1 mg/l)		3)
	M_{O_2}	3.125e-6 (=0.1mg/l)		3)
1) estimated; 2) Sigg and Stumm (1996); 3) MacQuarrie and Sudicky (2001); 4) based on Böttcher et al. (1989), Frind et al. (1990); 5) Hunter et al. (1998); 6) Kamei and Ohmoto (2000); 7) PHT3D/PHREEQC database (Prommer, 2002; Parkhurst and Appelo, 1999); 8) Min3P database (Mayer, 2000); 9) calibrated to tracer experiment 10) fitted to corresponding first-order or Monod approach				

3.3.5 Algorithm verification

The RT3D reaction-module was tested against an analogous formulation of the reaction system within the Min3P code (Mayer, 2000) in order to assess the accuracy of the mathematical formulations.

“The Min3P code is a multicomponent reactive transport model for variably saturated porous media in one, two or three spatial dimensions. Advective-dispersive transport in the aqueous phase as well as diffusive gas transport can be considered. Darcy velocities are calculated internally, using a variably saturated flow module. The model formulation is based on the global implicit solution approach (...), which considers reaction and transport processes simultaneously” (Mayer, 2000). RT3D, in contrast, is based on an operator-split strategy, where transport and reaction equations are solved in separate steps. As identical rate expressions were applied in both models, simulated turnover rates should be identical in both models.

A simple batch reaction problem was developed using identical sets of initial conditions (Table 6) and reaction parameters (default set) for both models. In the batch reaction problem the oxidation of organic matter by oxygen and nitrate was considered as well as the dissolution of calcite and carbonate equilibria.

Table 6: Initial component concentrations of the batch reaction problem [mg/l_{soil solution}]

H	O ₂	NO ₃	NH ₄	N ₂	SO ₄	HS	Fe	Ca	CO ₃	DOM	SOM	FeS ₂	Fe(OH) ₃	CaCO ₃
7	5	10	0	0	150	0	0	220	330	5	5000	0	5000	50000

It was found that all rate-limited reactions behaved identical in both models and thus proved a correct mathematical formulation (Figure 9). Deviations were found for total H, Ca and CO₃-concentrations, where concentration vs. time curves showed identical behaviour, but differed in a certain offset (Figure 10). This can be referred to different handling of ion activities, as the Min3P code allows a complex calculation of ion activities, whereas the RT3D reaction-module implements a straightforward, non-iterative calculation scheme. The identical behaviour proves an appropriate formulation of the problem. It was found that the solution of the equilibrium reactions increased calculation times considerably. As no feedbacks between pH and rate-limited reactions were considered in the reaction-module, the calculation of pH and carbonate species concentrations was omitted in the working version of the reaction-module.

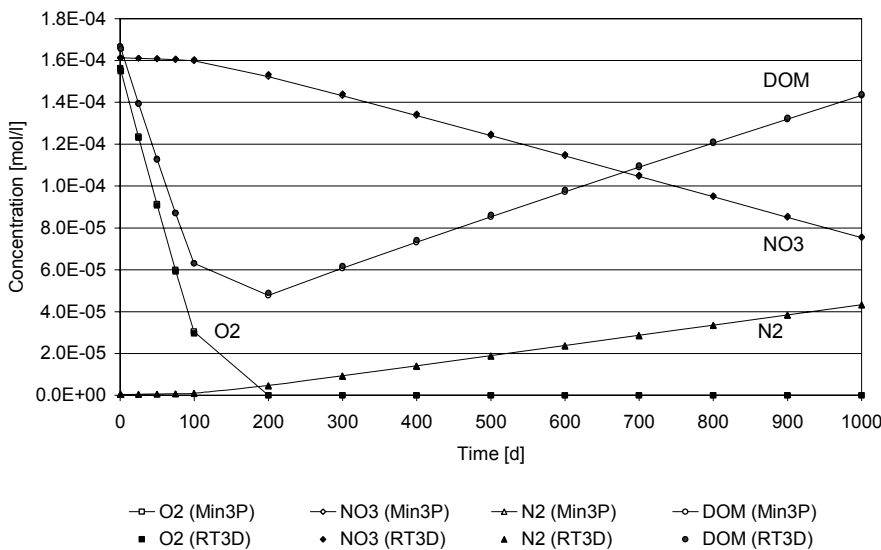


Figure 9: Concentrations vs. time for selected components calculated with the RT3D reaction-module and Min3P in batch mode.

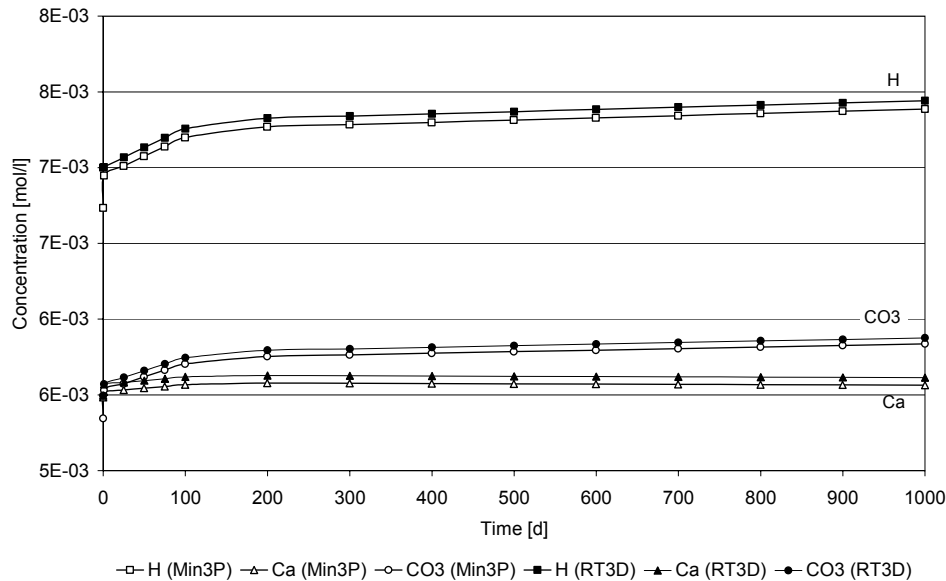


Figure 10: Concentrations vs. time for H, Ca and CO₃ calculated with the RT3D reaction-module and Min3P in batch mode.

3.3.6 Effect of cell-size on the behaviour of rate expressions

3.3.6.1 Introduction

In transport modelling, substance concentrations are always defined as mean cell concentrations. As a consequence, concentration gradients on a sub-cell scale can not be resolved. Advective mass fluxes applied via point sources or areal sources (e.g. groundwater recharge) are artificially diluted over the total cell-size, if the input flux of water is smaller than the cell volume. This effect causes a numerical spreading of solutes within the model domain, also known as numerical dispersion. This effect can be treated to some extent by using appropriate grid discretisation and transport algorithms. However, dispersion free transport algorithms as the Method of Characteristics (MOC) are not recommended for reactive transport simulations, as they are not entirely mass conserving (Chiang et al., 2002). In this study nitrate, oxygen and rOM are typical solutes transported to the groundwater domain by recharge water. Recharge fluxes of approximately 0.1m (100mm) are opposed by a vertical cell dimension of a few metres (and a horizontal discretisation of deka-metres). Thus, the recharge volume is only a small fraction of the cell volume, and a considerable artificial dilution has to be taken into account.

This artificial dilution poses a problem for reactive transport modelling, as zero-order, first-order and Monod-reactions implement different feedbacks on solute concentrations. Thus a response of turnover rates to cell-size and artificial dilution has to be expected, which may lead to different mass balances when using the same parameter sets for different grid resolutions. Therefore, it is generally considered good practice to test groundwater models with different cell-sizes and to analyze the effect of model discretisation, numerical dispersion and stability. In this study, the problem of cell-size and reactive transport modelling is looked at from a theoretical point of view: The effect of grid resolution on a simple one-dimensional reactive transport problem is examined for a zero-order, first-order and Monod-type rate expression, for a stand-alone Monod-half term and for an inhibition term, which is commonly used to describe sequential reaction schemes.

3.3.6.2 General considerations

A transport column for one dimensional transport is discretized in m volumes V_n . Transport is simulated by shifting cell contents from one cell to another. A mass load M_0 is applied to the first cell at $t=0$ and transported through the column (Figure 11).



Figure 11: One-dimensional transport problem

Different discretisation scenarios (index n) of the transport column are considered. The finest discretisation is denoted with the index 0. For each scenario, the cell volume V_n is a multiple of the elementary volume V_0 :

$$V_n = k \cdot V_0, \text{ with } V_n = \text{cell volume, } V_0 = \text{volume of elementary cell, } k = \text{scaling factor.}$$

The total model domain consists of i Volumes V_0 according to the equation

$$V^T = \sum_{j=1}^i V_n^j = i \cdot V_0, \text{ with } V^T = \text{total volume, } i = \text{number of elementary volumes, } k = \text{scaling factor, } i/k = \text{number of volumes.}$$

For each scenario n , the number of volumes i and of associated transport steps m is given by

$$m = \frac{i}{k}$$

Δt_0 is the time step after which cells are shifted through the column in Scenario 0. The total transport time T is given by the equation

$$T = i \cdot \Delta t_0$$

The transport step size Δt_n of each scenario n depends on the discretisation of the transport column and can be written as a multiple of Δt_0 as in the equation

$$\Delta t_n = k \cdot \Delta t_0$$

The same initial mass load M_0 is applied to the first cell volume in all discretisation scenarios. The resulting initial concentration C_n^0 of the first volume is given by the equation

$$C_n^0 = \frac{M_0}{V_n} = \frac{M_0}{k \cdot V_0} = C_0^0 \cdot \frac{1}{k}$$

These considerations are exemplified in Figure 12:

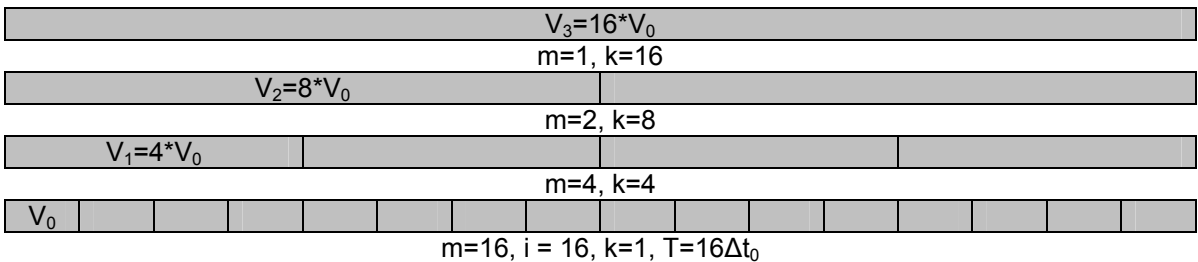


Figure 12: Example of a one dimensional model domain with different discretisations

3.3.6.3 Behaviour of a first-order reaction term

Considering a discretisation scenario n with m transport shifts, the final concentration at the outlet of the column can be calculated as follows:

$$\text{First transport step: } C'_n = C_n^0 \cdot e^{-r\Delta t_n} = C_n^0 \cdot e^{-rk\Delta t_0},$$

$$\text{Second transport step: } C'_n = \left(C_n^0 \cdot e^{-rk\Delta t_0}\right) \cdot e^{-rk\Delta t_0},$$

$$\text{m-th transport step: } C'_n = C_n^0 \cdot \left(e^{-rk\Delta t_0}\right)^m.$$

The final concentration at the end of the transport simulation can be written as in the equation

$$C'_n = C_n^0 \cdot \left(e^{-rk\Delta t_0}\right)^i = C_n^0 \cdot e^{-ri\Delta t_0} = C_n^0 \cdot e^{-rT} = C_0^0 \cdot \frac{1}{k} \cdot e^{-rT}$$

The resulting total substance mass is given by the equation

$$M'_n = C'_n \cdot V_n = C_n^0 \cdot e^{-rT} \cdot V_n = \frac{M_0}{V_n} \cdot e^{-rT} \cdot V_n = M_0 \cdot e^{-rT}$$

Both, final concentration and mass are independent of i or k and thus independent of specific grid settings. The change of mass follows the same law as the change of concentration. Applying the same rate constant r on several grid resolutions will have no effect on the overall mass balance.

This is due to the fact, that turnover rates are decreased proportionally to the decrease in concentrations due to the artificial dilution effect.

3.3.6.4 Behaviour of a zero-order reaction term

For a zero-order reaction term (constant reaction rate), the final concentration at the end of the transport simulation can be derived analogously:

$$\text{First transport step: } C'_n = C_n^0 - r \cdot k \cdot \Delta t_0,$$

$$\text{Second transport step: } C'_n = \left(C_n^0 - r \cdot k \cdot \Delta t_0\right) - r \cdot k \cdot \Delta t_0,$$

$$\text{m-th transport step: } C'_n = C_n^0 - m \cdot r \cdot k \cdot \Delta t_0.$$

This leads to the general equation

$$C'_n = C_n^0 - \frac{i}{k} \cdot (r \cdot k \cdot \Delta t_0) = C_n^0 - r \cdot i \cdot \Delta t_0 = C_n^0 - r \cdot T = C_0^0 \cdot \frac{1}{k} - r \cdot T$$

$$\text{with } \lim_{k \rightarrow \infty} (C'_n) = \lim_{k \rightarrow \infty} \left(C_n^0 \cdot \frac{1}{k} - r \cdot T \right) = -rT \text{ and } \Delta C = rT = \text{const}.$$

The resulting total substance mass at the end of the transport is given by

$$M'_n = C'_n \cdot V_n = \left(C_n^0 - r \cdot T\right) \cdot V_n = C_n^0 \cdot V_n - r \cdot T \cdot V_n = M_0 - r \cdot T \cdot V_n = M_0 - r \cdot T \cdot k \cdot V_0$$

$$\text{with } \lim_{k \rightarrow \infty} (M'_n) = \lim_{k \rightarrow \infty} (M_0 - r \cdot T \cdot k \cdot V_0) = -\infty \text{ and } \lim_{k \rightarrow \infty} (\Delta M) = \lim_{k \rightarrow \infty} (r \cdot T \cdot k \cdot V) = \infty.$$

Different laws apply to the change of mass and the change of concentration. If the same reaction rate r was applied to transport problems of increasing grid resolutions, the same concentration

change dC/dt would apply to a larger cell volume with a lower cell concentration and an increased residence time, compared to the finer grid resolution. Consequently, the total mass change increases with grid size as well. The mass change depends on the factor k and thus the relative change in grid size.

3.3.6.5 Behaviour of a Monod reaction term

With concentrations far above the half-concentration value, a Monod reaction term approaches a zero-order and thus comparable behaviour could be expected.

As before, the resulting concentration applying a Monod type equation can be derived as in the following equations

$$\text{First transport step: } C_n^1 = C_n^0 - r \cdot \frac{C_n^0}{H + C_n^0} \cdot k \cdot \Delta t_0$$

$$\text{Second transport step: } C_n^2 = C_n^1 - r \cdot \frac{C_n^1}{H + C_n^1} \cdot k \cdot \Delta t_0$$

which can be rearranged by substituting C_n^1 to

$$C_n^2 = \left(C_n^0 - r \cdot \frac{C_n^0}{H + C_n^0} \cdot k \cdot \Delta t_0 \right) \cdot \left(1 - \frac{r \cdot k \cdot \Delta t_0}{H + C_n^0 - r \cdot \frac{C_n^0}{H + C_n^0} \cdot k \cdot \Delta t_0} \right)$$

$$\text{m-th transport step: } C_n^m = C_n^{m-1} - r \cdot \frac{C_n^{m-1}}{H + C_n^{m-1}} \cdot k \cdot \Delta t_0.$$

This example is examined on a one-cell domain with a single transport step and on a two-cell domain with two transport steps, resulting from splitting cells of the one-cell domain..

For the one-cell domain, ($k=1$, $dt=T$) the final concentration is given by the equation

$$C_1' = C_1^0 - r \cdot \frac{C_1^0}{H + C_1^0} \cdot T$$

For the two-cell domain ($k=0.5$ and $dt=T/2=kT$) the final concentration is given according to the equation

$$C_2' = \left(C_1^0 \cdot \frac{1}{k} - r \cdot \frac{C_1^0 \cdot \frac{1}{k}}{H + C_1^0 \cdot \frac{1}{k}} \cdot k \cdot T \right) \cdot \left(1 - \frac{r \cdot k \cdot T}{H + C_1^0 \cdot \frac{1}{k} - r \cdot \frac{C_1^0 \cdot \frac{1}{k}}{H + C_1^0 \cdot \frac{1}{k}} \cdot k \cdot T} \right)$$

$$C'_2 = \left(C_1^0 \cdot \frac{1}{k} - r \cdot \frac{C_1^0}{H + C_1^0 \cdot \frac{1}{k}} \cdot T \right) \cdot \left(1 - \frac{r \cdot k \cdot T}{H + C_1^0 \cdot \frac{1}{k} - r \cdot \frac{C_1^0}{H + C_1^0 \cdot \frac{1}{k}} \cdot T} \right)$$

$$C'_m = \left(C_1^0 \cdot \frac{1}{k} - r \cdot \frac{C_1^0}{H + C_1^0 \cdot \frac{1}{k}} \cdot T \right) \cdot \left(1 - \frac{r \cdot k \cdot T}{H + C_1^0 \cdot \frac{1}{k} - r \cdot \frac{C_1^0}{H + C_1^0 \cdot \frac{1}{k}} \cdot T} \dots \right)$$

And the resulting mass is given by the equation

$$M'_1 = C'_1 \cdot V_1 = M_1^0 - r \cdot \frac{C_1^0}{H + C_1^0} \cdot T \cdot V_1 = M_1^0 - r \cdot \frac{M_1^0}{H + C_1^0} \cdot T$$

$$M'_2 = C'_2 \cdot k \cdot V_1 = \left(C_1^0 \cdot \frac{1}{k} - r \cdot \frac{C_1^0}{H + C_1^0 \cdot \frac{1}{k}} \cdot T \right) \cdot \left(1 - \frac{r \cdot k \cdot T}{H + C_1^0 \cdot \frac{1}{k} - r \cdot \frac{C_1^0}{H + C_1^0 \cdot \frac{1}{k}} \cdot T} \right) \cdot k \cdot V_1$$

$$M'_2 = \left(M_1^0 - r \cdot \frac{M_1^0}{H + C_1^0 \cdot \frac{1}{k}} \cdot k \cdot T \right) \cdot \left(1 - \frac{r \cdot k \cdot T}{H + C_1^0 \cdot \frac{1}{k} - r \cdot \frac{C_1^0}{H + C_1^0 \cdot \frac{1}{k}} \cdot T} \right)$$

with $M'_2 \neq M'_1$

Again, the change of mass and the change of concentration are not identical for the one-cell and two cell model domain.

3.3.6.6 Behaviour of the Monod-half term

Considering only the half concentration term for different cell-sizes yields the following expressions for increasing cell-size (=increased k-value)

$$k = 1 \left(\frac{C_0 \cdot \frac{1}{k}}{H + C_0 \cdot \frac{1}{k}} \right) = \frac{C_0}{H + C_0} \quad , \quad k = 10 \left(\frac{C_0 \cdot \frac{1}{10}}{H + C_0 \cdot \frac{1}{10}} \right) = \frac{0.1 \cdot C_0}{H + 0.1 \cdot C_0} < \frac{C_0}{H + C_0} \quad \text{and}$$

$$\lim_{k \rightarrow \infty} \left(\frac{C_0 \cdot \frac{1}{k}}{H + C_0 \cdot \frac{1}{k}} \right) = 0$$

$$\lim_{k \rightarrow 0} \left(\frac{C_0 \cdot \frac{1}{k}}{H + C_0 \cdot \frac{1}{k}} \right) = 1$$

For decreasing cell-size, the half-term approaches

It can be concluded that enlarging the grid cell-size will cause a reduction of reaction rates, applying a half concentration (Monod-) term, as cell concentrations are decreased due to artificial dilution. This effect is comparable to increasing the half concentration constant.

3.3.6.7 Behaviour of the inhibition term

The general inhibition term can be written as $\frac{I}{I + C_n} = \frac{I}{I + \frac{M_0}{k \cdot V_0}} = \frac{I}{I + C_0 \cdot \frac{1}{k}}$

Increasing grid size (increasing k-factor) leads to a relative decrease in inhibition as shown in the following equations:

$$k = 1 \rightarrow \frac{I}{I + C_0 \cdot \frac{1}{k}} = \frac{I}{I + C_0} \quad , \quad k = 10 \rightarrow \frac{I}{I + C_0 \cdot \frac{1}{k}} = \frac{I}{I + 0.1 \cdot C_0} \quad \text{and}$$

$$\lim_{k \rightarrow \infty} \left(\frac{I}{I + C_0 \cdot \frac{1}{k}} \right) = 1$$

Inhibition will decrease with enlarging cell-size, if the inhibition species is not ubiquitous but applied by a point or areal source. This effect may be negligible if concentration gradients are not resolved by grid size.

3.3.6.8 Discussion

These considerations for a one dimensional transport problem show that grid discretisation has an effect on reactive transport.

- First-order rate expressions maintain the mass balance with changing grid size and reaction parameters can therefore be applied under varying grid sizes. If the cell-size is enlarged and the resulting concentration is decreased, the reaction rate decreases proportionally.
- Using a zero-order term, mass turnover rates are over-estimated with enlarged cell-size. Finally, the system would approach an instantaneous stoichiometric turnover. However, this overestimation reduces solute concentrations effectively and limits the distribution of solute mass due to numerical dispersion.
- The behaviour of Monod-expressions is more complex and strongly depends on the setting of the half constants in relation to the given concentration ranges. As long as the reaction is in the range of unlimited turnover (\approx zero-order), a behaviour similar to zero-order expressions can be expected. The stand-alone half concentration term will increasingly reduce reaction rates until

no turnover takes place. This behaviour is equivalent to a relative increase in the half concentration constant.

- The effect of the inhibition term ceases with enlarging the cell-size. However, if cell-sizes become too large to resolve concentration gradients, sequential reactions take place simultaneously within a grid cell and an inhibition term is no longer meaningful. Therefore, this effect does not pose problems for transport simulations.

A straightforward approach to apply observed reaction rates with different cell-sizes and monod-type rate expressions, would be a scaling of reaction rates by a cell-size ratio. This requires the reaction rates to be related to a defined cell-size. However, this approach is only applicable for simple transport problems, as in two- or three dimensional model domains, the derivation of appropriate scaling factors requires consideration of irregular cell-sizes and orientation of flow vectors. Therefore, a scaling of reaction rates is not a feasible way to cope with a cell-size dependency of the behaviour of rate expressions.

The effect of cell-size on the behaviour of rate expressions only affects reaction rates, which means a modification of the temporal development of solute concentrations and masses. In short, a process will run faster or slower than defined by reaction parameters. The mass turnover is still defined by reaction stoichiometry and confined by the available amount of reaction partners.

Artificial dilution and cell-size-dependency of reaction rates can be neglected, if the reaction is a fast reaction. That means complete turnover takes place well within the average cell residence time and the reaction can be considered as instantaneous. These effects can also be neglected, if cell concentrations represent "real" concentrations. This is the case if the substances involved in the reactions, are ubiquitous (no artificial dilution, e.g. initial groundwater concentrations) or if input fluxes (e.g. recharge) lead to a complete exchange of water per transport step.

No general preference for a specific reaction approach is given. Dealing with small scale simulations, the choice of a reaction system more strongly depends on chemical considerations (a good process representation). On a regional scale, however, a phenomenological behaviour has to be simulated and the cell-size effect due to artificial dilution and increased numerical dispersion needs to be considered.

4 Materials and methods

4.1 Study area

The study area "Schaugraben catchment" is located SW of Osterburg/Altmark in the north of Saxony-Anhalt. The topographical catchment area has a size of app. 25 km² with a N-S extent of app. 8 km and an E-W extent of app. 6 km. The „Schaugraben“ is the central drain channel of the catchment, and discharges into the Uchte river close to Osterburg. The catchment area is framed by the Biese river to the North, the Uchte river to the East and the open drain Kleiner Markgraben to the West. Uchte and Biese unite at Osterburg (river stage 20.4 m NN). Approximately 40 km north of Osterburg, they discharge via the Aland river into the Elbe river (river stage 15 m NN). Uchte, Biese and Kleiner Markgraben define an extended study area, which is used as a basis for regional modelling studies (Figure 13).

Discharge values of the Schaugraben drain in the period of 1997 to 2002 were between 3.9 and 471 l/s, with a median discharge of 28.5 l/s. Observed annual runoff was 68 mm in 1998 and 117 mm in 2002. In the other years, measurements did not cover the complete years. Nitrate concentrations follow distinct seasonal cycles, ranging between 0 and 133 mg/l, with a mean concentration of 29 mg/l and a median concentration of 14 mg/l. For discharge, N-loads and concentrations see also appendix A.

The area was glaciated during the Warthe-stadial of the Saale-glaciation leading to a deposition of ground moraines. Concurrent and subsequent fluvio-glacial processes have led to formation of valleys and depressions and to deposition of fluvio-glacial sediments. The morphology is characterized by a mosaic of uplands (30-90 m a.s.l.) and lowlands (29-60 m a.s.l.). Glacial loam and till are dominating substrates in the uplands, whereas sandy fluvio-glacial deposits are dominating in the lower parts. Cover sands are widespread in the area. Soil types are determined by the distribution of sandy and loamy substrates on the one hand and the groundwater depth (between 1 and 6 m) on the other hand. Thus, at the higher locations, cambisols, luvisols, and podzoluvisols can be found, whereas at the lower positions gleysols and gleyic phaeozems are common. A soil map of the Schaugraben study area and extrapolated soil units for the extended study area is given in appendix A.

The geological situation can be characterized as follows, according to Jordan and Weder (1995) and GLA-SA (oral communications): The first aquifer is made up from glaciofluvial sands at the northern and eastern boundary of the area in the valleys of the rivers Biese and Uchte. It is unprotected and partly in contact with the second main aquifer. In the central plateau cover sands and glaciofluvial deposits form local unprotected aquifers. These upper aquifers have a thickness between 2 and 8 m. The most part of the study area is covered by glacial till of the Warthe-stadial, forming an aquitarde of sandy silt and loam. Aquifer thickness varies between 0 and 22 m. In the central part the till lies close to the surface, in the northern part the till extends below the first aquifer. Local hydrological contacts between upper and lower aquifers are possible. Considering the high heterogeneity of the till, its efficiency as an aquiclude or aquitarde is questionable. Below the till follows the main aquifer with a varying thickness of 10-40 m, which is present in the whole area. It is made up from glaciofluvial sands of different ages. The main aquifer is mostly protected. Below a sequence of sandy to clayey deposits can be found. According to Meissner (2000) conductivities of 17-34 m/d and an effective porosity of 10-15% are reported for the aquifer substrates (sand and gravel). Due to the low groundwater gradient, mean transport velocities of 0.1-0.5 m/d have to be expected.

The flow systems of the first and second aquifer are oriented to the rivers Biese and Uchte and to the central drain channels. Deep groundwater flow possibly follows the NE-direction to the Elbe-River. The area is not affected by infiltration water from the Elbe river during high river stages. A response of groundwater tables to the flood event in the Elbe river in August 2002 was not observed. However, groundwater stages were considerably high during that event due to excessive rainfall and corresponding rise of groundwater levels in June and July.

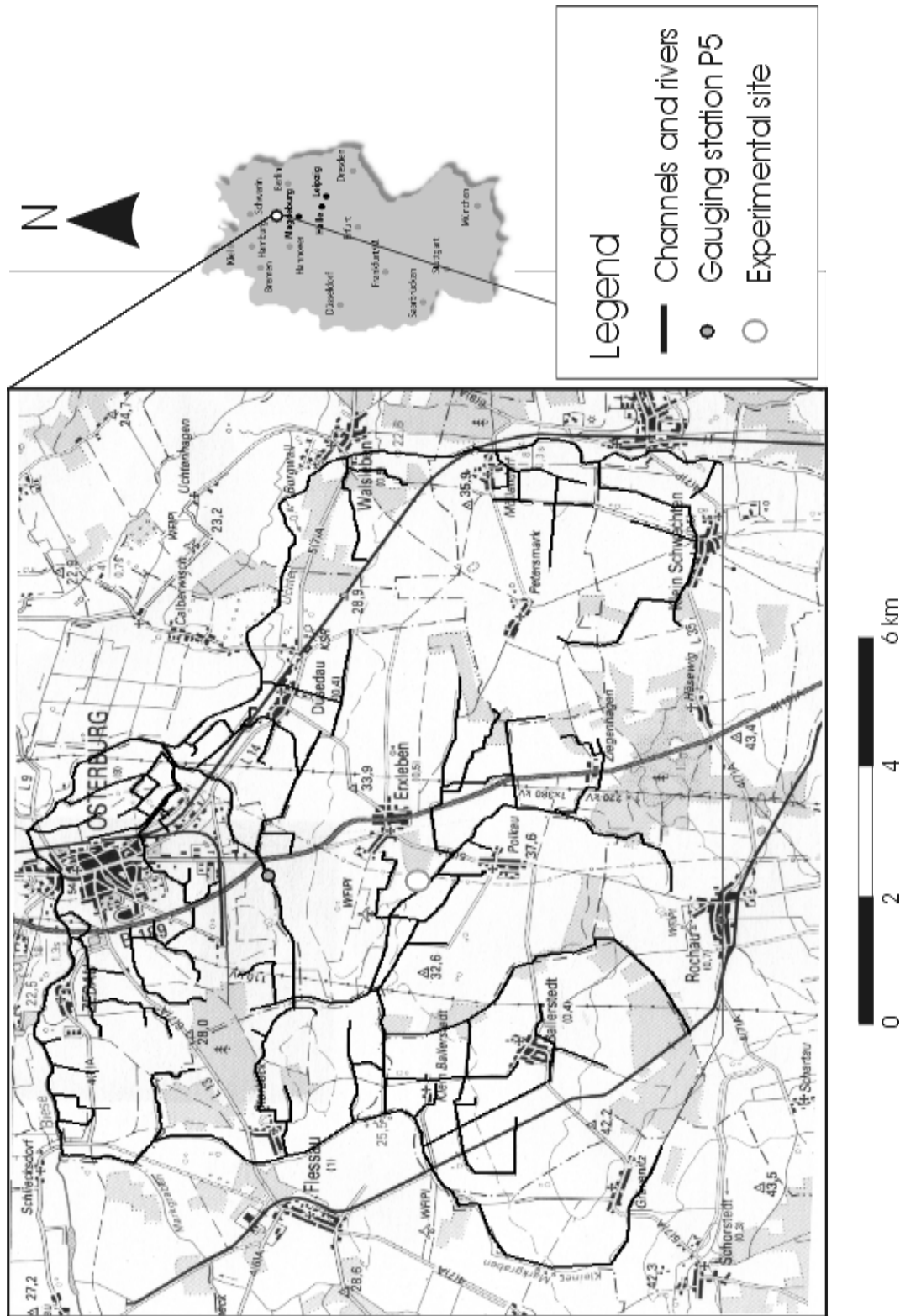


Figure 13: Map of the (extended) Schaugraben study area near Osterburg (Altmark)

The mean annual precipitation is 548 mm/a, potential evaporation calculated according to Penman-Wendling (DVWK, 1996) is 574 mm/a. Mean annual temperature is 9.0°C, ranging from Mean monthly temperatures of 0.8°C in January to 18.1 °C in Juli (Figure 14).

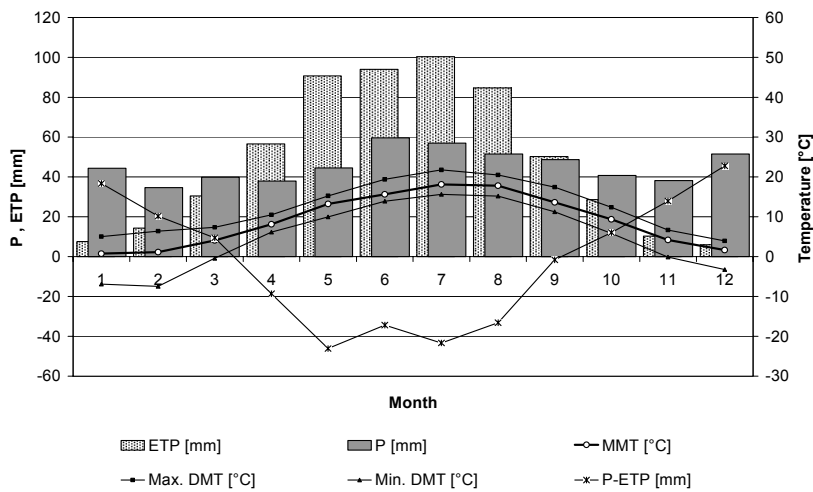


Figure 14: Mean monthly climatic data of UFZ Lysimeter station in Falkenberg (P=Precipitation, ETP = Evapotranspiration, MMT = Mean Monthly Temperature, DMT = Daily Mean Temperature), Data from 1982-2002

Agriculture is the dominating land use in the area. The lower areas are mostly used as grassland and pasture, although various fields can also be found in the lower areas, directly adjacent to the Schaugraben drain channel. The uplands are dominated by crop cultivation. In more sandy areas, mixed and coniferous forests are found (Figure 15). Since 1990, the year of German reunification, a structural change of agriculture has increasingly led to a market-oriented cultivation and abandonment of traditional crop rotation. The ratio of individual crops has changed considerably. A tendential increase in fallow, sugar beet, alfalfa and other (peas, flax sunflower, clover grass) to the cost of corn, potatoes and rape (=colza) can be observed (Meissner, 2000). This indicates general extensification of agriculture on the one hand and intensification in specific areas for a better utilisation of manure on the other hand. Most part of the Schaugraben study area is now operated by the farm cooperative in Erxleben. The UFZ Lysimeter station in Falkenberg has surveyed land use and management in the Schaugraben catchment since 1991.

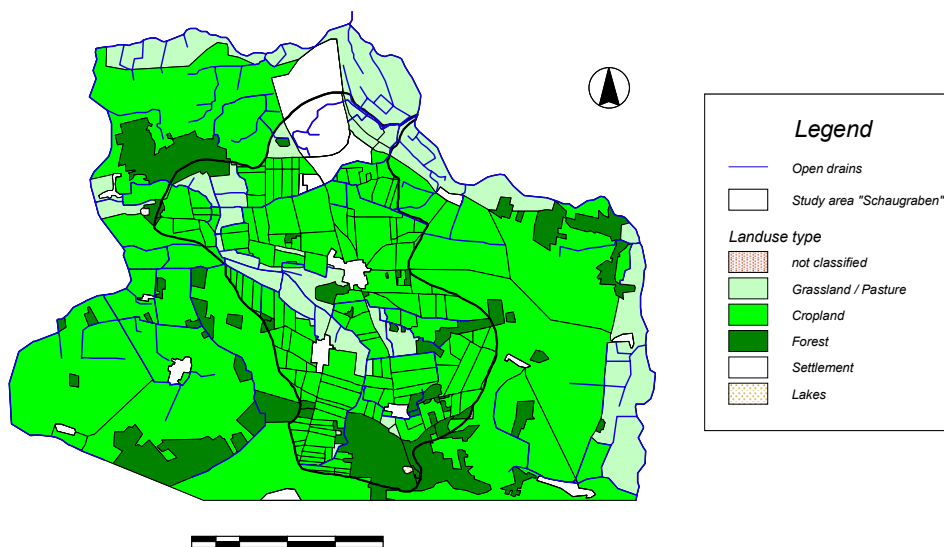


Figure 15: Distribution of land use classes in the study area

4.2 Data sources

In the Schaugraben catchment, various studies have been carried out by the UFZ Lysimeterstation in Falkenberg, including monitoring of land use and management since 1990, measurements of runoff and substance loads since 1997 and experimental investigation of N-transport in soils and shallow groundwater (Meissner et al., 1999; Meissner, 2000; Möller, unpublished; Blank, oral communications). These studies provide the database for this simulation work, together with additional data provided by public authorities such as the Geological Survey of Saxony-Anhalt (GLA-SA), the Environmental Protection Authority of Saxony-Anhalt (STAU). The following list is a summary of all experimental or published data sets used in this study.

Data from the UFZ Lysimeter station in Falkenberg:

- Lysimeter data including characterisation of original soils, management records, leaching rates and nitrate leaching
- Management data for the Schaugraben study area since 1990
- Soil map of the Schaugraben study area based on Soil Map of the GDR 1:50000 (MMK 50)
- Groundwater level observations and chemical groundwater analysis of the experimental site in the Schaugraben study area
- Single sampling of STAU groundwater wells 3236-0063 and 3236-0068
- Discharge measurements at gauging station P5 (weekly and continuous sampling, since 1997 with interruptions) and at gauging point P2 (weekly since November 2001)
- Chemical analysis of surface water samples at the gauging stations P5 (discontinuously since 1997) and P2 (since November 2001)
- Climatic data from the stations in Falkenberg and Seehausen
- Results of a field scale tracer experiment, carried out by B. Blank, UFZ Falkenberg

Data from the Geological Survey Saxony-Anhalt (GLA-SA):

- Borehole profiles of the extended study area, provided by GLA-SA
- Hydrogeological map HÜK 50 (GLA-SA)
- Geological map GK 50, 3236 Osterburg, scale 1:50000

Data from the Environmental Protection Agency Saxony-Anhalt (STAU):

- Groundwater level observations of the extended study area, provided from STAU

Data from the Bureau of Statistics in Saxony-Anhalt (STATLA-SA):

- Net plant N-uptake (harvest losses) from 1990-2000 for Saxony-Anhalt

Topographical Maps:

- Topographical maps TK 10, N-32-120-D-c-1 Polkau, N-32-120-C-b-4 Osterburg W, N-32-120-C-d-2 Ballerstedt, N-32-120-D-a-3 Osterburg, scale 1:10000
- Topographical maps, TK 25, 3236 Osterburg, 3237 Goldbeck, scale 1:25000

An overview on field data and a map showing the location of the various sampling stations in the study area is given in appendix A.

4.3 Soil water and nitrogen modelling with lysimeter data

4.3.1 Input data

Six lysimeters were used for modelling studies. They cover three management scenarios – grassland, cropland I (integrated management) and cropland II (conventional management) – and two soil textural classes, sand and loamy sand. The original soils were a sandy loam and a sand representing typical soils of the Altmark. They were analysed for soil physical parameters such as density, porosity and saturated conductivity. However, soil structure was completely destroyed during the filling process, and therefore, these data could only give an estimation of lysimeter properties. Thus soil physical data (pore volume, field capacity, wilting point, saturated conductivity) were assigned from textural data according to AG Boden (1994).

No literature data or transfer functions were available for parameterisation of the leaf interception storage and the infiltration storage. Initial values were set arbitrarily to 0.002 and 0.005 m and the effect was evaluated during sensitivity analysis.

Climatic data were taken from the UFZ Lysimeter station in Falkenberg and the climatic station in Seehausen, operated by the German National Meteorological Service (DWD). Input data for the soil simulation are precipitation, potential evapotranspiration and air temperature. Potential evapotranspiration was calculated according to the Penman-Wendling method described in DVWK (1996). In periods where global radiation was not measured, radiation data were calculated from sunshine duration according to DVWK (1996).

Lysimeter management records provided by the UFZ Lysimeter station included information on crops cultivated, irrigation measures and fertilizer additions. N-losses to harvest were provided as annual data.

For several crops (grassland, clover cultures and legumes) input of N via N-fixation had to be taken into account. The input of N via fixation was calculated as follows: The Fertilizer directives of Saxony-Anhalt (DVO-SA, Landesanstalt für Landwirtschaft und Gartenbau, 2002) provide estimates for total leguminal N-fixation [kg N/dt] and crop specific N-loss by harvest [kg N/ha]. It was assumed, that N-fixation is proportional to plant production, thus dividing N-fixation by N-Harvest yields a coefficient for N-fixation per N-Harvest (kg N by fixation / kg N harvested). Observed N-loss multiplied by the N-fixation coefficient yields total amount of N-fixation.

$$N_{\text{Fixation}} = \frac{N_{\text{Fixation}}^0}{N_{\text{Harvest}}^0} \cdot H \cdot T$$

with N_{Fixation} = N-Fixation [kg N/ha], N_{Fixation}^0 = total leguminal N-Fixation [kg N/ha] (DVO-SA), N_{Harvest}^0 = Loss of N by harvest [kg N/ha] (DVO-SA), H= Harvest [dt FM/ha], T =specific crop N-content [kg N/dt DM]

Observed bulk deposition is 12 kg N/ha on average. According to recent experimental studies (Böhme and Russow, 2002, see also chapter 4.7.2.4), the total atmospheric deposition can be considerably higher but is still difficult to quantify. Therefore, atmospheric deposition was set to a worst-case input of 60 kg N/ha/a.

Observed percolation (groundwater recharge) and nitrate-leaching were used for model validation. The data were provided on a monthly base.

The denitrification constant was set to 0.0001 for all horizons assuming no significant denitrification.

Frequently used mineralisation functions are those of Kersebaum and Richter (1991) for two (rapidly and slowly) mineralisable N-Pools. Mineralisation rate constants determined by Kersebaum and Richter (1991) on loess soils are 0.01263 d⁻¹ for rapidly and 0.0059 d⁻¹ for slowly mineralizing organic matter. These rates are frequently used as standard values in mineralisation functions. Heumann et al. (2002) determined mineralisation rate constants on sandy soils (0.00865 d⁻¹ and 0.0023 d⁻¹) and conclude that different rate constants apply on sandy and loess soils. As a consequence, mineralisation rate constants have to be considered as site specific and not as universal constants. The conventional values given by Kersebaum and Richter (1991) and the values determined by Heumann et al. (2002) for sandy soils are taken here to define a range of possible values to be used in simulations. The initial rate constants were set to intermediate values of 0.00405 and 0.01064 1/d.

4.3.2 Sensitivity analysis

A sensitivity analysis was carried out to obtain a first overview of model behaviour and to assess the importance of single parameters for model calibration. In a first step, a local sensitivity analysis was carried out to analyse the effect of soil physical and chemical parameters on average soil model results. Model observations were total averages of evapotranspiration, groundwater recharge, storage change, mineralisation, denitrification, and nitrate leaching. A normalized sensitivity function e was used according to Reichert (1998):

$$e = \frac{\partial O}{\partial P} \cdot \frac{P}{O}, \text{ which can be modified into } e_{10} = \frac{\Delta O}{\Delta P} \cdot \frac{P}{O} = \frac{O_1 - O}{1.1P - P} \cdot \frac{P}{O} = \frac{(O_1 - O)}{0.1 \cdot O}$$

with e = normalized sensitivity index, O = reference observation value, $\partial O/\partial P$ = , P = reference parameter value, O_1 = observation value corresponding to 10% change of the parameter value.

This index is known as the normalized 10%-elasticity index e_{10} in economic literature. The elasticity index e_{10} is a measure of the relative change of an observation to a relative change of the parameter. The index was calculated for a 10% increase and decrease in the parameter value. The analysis was conducted for Lysimeter 03 (grassland, sandy loam), Lysimeter 04 (grassland, sand), Lysimeter 05 (integrated management, sandy loam) and Lysimeter 53 (conventional management, sandy loam).

In a second step, the effects of single parameters were evaluated over a range of possible parameter values for each lysimeter. The modified parameter values are given in Table 7.

A substantial problem in modelling the mineralisation is the estimation of initial organic N-pools, as there are no accepted methods to identify specific N-pools (Heumann et al., 2002). A separation into functional groups has not proven to be applicable according to Kersebaum (1999). In this study, initial N-pools are derived from subsequent simulation runs approaching steady state conditions.

The initial parameters for the reference simulation are defined in Table 8.

Table 7: Simulation runs and parameter ranges used in sensitivity analysis

ID	Parameter	Parameter values	
1	Rapid mineralisation rate constant [1/d]	0.01263 – 0.01164 – 0.01064 – 0.00965 – 0.00865	Range according to Heumann et al. (2002)
2	Slow mineralisation rate constant [1/d]	0.0058 – 0.00493 - 0.00405 – 0.00318 - 0.0023	Range according to Heumann et al. (2002)
3	Groundwater depth [m]	2 - 2.5 – 3 – 4 – 5 – 6	Range of groundwater depths in the study area
4	Saturated conductivity [m/d]	0.02 – 1.36 (reference /8, /4, /2, *2, *4, *8)	
5	Field capacity [m]	0.20-0.35/0.15-0.30/0.15-0.30, in steps of .03	
6	Interception storage capacity [m]	0 – 0.001 – 0.002 – 0.003 – 0.004	
7	Infiltration storage capacity [m]	0 – 0.001 - 0.0025 – 0.005 – 0.0075 – 0.010	3 cm soil layer with porosity of 0.3
8	Denitrification rate constant [1/d]	0.0001 – 0.0005 – 0.001 – 0.005 – 0.01	0.01 = RISK-N default value

Table 8: Initial soil parameters used in sensitivity analysis

Parameters	Unit	Reference soil: Loamy Sand	Reference Soil: Sand
Porosity (URZ/LRZ/IVZ)	[-]	.39/.33/.33	.46/.37/.37
Field Capacity (URZ/LRZ/IVZ)	[-]	.27/.22/.22	.22/.16/.16
Reduction point (URZ/LRZ/IVZ)	[-]	.22/.18/.18	.18/.13/.13
Wilting point (URZ/LRZ/IVZ)	[-]	.09/.05/.05	/.06/.04/.04
K_f (URZ/LRZ/IVZ)	[m/d]	.42/.22/.22	.67/5.8/5.8
Leaf storage capacity / Infiltration storage capacity	[m]	.002/.005	.002/.005
K_{den} (URZ/LRZ/IVZ)	[1/d]	.0001/.0001/.0001	.0001/.0001/.0001
Rapid and slow mineralisation rate constant	[1/d]	.01064/.00405	.01064/.00405
Groundwater depth	[m]	2	2
URZ = Upper root zone, LRZ = Lower root zone, IVZ = Intermediate vadose zone			

4.3.3 Calibration and validation procedure

Observations of groundwater recharge and nitrate leaching from 1992-1996 were used for calibration. Data from 1997 to 2000 were used for validation. The calibration process followed a two step procedure. First, groundwater recharge was calibrated. Model parameters were calibrated sequentially within physically reasonable boundaries in the order field capacity, reduction point, hydraulic conductivity, infiltration storage capacity. Each calibration run was automated using the software PEST (Waterloo Hydrogeologic, 2000), which implements a Gauss-Marquardt-Levenberg algorithm for parameter optimisation. Basically, this method finds local minima of an objective function, in this case the RMSE of observed and simulated values. Parameters are optimized iteratively based on the local sensitivity of the objective function in each loop. In a second step, nitrate leaching was calibrated by optimisation of denitrification rate constants first and mineralisation rate constants second, again supported by the PEST algorithm. For model calibration both monthly and annual leaching rates were used as observations, in order to get a good fit of inter-annual variations, while at the same time maintaining seasonal dynamics. For the final calibration run, Root Mean Squared Error (RMSE) and the Nash-Sutcliffe coefficient of Efficiency (NS-CoE, Nash and Sutcliffe, 1970) were calculated as performance measures for the calibration period, the validation period and the total simulation period.

4.4 Sensitivity analysis of the groundwater-reaction-module

A sensitivity analysis of the reaction-module was made for a batch reaction, representing only chemical processes. In this case, the analysis of model response to parameter variations was part of model verification, as model response should be in accordance with theoretical behaviour, defined by the functional relationships of the reaction-module. The analysis was carried out by variation of individual parameters over a certain range of possible values. Both, substance concentrations and reaction parameters were varied. For evaluation of model behaviour, concentration vs. time – curves were plotted for selected species. The concentrations used in the reference simulation and the individual sensitivity runs are given in Table 9.

Table 9: Parameter values used for sensitivity analysis of the groundwater-reaction-module

Parameter	Reference simulation	Variations
H	7.00007 mg/l _w	-
O ₂	5 mg/l _w	0 – 2 – 4 – 6 – 8 – 10
NO ₃	50 mg/l _w	10 – 25 – 50 – 75 – 100
N ₂	0 mg/l _w	-
NH ₄	0 mg/l _w	-
SO ₄	20 mg/l _w	20 – 40 – 60 – 80 – 100
HS	0 mg/l _w	-
Fe	0 mg/l _w	-
Ca	280 mg/l _w	-
CO ₃	330 mg/l _w	-
rOM	15 mg/l _w	0 – 5 – 10 – 15 – 20
SOM	500 mg/l _w (0.01 Mass-%)	500 – 5000 – 50000 – 500000
FeS ₂	500 mg/l _w (0.01 Mass-%)	500 – 1000 – 5000 – 10000
Fe(OH) ₃ (am)	0 mg/l _w	-
k _{eff} ¹ -O ₂	0.961	0.481 – 1.44 (+/- 50%)
k _{eff} ² -NO ₃	5.6	2.80 – 8.40 (+/- 50%)
k _{eff} ³ -SO ₄	1.32e-5	6.60e-6 – 1.98e-5 (+/- 50%)
k _{eff} ⁴ -SOM	1.0e-9	1.0e-9 – 1.0e-8 – 1.0e-7 – 1.0e-6
rOM _{max}	0.00067 mol/l	x1 x2 x4 x8
K _{eff} ⁶ -Pyrite-NO ₃	3.92e-9	(+/- 50%)
Temperature	10°C	0° - 5° - 10° - 15° - 20°

4.5 Simulation of a field scale tracer experiment

4.5.1 Description of the tracer experiment

The Schaugraben tracer experiment was carried out by B. Blank UFZ Falkenberg (Blank, oral communications; Wriedt et al., 2001). Only a short summary of experimental setup and layout will be given here. The experimental site was located on a pasture within the Schaugraben catchment in direct vicinity to the Schaugraben drain.

Soils in the area are a mosaic of gleyic soils on loamy and sandy substrates. The well field for the tracer experiment was placed on a sandy plot of the pasture area. Groundwater observation wells were constructed from June 2000 - May 2001. The observation wells are located on circular arcs at a distance of 3, 8 and 13 m from the injection well. The well screens were located in a depth of 2-3 m below surface. Groundwater depths lie between 1 and 1.5 m below surface. A general sketch of the well field is given in Figure 16. Samples were taken from the observation wells T1-1, T2-1, T3-1 weekly from summer 2001 until autumn 2002.

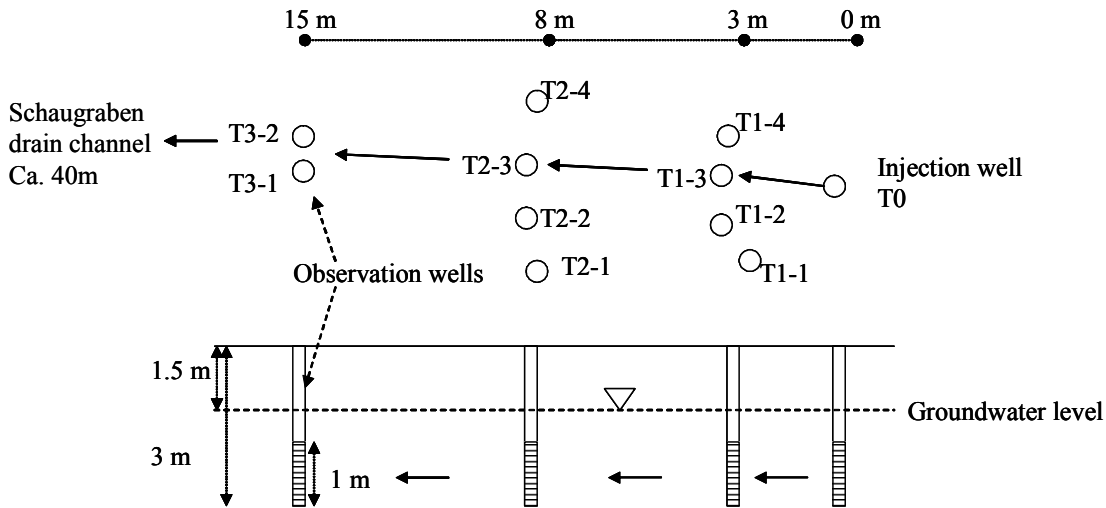


Figure 16: Experimental layout of the tracer experiment

For the tracer experiment Nitrate was used as a reactive tracer and bromide as a conservative tracer. In June 2001 110 g $\text{NO}_3\text{-N}$ (as KNO_3) and 110 g Br (as KBr) were injected into the aquifer at well T0. During the tracer experiment, samples were taken twice a week from all wells, where a tracer breakthrough was expected. The samples were analyzed for $\text{NO}_3\text{-N}$, $\text{NH}_4\text{-N}$, $\text{NO}_2\text{-N}$, Br^- , SO_4^{2-} , DOC and TIC. A tracer breakthrough was observed after a travel distance of 3, 8 and 15 m (Figure 17).

The breakthrough curves show a considerable decline of the nitrate concentrations compared to the bromide concentrations. In well T1-3 the tracer breakthrough showed also a distinct peak of nitrite concentrations, which can be interpreted as an intermediate product of denitrification processes. No corresponding peaks of TIC or Sulphate could be observed. A preliminary pumping test indicates hydraulic conductivities in the order of $10\text{e-}4$ m/s (approximately 9 m/d).

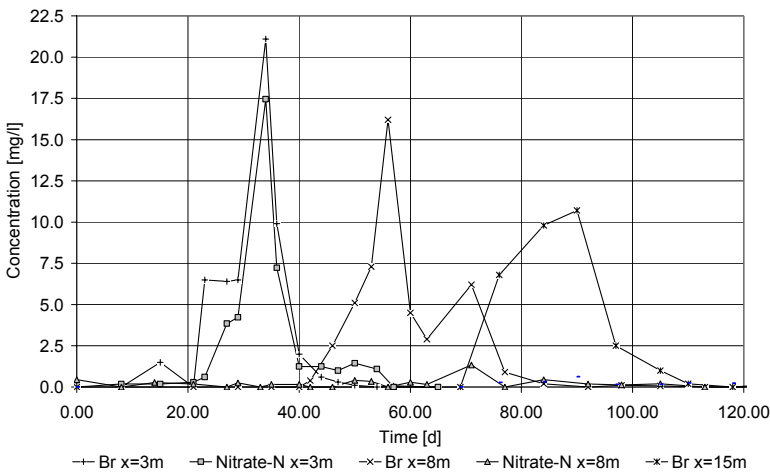


Figure 17: Observed breakthrough-curves of bromide and nitrate-N after a travel distance of 3, 8 and 15 m

4.5.2 Evaluation of the tracer experiment

The observed BTC's are of quite irregular shape and indicate a variety of processes, which were not observed or can not be considered by the model, e.g. preferential flow paths and small scale substrate heterogeneity or changes of hydraulic conditions. Thus observed BTC are not suited for direct model comparison. A quantitative description is needed that allows estimation of mass fluxes rather than concentrations.

Such a quantitative description of BTC was obtained by a temporal moment analysis, as described

in Vanderborght and Vereecken (2001). The zero-order moment is the area under the BTC, the first-order moment is the mean solute travel time μ_t , the second order moment is the variance of solute travel times. From these information equivalent particle velocity u_{eq} and the equivalent dispersivity λ_{eq} were calculated. These data are consistent with the 1D CDE and allow calculation of the equivalent analytical breakthrough curves.

A reference mass flux was defined as:

$$\Omega(x) = \int_{t=0}^{\infty} C(x,t) \cdot v_c dt = T0(x) \cdot v_c$$

where $\Omega(x)$ =mass equivalent in location x [M], $T0$ = area under BTC [$ML^{-3}T$], $C(x,t)$ =concentration at location x and time t [ML^{-3}], v_c =local transport velocity [LT^{-1}].

Ω is a measure for the mass flux per unit cross sectional area, observed at an individual observation site. This indicator allows comparison of different BTC. It is, however, no estimator for the actual mass flux, as it expands a point measurement over a homogeneous cross sectional area without taking into account lateral and vertical concentration distributions. Thus Ω can also be higher than the initial tracer mass applied. However, as experimental findings limit lateral extent of the tracer plume to approximately 1-2m, Ω can be taken as an indicator for the maximum possible tracer mass in the system which can be compared to the injected tracer mass. In an ideal transport system all observed Ω -values should be identical. Different Ω -values between observation wells indicate that the observation wells cut the tracer plume at different positions.

From the BTC analysis a quantitative description of observed BTC's was obtained, allowing calculation of equivalent analytical BTC's, which can be used as reference BTC's for model comparison. For the case of different Ω -values, the BTC's can be scaled to each other by their Ω -ratios to get a consistent series of BTC's.

4.5.3 Model setup and flow simulation

The well field was placed entirely into a sandy deposit. The substrate can be characterized as medium sand of a uniform distribution. The model domain is a 2D-transect cutting through the well field. The left margin of the model domain is given by the Schaugraben drain, which is implemented as a head-dependent flux boundary (Cauchy-boundary condition) in the first layer. The drain water level was set to 29.9 m. The right margin is described by a fixed-head boundary (Dirichlet-Boundary), corresponding to groundwater well GM5. The constant head value was set to a value of 30.5 meters, which was derived from the observed data. Recharge or evaporation from groundwater were not considered, as calculations with a soil-water-model indicate that there was no recharge during the period of investigation. The injection well is implemented as a specified flux boundary. A summary of the model layout is given in Figure 18.

During the tracer experiment, transport velocities and groundwater levels were observed. For the

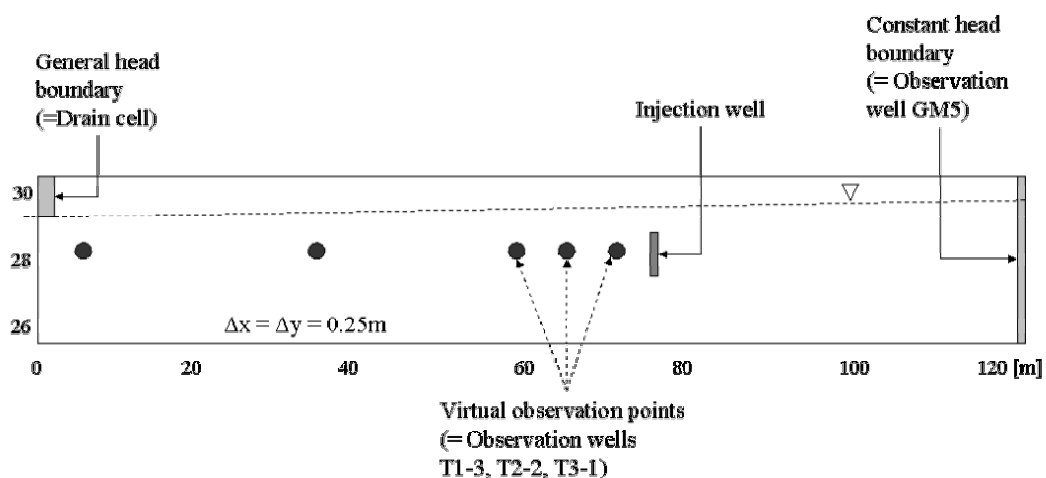


Figure 18: Model setup for simulation of the tracer experiment

steady state simulation, the corresponding hydraulic conductivity can be calculated applying Darcy's Law using the equation

$$K_f = Q \cdot \frac{\Delta x}{\Delta H}$$

K_f = saturated conductivity [$L T^{-1}$], ΔH = Head difference [L], Δx = distance between heads [L], Q = Flux [$L^3 T^{-1}$].

From the observed transport velocity $u_a = 0.22$ m/d and an assumed porosity of 0.3 the calculated flux is 0.066 $m^3/m^2/d$, which equals a flux of 0.29 $m^3/m/d$ per m channel length. This is a reasonable value compared to the flux estimated by relating the fluxes of the gauging station P5 to the total length of the drain network. Assuming that the entire drain contributes to discharge, the discharge flux is 0.26 $m^3/m/d$. It is likely that only a fraction of the channel system contributes to discharge due to the distribution of sandy and loamy sediments. If only half of the drain contributed to discharge, the corresponding flux would be 0.52 $m^3/m/d$. The transect was subdivided into several sections between single observation wells and saturated conductivities were calculated for each section. Following this approach, all parameters of the flow model (fluxes, hydraulic heads and conductivities) are identified, if the flux is given and no further calibration is needed.

The steady state model neglects the fact that groundwater gradients decreased considerably during the tracer experiment, which also leads to a decrease in transport velocities. Consequently, deviations in the travel time of the simulated breakthrough-curves compared to the observed breakthrough-curves have to be expected.

4.5.4 Calibration of the transport model

The simulation of the conservative bromide tracer transport required calibration of porosity, dispersivity and initial tracer mass. The initial tracer mass was set equal to the highest observed Ω . The appropriate tracer mass is equal or lower to the Ω value and has to be calibrated to the observed BTC's. Only the third BTC was used as a reference for initial tracer mass, as it provided the most reliable measurement. In a first approach, a uniform distribution of dispersivity and porosity was assumed. The initial porosity was set to 0.3, the initial longitudinal dispersivity was set to 0.1 m. Longitudinal and vertical dispersion were set to a constant ratio of 0.1. Initial tracer mass and transport parameters were calibrated based on the best fit of the BTC at well T3-2. This approach did not achieve a good fit of travel times for all BTC's simultaneously and inhomogeneous conditions needed to be incorporated into the model. In a second approach, the experimental site was divided into three sections between observation wells. Dispersivities assigned were identical to the values achieved from BTC-analysis and only porosity values had to be calibrated. All parameters were adjusted systematically by trial and error. Model fit was assessed by calculating the root mean squared error (RSME) of observed and calculated BTC's.

4.5.5 Simulation of reactive nitrate transport

The transport model was extended for reactive transport simulations. The same transport parameters as for bromide transport were applied to nitrate transport as well. Turnover reactions were implemented by a user-defined reaction-module, running with the RT3D transport code (see chapter 3.3). The reaction-module considers decay of dissolved organic matter using Oxygen, Nitrate and Sulfate as possible electron acceptors as well as pyrite oxidation by oxygen and nitrate (autotrophic denitrification). In this simulation study an earlier version of the reaction-module was used (Reaction-module A), which was completely based on Monod-type reaction kinetics.

As experimental data did not allow a separation of heterotrophic and autotrophic denitrification, heterotrophic denitrification was considered as the only nitrogen turnover process, and pyrite oxidation (autotrophic denitrification) was neglected. The initial concentrations of oxygen and nitrate were set to 0 mg/l, the concentration of rOM was set to 10 mg/l, which is within the range of observed aquifer solute concentrations and SOM-concentrations were set to 5000 mg/l (=0.1 Mass-% at a porosity of 0.3). Other concentration values were set arbitrarily within the range of observed data. The concentrations of the injection well were set equal to the aquifer concentrations, with the exception of NO_3^- . The initial Nitrate-N mass was set equal to the calibrated initial bromide mass of 22.5 g (see chapter 5.3.2). The resulting NO_3^- -concentration in the injected volume of 5 l is 19928 mg/l.

The actual nitrate turnover is strongly restricted by availability of electron donors. In this model, supply of DOM can be controlled by two factors, the release of organic matter from the SOM-pool or the linear sorption coefficient of organic matter. Whereas release of SOM would constantly increase OM concentrations, the sorption process would maintain a stable OM concentration by exchange with the sorbed phase. The effect of SOM release and of DOM sorption was investigated in two simulation studies, using the same model as described above. A third study shows the effect of decreasing the denitrification rate constant, assuming unlimited supply of organic matter. Model parameters were set according to Table 10.

Table 10: Model runs and parameter settings for tracer transport simulations

Simulation study:	(1) Effect of SOM release	(2) Effect of rOM sorption	(3) Effect of denitrification rate
Changed parameter:	SOM release coefficient [1/s]	Linear sorption coefficient [m ³ /mg]	Denitrification rate constant [1/s]
Model run	Parameter values		
A	1.0e-10	No sorption	1.9e-09
B	1.0e-8	1e-7	9.5e-10
C	1.0e-7	3e-7	5.225e-10
D	1.0e-6	1e-6	9.5e-11
E	1.0e-4	1e-4	-

4.6 Simulation of nitrogen transport and turnover at the transect scale

4.6.1 Model setup

In order to investigate basic interactions between chemical and physical properties and nitrate turnover in groundwater, a variety of simulations were performed on a synthetic transect cutting an upper and lower aquifer in a lowland catchment. Due to the reduction to a two-dimensional problem with a simple flow situation, a variety of processes and model behaviour could be investigated more closely than in a large scale model. Simulations focussed on general system characterisation, investigating varying flow situations, transport properties and chemical properties and on practical questions, as the effect of buffer areas and changed N-loads.

A synthetic transect was chosen, as the investigations focussed on general processes and model behaviour, rather than on site specific problems. Additionally, there were no field data available allowing setup of suitable transect simulations. Geological information of the study site were too sparse to derive a hydrogeological model of the transect and only the uppermost groundwater was investigated at the experimental site. Relevant information on background concentrations or field observations for model validation was not available. Thus an extension of the model domain would be necessary, adding further assumptions to the model. In order not to imply relations to real world situations, not supported by observation data, the simulations were completely defined for a synthetic transect.

However, model layout was derived according to observed or assumed field conditions occurring in the Schaugraben study catchment. Although hypothetical, the model thus can be considered as a realistic model.

The model grid had an extent of $x=600$, $y=10$ m and $z=30$ m, with a grid resolution of $dx=dy=10$ m and $dz=2$ m (15 layers). A drain was located in cell (1,1,1), being described by a fixed head boundary in cell (1,1,1), with a constant head set to $x = 28.5$ m. A specified flux boundary was assigned to the upper boundary representing groundwater recharge. The opposite vertical boundary implemented a constant head boundary condition, allowing for head dependend flux into the model domain. The model domain was subdivided into an upper aquifer (layer 1-4), a lower aquifer (layer 9-15) and an intermediate horizon (layer 5-8). The model domain was further divided into subsections with an extent of 200m. Thus, the model domain was partitioned into a total of nine (3x3) subsections. Parameters could be specified individually for each of these subsections in order to generate various hydraulic and geochemical situations. Virtual observation points were

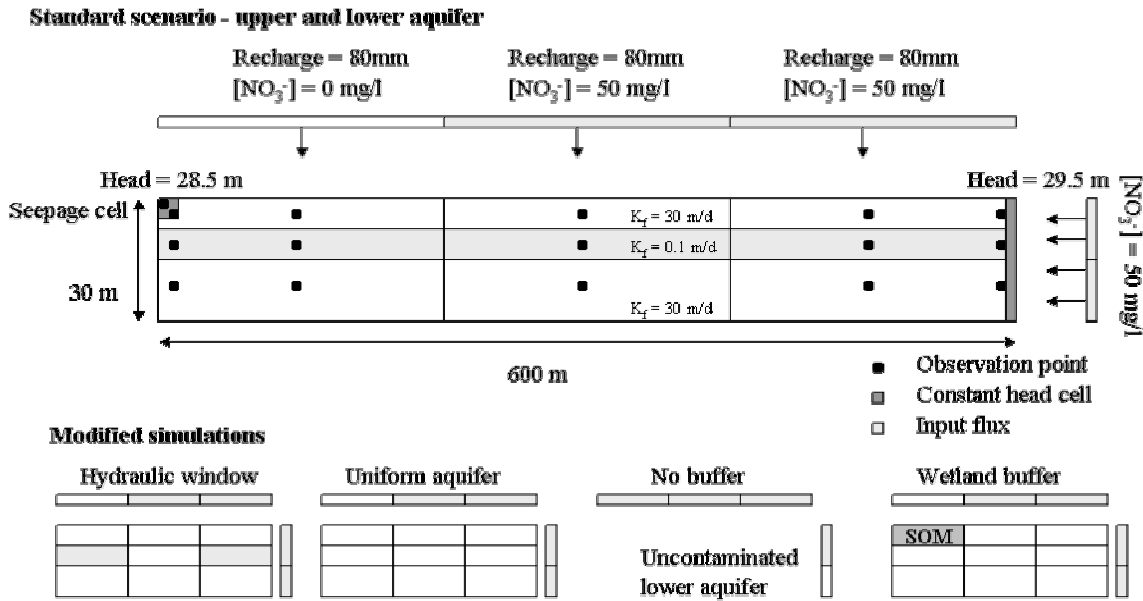


Figure 19: Model layout for artificial transect simulations

defined within the model domain. For each observation point and component concentration vs. time curves were automatically extracted. As the results were written for each transport step, a special macro had to be written in order to reduce the amount of data and to write concentration records with larger time intervals. A general overview on model layout is given in Figure 19.

4.6.2 Definition of flow simulations

Several flow scenarios were developed in order to define specific flow situations. They address various hydraulic situations such as interaction between upper and lower aquifer and different groundwater fluxes (i.e. changed hydraulic gradients). In simulation 1 the model domain was a homogeneous aquifer of good conductivity. In simulation 3 an upper and a lower aquifer were separated by a low-conductivity layer. In simulation 5, the low-conductivity layer was interrupted by a hydraulic window of high conductivity, connecting upper and lower aquifer. Simulation 8 was defined identical to simulation 3, but the hydraulic gradient is decreased by 50%. The model parameters are given in Table 11. A schematic illustration is given in Figure 19. For each flow simulation a particle tracking simulation was run using MODPATH. 19 Particles were placed along the recharge boundary (upper boundary) in a distance of 50m and along the constant head boundary (right boundary) in a distance of 2 m.

Table 11: Definition of flow simulations

Parameter ↓	Flow → simulation	1	3	5	8
Description		Homogeneous Aquifer	Upper aquifer, Aquitarde, lower aquifer	Hydraulic window within Aquitarde	As 3, decreased gradient
K _f Aquifer 1 [m/d]	Layers 1-4	30	30	30	30
K _f Intermediate layer [m/d]	Layers 5-8	30	0.1	0.1 / 30 / 0.1	0.1
K _f Aquifer 2 [m/d]	Layers 9-15	30	30	30	30
Recharge [m ³ /d]	-	0.00023	0.00023	0.00023	0.00023
Const.Head	Inflow boundary	29.5	29.5	29.5	29.0

4.6.3 Reference reaction scenario

All reactive transport simulations were based on a reference simulation, from which specific simulations were derived by modification of boundary conditions, initial conditions and model parameters. This reference or standard scenario involved all basic processes considered in the reaction-module and was defined as follows:

The first section of the upper aquifer represented a buffer area with no input of nitrate but with higher initial and recharge concentrations of reactive organic matter. The second section represented cultivated land and was considered a source area for nitrate. A second source was flux of contaminated groundwater across the constant head boundary into the upper and lower aquifer system. The intermediate layer and the lower aquifer were initially nitrate free and contained reduced groundwater, with high concentrations of sulphate and pyrite. Temperature for the standard scenario was set to 10°C.

The aquifer was initially free of oxygen and nitrate. Sulphate concentrations were set to 10 mg/l in the upper aquifer and to 100 mg/l in the lower aquifer (In the lower aquifer, higher sulphate concentrations result from pyrite oxidation). The initial content of SOM was set to 0.1 Mass-% (5000 mg/l) and of pyrite to 0.01 Mass-% (500 mg l⁻¹). Whereas SOM was present in the whole aquifer, pyrite was present in the lower and intermediate layer only. Concentrations of rOM were set to 5 mg/l and to 15 mg/l in the left section of the upper aquifer, indicating an increased availability of OM in this buffer area. Concentrations at the constant head boundary were set corresponding to initial aquifer concentrations. Only nitrate concentrations were set to 50 mg/l in all layers.

Recharge water in the first section (buffer area) was free of oxygen and nitrate and rOM concentrations were set to 15 mg/l. In the second section (representing cultivated land) oxygen concentrations were set to 6 mg/l and nitrate concentrations to 50 mg/l (limit for drinking water). rOM concentrations were reduced to 5 mg/l, which was equal to the aquifer background concentrations.

4.6.4 Definition of transport simulations

Interactions between upper and lower aquifer were investigated by comparing model behaviour under different flow simulations considering i) a homogeneous aquifer, ii) a separated upper and lower aquifer and iii) a hydraulic window in the intermediate layer. The effect of transport velocity on nitrate transport and turnover was evaluated by changing i) the overall hydraulic gradient and ii) the porosity of the substrate. The effect of temperature was evaluated for 5, 10 and 15°C. Modified reaction scenarios considered i) a nitrate free lower aquifer and ii) absence of a buffer area close to the drain and iii) the contribution of various reactive pools (rOM, SOM and pyrite) to nitrate turnover.

A set of simulation runs was defined respectively. The individual runs are specified in Table 12, including the model parameters changed with respect to the standard scenario. For each simulation run a corresponding conservative transport simulation was calculated, if flow situation or solute fluxes were different from the standard simulation sim03a. The simulation runs covered a period of 31025 days (=85 years). However, reactive simulations partly stopped execution earlier. A TVD algorithm was used to solve the transport equation. The longitudinal dispersivity was set to 1.0 m, vertical and lateral dispersion to 0.1 m. Reaction parameters were set to standard parameters as defined in Table 5.

Model results were evaluated by pairwise comparison of corresponding simulation runs.

Table 12: Definition of simulation runs for the artificial transect model.

Transport simulation identifier	Corresponding flow simulation	Reactive transport setup
Sim01a *	Flow 1	Reference scenario, homogeneous aquifer
Sim03a *	Flow 3	Reference scenario, upper and lower aquifer, 10°C
Sim05a *	Flow 5	Reference scenario, hydraulic window connecting upper and lower aquifer
Sim07a *	Flow 7	Reference scenario, homogenous aquifer with decreased hydraulic gradient
Sim08a *	Flow 8	Reference scenario, upper and lower aquifer with decreased hydraulic gradient
Sim03b *	Flow 3	Uncontaminated lower aquifer: nitrate concentration at inflow boundary = 0 mg/l
Sim03c	Flow 3	Temperature = 5°C
Sim03d	Flow 3	Temperature = 15°C
Sim03e	Flow 3	Reactive pools: rOM-pool only, no SOM, no pyrite
Sim03f	Flow 3	Reactive pools: rOM and SOM-pools only, no pyrite
Sim03g	Flow 3	Reactive pools: pyrite only, no SOM
Sim03h	Flow 3	Reactive pools: reduced pyrite-content (100 mg/l), no SOM
Sim03i *	Flow 3	Increased transport velocity (porosity=0.15)
Sim03j *	Flow 3	Decreased transport velocity (porosity= 0.45)
Sim03q *	Flow 3	Buffer area: no buffer area
Sim03l	Flow 3	Buffer area: Effective buffer area (Wetland, Peat) with high SOM concentrations and reduced SOM outside buffer area
Sim03m *	Flow 3	Higher input of nitrate (Recharge concentration = 100 mg/l)
* with corresponding conservative transport simulations		

4.7 Simulation of water and nitrogen fluxes at the catchment scale

4.7.1 Outline of the modelling procedure

The catchment scale simulations followed a nested modelling approach, starting from a regional flow model to cut-outs at catchment and sub-catchment scale (Figure 20). All input data were inherited from the previous model (Figure 21).

1. Regional flow model: A regional model served as a base for delineation of catchment boundaries and provided the necessary boundary conditions (constant head boundaries) needed for the following sub-models.
2. Catchment model (Schaugraben P5 catchment): The catchment model is the first cut-out of the area and covers the catchment area of the Schaugraben at the gauging station P5. Regional soil simulations as well as conservative and reactive nitrogen transport were combined at this scale, focussing on interactions between spatial distribution of N-sources and N-discharge into the surface water system.
3. Subcatchment model: The subcatchment model considered a smaller cut-out located within the catchment model. The simulations runs were identical to the simulations of the Schaugraben P5 catchment. However, on this scale a finer grid resolution was used.

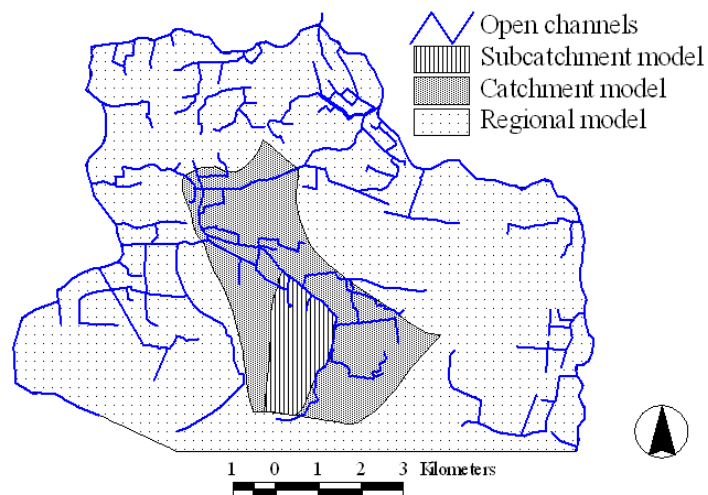


Figure 20: Nested modelling domains

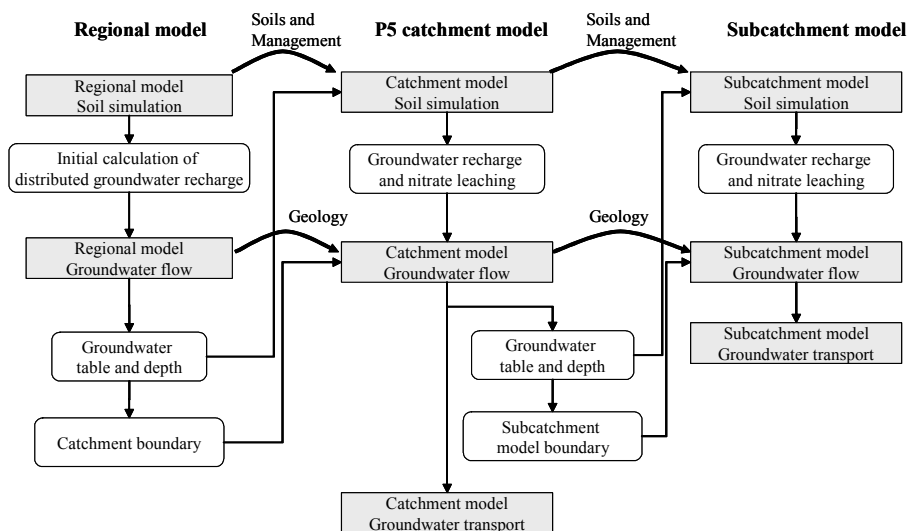


Figure 21: Data inheritance between the nested modelling domains

4.7.2 Simulation of groundwater recharge and nitrogen leaching at the catchment scale

4.7.2.1 Climatic data

Climatic data were taken from the UFZ Lysimeter station in Falkenberg and the climatic station in Seehausen, operated by the German National Meteorological Service (DWD). Both stations are located approximately 15 km north of the study area. Potential evapotranspiration was calculated according to the Penman-Wendling Method described in DVWK (1996). In periods where global radiation was not measured, radiation data were calculated from sunshine duration according to DVWK (1996).

4.7.2.2 Soil data

The soil map of the Schaugraben area is based on the Soil Map of the GDR 1:50000 (MMK 50). About 14 soil units are mapped in the Schaugraben catchment area (see appendix A). For areas outside the catchment area, the distribution of soil units was extrapolated based on the given soil and geological information (distribution of sandy and loamy areas).

Schwartz (1999a, 1999b) characterized physical and chemical characteristics of 6 soil profiles representing typical soil types. Due to the simplified structure of the mRISK-N model, observed soil profiles could not directly be transferred into the model. On the one hand, experimental data had to be averaged to match the soil discretisation of the model, on the other hand, only 6 profiles were given representing soils in a highly heterogeneous area. Thus, soil parameterisation was based on mapped soil units and pedotransfer functions using textural classes.

For the mRISK-N model soil profile information needed to be much more simplified, as only two model horizons cover the soil layer. From the TGL 2400 classification a sequence of substrates and the substrate depths were derived for each soil type. Substrate parameters as pore volume, field capacity, wilting point and hydraulic conductivities were derived using pedotransfer functions according to Kainz and Hartmann (1997) and AG Boden (1994) (KA4).

Mineralisation parameters were set as follows: 0.01064 1/d for the rapid mineralisation rate constant, 0.00405 1/d for the slow mineralisation rate constant (see chapter 5.1). The default denitrification rate constant was set to 0.0001 for all horizons (low denitrification). For soils rich in organic matter (humic gleysols etc.) higher values were assigned to the upper and lower root zone to account for increased availability of organic matter. Upper root zone denitrification rate constants were set to 0.004 for mollic and humic gleyic soils, 0.002 for gleyic soils, 0.001 for luvisols and 0.0001 for sandy cambisols. According to the results of the sensitivity analysis of the mRISK-N model (5.1.1), these values should account for denitrification rates of approximately 20, 15, 10 and 1 kg N/ha/a. Denitrification rate constants for the intermediate vadose zone were set to the default value for all soils.

Soil properties defined for the specific soil units are given in appendix A.

4.7.2.3 Landuse data and management practices

Management records to be used with the mRISK-N model include plant specific data such as N-uptake, root depth and leaf area index as well as management data on fertilizer input on a monthly basis.

Landuse data and management practices of the Schaugraben catchment have been surveyed by the UFZ Lysimeter station in Falkenberg since 1990. The data include site specific information on crop, yield, mineral and organic fertilizer and irrigation. A first survey covered the period of 1990 to 1997. A second survey was made in 2002 to complete the management data. Both surveys included crop cultivation only. The management data were implemented into a database for the CANDY-model (Franko et al., 1995) and serve as a base for the mRISK-N simulations as well. Crop specific data such as specific N-uptake or rootdepths were taken from the CANDY-database. The CANDY-database was cross-checked to data provided by official fertilizing guidelines (DVO-SA) and no considerable differences were found. Crop yields and net plant uptake by harvest were partly completed with annual statistics for Saxony-Anhalt provided by STATLA-SA.

Data were missing for various fields in the first or second survey. The corresponding management records were completed by the total monthly averages of surveyed plant and management data.

A management record for grassland areas was developed by the UFZ Lysimeter station in Falkenberg, based on information of local farmers (total living stock per grassland area), and literature data on excretion and N-content (Faustzahlen für Landwirtschaft und Gartenbau, 1993). Plant parameters and fertilizer input were assigned according to corresponding grassland lysimeter records. Nitrate fluxes due to grazing were considered as follows: The cooperative in Erxleben has a life stock of 560 cows and a pasture area of 520 ha. Within a grazing period of 5 months from Mai to September each plot is grazed for approximately 100 days per year. The following N-fluxes can be calculated (data taken from Faustzahlen für Landwirtschaft und Gartenbau, 1993):

Input of urea: 15 kg urea/cow/d, N-content 1% = 16 kg N/ha/a (3.2 kg N/ha/month)
Input of manure: 25 kg manure/cow/d, N-content 0.3% = 8 kg N/ha/a (1.6 kg N/ha/month)
Uptake by grazing: 40 kg grass/cow/d, N-content 0.5 kg N/dt Grass = 21.5 kg N/ha/a (4.3 kg N/ha/month)

The forest management records generated for the mRISK-N model include deciduous, coniferous and mixed forest. It was assumed that the root zone extends to a maximum depth of 2 m. Monthly

leaf area indices were assigned according to DVWK (1996) for each forest type. Nitrate uptake rates of forest areas are less readily available than for agricultural areas and difficult to compare, due to the different approaches and methods applied. Literature data given by Verburg and Johnson (2001), Matzen (1988) in Verburg (2001), Thomas and Büttner (1998), Rytter (2001), Watmough and Dillon (2003) suggest net uptake rates in the range of 7-17 kg N/ha/a, and gross uptake rates range between 56 and 193 kg N/ha/a (see also summary in Appendix A). Nitrogen fluxes were set equal for all forest types. A net nitrogen uptake of 10 kg N/ha/a was considered as difference between total uptake and residue production, in accordance with the literature values cited above. Total N-uptake was set to values of 150-190 kg N/ha.

The surveyed area covers only a part of the regional model domain and is also not identical to the model domain of the P5 catchment simulation. For areas outside of the surveyed area, distribution of cropland, grassland and forest was derived from the topographical map 1:25000. Management of cropland areas outside the surveyed areas was defined by average monthly plant and management data. (However, for the extended study area groundwater recharge was simulated only.)

4.7.2.4 Atmospheric deposition

The atmospheric N-deposition includes gaseous, particular and dissolved components, such as NO_x , NH_y , organic N-compounds, NO_3^- , NH_4^+ . According to Böhme and Russow (2002), conventional sampling methods such as wet-only and bulk samplers allow the analysis of Ammonium and Nitrate input only and neglect gaseous deposition and input of organic N-compounds. With the newly developed ITNI (Integral Total Nitrogen Input)-Method they were able to determine atmo-genous N-deposition rates of 46-74 kg/ha/a for Sachsen-Anhalt, compared to values of 30-35 kg/ha/a based on bulk sampler measurements. They also point out, that gaseous deposition is at least partly an active plant uptake process. These findings are supported by long time fertilizing experiments. Merbach (2002) could quantify the total N-deposition using the reference-fields (without fertilizer addition) of the static and extended static fertilizing experiments in Bad Lauchstädt, with a mean of 52 kg/ha/a. They also found that the total atmo-genous N-deposition is plant specific. Similar results were found in long time fertilizer experiments in Ascov(Danmark) and Rothamstedt (Great Britain) (Christensen, 1989; Poulton, 1996, both cited in Merbach, 2002).

According to these findings, bulk deposition underestimates the total atmo-genous N-deposition. Gaseous deposition is at least partly an active and plant specific process. Conventional methods do not allow a secure estimation of total N-deposition. Bulk deposition observed at the UFZ Lysimeter station in Falkenberg is low with a mean annual N-Input of 12 kg N/ha (Range 5.7-31.1 kg N/ha, data from 1991-2000, UFZ Falkenberg), currently there are no measurements of total N-deposition using long-term experiments or the ITNI- method available. For soil simulations an atmospheric deposition of 60 kg N/m² was used as a worst case scenario.

4.7.2.5 Initial conditions

Initial conditions for organic N contents were generated by subsequent simulation runs approaching equilibrium conditions. This procedure also provided an initial state of soil water content.

4.7.2.6 Setup of model runs

Distributed soil simulations were based on the mRISK-N model, using the RISKREGIO-processor for data organisation and extraction of model results. Climatic data, management records and soil data were defined in the corresponding mRISK-N input files. In order to simplify data transfer from the soil to the groundwater model, all distributed input data and simulation runs were based on a grid structure consistent with the groundwater model grid. Soil map and landuse distribution were converted into grid format from polygon coverages. Groundwater depths were calculated directly from an initial groundwater flow simulation as difference between observed groundwater head and surface elevation.

For the extended study area (regional simulation), only soil water balance was calculated. On

catchment scale, four simulations were defined combining distributed and uniform groundwater depth and uniform and soil specific denitrification rates (Table 13). This approach allowed to evaluate the effect of a distributed groundwater table and vadose zone transport and turnover, considering uniform and soil specific assignment of denitrification rate constants. The uniform groundwater depth was set to a value of 2 m. The uniform denitrification rate constant was set to the default value 0.0001 1/d (=very low denitrification). Simulation 3, which considers soil specific denitrification and distributed groundwater depths, provides the input data for subsequent groundwater simulations and was also used in the regional (no evaluation of N-dynamics here) and in the subcatchment simulation.

Table 13: Definition of distributed soil simulations for the P5 catchment model

Simulation	Groundwater depth	Denitrification	Comments
1	Constant (=2m)	Soil specific	
2	Constant (=2m)	Default (0.0001 1/d)	
3	Distributed (0.0-7m)	Soil specific	Reference simulation for groundwater simulations
4	Distributed (0.0-7m)	Default (0.0001 1/d)	

4.7.3 Regional groundwater flow modelling

4.7.3.1 Model Setup

The model domain extends to the rivers surrounding the Schaugraben catchment in order to get suitable boundary conditions and to minimize the effect of uncertainties in model boundaries on groundwater flow and head distribution in the catchment area. The northern margin of the modelling domain was defined by the Biese-river, the eastern margin by the Uchte-River. The westerly margin is defined by the drain channel "Kleiner Markgraben". The southern margin is not defined by drains or river systems or watersheds and was placed arbitrarily as a cut through the area well off the Schaugraben catchment.

The model grid for the flow model was discretized into cells of $dx=dy=100m$ and into 6 layers of varying thickness between 4-8 m. Courses of drain channels and rivers and their water stages as well as surface elevations were taken from the topographical maps 1:10000 and 1:25000. A surface elevation model was compiled from digitized contour lines and point elevations. All channels and rivers within the model domain and at the model boundaries were included as a general head boundary using the Modflow drain-package. The northern, eastern and western model boundaries were considered as no-flow boundaries. As the southern boundary was not defined by natural boundaries (surface waters, flow paths or watersheds), an exchange of water across this boundary had to be allowed in order to retain the natural flow system. The boundary was defined as a constant head boundary, with head elevations interpolated from groundwater head observations at selected observation wells. Recharge fluxes were assigned separately for the sensitivity and calibration studies. They will be defined in the corresponding chapters.

A hydrogeological model defining subsoil substrate distributions was constructed from the available borehole profiles. Borehole descriptions were provided by the Geological Survey of Saxony-Anhalt. They include borehole profiles of the geological map GK 1:50000 Osterburg as well as borehole profiles from commercial drillings for wells within the study area and give information on substrate types and depths. Most wells extend to a depth less than 10 m below surface, only a few wells extend to the second aquifer or deeper (see appendix A). The vertical extent of the model domain was defined by the soil surface and a clay layer below the main aquifer. Borehole information was sufficient to give a general overview of the general geological situation in the study area, but on the other hand was too sparse to allow a detailed classification of substrate types or an exact location of substrate boundaries. Although the preprocessing software GMS provides a variety of tools for spatial interpolation and development of geological models, they could not be applied in a reasonable fashion with the data on hand. Thus, the geological model was constructed by simple linear interpolation of substrate boundaries between boreholes. The substrate information was reclassified into three materials only: upper sand, glacial till and deep sand. "Upper sand" and "deep sand" consider all materials with sand as the major component, whereas "glacial till" involves

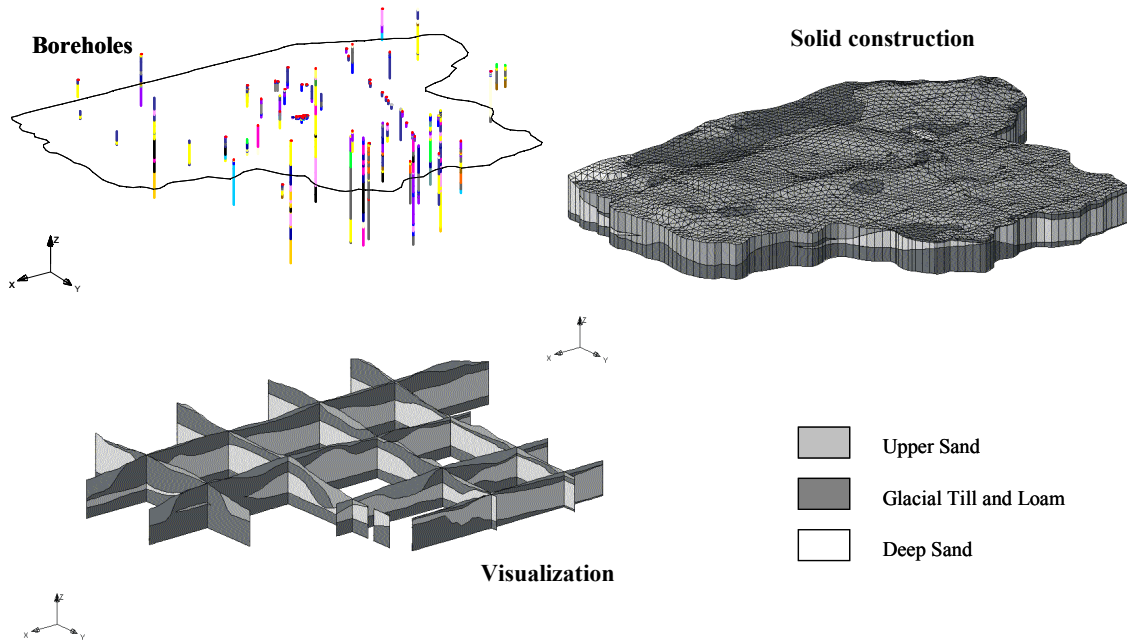


Figure 22: Derivation of the hydrogeological model

the major substrate classes Silt, Loam and Clay. The upper and lower boundaries of the materials were defined by linear interpolation between borehole contacts. These boundaries were used for construction of a set of three dimensional geometrical bodies (solids) representing substrates in the modelling domain. The creation of solids allows definition of substrate bodies independent from the specific model grid, thus one geological model can be used for the generation of various submodels of different extent or grid resolution (Figure 22). Conductivity values were based on parameter ranges given by Dyck and Peschke (1995). Initial saturated conductivities were set to 6 m/d for upper sand, 6 m/d for lower sand and 0.2 m/d for glacial till. The substrate classes and boundaries defined in the hydrogeological model were then transferred to the model grid of the regional groundwater flow model.

Groundwater levels were provided as time series for the period of 1990-2001 by STAU (Environmental protection agency of Saxony-Anhalt) for various groundwater observation wells of the extended study area (see appendix A). Mean groundwater stages were calculated from the varying time series as reference data for the steady state flow model. The initial groundwater surface was compiled from average groundwater levels and surface water stages.

The flow simulation was carried out as a steady state simulation, using constant boundary conditions.

4.7.3.2 Sensitivity analysis of the regional flow model

A sensitivity analysis was carried out to investigate model response to changes of hydraulic parameters. Distributed groundwater levels and seepage fluxes to the Schaugraben channel system were used as observations. Variation parameters were hydraulic conductivity of all three substrate classes and drain bed conductivity. Substrate conductivities were changed by 10% to the initial value and the 10%-elasticity index e_{10} was calculated as sensitivity measure. Drain bed conductivity showed no effect when changed by 10% only and was varied over specified values of 1, 4, 40 and 400 $1/m^2$. Groundwater level sensitivity was evaluated on a cell-by-cell base, giving the spatial distribution of groundwater sensitivities. The sensitivity analysis was carried out as an exploratory simulation before the distributed soil simulation the calibration of the regional flow model. A uniform groundwater recharge of 100 mm/a was applied to the model domain in accordance to observed lysimeter fluxes.

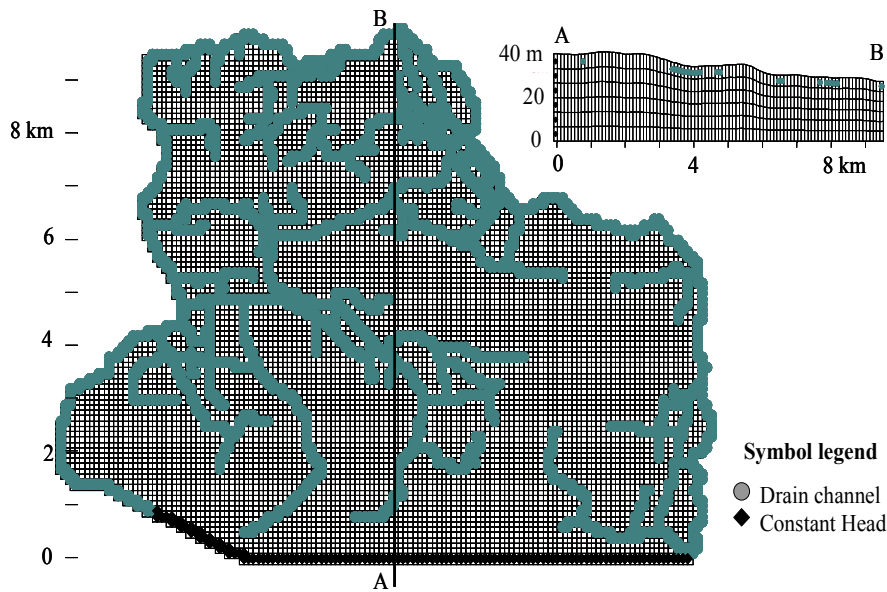


Figure 23: Regional flow model – Boundary conditions and model grid

4.7.3.3 Calibration of the regional flow model

For model evaluation mean groundwater levels of observation wells within the model area were used together with observed discharge fluxes of the “Schaugraben” drain. The groundwater flow model was manually calibrated by sequentially varying conductivity parameters. As model performance measures mean error (ME), mean absolute error (MAE) and root mean squared error (RMSE) of groundwater level observations were used together with seepage flux into the channel system; which was compared to a reference discharge at gauging station P5. A mean recharge flux of 83 mm/a was calculated from the regional soil simulation over a period of 13 years. The theoretical discharge at gauging station P5 is 52.6 l/s (=83 mm/a). Discharge observations at gauging station P5 were given from 1997-2001, but contain only 4 complete years of observation. A reference discharge was calculated by scaling the observed discharge by the ratio of average recharge over 13 years to average recharge during years with discharge observations (see Table 14). This method yields a reference discharge of 43.9 l/s (69 mm/a).

As the theoretical discharge was not observed and the scaled reference discharge might be rather uncertain, both discharge values were considered to define a range of reasonable discharge values. The target discharge was set halfway between these values to 48.3 ± 4 l/s (76 ± 7 mm/a).

Table 14: Calculation of reference discharge fluxes

Lysimeter year	Simulated recharge [mm/a]	Observed discharge [l/s (mm/a)]
1997	23	28.7 (45)
1998	178	91.2 (144)
1999	74	50.1 (79) (incomplete data)
2000	77	50.1 (79) (incomplete data)
2001	165	64.1 (101)
Mean	103 (average between 1997-2001)	56.8 (90)
Reference 1	83 (average over 13 years)	52.6 (83)
Reference 2	Scaling ratio = 83/103	43.9 (69)

4.7.3.4 Delineation of the Schaugraben catchment

With the final simulation of the calibration run, a particle tracking simulation was carried out using MODPATH (Pollock, 1994) in order to evaluate the catchment boundary of the Schaugraben drain at gauging station P5. Particles were placed in each grid cell on top of the water table. Catchment boundaries were determined by analysis of flow paths and watersheds.

4.7.4 Groundwater modelling on catchment and subcatchment scale

4.7.4.1 Model setup and flow simulation

At the beginning of simulation runs, it was not clear, if the reaction-module could be run with the grid resolution and time steps defined for the catchment model. For practical reasons, a reduction of time steps or cell-size was not possible. In case of failure of the reaction-module, only simulation of conservative transport would be possible. Thus simulations were prepared for two model domains, a catchment model (P5 catchment) and a three-dimensional cut-out of the catchment, which could be run with a smaller grid resolution. The definitions of flow and transport simulations were identical in both model domains.

The catchment scale submodel was derived from the regional flow model. The calculated groundwater levels and flows allowed identification of groundwater surface and flow directions. The model domain was based on the catchment area of the Schaugraben drain channel at gauging station P5. A particle tracking simulation using MODPATH (Pollock, 1994) allowed an exact identification of watersheds and was used to define the catchment area (see chapter 4.7.3.4 and Figure 24). Boundaries parallel to pathlines (to the north, east and west of the catchment) were defined as no-flux boundaries. The watershed at the southern margin was defined as a constant head boundary. This was necessary, as the model boundary does not necessarily coincide with the watershed in deeper layers, due to its three dimensional nature. A specific exchange flux forced by the observed groundwater head distribution is necessary, to retain the natural flow system. It was observed in exploratory model runs, that a no-flow boundary may result in flooding of the area or levelling out of the groundwater surface. North of gauging station P5, the model domain extends across the catchment boundary. This extension allowed i) to place a constant head boundary at the model outlet ii) to include deep groundwater pathlines, which cross the Schaugraben drain and leave the area on a subsurface flow path.

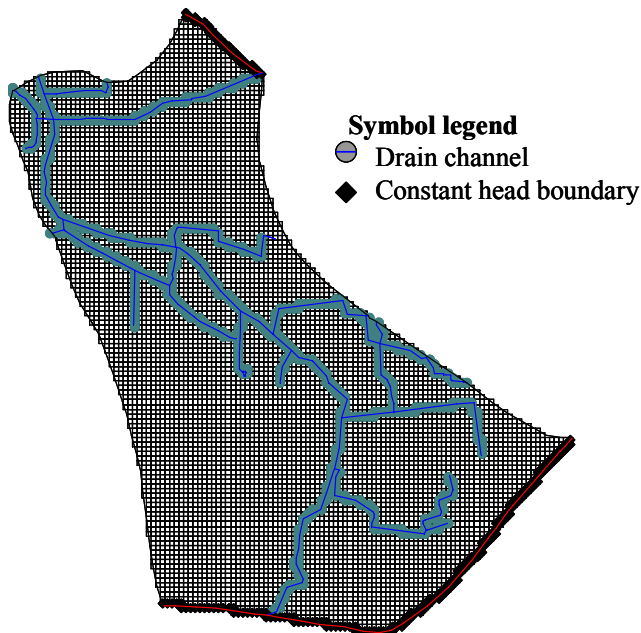


Figure 24: Boundary conditions and model grid of P5 catchment model

The subcatchment is of triangular shape, with two sides being defined as a closed boundary following flow pathlines and a drain defined as constant head boundary in the first layer at the other side of the triangle (Figure 25). Initial and boundary conditions as well as substrate properties were inherited from the P5 catchment model by regional to local model conversion. Cell-sizes were decreased to $dx=dy=10m$. All landuse classes (grassland, cropland, forest and settlement), are present within the cut-out. Groundwater depths range between 0.75 m close to the drain and 6 m at the opposite edge of the model domain.

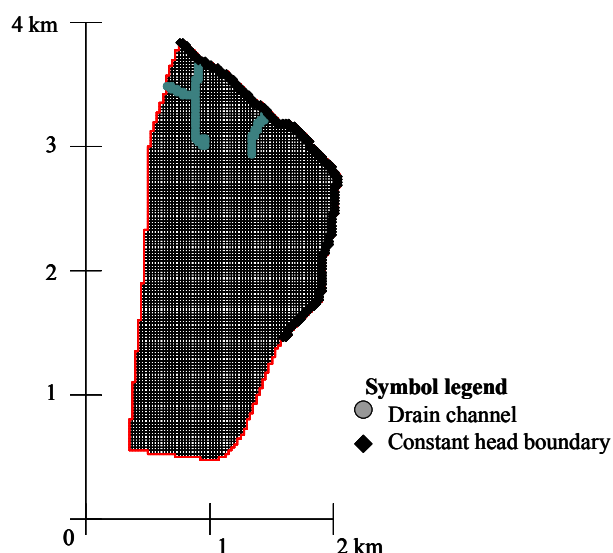


Figure 25: Subcatchment model - Boundary conditions and model grid

The GMS-software facilitates a regional to local model conversion, where all information concerning substrate boundaries, hydraulic properties, initial and boundary conditions and grid definitions are automatically transferred to the new submodel. Thus, all input data are inherited from the regional model. During regional to local model conversion, all layers were subdivided in two layers and grid resolution was increased to $dx=dy=25m$.

Groundwater recharge and nitrate leaching were re-calculated with the mRISK-N model using the same input data as for the regional model, but with increased spatial resolution. All other model parameters are identical to the regional model. The simulated groundwater recharge was then used, to calculate a steady state solution of groundwater flow for the P5-catchment model and the subcatchment model.

4.7.4.2 Transport scenarios

The chemical properties used in the transport simulations were defined as follows: A background content of 0.01 Mass-% (500 mg/l_{H_2O}) of organic matter was assumed in all layers. As soils in the area are predominantly gleyic soils with high content of organic matter, the content of organic matter was modified in the upper layer as follows: In the first layer, a background concentration of 0.1 Mass-% (5000 mg/l) was assumed. If groundwater depth was below 2m, cells with high contents of organic matter representing peat or humic gleysols were placed randomly with a probability of 0.1 (10%). In these cells, SOM-content was set to 10 Mass-% (500000 mg/l_{H_2O}), if groundwater depth was lower than 1 m and to 1 Mass-% (50000 mg/l_{H_2O}), if groundwater depth was between 1 and 2m. This depth dependent setting was made in order to account for interaction between humic soil layers and groundwater table dynamics, assuming that humic layers of gleyic soils or peat formations do not extent to greater depths. As no experimental data were available describing rOM leaching from the soil, rOM input to groundwater was compiled as follows. The initial soil leachate concentration was set to 30 mg/l . An exponential decay in the vadose zone was applied with a half depth of 1m. This yields a concentration of 7.5 mg/l in a depth of 2m. This concentration corresponds to groundwater concentrations at the experimental site, which have a median DOM concentration of 15 mg/l , assuming that half of the DOM belongs to the reactive fraction rOM. Following this approach, only locations with high groundwater tables (humic and

gleyic soils) receive considerable loads of organic matter from the soil. Initial concentrations of reactive organic matter in the groundwater were set to a value of 3 mg/l. This concentration (approximately 1%-quantil of observed rOM concentrations in shallow groundwater) was set arbitrarily, as experimental data, especially for deep groundwater were lacking. During the simulation run, this concentration will be modified by i) input from recharge and ii) release from SOM. A constant pyrite content of 0.002 Mass-% (100 mg/l) was assumed for all layers but the first. Observed sulfate concentrations were about 150 mg/l. These high concentrations have to be considered as a result of pyrite oxidation processes, which are to be simulated by the model. Thus the initial concentration for the simulation was set to a lower value of 10 mg/l. For reactive transport simulations, reaction-module B (first-order approaches) was used, the reaction constants were set to standard values as defined in Table 5.

In order to investigate interactions between spatial distribution of N input to groundwater and N-discharge to surface waters, distributed groundwater recharge and N-leaching taken from the soil simulation were simplified in two steps. Starting from the initial, distributed input-scenario, in a first step recharge and N-leaching were classified by landuse type (grassland, agriculture and forest) and in a second step, uniform recharge and N-leaching was applied. This approach leads to a stepwise loss of spatial information while at the same time total recharge and N-leaching to groundwater are preserved. Additionally, the effect of buffer stripes was investigated. For the subcatchment model, all drains were buffered by buffer stripes with a width of 50, 100 and 200m, for the catchment model only one buffer of 100m width was applied. In these areas, N-load was set to zero and recharge was set intermediate between recharge from forest and grassland areas. These settings are based on the assumption, that no leaching of nitrate occurs due to effective plant uptake, soil storage and denitrification and vegetation of the buffer areas combines open and forested patches or bush-land. The corresponding simulation scenarios are summarized in Table 15. For each scenario, a steady state flow simulation, a reactive transport simulation and a conservative transport simulation were calculated. Transport was considered as advective transport only. Dispersion was not considered explicitly. A setting of appropriate dispersivities would be rather uncertain, as the dispersivity value of a porous medium depends on aquifer heterogeneity and on the integral transport scale (Gelhar et al., 1992; Kinzelbach and Rausch, 1995). Dispersivity also accounts for unknown heterogeneity in the aquifer. Therefore, the density of information affects the dispersivity value as well (Chiang et al., 2002). However, some dispersion will be introduced by the effect of numerical dispersion.

Table 15: Simulation runs defined for catchment and subcatchment scale transport simulations

Simulation 1.1 "Distributed landuse"	Groundwater recharge and nitrate leaching were taken from the distributed RISK-N simulation as cell means over the simulation period. This simulation represented actual land-use and management patterns.
Simulation 1.2 "Classified landuse"	Landuse distribution classified by actual land-use into cropland, grassland, forest and settlement. Mean recharge and N-loads per land-use class were assigned as calculated from the distributed soil simulation.
Simulation 1.3 "Uniform landuse"	Uniform recharge and N-Load were supplied as means over the total study area.
Simulation 2.1-2.3 "Implementation of buffer stripes"	All drain channels were buffered by a buffer area of 100m width for the catchment model and 50, 100 and 200m width for the subcatchment model.

4.7.4.3 Data Analysis

The groundwater model yields fluxes and substance concentrations for each cell at specified times. Results were given after 1,2,4,7 and 10 years and in 10 years intervals thereafter. For each drain-cell seepage fluxes (Q) and solute concentrations (C_i) were extracted and solute loads were calculated according to the equation

$$L_i(x, y, t) = Q(x, y, t) \cdot C_i(x, y, t)$$

where L = load [g/d/cell], Q = seepage flux [m³/d/cell], C = solute concentration[mg/l=g/m³], i = solute index, x and y = cell indices, t = time step.

Summarizing all fluxes and loads for the total channel system, yielded total seepage fluxes (Q^T_i), total loads (L^T_i) and average seepage concentrations (C^T_i):

$$Q^T(t) = \sum_{x=1}^n \sum_{y=1}^m Q(x, y, t) \quad L_i^T(t) = \sum_{x=1}^n \sum_{y=1}^m L_i(x, y, t) \quad C_i^T(t) = \frac{\hat{L}_i(t)}{\hat{Q}(t)}$$

The simulation results were evaluated as

- Cell based average seepage fluxes and concentrations as a grid map at the end of the simulation run (where maximum concentrations are reached)
- Total fluxes and concentrations of the channel system (referred to sampling station P5 or the channel system of the submodel) as function of time (graph)

Additionally, the development of subsurface solute concentrations of nitrate, pyrite and OM were exemplified on a cross-section cutting the model domains for selected simulation times.

5 Results and Discussion

5.1 Soil water and nitrogen modelling with lysimeter data

5.1.1 Results of lysimeter sensitivity analysis

The results of the 10% elasticity analysis are similar in all four simulation runs. Thus they are exemplified by results of Lysimeter 03 (grassland on sandy loam). Sensitivities for all lysimeter simulations are given in the appendix A.

Actual evapotranspiration and groundwater recharge are mostly influenced by field capacities and reduction points of the upper and lower root zone (Figure 26 and Figure 27). There is no effect of saturated conductivities and only a small effect of interception and infiltration storage capacity. The sensitivities of evapotranspiration are reversed to recharge. Mineralisation and nitrification depend on field capacity and reduction point in the upper root zone and, to a smaller degree, on mineralisation rate constants (Figure 29 and Figure 30). Nitrification directly depends on mineralisation, which provides ammonium for the nitrification process. Denitrification (Figure 31) is sensitive to a variety of parameters, such as pore volume, field capacities, reduction point (URZ), denitrification and mineralisation rate constants, indicating the complex interactions between soil water dynamics and reaction characteristics. Denitrification is the only process, in which pore volume is directly considered in the mathematical formulation of the reaction process. Nitrate leaching, as groundwater recharge, is most sensitive to field capacity and reduction point of upper and lower root zone. This indicates the strong dependency of nitrate leaching on the water flux (Figure 28). Other factors are of minor importance.

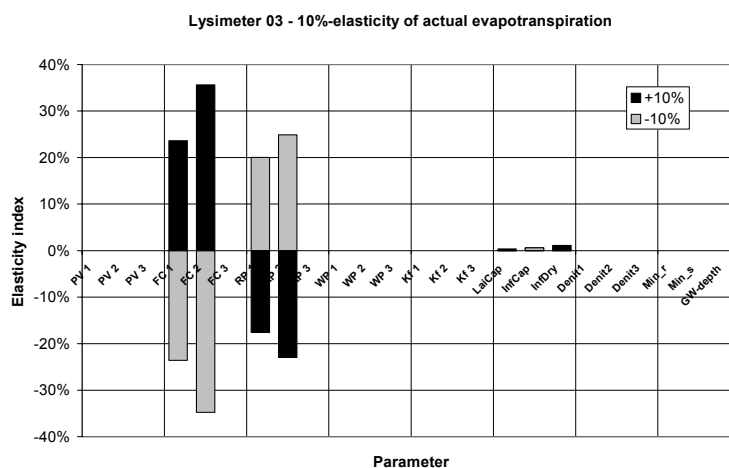


Figure 26: Local sensitivity of annual evapotranspiration to selected parameters

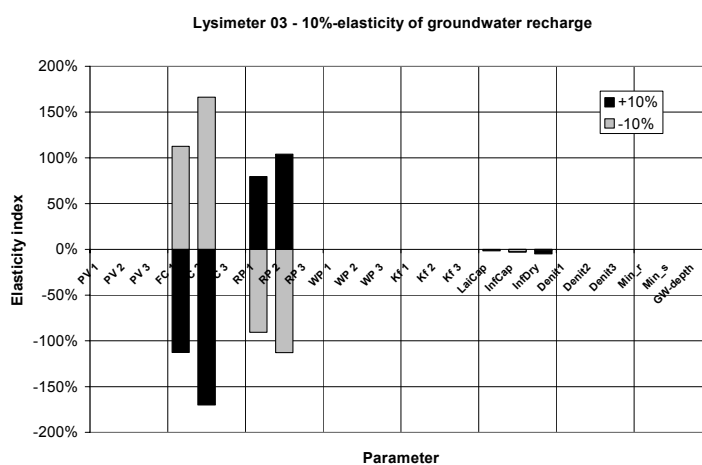


Figure 27: Local sensitivity of annual groundwater recharge to selected parameters

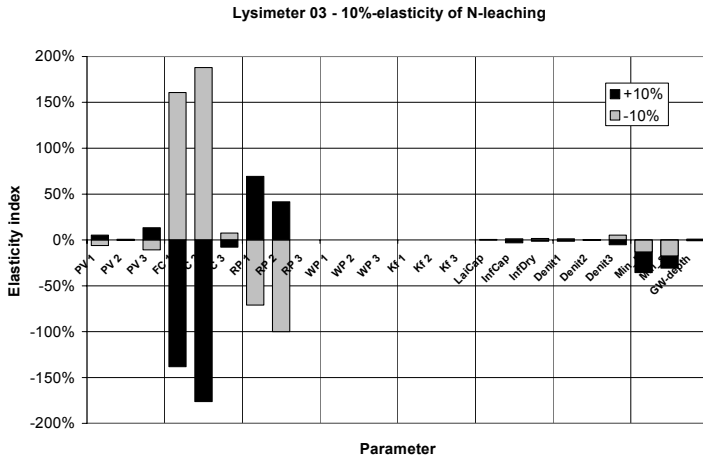


Figure 28: Local sensitivity of annual N-leaching to selected parameters

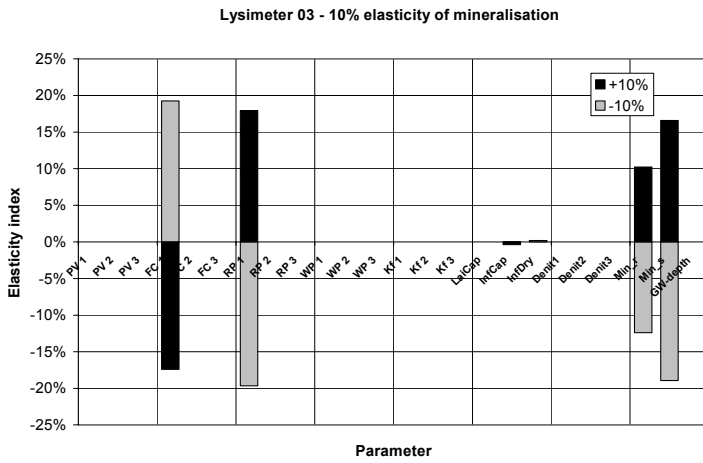


Figure 29: Local sensitivity of annual nitrification to selected parameters

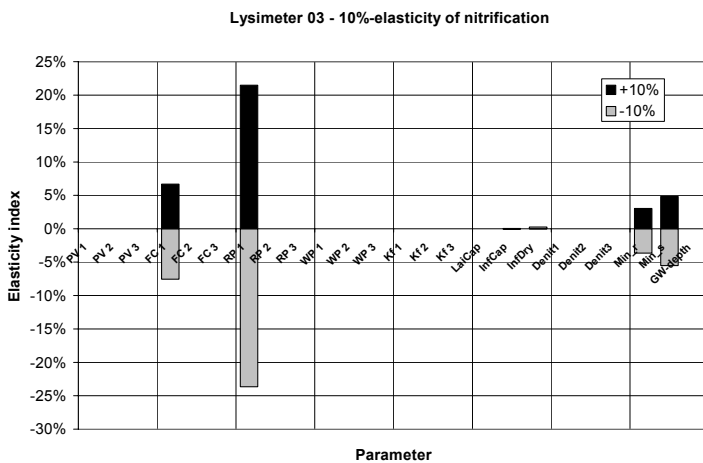


Figure 30: Local sensitivity of annual mineralisation to selected parameters

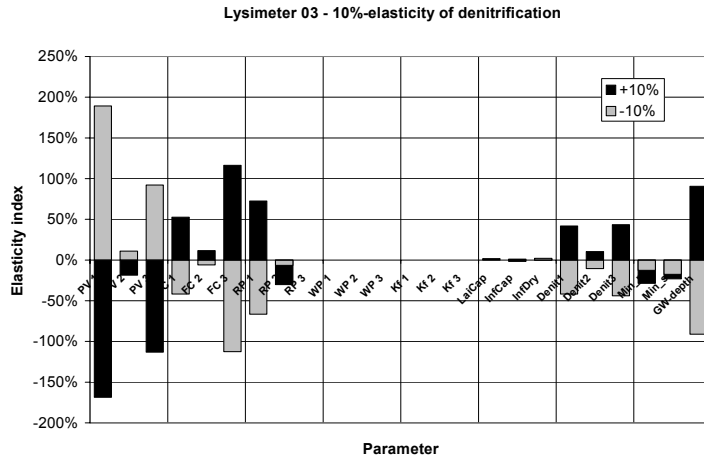


Figure 31: Local sensitivity of annual denitrification to selected parameters

Figure 32 - Figure 39 show the response of groundwater recharge, evapotranspiration, denitrification and N-leaching to the variation of specific model parameters. Groundwater depth (Figure 32) does not effect groundwater recharge, as i) the model does not consider capillary rise and ii) no evapotranspiration takes place in the IVZ. Nitrate leaching increases and denitrification increases with groundwater depth due to longer residence time in the intermediate vadose zone. It can roughly be said that changing groundwater depth by 1m decreases Nitrate leaching by 0.16 g N/m². Variation of field capacity (Figure 35) over a range of 15 Vol-% changes evapotranspiration and groundwater recharge by approximately 0.050 m. The increase in denitrification and decrease in N-leaching is partly caused by the fact that total porosity was kept constant, and modifications of field capacity also changes the soil aeration state. Infiltration storage capacity (Figure 33) has only a weak effect on evapotranspiration and groundwater recharge. Applying values between 0 m and 0.010m causes reduction of groundwater recharge of 0.020 m/a. Leaf storage capacity (Figure 39) and saturated conductivity (Figure 34) have no effect on recharge, evapotranspiration and n-leaching, comparable to the local sensitivity analysis. Varying the slow mineralisation rate constant (Figure 36) over the given range has a stronger effect on mineralisation than varying the rapid mineralisation rate constant (Figure 37) (2.5 g N/m² versus 1.0 g N/m²). The effect on N-leaching, however, is low with changes of 0.5 g N/m² and 0.3 g N/m² over the total range of parameters. Increasing denitrification (Figure 38) causes a reduction of N-leaching.

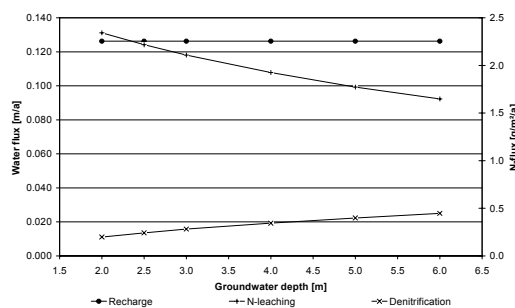


Figure 32: Model response to ground-water depth, Lysimeter 05

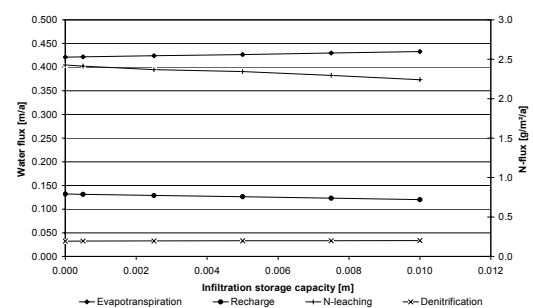


Figure 33: Model response to infiltration storage capacity, Lysimeter 05

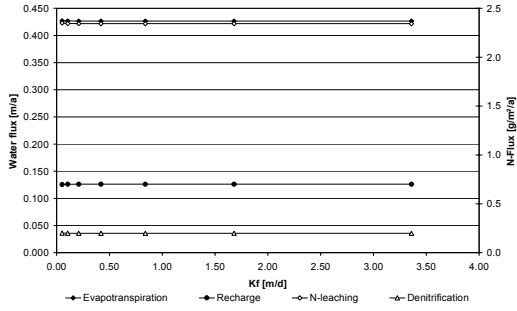


Figure 34: Model response to saturated hydraulic conductivity, Lysimeter 05

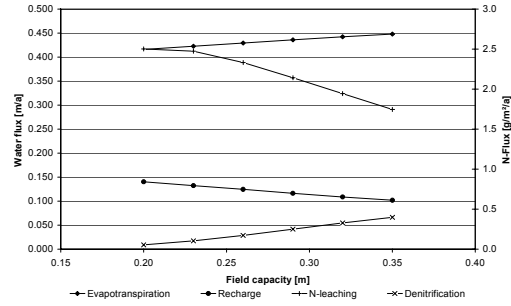


Figure 35: Model response to field capacity, Lysimeter 05

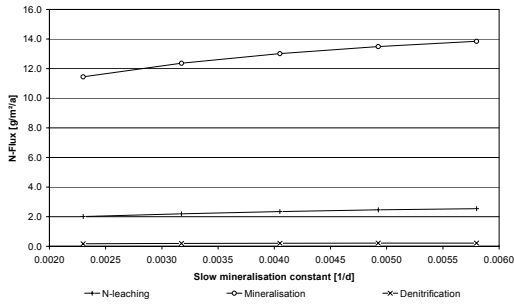


Figure 36: Model response to slow mineralisation constant, Lysimeter 05

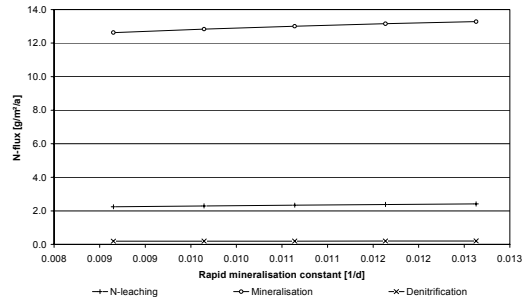


Figure 37: Model response to rapid mineralisation constant, Lysimeter 05

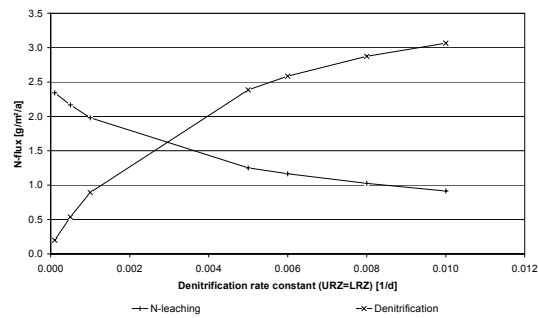


Figure 38: Model response to denitrification rate constant (equal for upper and lower root zone), Lysimeter 05

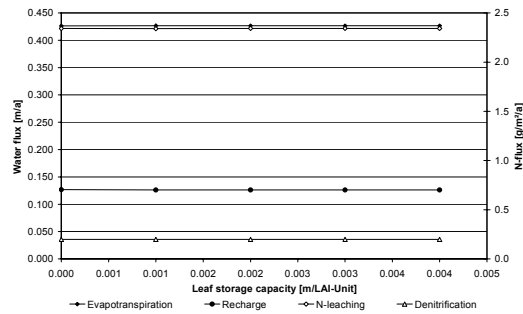


Figure 39: Model response to leaf storage capacity, Lysimeter 05

5.1.2 Calibration and validation of the mRISK-N model using lysimeter data

During the PEST-assisted calibration it was found that after optimisation of field capacities, subsequent calibration of reduction points and wilting points did not change parameter values. All three parameters define the soil water storage available for evapotranspiration and either increase or decrease groundwater leaching. Thus optimisation of field capacities substitutes the effect of the other two parameters. It was also found, that the remaining model parameters were insensitive, as it was expected from the sensitivity analysis. Therefore, calibration of field capacities was sufficient to fit the model to observed data.

An optimisation of mineralisation rate constants did not suggest other rates than the initial ones. The effect of mineralisation rates is too low to change N-leaching rates substantially.

Figure 40 shows the cumulative observed recharge and model results from the two calibration strategies for lysimeter 03. The PEST-assisted calibration results in a significant underestimation of annual groundwater recharge over all years. In order to maintain the observed annual water balance, a second calibration run was carried out manually, aiming at an “optical” fit with the cumulative groundwater recharge curve and annual recharge values.

Model performance was measured as root mean squared error (RMSE) and Nash-Suttcliffe Coefficient of Efficiency.

Table 16 and Table 17 show the corresponding model performance measures for the calibration and validation period for the individual calibration runs. Although groundwater recharge is represented much better by the second calibration strategy (“optical fit”), model performance is worse than in the PEST-assisted calibration, with exception of the lysimeter 04.

The resulting parameter sets of the calibration runs are given in Table 18. In the first calibration procedure (PEST-assistance) storage parameters were heavily modified, whereas during the second calibration run (“optical fit”), the initial parameter set proved to be a good estimate and only few modifications were necessary.

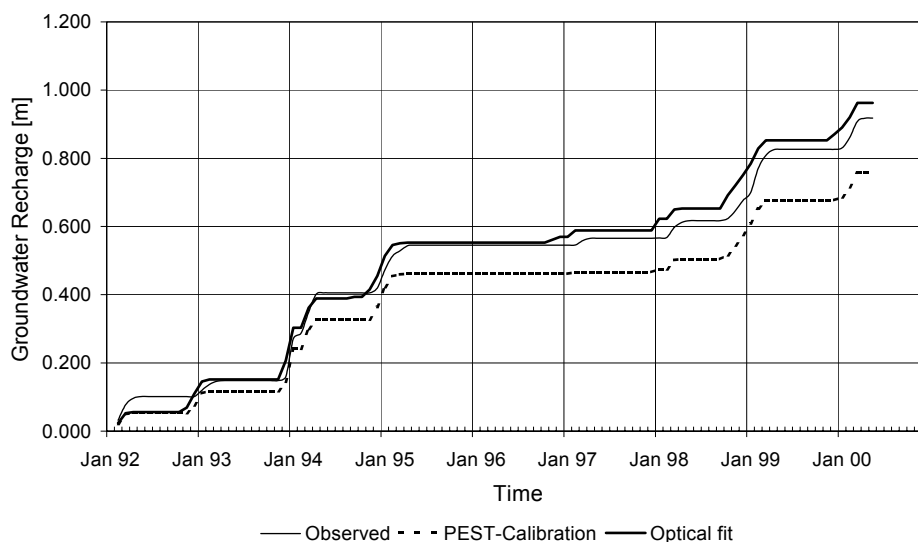


Figure 40: Cumulative groundwater recharge for Lysimeter 03 – observed, PEST-assisted calibration and manual calibration

Table 16: Model performance measures for groundwater recharge (RMSE = Root mean squared error, NS-CoE = Nash-Sutcliff coefficient of efficiency)

Period		Calibration (1990-1996)		Validation (1997-2001)		Total (1990-2001)	
Lysimeter	Simulation	RMSE	NS-CoE	RMSE	NS-CoE	RMSE	NS-CoE
03	Initial	15	0.45	16	-0.22	16	0.25
	C-1	8	0.83	6	0.81	7	0.83
	C-2	11	0.68	11	0.47	11	0.62
04	Initial	15	0.40	17	-0.35	16	0.17
	C-1	15	0.40	17	-0.35	16	0.17
	C-2	10	0.72	11	0.47	11	0.64
05	Initial	13	0.50	14	0.21	13	0.41
	C-1	8	0.81	10	0.55	9	0.73
	C-2	13	0.50	14	0.21	13	0.41
07	Initial	16	0.16	15	-0.15	16	0.06
	C-1	9	0.72	9	0.55	9	0.67
	C-2	11	0.59	11	0.42	11	0.54
53	Initial	16	0.19	15	-0.11	16	0.09
	C-1	10	0.67	10	0.53	10	0.63
	C-2	16	0.19	15	-0.11	16	0.09

Table 17: Model performance measures for nitrate leaching

		Calibration period (1990-1996)		Validation period (1997-2001)		Total period (1990-2001)	
Lysimeter	Simulation	RMSE	NS-CoE	RMSE	NS-CoE	RMSE	NS-CoE
03	Initial	4.8	0.15	2.7	0.38	4.0	0.21
	C-1	4.2	0.34	2.4	0.48	3.5	0.38
	C-2	4.7	0.17	2.5	0.45	3.9	0.25
04	Initial	1.9	0.45	2.8	0.15	2.4	0.30
	C-1	1.7	0.57	2.7	0.23	2.2	0.39
	C-2	1.6	0.60	2.6	0.28	2.1	0.44
05	Initial	8.9	0.24	5.7	0.54	7.7	0.34
	C-1	8.9	0.24	6.7	0.35	8.0	0.28
	C-2	8.9	0.24	5.7	0.54	7.7	0.34
07	Initial	9.7	0.26	4.2	0.61	7.9	0.33
	C-1	0.7	0.12	5.4	0.35	8.8	0.17
	C-2	9.6	0.28	4.4	0.56	7.9	0.34
53	Initial	5.5	-2.39	3.5	0.32	4.7	-0.76
	C-1	1.9	0.60	4.2	0.01	3.1	0.25
	C-2	2.2	0.46	4.0	0.10	3.1	0.25

Table 18: Model parameters (field capacity FC, reduction point RP and denitrification rate constant kden) for initial model run (Initial), for PEST-assisted calibration (C-1) and for manual calibration (C-2), AWC = FC-RP.

Lysimeter	Model run	FC URZ	FC LRZ	FC IVZ	RP UVZ	RP LRZ	RP IVZ	AWC URZ	AWC LRZ	AWC IVZ	kden URZ	kden LRZ	kden IVZ
		[-]	[-]	[-]	[-]	[-]	[-]	[-]	[-]	[-]	[1/d]	[1/d]	[1/d]
03	Initial	0.27	0.22	0.22	0.22	0.18	0.18	0.18	0.17	0.17	0.0001	0.0001	0.0001
	C-1	0.3	0.23	0.22	0.18	0.14	0.13	0.21	0.18	0.17	0.0001	0.0001	0.0001
	C-2	0.27	0.27	0.22	0.22	0.18	0.18	0.18	0.22	0.17	0.0001	0.0001	0.0001
04	Initial	0.22	0.16	0.16	0.18	0.13	0.13	0.16	0.11	0.11	0.0001	0.0001	0.0001
	C-1	0.22	0.16	0.16	0.18	0.13	0.13	0.16	0.11	0.11	0.0001	0.0001	0.0001
	C-2	0.22	0.22	0.22	0.18	0.13	0.13	0.16	0.17	0.17	0.005	0.005	0.0001
05	Initial	0.27	0.22	0.22	0.22	0.18	0.18	0.18	0.17	0.17	0.0001	0.0001	0.0001
	C-1	0.3	0.28	0.22	0.22	0.18	0.18	0.21	0.23	0.17	0.0001	0.0001	0.0001
	C-2	0.27	0.22	0.22	0.22	0.18	0.18	0.18	0.17	0.17	0.0001	0.0001	0.0001
07	Initial	0.22	0.16	0.16	0.18	0.13	0.13	0.16	0.11	0.11	0.0001	0.0001	0.0001
	C-1	0.28	0.28	0.15	0.18	0.13	0.13	0.22	0.23	0.1	0.0001	0.0001	0.0001
	C-2	0.22	0.22	0.22	0.18	0.13	0.13	0.16	0.17	0.17	0.0001	0.0001	0.0001
53	Initial	0.27	0.22	0.22	0.22	0.18	0.18	0.18	0.17	0.17	0.0001	0.0001	0.0001
	C-1	0.34	0.32	0.27	0.22	0.18	0.18	0.28	0.27	0.22	0.0001	0.0001	0.0001
	C-2	0.27	0.22	0.22	0.22	0.18	0.18	0.18	0.17	0.17	0.007	0.011	0.0001

Figure 41 - Figure 46 show annual and cumulative groundwater recharge and nitrate leaching for the lysimeters 03, 05, and 53, based on the second calibration run. The results for the lysimeters 04 and 07 are given in appendix A. The grassland lysimeters 03/04 give the best representation of groundwater recharge, recharge of the cropland lysimeters 05/07 is slightly overestimated in most years. This can be attributed to the definition of vegetation data, which was based on literature values. Grassland vegetation dynamics are more or less similar in all years, whereas crop cultivation is characterized by inter-annual variations and more pronounced seasonal dynamics. A strong overestimation of recharge was found in lysimeter 53. In addition to the more complex dynamics of plant data, these lysimeters were intensively irrigated. Irrigation does not lead to increased percolation and groundwater recharge during summer, calculated recharge, however, shows distinct peaks in the dry period following irrigation. Observed and simulated N-leaching is best represented in Lysimeters 03/04. Due to the insufficient representation of soil water dynamics, Lysimeters 53/54 show stronger deviations than the other simulations. Observed and simulated N-leaching rates stay within the same order of magnitude and roughly follow the same inter-annual dynamics. However, calculated N-leaching rates generally underestimate observed N-leaching.

Monthly recharge rates are shown in Figure 47 for lysimeter 03. Although seasonal dynamics are well reflected, monthly recharge rates show poor coincidence.

Lysimeter balances suggest little or no denitrification at all, consequently low denitrification rate constants of 0.0001 were appropriate to predict nitrate leaching in Lysimeters 03, 05 and 07. Only lysimeter 04 required assumption of denitrification.

The corresponding loamy and sandy lysimeters show similar groundwater recharge and nitrate leaching, thus there were no substantial differences of soil physical parameters to be expected. In fact, although the soils differ in field capacity and wilting point according to their texture, the available water contents do not differ substantially, causing a similar behaviour in the field and in the model. The two sandy soils (04 and 07) run with identical soil physical parameters, whereas small differences are found between the two loamy sand lysimeters (03 and 05).

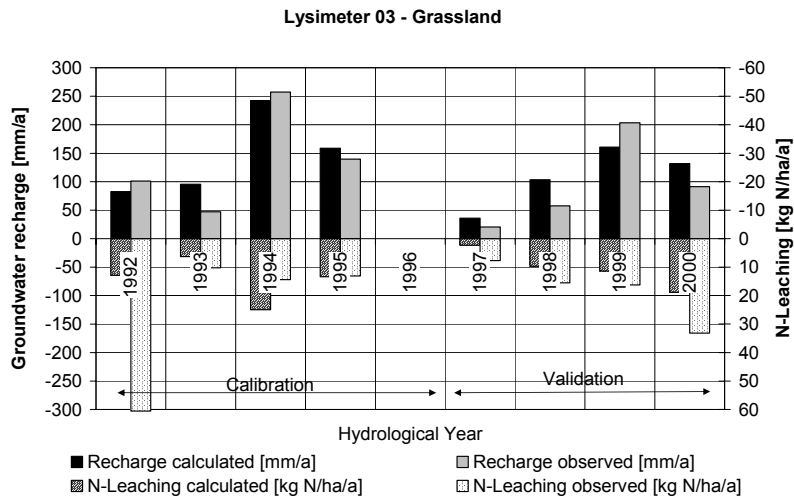


Figure 41: Annual groundwater recharge and N-Leaching of Lysimeter 03

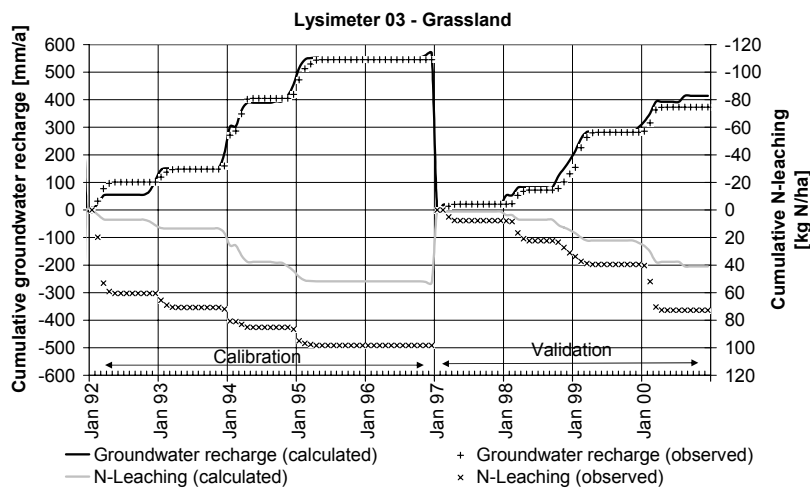


Figure 42: Cumulative annual groundwater recharge and N-Leaching of Lysimeter 03

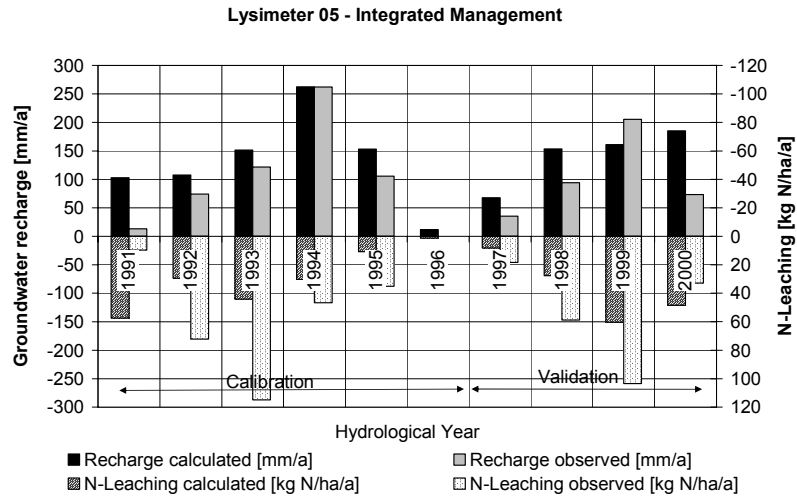


Figure 43: Annual groundwater recharge and N-Leaching of Lysimeter 05

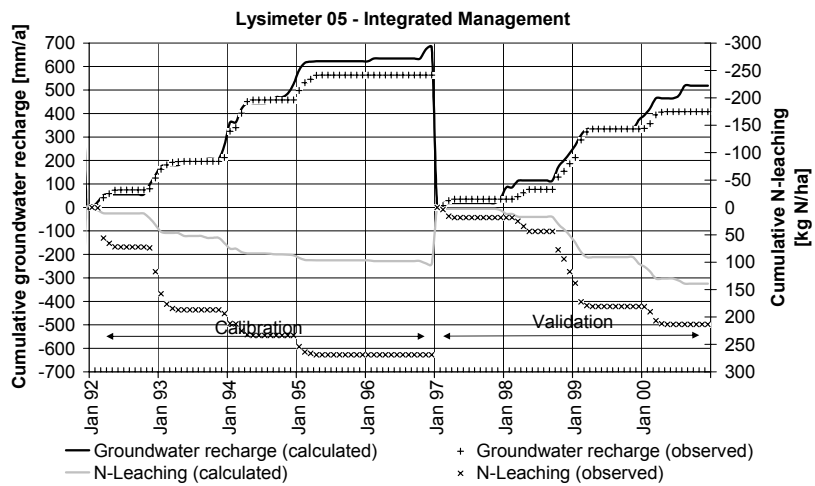


Figure 44: Cumulative annual groundwater recharge and N-Leaching of Lysimeter 05

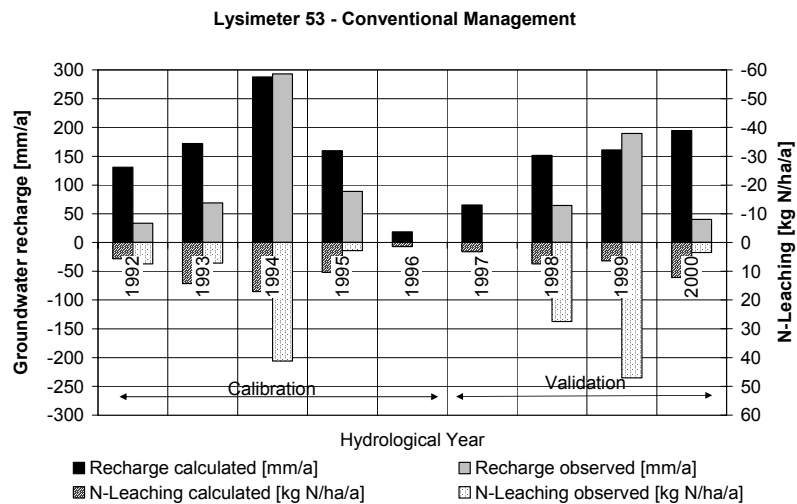


Figure 45: Annual groundwater recharge and N-Leaching of Lysimeter 53

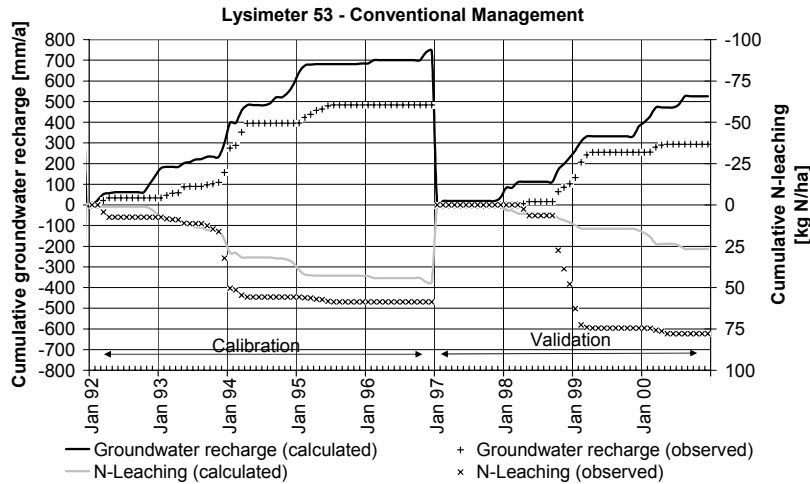


Figure 46: Cumulative annual groundwater recharge and N-Leaching of Lysimeter 53

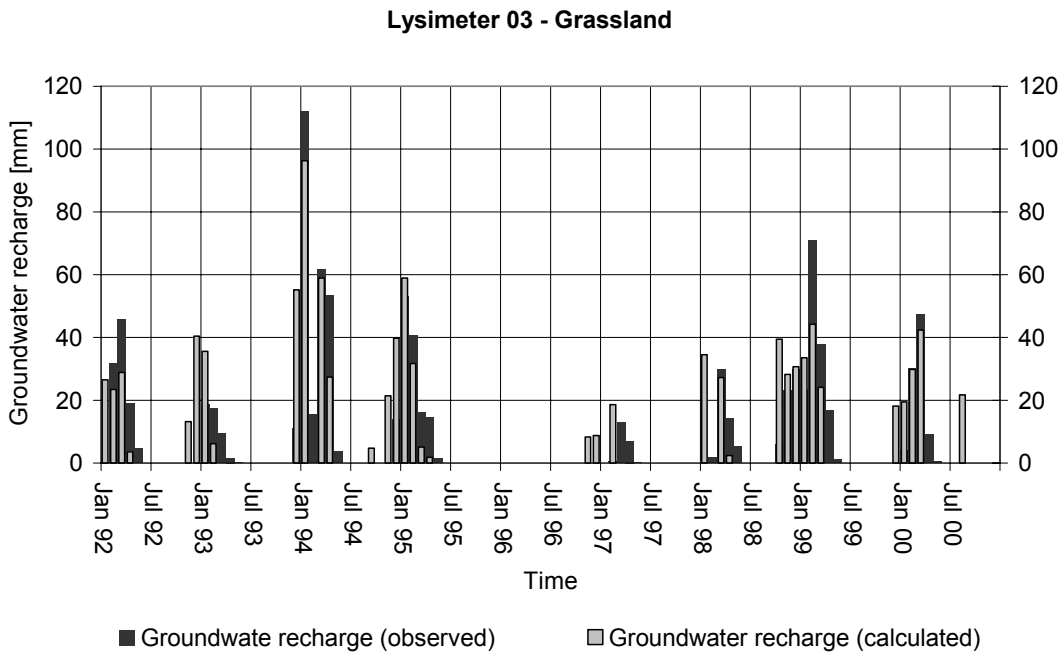


Figure 47: Monthly groundwater recharge of Lysimeter 03

5.1.3 Uncertainty of input data

In contrast to model parameters, which may be calibrated if suitable observations were made, input data are boundary conditions and thus remained unchanged. Consequently, the best possible model fit to observed data is limited by the quality of input data. In this chapter, the attempt is made to estimate uncertainty of selected input data and to compare data accuracy with N-leaching and denitrification rates.

Considering gaseous deposition as an additional component of atmospheric deposition, bulk deposition underestimates total deposition. Literature data indicate total deposition rates between 50-70 kg N/ha/a (Böhme and Russow, 2002, see 4.7.2.4), possibly independent of the bulk deposition rate. The average bulk deposition recorded at the climatic station of the UFZ Lysimeter station in Falkenberg ranges between 6.2 and 31.1 kg N/ha/a ($\mu_{\text{deposition}}=12.5$ kg N/ha/a, $\sigma=8.7$ kg N/ha/a, Data from 1991-2000). Using a total deposition rate of 60 kg N/ha instead of bulk deposition rates will introduce a gap of 48 kg N/ha which has to be verified.

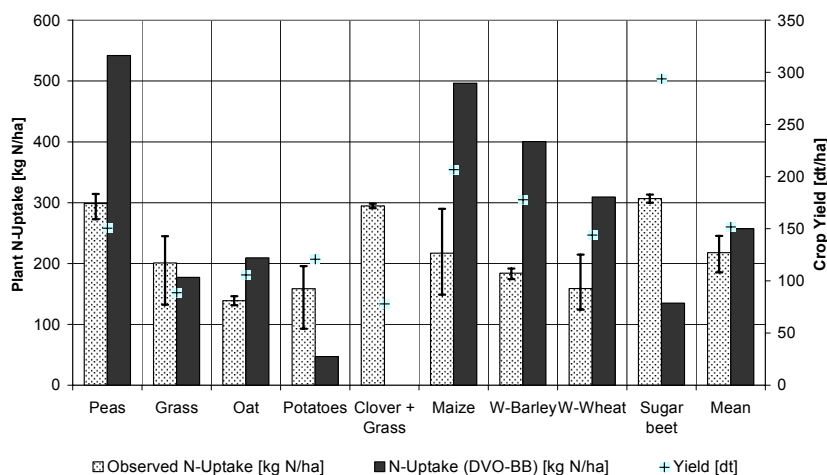


Figure 48: Average crop yields and comparison of crop specific N-Uptake rates, taken from Lysimeter data and calculated according to data taken from fertilizing directives

Official fertilizer directives give estimates of nitrogen sources and sinks for agricultural practice. Observed nitrogen losses to harvest (net plant N-uptake) vary considerably for the same crop and do not coincide with the estimates taken from the fertilizer directive. N-uptake [kg N/ha] is generally calculated by multiplying the amount of harvest [dt/ha] with an uptake coefficient T [kg N/dt]. In Figure 48 average N-uptake rates are compared, that were calculated from i) uptake coefficients taken from official fertilizing directives (DVO-SA), ii) average crop specific uptake coefficients calculated from observed amounts of harvest and plant N-contents and iii) minimum and maximum uptake coefficients derived from observed data.

Differences between the two calculation-schemes lie between 250 kg N/ha (Peas) and 30 kg N/ha (Grass). Observed plant N-contents vary considerably from year to year and even between lysimeters and so do uptake coefficients derived from observed data. From lysimeter data at hand average errors (over all crops and years) of ± 30 kg N/ha have to be taken into account using mean uptake coefficients. Related to average plant N-uptake, this is a variation of $\pm 16\%$ on average, ranging from 1% (mixed clover-grass) to 41% potatoes. Although this is just a rough estimate for a small data set, they indicate possible uncertainties in N-uptake.

However, the above calculation of N-uptake refers to plant N-uptake lost by harvest of crops. Gross plant N-uptake also needs to consider N-content of plant residues such as roots and leaves. This mechanism is an additional sink for mineral N and a source for organic N.

The amount of N-fixation for legumes was not measured for the single lysimeters. Assuming no internal storage changes and denitrification, a theoretical N-fixation rate can be calculated from the lysimeter N-budget and compared to N-fixation derived from fertilizing directives. It was found that both methods result in completely different fixation rates. This is shown in Figure 49 for lysimeters 05 and 07 where clover cultivation and leguminal intercrops cause intensive N-fixation. The RMSE of both methods is 85 kg N/ha/a for Lysimeter 05 and 99 kg N/ha/a for Lysimeter 07. As a consequence, N-fixation rates have to be considered as unknown inputs, as long as no direct measurements are available.

A good estimation of N-Fixation is essential for simulating soil nitrogen dynamics, as fixation rates can be well within the order of plant uptake rates. This is shown in Figure 50 for the lysimeters 05 and 07.

This discussion can be summarized as follows: Errors due to atmospheric deposition range between 0-50 kg N/ha/a. For plant N-Uptake an uncertainty around ± 30 kg N/ha/a or higher has to be taken into account. N-fixation rates can only roughly be estimated, two different calculation methods show average differences of approximately 85-100 kg N/ha/a. average N-leaching rates are between 10 and 30 kg N/ha/a (lysimeter simulation), which is well below or in the order of the errors to be expected due to data uncertainty.

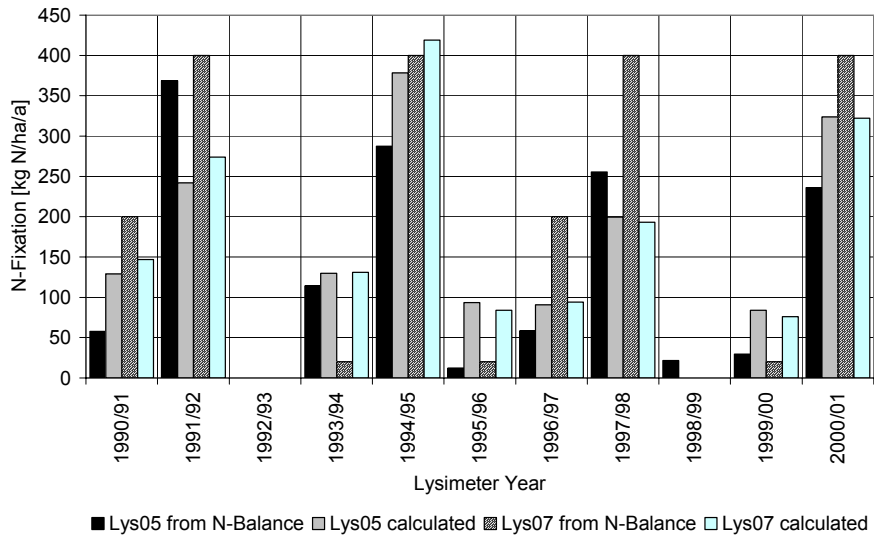


Figure 49: N-fixation of lysimeter 05 and 07 as postulated from the N-budget and calculated.

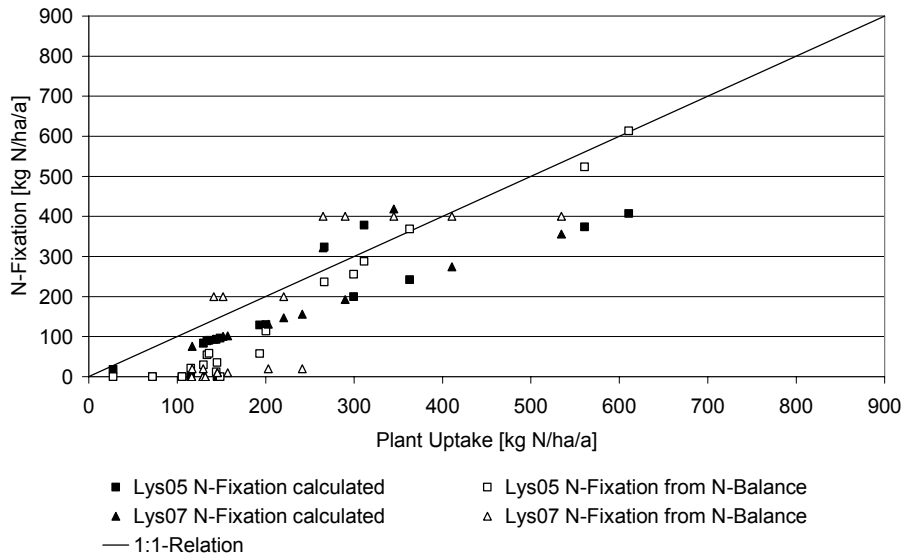


Figure 50: Calculated total N-Fixation in relation to plant N-uptake for the Lysimeters 05 and 07

5.1.4 Discussion

The sensitivity analysis shows well defined model behaviour and allows separation of sensitive and insensitive parameters. Storage parameters as field capacity and reduction point are the most sensitive parameters determining groundwater recharge, as they define actual evapotranspiration. Saturated conductivity, Interception and infiltration storage capacity are of minor importance and the initial parameter values did not need to be modified. Further optimisation of mineralisation rate constants is not meaningful. The initial parameters are good estimators, as parameter variations over a range of reasonable values have only little effect on N-leaching. N-leaching, used as the observed model output, is influenced by slow and fast mineralisation as well as by denitrification. Therefore, the optimisation of mineralisation rate constants is ambiguous. Model observations are based on average values over the simulation period, thus insensitive parameters in this study may be sensitive on an intra-annual base. They do not change water balance but may have an effect on intra-annual dynamics, e.g. delay or smoothing of the recharge function. From screening simulations, it is known, that intra-annual patterns are generally maintained and parameter changes only affect the amount of recharge and N-leaching. For interpretation of the time specific model results, sensitivity measures could be based on an objective function (e.g. Root mean

squared error) or multi-observation sensitivity measures could be applied. Using the e10-index on average data, however, is a simple method allowing a meaningful interpretation of sensitivities.

The PEST-assisted calibration scheme failed in giving a reasonable parameter set although model performance measures are better than in the manual calibration run. The latter gives a better interpretation of observed data, while at the same time worse model performance measures. This effect can be explained by the effect of temporal coincidence of observed and calculated model results. The soil-water-model does not sufficiently represent translation of groundwater recharge in time, thus precipitation excess is moving through the system much faster than in the natural system, i.e. instantly. The PEST-assisted calibration aims at reduction of the RMSE. Calculated monthly recharge peaks may occur in advance to observed recharge, contributing considerably to the objective function. As stated before, changes of model parameters only tend to increase or decrease model observations, but there are no parameters changing seasonal patterns and allowing better coincidence of observed and calculated values. Thus the contribution of these imbalanced peaks can only be reduced by decreasing recharge in total. During the second calibration run, seasonal patterns remained constant, and the imbalanced peaks are the reason for worse model performance measures while annual and cumulative recharge are represented better. This effect is explained in Table 19.

Table 19: Effect of temporal displacement on model performance measures

X	$f_0(x)$	$f_1(x)=f_0(x+1)$	$f_2(x)=0.5 f_0(x)$	An observation function $f_0(x)$ is defined. A model function $f_1(x)$ is given by temporal displacement of $f_0(x)$ by one x-unit ($f_1(x)=f_0(x+1)$), a second model function $f_2(x)$ is defined as half the value of $f_0(x)$ ($f_2(x)=0.5f_1(x)$). f_1 is be equivalent to the second calibration strategy, whereas f_2 is equivalent to the PEST-assisted calibration. f_2 would be a better representation of f_0 in terms of performance measures than f_1 , although f_1 is in fact identical to f_0 , except for temporal displacement. Temporal delay of recarge can only poorly be influenced by model parameters, thus the calibration algorithm forces the model to calculate lower recharge values in order to increase model fit.
1	0	0	0	
2	0	5	0	
3	5	10	2.5	
4	10	20	5	
5	20	5	10	
6	5	0	2.5	
7	0	0	0	
Sum	40	40	20	
RMSE	-	6.3	3.7	
NS-CoE	-	-0.03	0.65	

N-leaching rates were underestimated in the lysimeter simulations, although a worst case deposition of 60 kg N/ha/a and input via N-fixation were considered. At the same time, mineralisation rates proved to be rather insensitive and no considerable denitrification was simulated. Thus a further increase in N-leaching rates can not be achieved by modifying reaction parameters. A possible explanation for the underestimation of N-leaching is an overestimation of gross plant N-uptake, causing an effective reduction of mineral N-content and N-leaching rates.

The data set included only input and output fluxes, but no state variables or internal fluxes. Both percolation of water and N-leaching are the result of various interacting processes. These processes and their parameters can not be calibrated with this dataset due to parameter ambiguity. The calibration process is in fact a black-box calibration and the "optimum" parameter set does not identify the underlying processes.

The soil-water-model gives reasonable annual leaching rates, but representation of intra-annual dynamics is not satisfying. The soil-water-model is based on three serial storages. As shown by Beven (2002), the output signal of a linear storage cascade is not independent on the number of storages (while maintaining total storage capacity). This observation partly explains why the model shows no sensitivity to saturated conductivity and why a temporal delay of the output signal was

not possible. A more complex soil water submodel (e.g. increased number of storages) would probably show a better performance.

A major limitation of the analysis resulted from uncertainties of input data. The uncertainties introduced into the model are higher than expected N-leaching or denitrification rates. A soil nitrogen simulation is basically a calculation of a nitrogen balance. Thus errors of given N-budget terms (plant uptake, fertilizer) are directly reflected in calculated N-budget terms (n-leaching, denitrification). This is the case regardless of model complexity. For plot simulations, these problems can partly be overcome by direct measurement of all input data. For regional simulations various input data (plant uptake, n-fixation) can not be measured but have to be calculated from other data sources (statistics, guidelines, etc.). Additionally, there is a need to define effective values for elementary areas or patches, introducing further uncertainties. Using lysimeter data for parameterisation of plant uptake and n-fixation for regional simulations does not necessarily improve the simulation results, as i) lysimeter conditions may differ from field behaviour and thus may not be representative and ii) lysimeter data cover only a small selection of crops and provide only some of the data needed. The complexity of the soil nitrogen sub-model RISK-N is sufficient for simulation of lysimeter N-budgets with the given data. For regional application, a further increase in input data uncertainty can be expected, as more N-budget related input data have to be derived via transfer functions. Thus increasing complexity of the nitrogen-submodel will not improve simulation results, especially when performing distributed regional simulations.

The mRISK-N model can be used for scenario simulations, as key processes are reflected reasonably well. Limited capabilities of simulating real world situations (comparison to observed data) result from model simplifications as well as from uncertainties of input data. Although complexity of the soil-nitrogen-model RISK-N is considered to be sufficient, a more complex soil-water-model is expected to improve calculation of soil water dynamics considerably, allowing for a better intra-annual representation of soil water dynamics.

5.2 Sensitivity analysis of the groundwater-reaction-module

Figure 51 to Figure 58 show model response to initial oxygen concentration, initial nitrate concentration, initial content of SOM, transfer rate of SOM, autotrophic denitrification rate constant and temperature. Concentration as a function of time is given for nitrate, pyrite, sulfate, SOM and rOM. These species are directly involved in the turnover processes as reaction educts or products.

An instantaneous initial drop of nitrate concentrations is found in all simulations due to heterotrophic denitrification, as model parameters define a high reaction velocity. The subsequent turnover rates are determined either by limited release of rOM or by rate-limited autotrophic denitrification (pyrite oxidation). rOM is readily transformed with oxygen, thus the initial oxygen content also controls the amount of initial rOM left for denitrification (Figure 51). Changing autotrophic denitrification rate constants directly effects half life of nitrate and corresponding decay of pyrite (Figure 52). Increasing the content of SOM also increases transfer rates from SOM to rOM, causing a faster restoration of rOM-content. Nitrate turnover rates increase correspondingly (Figure 53). A similar effect can be achieved directly changing the SOM transfer rate (Figure 54). In both cases, the release of rOM is stopped after reaching the threshold concentration. Temperature dependency strictly follows the Van t'Hoff relation (Figure 56).

Model response to the various parameters is well in accordance to the model equations. Concentration changes are not contradictory to theoretical considerations. Figure 57 and Figure 58 are equivalent to Figure 55 and Figure 56, but the full Monod reaction-module was used for calculations here. The general behaviour is similar to the corresponding results using the first-order reaction-module, but concentration changes follow a more or less linear trend. For a given range of concentrations, a more or less equivalent behaviour of both reaction-modules can be achieved by appropriate parameter settings.

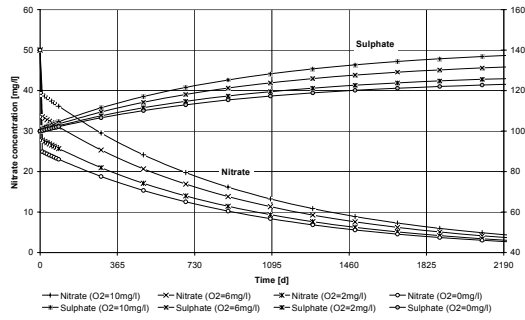


Figure 51: Model response to initial oxygen concentration

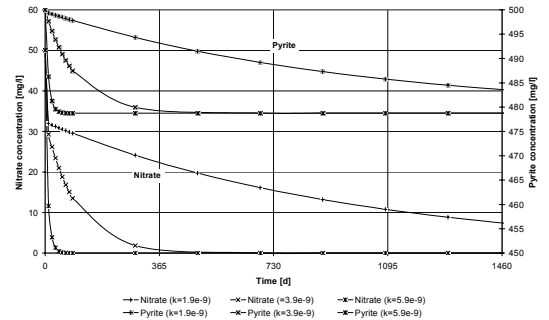


Figure 52: Model response for different rate constants of autotrophic denitrification

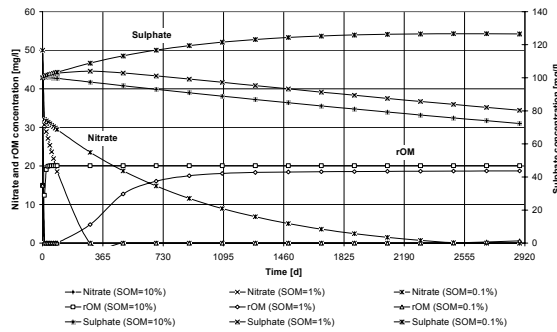


Figure 53: Model response to initial content of SOM

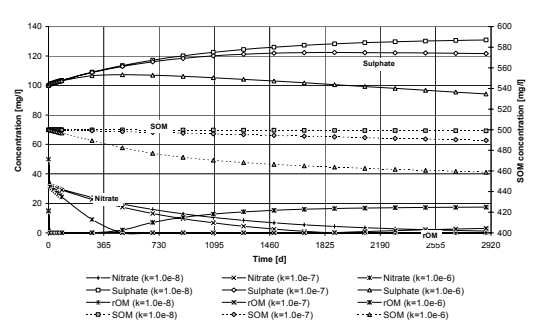


Figure 54: Model response to different SOM-release coefficients

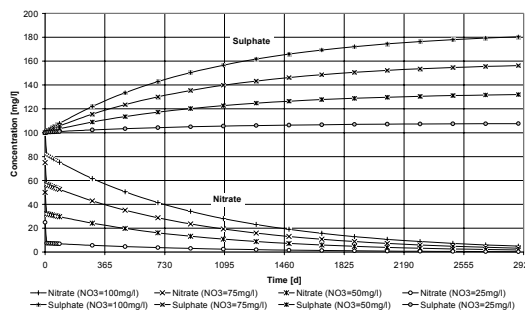


Figure 55: Model response to initial nitrate concentration

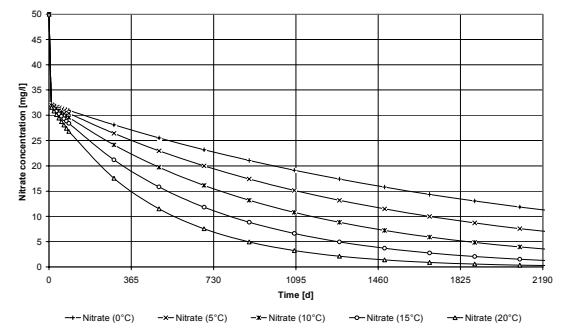


Figure 56: Model response to different temperatures

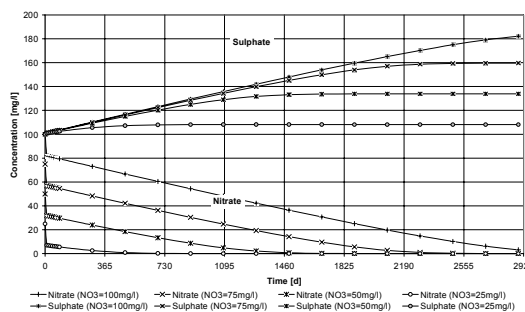


Figure 57: Model response to initial nitrate concentration using the full Monod reaction-module

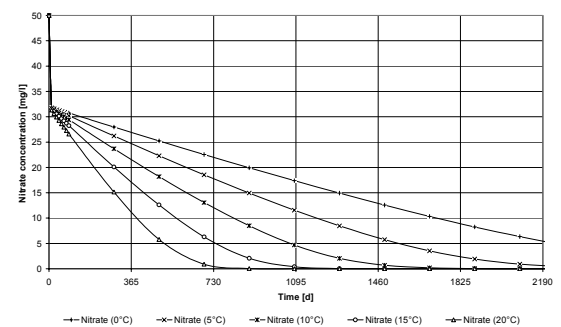


Figure 58: Model response to temperature, using the full Monod reaction-module

5.3 Simulation of a field scale tracer experiment

5.3.1 Evaluation of experimental results

The results of the analysis of temporal moments are summarized in Table 20.

Table 20: Results of the tracer experiment, based on analysis of temporal moments

Unit	Well T1-3	Well T2-4	Well T3-1	Explanation
Injection				
06/06/2001: 110 g Br and 110 g NO ₃ -N in Well T0				
Location	T1	T2	T3	Observation well
X [m]	3	8	15	Distance from injection well T0
Δx [m]	3	5	7	Distance between observation wells
Bromide breakthrough curves [Br ⁻]				
C _{max} [mg/l]	21.1	16.2	10.7	Maximum concentration of BTC
T ₀ [mg·d/l]	186	191	216	Area under BTC
μt [d]	31.4	53.9	88	Average solute travel time
σt [d]	6.2	9.1	7.4	Standard deviation of solute travel time
$v t$ [m/d]	0.1	0.15	0.17	Equivalent solute particle velocity
λt [m]	0.06	1.11	0.05	Equivalent dispersivity
Ω_{Bromide} [g/m ²]	29.6	40.8	44.4	Total mass flux
Nitrate breakthrough curves [NO ₃ -N]				
C _{max} [mg/l]	17.5	1.3	0.6	Maximum concentration of BTC
T ₀ [mg·d/l]	136	28	14	Area under BTC
μt [d]	34.5	59.9	96.6	Average solute travel time
σt [d]	7	30	-	Standard deviation of solute travel time
$v t$ [m/d]	0.09	0.13	0.16	Equivalent solute particle velocity
λt [m]	0.1	1	0.1	Equivalent dispersivity
Ω_{Nitrate} [g/m ²]	23.7	5.1	2.9	Total mass flux
Transport characteristics				
Δt [d]	31.4	22.6	34	Transport time from last well
v_a [m/d]	0.1	0.22	0.21	Average transport velocity between wells
v_c [m/d]	0.16	0.21	0.21	Local transport velocity at well
Decay				
[g/g]	0.73	0.14	0.06	Mass ratio NO ₃ -N / Br
[%]	27%	86%	94%	Nitrate decay
[g/m ²]	44.4	44.4	44.4	Scaled Bromide mass
[g/m ²]	32.3	6.3	2.9	Scaled NO ₃ -N mass
[mg/l/d]	5.1		0.44	Nitrate decay rate between wells
[mol/l/s]	9.50E-010		8.30E-011	Nitrate decay rate between wells

The analysis of the experimental data showed that

- The maximum calculated Ω was considerably lower than the initial mass of tracer applied (44g Ω_{Bromide} vs. 110g of Tracer). This indicates that a substantial part of the bromide applied either did not pass the observation wells or that maximum concentrations were not caught within the sampling interval.
- The dispersion coefficient is in the order of 0.05 m. The second Bromide-BTC shows two peaks and thus yields a higher dispersion of 1.1 m.
- Nitrate and bromide have slightly different transport characteristics. Nitrate moves slower and dispersion is less (in the first BTC).
- A denitrification rate of 9.5×10^{-10} mol/l/s was observed, assuming a linear decay of Nitrate.

It was found, that mass equivalent increases with travel distance, suggesting a different position of the observation wells relative to the plume centre. The maximum observed mass equivalent was found in well T3-2. Reference bromide BTC's were derived from the analytical BTC scaled to the maximum observed mass equivalent, according to the ratio $\Omega_{\text{Br}}^{\text{max}} / \Omega_{\text{Br}}^{\text{i}}$.

BTC analysis suggests different transport characteristics of nitrate and bromide transport. For the simulation, however, transport parameters like adsorption can not be set individually for each species. Thus reference nitrate BTC's were recalculated assuming the same dispersion than bromide BTC's. The relative mass ratio of Nitrate and Bromide BTC ($T_{\text{NO}_3} / T_{\text{Br}}$) was maintained.

For model comparison these BTC were used as reference together with mass equivalents and the zero-order moment (=area under BTC). They are not identical with the observed BTC's, but are consistent with the actual transport characteristics of the model, maintaining observed mass fluxes. The observed BTC's and their analytical counterparts are given in Figure 59 for bromide breakthrough and in Figure 60 for nitrate breakthrough.

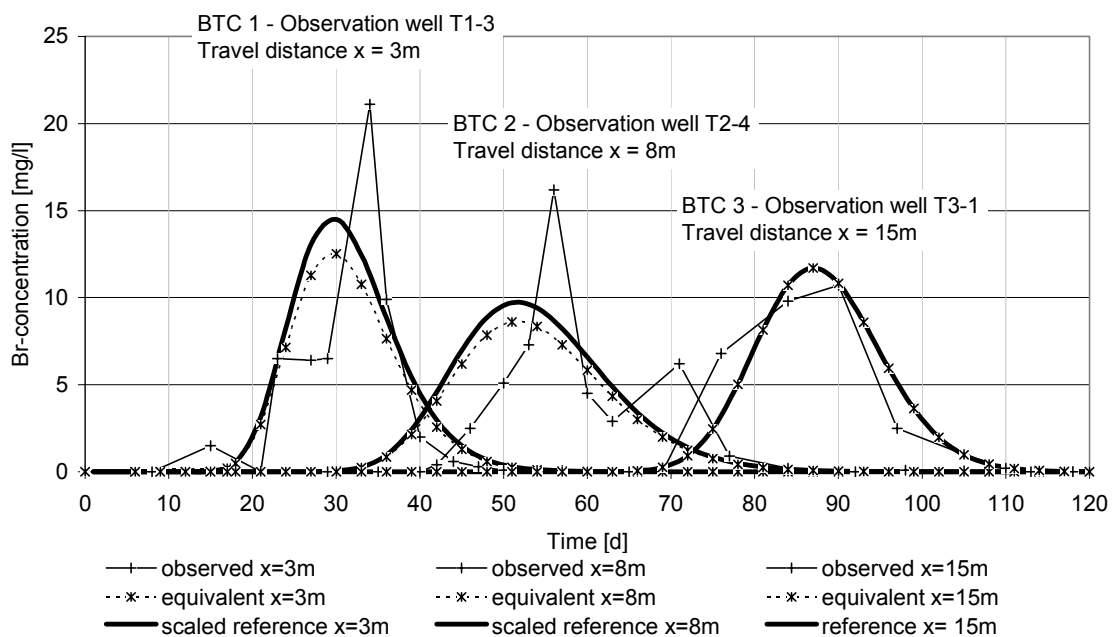


Figure 59: Processing of Bromide BTC's: observed, analytical equivalent and scaled reference BTC's.

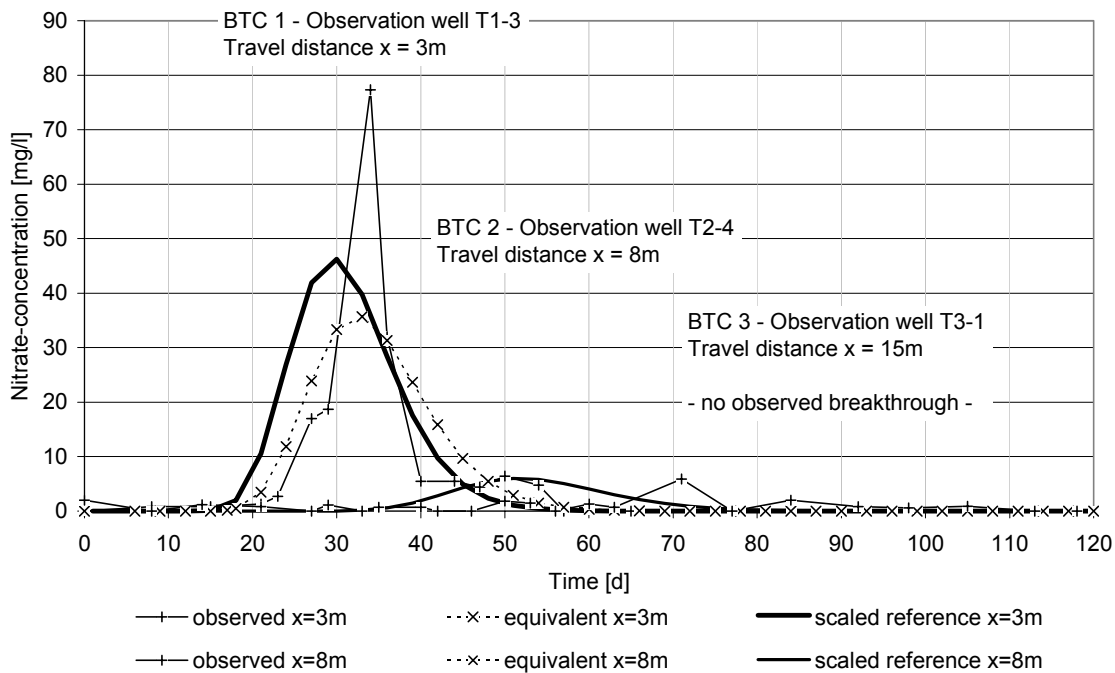


Figure 60: Evaluation of Nitrate BTC's: observed, analytical equivalent and scaled reference BTC's.

5.3.2 Calibration results

During calibration, porosity values were used to optimize travel times of the BTC's and the initial tracer mass was optimized to fit the shape of the BTC's. The final model parameters are given in Table 21, calculated and reference BTC's are given in Figure 61.

Table 21: Result of bromide transport calibration

	θ [-]	α [m]	M_i [g]	ME	MAE	RSME
Result	0.4/0.35/0.23/0.6	0.05/0.11/0.06	22.5	34.28	37.28	71.58

Considerable adaption of porosity values was necessary, indicating that the aquifer is by far not homogeneous. Within the sandy substrate variations of porosity or conductivities occur, which have a considerable effect on transport velocities.

Travel times of observed and simulated BTC's coincide quite well. Concentrations of BTC 1 and 2, however, are considerably higher than concentrations of the reference BTC's and a good representation is only found in BTC 3, which was used to optimize initial tracer mass.

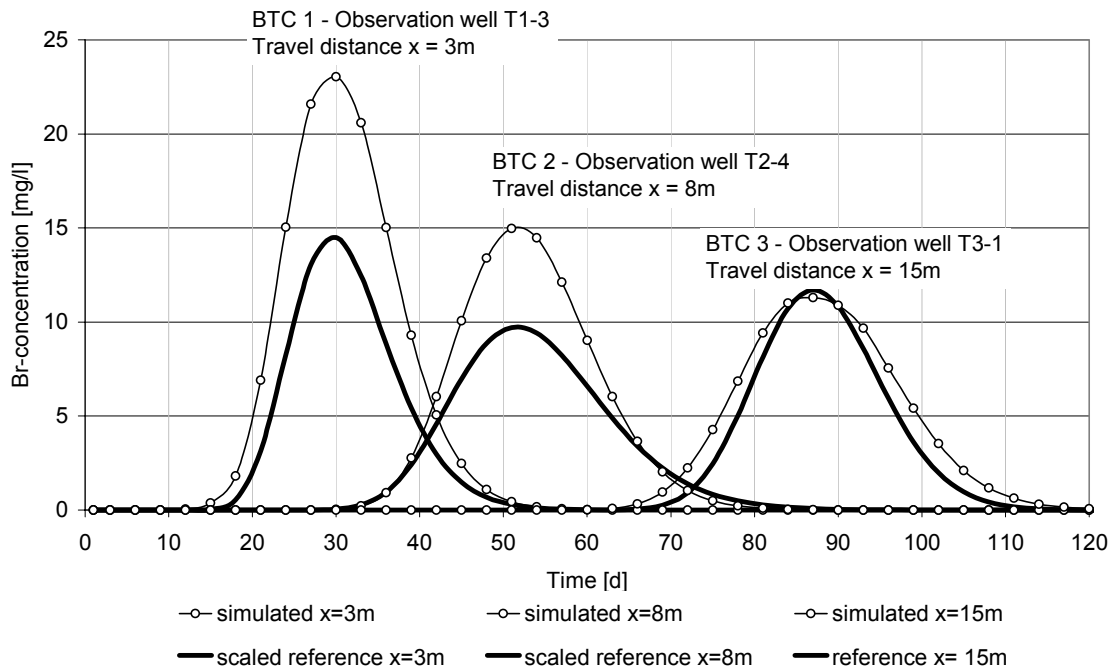


Figure 61: Bromide-breakthrough curves – scaled reference BTC and simulated BTC (best fit)

5.3.3 Nitrate transport simulation results

The effect of different SOM release coefficients on Nitrate and OM-concentrations is shown in Figure 62. The higher the release coefficient, the faster reactive organic matter can be made available from the sedimentary organic matter pool.

The effect of considering linear sorption of OM is shown in Figure 63. The highest nitrate peak corresponds to the no sorption run. Increasing sorption of OM buffers OM-concentrations due to exchange with the sorbed phase. Denitrification is no longer limited by availability of OM and nitrate concentrations decrease. The overall effect on nitrate concentrations, however, is low, as the denitrification process is also limited by the denitrification rate constant.

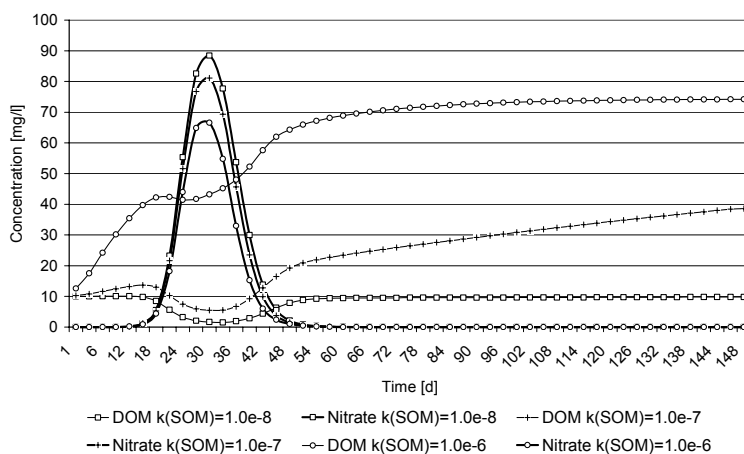


Figure 62: Effect of different SOM-release coefficients on Nitrate and DOM-concentrations observed after a travel distance of 3m (BTC 1).

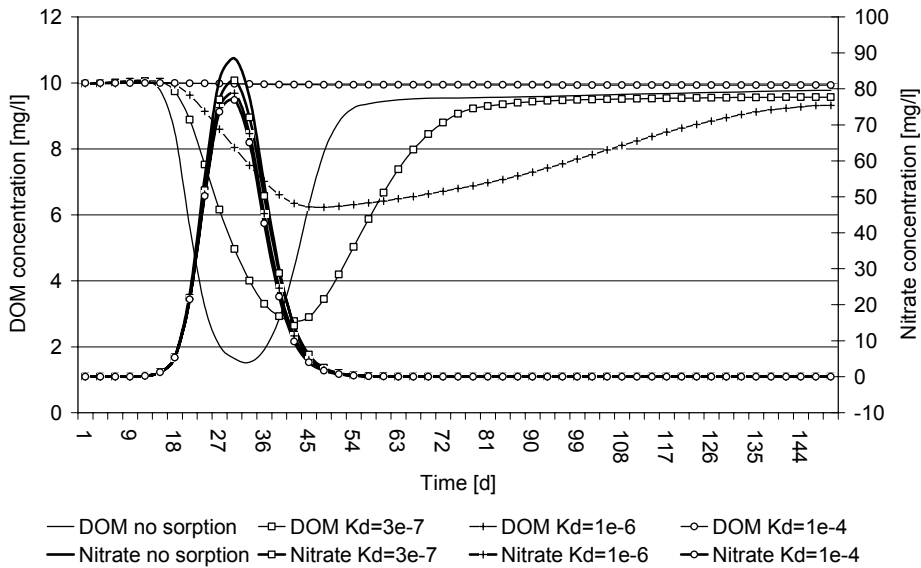


Figure 63: Effect of different DOM sorption coefficients K_d on DOM and Nitrate concentrations observed after a travel distance of 3m (BTC 1).

Figure 64 shows breakthrough curves for various denitrification rate constants. Figure 65 shows the simulated and reference BTC's for the best model fit. The denitrification rate constant of $9.5 \cdot 10^{-10}$ derived from BTC-analysis seems to underestimate nitrate turnover. A better representation was found using a rate constant of $4 \cdot 10^{-9}$, which is approximately five times higher than the value derived from observation data.

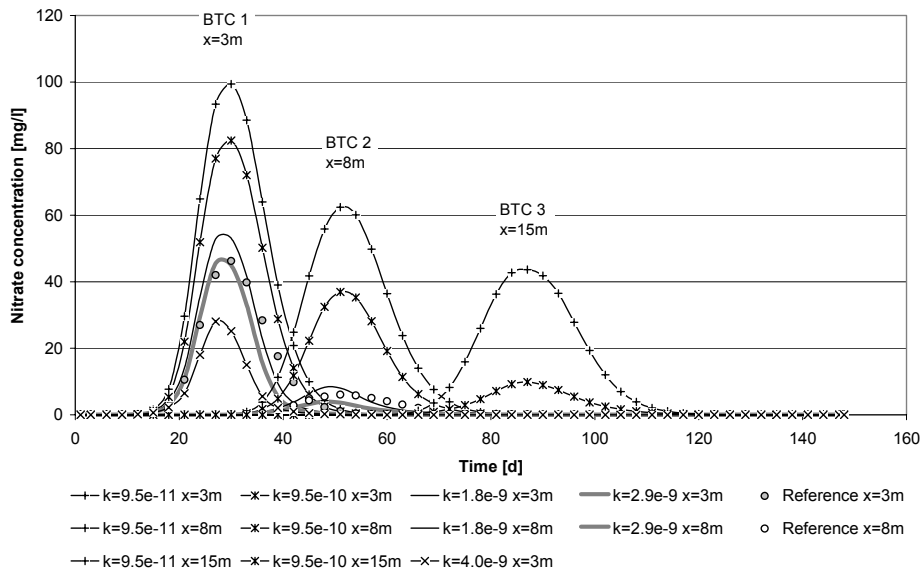


Figure 64: Calibration of denitrification rate constant – simulated and reference nitrate breakthrough-curves

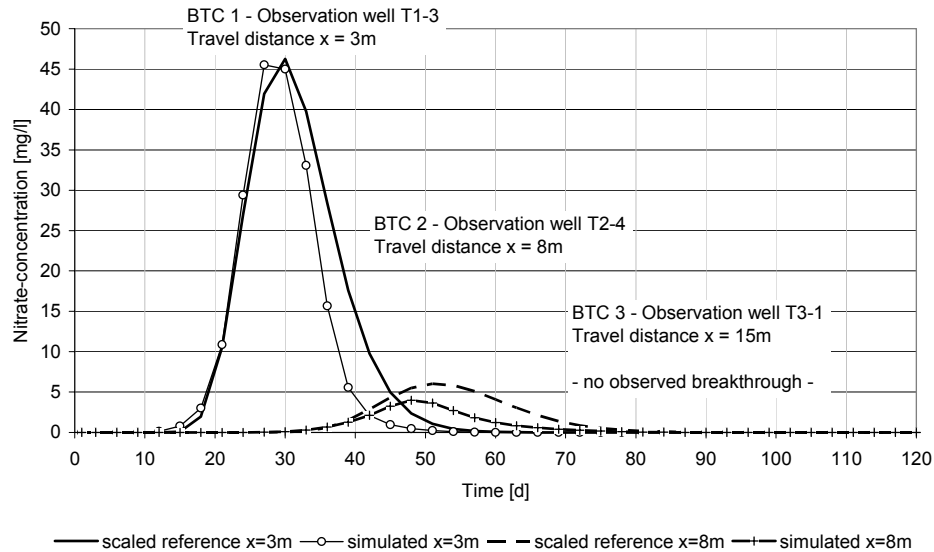


Figure 65: Nitrate breakthrough curves –scaled reference BTC and simulated BTC (best fit)

5.3.4 Discussion

In the field experiment, the observed mass equivalent Ω is influenced by three factors: i) lateral and vertical dispersion, leading to a decrease in mass equivalent with increasing distance from the injection well, ii) sampling interval, which may be too large to catch the peak concentration and thus yields a different BTC-curve and iii) the position of the observation well relative to the plume centre. Neglecting dispersion processes, all observed mass equivalents should be equal if all wells catch the same cross section through the tracer plume. The maximum mass equivalent is found in a cross section through the plume centre, lower values indicate marginal cuts through the tracer plume.

The bromide mass in the system is lower than 44.4g (mass equivalent calculation). From model calibration a mass of 22.5 g was determined, whereas the initial mass injected was 110g. Taking the calibrated mass of 22.5g, only 20% of the tracer initially applied could be found in the experiment. The fate of the remaining tracer is unknown. The most probable explanations are:

1. Incomplete exchange between injection well and aquifer. This well was not sampled during the tracer experiment, thus an experimental verification could not be made.
2. The observation wells did not catch the plume centre, either because the plume was cut at the margin by all wells or because of subsidence of the tracer plume due to density effects: The high concentration of the tracer salts leads to an increase in density and thus causes the tracer plume to sink. The tracer may be transported below the well screens and only the upper part of the plume was sampled during the experiment. Similar observations were made by Vereecken et al. (2000) in the Krauthausen tracer experiment using bromide as tracer.
3. Peak concentrations of bromide breakthrough were missed by sampling intervals, and thus the observed BTC does not equal the “real” BTC.

The simulated observation wells are consistent with the transport system defined by the model. As concentrations of observed and simulated BTC show a good fit only in the third observation well, it can be concluded that the way of scaling the observed BTC's to reference BTC is an inappropriate method in this case. The fact that observed tracer masses do not correspond to the tracer masses initially applied show that considerable elements of flow and transport are neither understood nor can be resolved by observed data.

Calibrated porosities no longer coincide with the homogeneous porosity of 0.3 assumed for the flow model. The flow model determines groundwater fluxes only and model parameters were derived from fixed assumptions. Alternative combinations of porosity and conductivity could be used to describe the same flow system. Thus a change of porosity values in the transport model does not

indicate inconsistency of flow and transport model.

Experimental data did not allow differentiation of heterotrophic and autotrophic denitrification. Neither sulphate nor dissolved organic carbon or inorganic carbon concentrations showed distinct patterns during nitrate breakthrough, which could be distinguished from background scatter.

Heterotrophic denitrification leads to a consumption of organic matter and a production of TIC. Observations of DOM were too irregular and unsuited for further evaluation. TIC-concentrations are determined by carbonate dissolution and CO₂-partial pressure, thus production of TIC by denitrification would not be reflected adequately in TIC concentrations. Similarly, DOM concentrations may be balanced by sorption or turnover of SOM. Total OM-concentrations, however, may be too insensitive to reflect consumption of OM due to denitrification.

Well (2003, oral communications) stated that the observed denitrification rates are considerably high and typical for those areas, where reduced sulphur sources such as pyrite are available for denitrification. An increase in sulphate concentrations indicating Pyrite oxidation was not observed, however, background scatter of sulphate-concentrations was too high to identify a clear sulphate peak. Measurements of sediment pyrite content, which could give a likelihood for autotrophic denitrification, were not made. If autotrophic denitrification was assumed as dominating turnover process, an equivalent calibration of the model is to be expected.

Assuming heterotrophic denitrification only, the observed turnover rate can only be maintained if availability of organic matter does not limit the denitrification process. This was shown by i) including sorption as a process controlling rOM concentrations and ii) by increasing the transfer rate between SOM- and rOM-pool.

The relative importance of these processes could not be assessed with the experimental data at hand and the specific model parameters were applied over a broad range of values. However, it can be shown, that consideration or neglect of these processes does have a strong effect on simulated nitrate concentrations. The observed decay of nitrate can not be related to specific processes, but is a phenomenological behaviour. Extensive process studies would be necessary to study the interaction of these processes in detail.

Putting it all together, the following conclusions can be drawn:

- As shown above, a variety of processes may influence transport and turnover. These processes can not be identified from the observed data. Consequently, the modelling study is characterized by a high degree of freedom and can only be considered as an interpretation of the actual processes.
- Experimental data required considerable data interpretation and processing in order to facilitate model application. Although relevant data were lacking or could not be observed, an interpretation of the tracer experiment could be made. The calibration process revealed that flow and transport processes are not completely understood. Small scale heterogeneities can not be neglected in model setup, but can not be observed with the field methods applied.
- Considerable high denitrification rates were observed and simulated. They indicate high availability of electron donors (pyrite or organic matter). If such conditions are likely to occur along the whole Schaugraben drain, an effective reduction of nitrogen loads should be expected. However, experiments were made during summer, and seasonal temperature-variations will lead to reduced denitrification rates in winter. If N-source areas are close to the drain, i.e. if N-loads reach the drain within a seasonal cycle, they may contribute to higher seepage concentrations during winter. If N-source areas are in greater distance, they will undergo more seasonal cycles and reduction of N-loads will depend on reactive pools rather than on temperature.

5.4 Simulation of nitrogen transport at the transect scale

5.4.1 Flow simulation results

The results of the flow simulations are given in Figure 66 as hydraulic head distribution and pathlines and in Table 22 as water fluxes and average particle travel times.

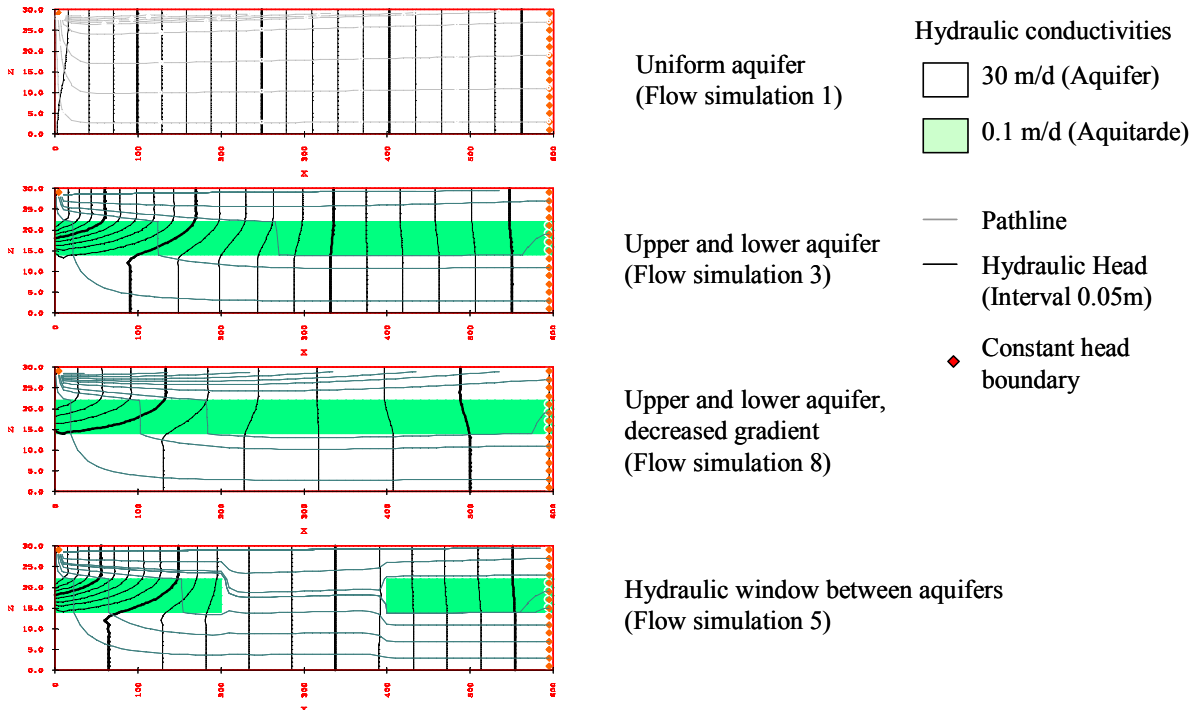


Figure 66: Flow simulations – hydraulic heads and pathlines

In the homogeneous aquifer gradients are quite constant and more or less horizontal flow paths are to be found. At the left boundary, water rises almost vertically to the seepage face (drain cell in upper left corner) and the zone of upwelling deep groundwater is confined to a distance of ca. 20m from the drain cell.

In contrast, separating upper and lower aquifer with a low-conductivity-layer forces particles in the lower aquifer to cross the impermeable layer, and higher gradients evolve around the drain cell. A zone of upwelling water extends far ahead of the drain cell, where deep ground-water crosses the intermediate layer and is integrated into the upper flow system. This zone extends to approximately 300m distance from the drain cell. In the decreased gradient scenario, the extent of this zone is lower (about 200m) as the total flux through the model domain is lower as well.

The inclusion of a hydraulic window connecting upper and lower aquifer system allows some more exchange of water from the lower to the upper layer.

The resulting seepage flux is the sum of recharge flux and flux across the constant head boundary. The latter depends directly on hydraulic conductivity and hydraulic gradients. Introduction of a less permeable layer in simulation 3 causes a considerable reduction of seepage fluxes, an additional reduction is observed in simulation 8 due to the decreased hydraulic gradient. Introduction of a hydraulic window causes only a weak increase in fluxes.

Travel times in the uniform aquifer are quite homogeneous. Introducing a less permeable layer between upper and lower aquifer increases the average travel times by a factor of 4.5, whereas the maximum travel time is increased by a factor of 28, but only 10% (2 particles) of all particles have travel times more than the average. The highest travel times are bound to the two particles moving completely within the intermediate layer, particles moving through the lower layer however move through the system as fast as particles in the upper layer. Due to the increased gradient at the seepage boundary, the low conductivity of the intermediate layer does not lead to a considerable retardation of particles. Simulations 5 and 8 show similar patterns as simulation 3, with travel times

in simulation 8 roughly doubled corresponding to the decreased hydraulic gradient.

Introducing a hydraulic window connecting upper and lower aquifer causes a slight increase in total flux and a slight reduction of travel times.

Table 22: Results of flow simulations: Seepage fluxes and travel times

Flow simulation	Seepage flux [m ³ /d]	Minimum travel time [years]	Maximum travel time [years]	Average travel time [years]	% of particles with travel times below average
1 – uniform aquifer	14.8	0.29 (105 d)	10.5	6.7	42%
3 – upper and lower aquifer	8.4	0.18 (66 d)	291	30.6	90%
5 – hydraulic window	9.0	0.17 (61 d)	268	28.7	90%
8 – upper and lower aquifer, decreased gradient	4.4	0.34 (124 d)	424	56.1	84%

5.4.2 Chemical interactions

The evolution of aquifer geochemistry is demonstrated for the reference simulation (sim03a) (standard reaction scenario for separated upper and lower aquifer). The distribution of nitrate is given for conservative transport and reactive transport in Figure 67 and Figure 68. During conservative transport nitrate moves equally fast in upper and lower groundwater and the aquifer is completely contaminated after 23 years. In the reactive transport simulation, pyrite oxidation in deep groundwater leads to a greater retardation of nitrate than in the upper groundwater, where only organic matter is involved in denitrification. Nitrate pollution has not yet reached the seepage cell. For the reactive transport scenario, the corresponding concentrations of sulphate and pyrite are given in Figure 69, of DOM, inorganic carbon, hydrogensulfide and nitrogen in Figure 70. The depletion of pyrite is also reflected in production and movement of sulphate. A desulfurikation zone, indicated by high concentrations of hydrogensulfide, is slowly replaced by fresh, nitrate contaminated groundwater.

Generally, well defined concentration gradients can be observed for most substances, which move slowly through the system, corresponding to transport of the solute and depletion of reaction partners. At specific observation points, a gradual increase in concentrations over time could be expected. The steepness of the gradients is defined by transport velocity and reaction kinetics. Steeper gradients require higher turnover rates or reduced transport velocities.

Nitrate (conservative transport)

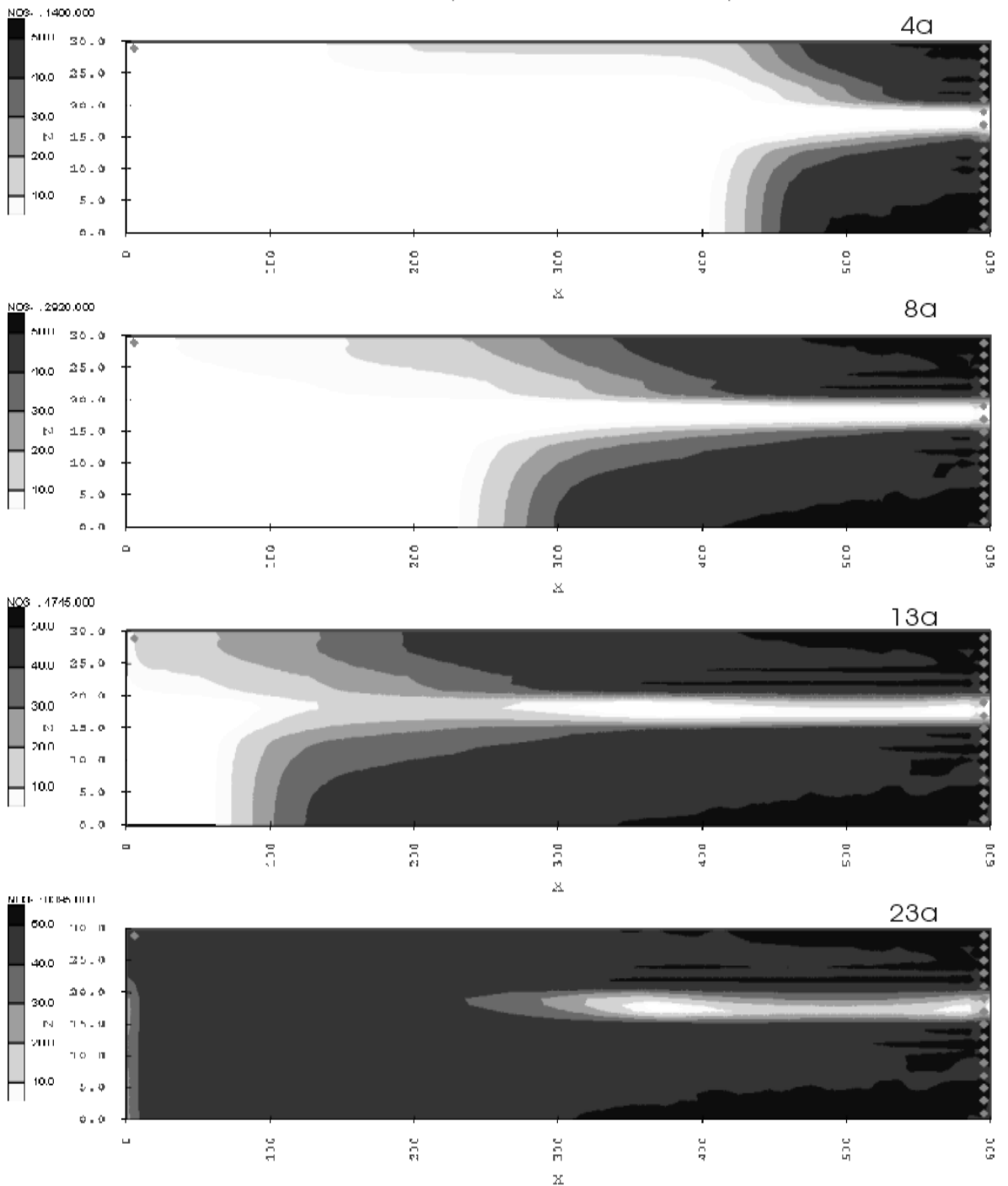


Figure 67: Distribution of nitrate (conservative transport) after 4, 8, 13 and 23 years.

Nitrate

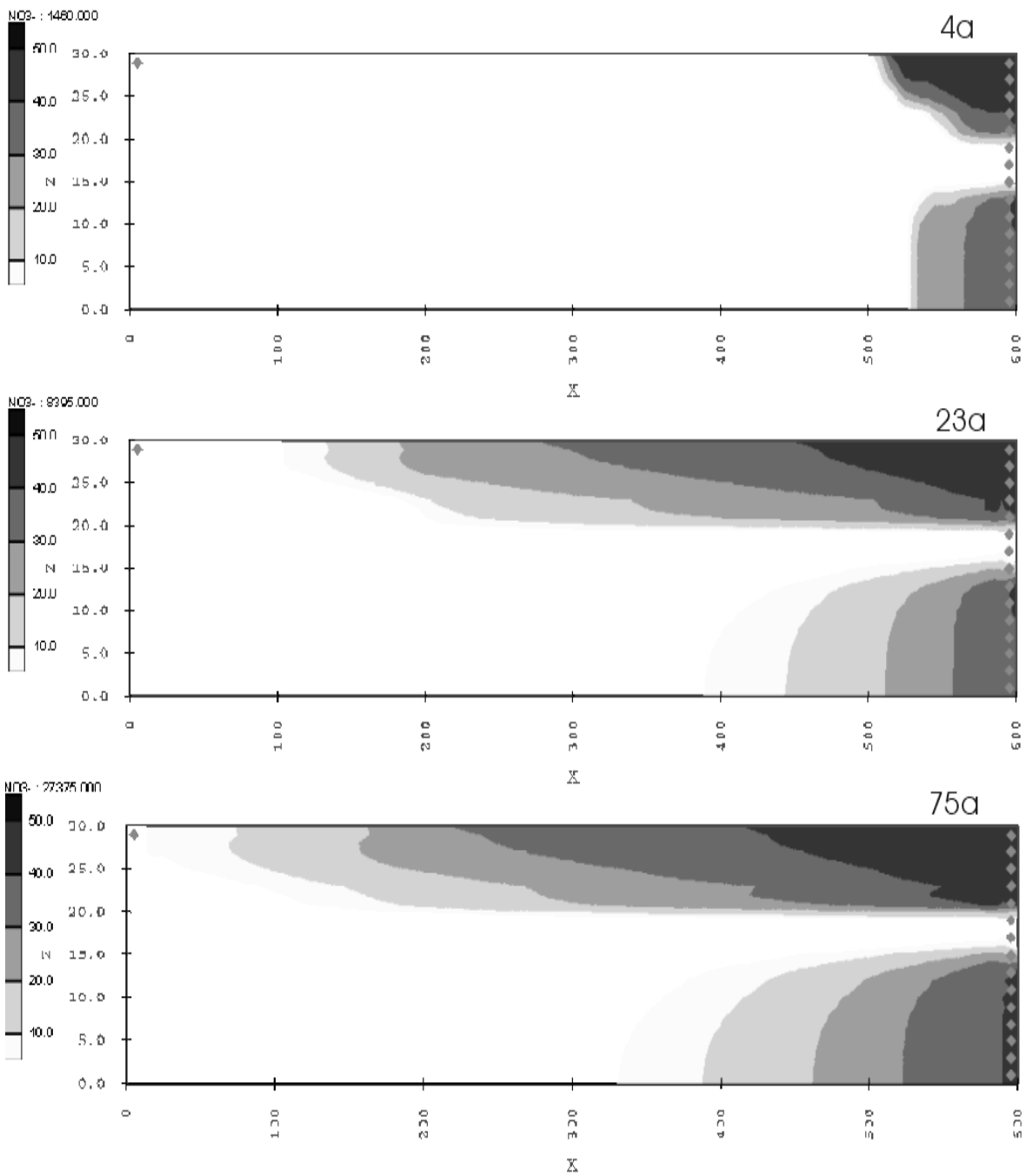


Figure 68: Distribution of nitrate (reactive transport) after 4, 23 and 75 years.

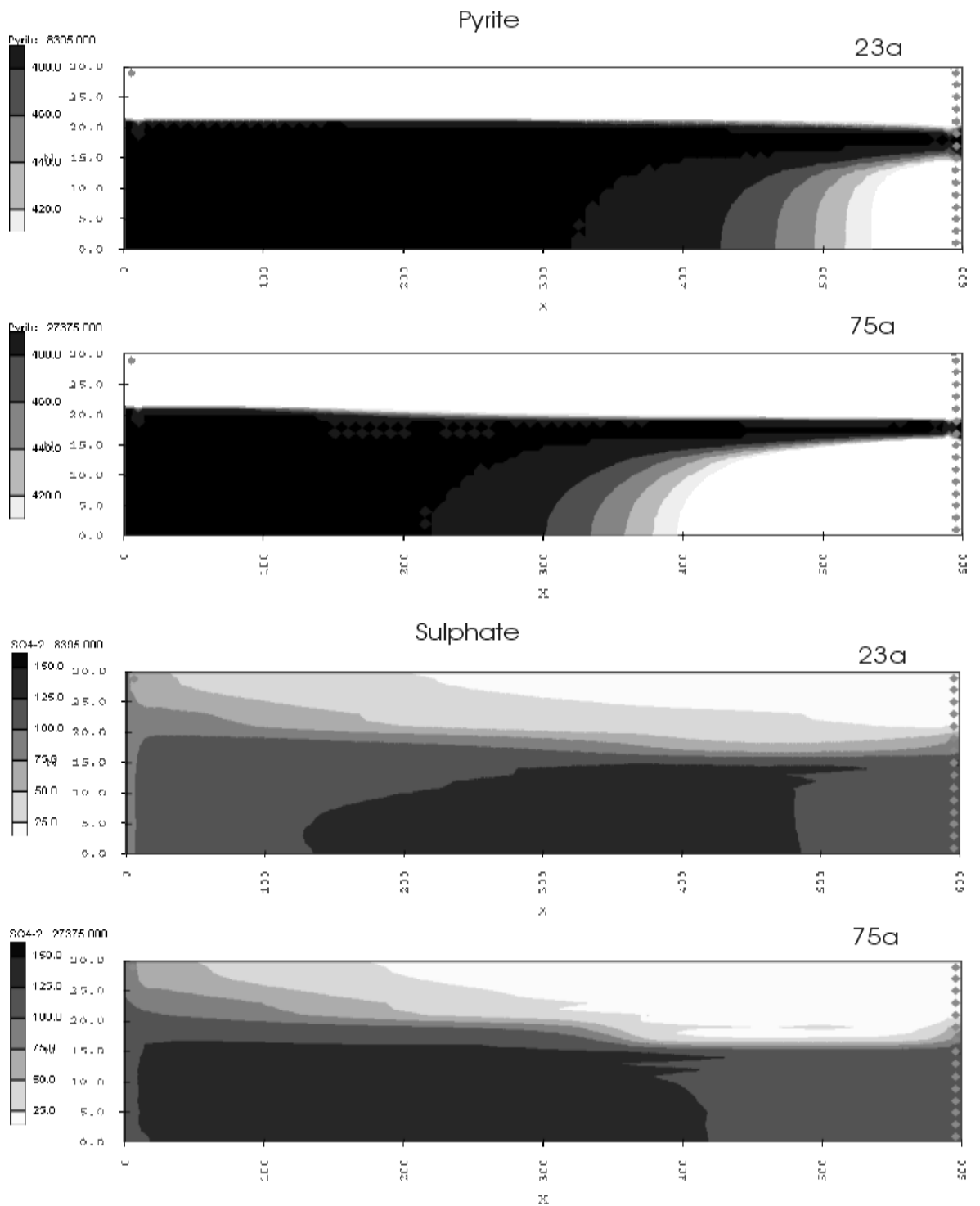


Figure 69: Distribution of pyrite and sulphate after 23 and 75 years

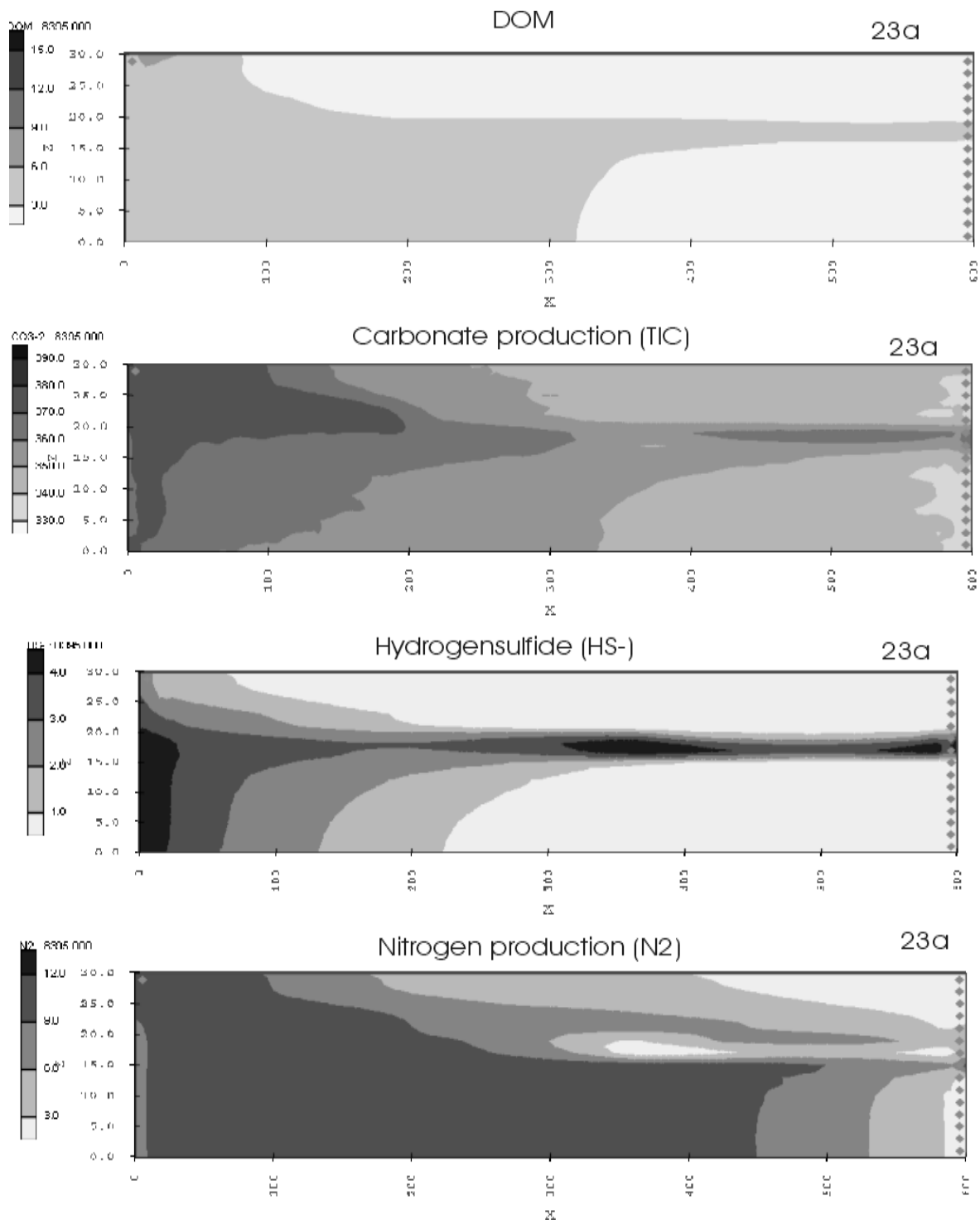


Figure 70: Distribution of DOM, hydrogensulfide, nitrogen and inorganic carbon after 23 years

5.4.3 Investigation of controlling factors

The following results are given as concentration vs. time curves of Nitrate at cell (1,1,1), which represents seepage to the drain channel. Cell concentrations are equivalent to concentrations in seepage water. As flow is constant throughout time, concentrations and loads behave identical and loads were not calculated explicitly. Due to the application of different flow scenarios in various simulations, transport velocities and seepage fluxes differ in some simulations, resulting in modified loads as well.

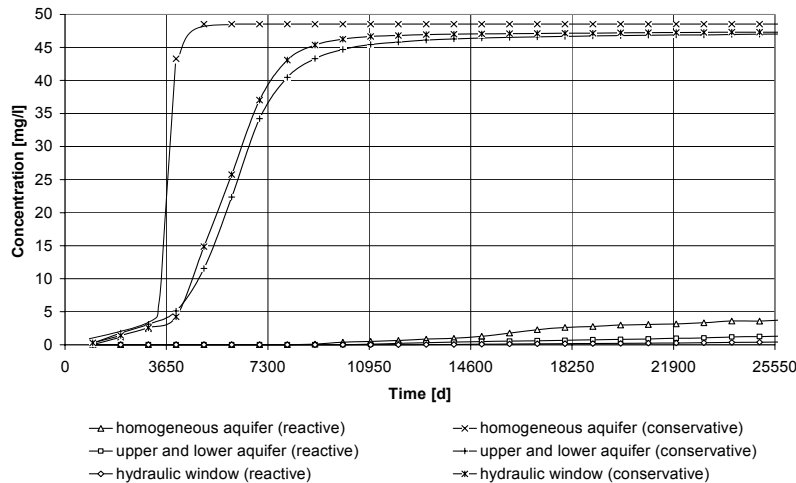


Figure 71: Nitrate concentrations in seepage water – effect of different flow systems

Figure 71 shows the development of Nitrate concentrations in seepage water for three different flow situations: i) homogeneous aquifer, ii) upper and lower aquifer separated by a low-conductivity layer and iii) a hydraulic window connecting upper and lower aquifer.

Considering conservative transport simulations, all breakthrough-curves follow a sigmoidal shape approaching a maximum concentration dependent on the average concentration of all input fluxes. The maximum concentration is reached after complete exchange of the initial groundwater. The development of concentrations depends on the relative contribution of short and long flow paths, as pollutants following longer flow paths reach the drain cell later than pollutants on short flow paths. The BTC of the homogeneous aquifer simulation is much steeper than for the other flow situations. In the homogeneous aquifer, flow velocities and travel times show only small variation, whereas a low-conductivity layer causes a retardation of solutes passing through this layer and the range of travel times is increased as well. Maximum nitrate concentrations are slightly different in all three simulations. All nitrate source concentrations are equal (50 mg/l), only the first recharge section is not contaminated with nitrate. Thus the final concentration depends on the relation between the uncontaminated recharge flux to the total flux, which differs between the various flow situations.

The reactive transport simulations show considerably lower nitrate concentrations, which increase constantly over time. Nitrate concentrations stay well below 5 mg/l within the simulation period, indicating an effective reduction of nitrate concentrations compared to the conservative transport simulation. Nitrate concentrations in the homogeneous aquifer are higher than in the other two simulations, as higher transport velocities result in a reduction of reaction time and total turnover. For conservative transport 50% of the maximum concentration is reached after 10 years in the homogeneous aquifer simulation and after approximately 16 years in the low-conductivity simulations. Concentrations remain low and increase slowly during the first 10 years and show a sharp increase thereafter. Nitrate reaching the seepage cell during the first 10 years, originates from the recharge boundary, the sharp increase takes place, when contaminated groundwater, entering the system at the inflow boundary, has reached the seepage cell (see also Figure 67). For reactive transport, it takes between 20 and 40 years, to find nitrate in the seepage water.

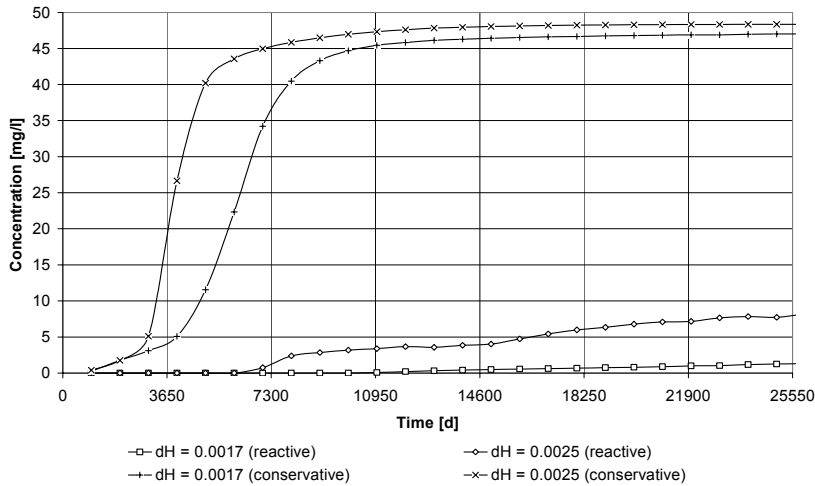


Figure 72: Nitrate concentrations in seepage water at different hydraulic gradients

Figure 72 shows nitrate concentrations under different hydraulic gradients. Increasing the gradient causes a faster response of seepage concentrations in the case of conservative transport and also a considerable output of nitrate after 20 years in the case of reactive transport, due to the decreased reaction time.

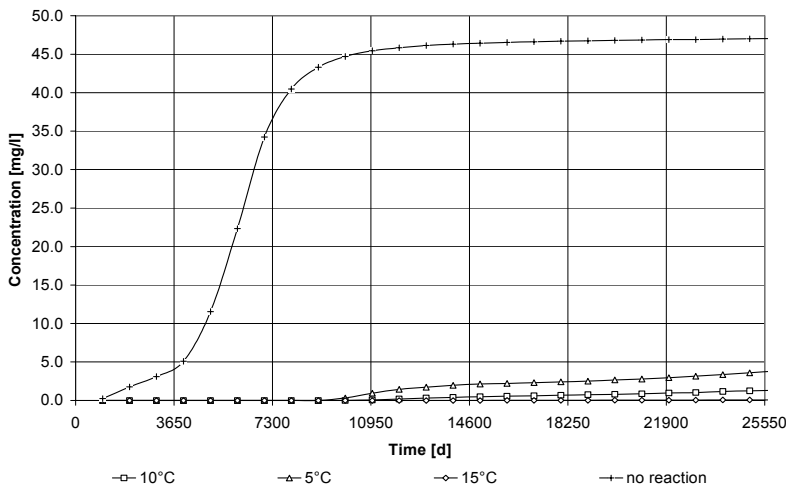


Figure 73: Nitrate concentrations in seepage water at different temperatures (5°, 10° and 15°C)

The effect of different temperatures on seepage concentrations of nitrate is shown in Figure 73. Nitrate concentrations decrease with increasing temperature, according to the temperature dependency of reaction rates defined in the reaction-module.

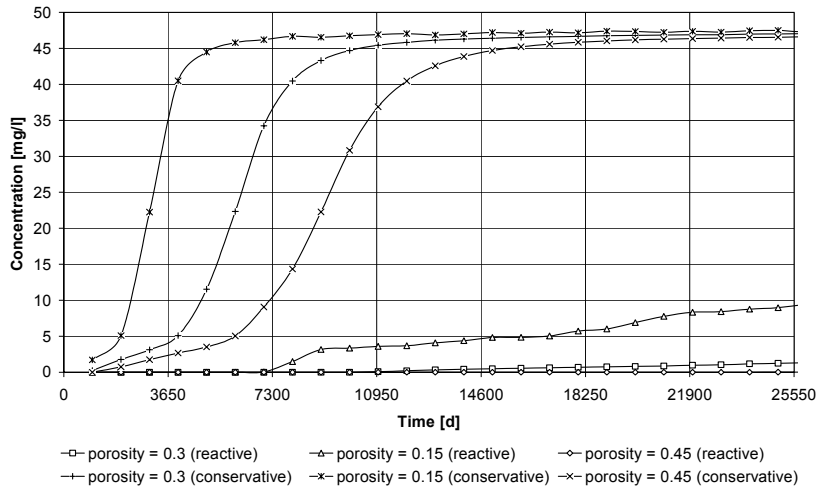


Figure 74: Nitrate concentrations in seepage water at different porosities

Porosity is directly connected to transport velocities, as are hydraulic gradients. Thus the effect of changing porosities is similar to changing hydraulic gradients (Figure 74). For conservative simulations, increasing porosity causes a smoothing of BTC and a delay of nitrate breakthrough (50% of maximum concentration are reached after 8, 16 and 25 years). For reactive transport simulations, higher porosities (and lower transport velocities) lead to decreased nitrate concentrations, as lower transport velocities increase reaction time.

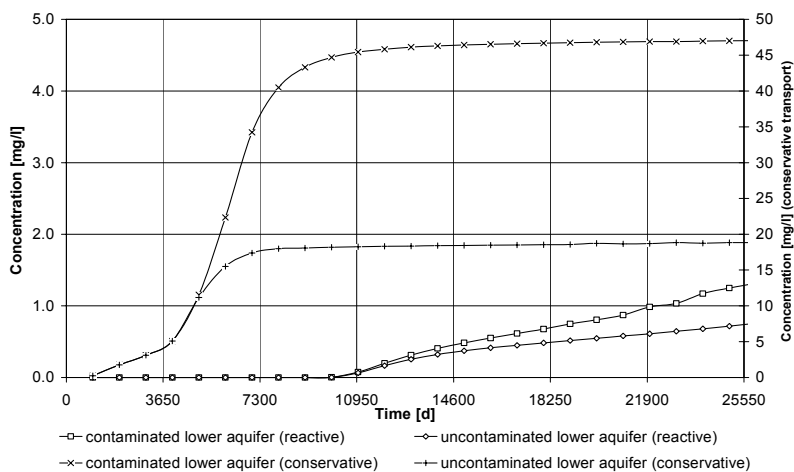


Figure 75: Nitrate concentrations in seepage water with contaminated and uncontaminated lower aquifer

If no contamination of the lower aquifer is considered (i.e. no contaminated groundwater enters the system over the constant head boundary, Figure 75), the maximum concentration in the conservative case is reduced considerably due to mixing of contaminated water from the upper aquifer and uncontaminated water from the lower aquifer. Consequently, nitrate concentrations are also lower in the reactive transport simulation, compared to the reference simulation.

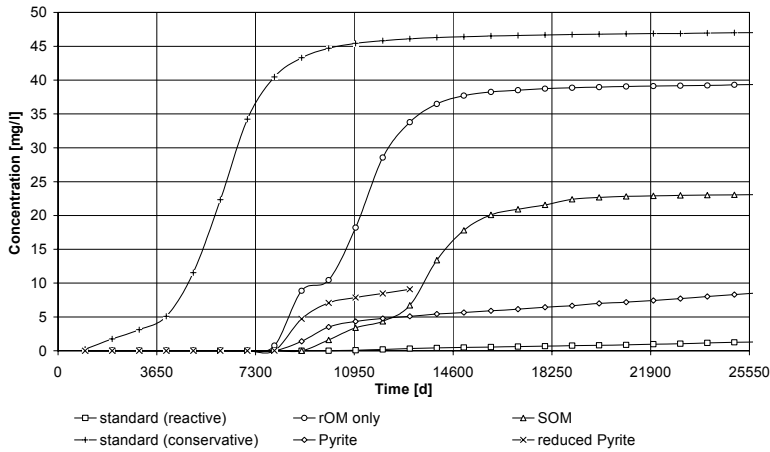


Figure 76: Nitrate concentrations in seepage water using different reactive pools

The availability of reactive substances has a considerable effect on nitrate turnover. Figure 76 shows the effect of separate application of different reactive pools compared to the standard scenario, where all pools are considered simultaneously. Reactive pools are reactive organic matter (rOM), sedimentary organic matter and pyrite. All simulations show a clear reduction of nitrate concentrations and retardation of breakthrough compared to the conservative transport simulation. Considering rOM as the only reactive substance, a distinct breakthrough takes place after 22 years, directly followed by a second breakthrough from deep groundwater after 30 years. Including SOM as a reactive pool leads to a higher reduction of nitrate concentrations, as the transfer of SOM to the rOM-pool allows a certain regeneration of rOM. This effect also takes place in the lower aquifer and thus leads to a considerable retardation of nitrate breakthrough from the lower aquifer. If only pyrite is considered as reactive substance, the decrease in nitrate concentrations is considerably higher than in the preceding simulations. The nitrate concentration curve shows no steps or sharp fronts, indicating that nitrate is completely retained in the lower aquifer and all observed nitrate originates from the upper aquifer. A simulation with reduced content of pyrite (0.002 Mass-%) was carried out but failed after a simulation period of 35 years. Up to then, Nitrate concentrations are about twice as high as in the preceding simulation. Due to the mineral updating, turnover rates are decreased corresponding to the decrease in pyrite content and more nitrate will leave the system. In the standard simulation, nitrate concentrations are lowest, as they result from the combined interaction with rOM, SOM and pyrite.

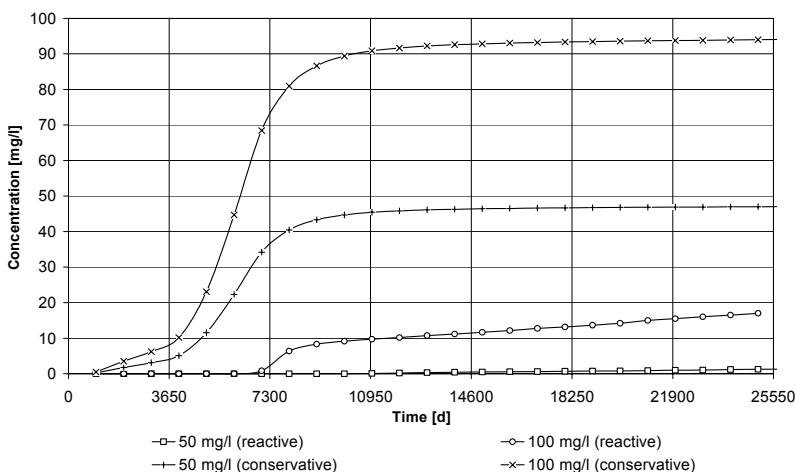


Figure 77: Nitrate concentrations in seepage water under different N-loads

The effect of increasing the nitrate load to a source concentration of 100 mg/l (vs. 50 mg/l) is shown in Figure 77. The shapes and breakthrough times of conservative transport breakthrough-curves are similar, but concentrations are doubled. In the reactive transport simulation, nitrate concentrations are overproportionally higher than in the reference simulation (with maximum

concentrations of 17 mg/l vs. 2mg/l). The higher input leads to an increased consumption of organic matter, subsequently limiting further denitrification, as organic matter is released only slowly from the SOM-pool. The shape of the nitrate concentration curve is similar to the corresponding curve in simulation “sim03h”, where pyrite is the only reactive substance. It can be concluded, that the observed nitrate concentrations originate from the upper layer, where no pyrite is present and availability of organic matter is not sufficient to counterbalance the increased nitrate input.

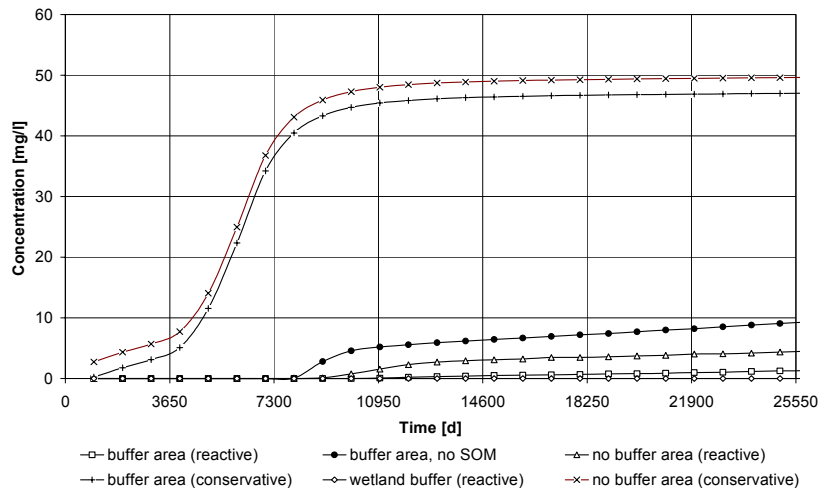


Figure 78: Nitrate concentrations in seepage water – effect of different buffer areas

Figure 78 shows the effect of different buffer area implementations. Conservative simulations consider a buffer area of 200m width compared to a no-buffer simulation. In the no-buffer simulation all input fluxes are contaminated, including the first recharge section. Thus the maximum concentration is equal to the source concentration of 50 mg/l and nitrate enters the seepage cell from the beginning. The standard scenario implements a buffer area in the first model section, which is characterized by lacking input of nitrate only. The reactive transport simulations show a clear reduction of seepage concentrations in the order “no buffer” (up to 10 mg/l), “standard buffer” (up to 5 mg/l) and “effective buffer” (up to 1 mg/l). The effect of the “standard buffer”-simulation is mainly caused by reducing the total input of nitrate, whereas the “effective buffer”-simulation additionally has a higher denitrification capacity due to increased availability of rOM.

Nitrate reaching the drain cell originates from different source areas. The different flow paths and travel times result in a characteristic shape of the BTC. For conservative transport, recharge water from the first three model sections enters the drain cell first, and concentrations remain low due to mixture with initial, uncontaminated groundwater but increase constantly. Second, a sharp increase in nitrate-concentrations as contaminated water from the constant head boundary reaches the drain cell. This contaminated water has replaced uncontaminated deep groundwater and is now entering the channel system. Finally, a maximum concentration is reached, defined by the proportion of uncontaminated and contaminated input fluxes. For reactive transport, the concentration function shows following characteristics: first, a more or less pronounced breakthrough of nitrate, considerably delayed with respect to conservative nitrate breakthrough, followed by a slow but constant increase in nitrate concentrations. Second, a more or less pronounced step of the concentration curve indicating breakthrough of deep groundwater nitrate. This step vanishes with increased reductive capacity of the aquifer. Whereas it takes about 10 years, until a considerable breakthrough of nitrate is observed in conservative transport simulations, 20-30 years are needed for reactive transport. In reactive transport simulations, total change of seepage concentrations after breakthrough is low and does not exceed 5 mg/l over a period of approximately 40 years.

5.4.4 Discussion

As shown in the flow simulations, a zone of upwelling deep groundwater extends into some distance of the aquifer, depending on hydraulic characteristics such as hydraulic gradient and conductivities. If this zone is narrow, mixing of deep and upper groundwater is confined to the

channel system and to a small area around the drain. If this zone is wide, a substantial part of deep groundwater enters the upper aquifer and is transported to the drain in the upper aquifer system. If the upper groundwater contains considerably pools of organic matter (e.g. peat, humic soils), the extent of this zone defines the possibility of contact between contaminated deep groundwater with reactive pools in the upper aquifer.

All factors influencing transport velocities, for example conductivities, porosities and hydraulic gradients do change residence times and thus the time available for reactions in groundwater. As all reactions are kinetically controlled, an increase in transport velocity will cause a reduction of total turnover and increased seepage loads and concentrations.

In the given system it takes years to decades, until breakthrough of nitrate is observed in the drain channel. The evaluation of seepage concentrations does not consider intermittent contribution of tile drains, allowing a short-cut of soil water and channel water. In the various reactive transport simulations seepage concentrations change only little over long periods of time. It can be questioned, if field observations allow a significant identification of such slow concentration changes. If observation periods are too short, concentration trends may not be significant, as a certain natural variability has to be taken into account as well. Thus, long observation periods are needed, covering periods of decades, rather than a few years. Of course, concentration changes will be more or less pronounced depending on the hydraulic and geochemical characteristics of the specific system. Shorter residence times or lower reductive capacity in the catchment will result in a faster response of seepage concentrations and in elevated nitrate concentrations as well.

A buffer area contributes to reduced seepage concentrations i) by reducing the total load of nitrate into the aquifer system and ii) by increased denitrification capacity provided that suitable hydraulic and geochemical conditions are present. If the reductive capacity of the aquifer system is low, a buffer area would not substantially contribute to reduction of nitrate loads. If the reductive capacity of the aquifer is high, reactive substances may cause an effective removal with or without buffer areas. As geochemical conditions are fixed and can not be modified, model-based evaluation of the effect of buffer areas can be a useful tool for planning buffer areas. However, in this study the effect of plant N-uptake from groundwater was not considered. If a modified vegetation in buffer areas results in an increased N-uptake from groundwater, this process contributes to the removal of nitrate from groundwater.

5.5 Simulation of nitrogen transport in the Schaugraben catchment

5.5.1 Distributed soil nitrogen modelling of the Schaugraben catchment

A first simulation was made for the extended study area to provide groundwater recharge for the regional groundwater flow simulation. Further simulations were made for the Schaugraben P5 catchment and the subcatchment, providing groundwater recharge and nitrate leaching for subsequent groundwater flow and transport simulations. All simulations were based on the same input data. They differed in spatial extent and spatial resolution only, according to the corresponding groundwater simulations. Therefore, the following sections confine to the results and discussion of to the four P5 catchment simulations.

Although the term “soil simulation” is commonly used in this study, it has to be kept in mind that the soil model includes the intermediate vadose zone and recharge and N-leaching rates are given at the groundwater surface and not at the lower boundary of the root zone.

Average groundwater recharge, N-leaching and denitrification of the four soil simulations are given in Figure 79. Groundwater recharge was identical in all simulation runs, as the same soil physical parameters were used in all simulations and a capillary rise and evaporation from groundwater was not considered by the model. Using the default denitrification rate constant of 0.0001 1/d caused an average denitrification of 2-4 kg N/ha/a (simulations 2 and 3). Applying higher and soil specific denitrification rate constants (simulations 1 and 3) increased total denitrification considerably, and denitrification rates in the catchment area ranged from 0-30 kg N/ha/a.

The effect of applying distributed groundwater depths, as in simulations 1 and 3, was rather low compared to the simulations 2 and 4 with a constant groundwater depth of 2m. The difference of denitrification and N-leaching was approximately 1 kg N/ha/a. In the intermediate vadose zone the default denitrification rate constant was set very low and identical in all simulations. Thus no

considerable denitrification was simulated in the vadose zone. Using higher rate constants, would also pronounce the effect of considering distributed soil depths.

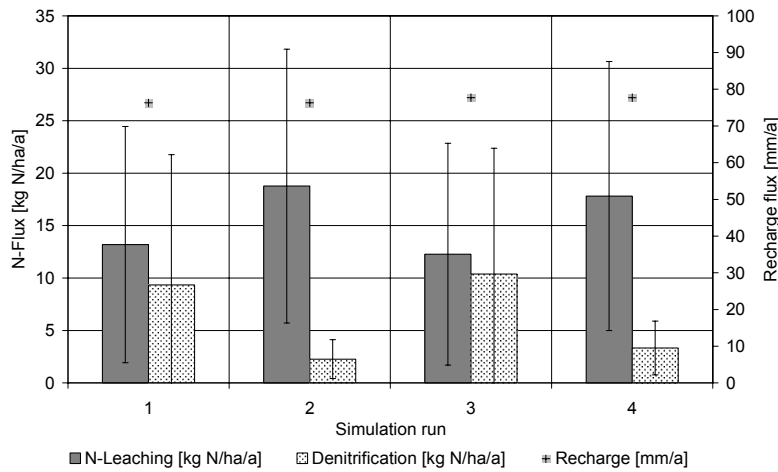


Figure 79: Comparison of distributed soil simulation runs 1-4

Figure 80 - Figure 82 show the distribution of mean annual groundwater recharge, N-leaching and denitrification in the model domain for simulation 3 (distributed groundwater table and soil specific denitrification). Groundwater recharge patterns (Figure 80) roughly reflect landuse patterns, with modest groundwater recharge in the grassland areas along the drain channels, highest recharge on arable land and lowest recharge in forested areas. This figure, however, is modified by soil properties as well. High denitrification rates concentrate along the drain channels, whereas modest denitrification is found in the remaining areas (Figure 81). This pattern corresponds roughly to distribution of grassland and arable land, but also to the distribution of gleyic soils with higher potential denitrification. Again, N-leaching rates (Figure 82) are roughly distributed in a complementary fashion.

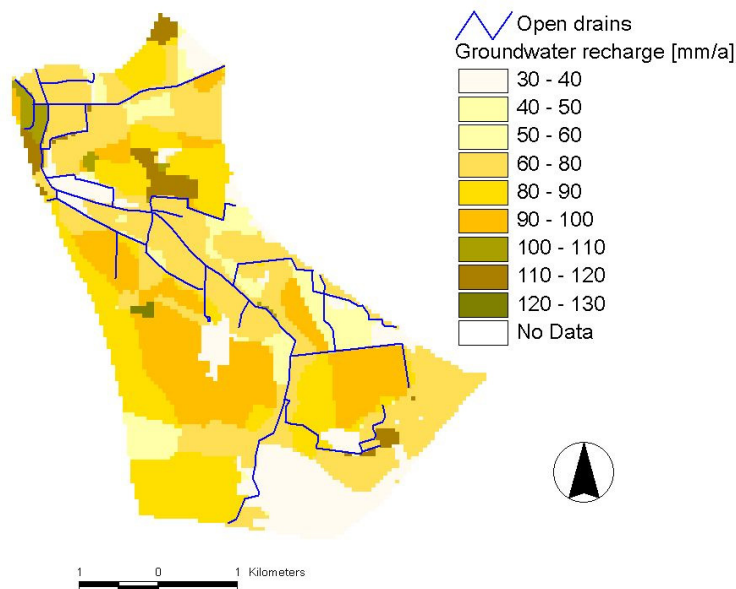


Figure 80: Simulated mean annual groundwater recharge

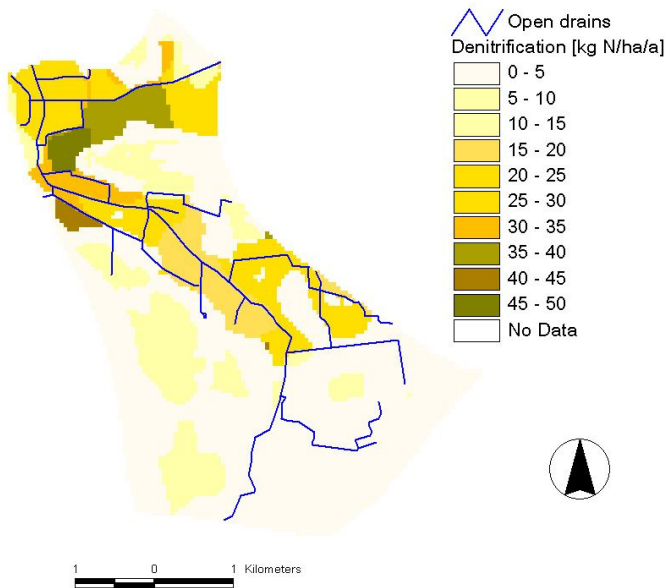


Figure 81: Simulated mean annual denitrification

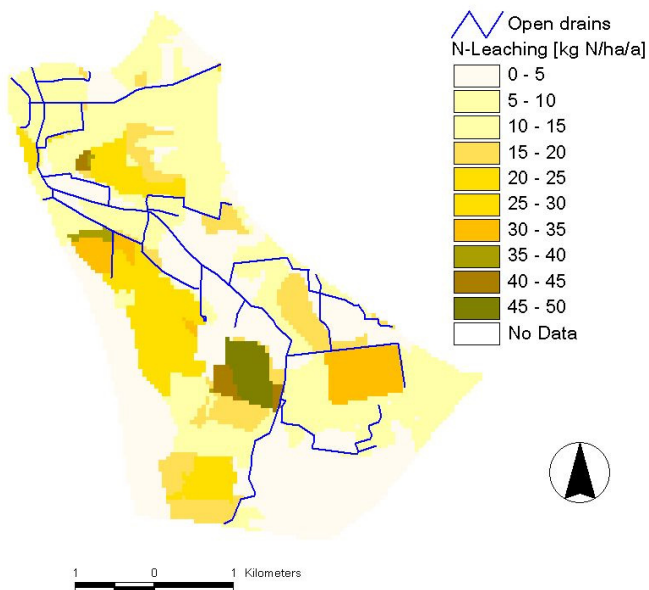


Figure 82: Simulated mean annual N-leaching

Figure 83 and Figure 84 show calculated annual water and nitrogen balances for the model domain over the simulation period. Wet and dry years are clearly reflected in the annual catchment water balances (Figure 83). Annual N-budgets (Figure 84) show less variation. The mineral N-Pool acts as a net sink of nitrogen caused by sorption of ammonium and storage in the soil column. It is clearly to be seen that N-leaching is only a fraction of total N-Input (maximum: 40 kg N-Leaching/ha vs. 240 kg N-Input/ha).

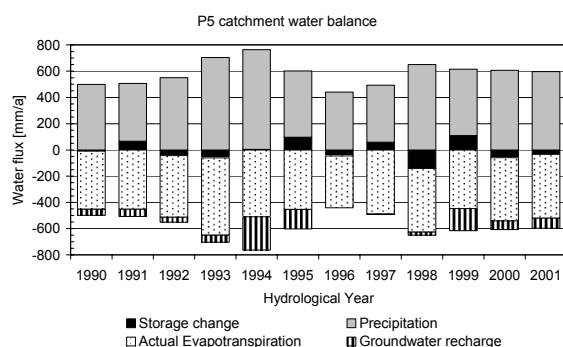


Figure 83: Simulated annual water balances

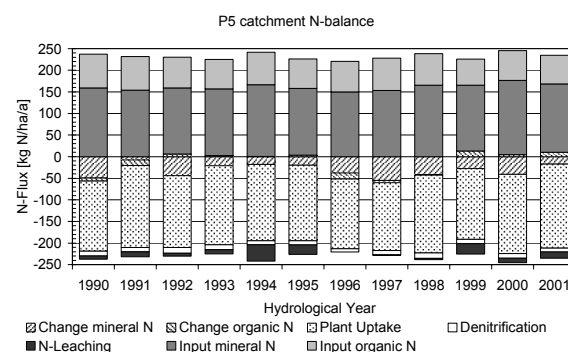


Figure 84: Simulated annual N-budgets

For subsequent groundwater simulations, groundwater recharge and N-leaching were averaged over the entire simulation period. The data were prepared as i) distributed input data, ii) averaged data by landuse class and iii) total averages. A short characterisation of the input data is given in Table 23 for the P5 catchment simulation and in Table 24 for the subcatchment simulation.

Table 23: Input data for the P5 catchment simulation, groundwater recharge and N-leaching are given as total averages and averages by landuse type, based on simulation 3

Landuse class	Area [ha]	Groundwater recharge [mm/a] $\pm \sigma$	N-Leaching [kg N/ha/a] $\pm \sigma$	Nitrate-concentration [mg/l]
Not specified	1	36 \pm 0	60 \pm 0	77
Grassland/Pasture	345	64 \pm 14	80 \pm 5	53
Cropland	1258	89 \pm 12	160 \pm 11	78
Forest	258	49 \pm 14	30 \pm 2	31
Settlement	59	39 \pm 5	30 \pm 1	37
Total	1920	78 \pm 9	120 \pm 4	70

Table 24: Input data for the subcatchment simulation, as total averages and averages by landuse type

Landuse class	Area [ha]	Groundwater recharge [mm/a]	N-Leaching [kg N/ha/a]	Nitrate-concentration [mg/l]
Not specified	0	0	0	0
Grassland/Pasture	75	73	70	44
Cropland	271	97	240	110
Forest	8	49	30	26
Settlement	23	41	30	37
Total	377	88	190	96

There are no possibilities to validate model results on a catchment scale, as further transformations in ground- and surface waters as well as a long residence time do not allow comparison of stream loads to N-leaching rates. Simulation results were strongly affected by parameterisation (especially assignment of denitrification rate constants to soil types) and all uncertainties inherent to the input data (see discussion in 5.1.3). However, the simulated recharge and leaching rates lie within reasonable ranges. Spatial patterns of recharge and leaching clearly reflect distribution of soil types

and landuse. Low leaching rates coincide with highly denitrifying environments or low input areas and vice versa. A crosscheck of recharge and leaching by landuse class and soil type did not suggest anomalies contradictory to expected model behaviour.

5.5.2 Regional flow model

5.5.2.1 Results of the sensitivity analysis

Figure 85 - Figure 88 present distributed elasticities of groundwater levels to changes of substrate and drainbed-conductivities. The effect on seepage fluxes is presented in Figure 89 - Figure 90.

Sensitivities of groundwater level observations to changes of hydraulic conductivities are generally low, but lie within comparable ranges for all substrate types (e_{10} between -0.09 and 0.08). However, distinct sensitivity patterns can be found for the three substrate types upper sand, till and deep sand. As can be seen from the distribution of groundwater observation wells (appendix A) within the model domain, most wells lie more or less close to an open drain channel. Thus groundwater levels are determined by drain elevations rather than by other factors. It can roughly be said, that groundwater-level sensitivity increases with distance from drains and rivers and that drain water levels (which specify a head dependent flux boundary) largely determine the groundwater surface. Sensitivity of groundwater levels to drainbed conductivity (Figure 92) is about one order of magnitude lower than to substrate conductivities. Again, the highest sensitivities are found far off the drain channels.

The effect of substrate conductivity on seepage fluxes was evaluated for high (100 mm/a) and low (50 mm/a) groundwater recharge (Figure 89). Elasticities lie between 0.11 and 0.13 for the low recharge simulation and 0.6 and 0.4 for the high recharge simulation. Using the high recharge value, the relative effect of hydraulic conductivities is decreased and displaced by the effect of increased hydraulic gradients and fluxes within the system.

The effect of drain-bed conductivity on seepage fluxes was evaluated as relative change of seepage flux for discrete drain-bed conductivities (1, 4, 40 and 400 d/m², Figure 90). The relative change of seepage flux is considerably low and lies between +1 and -3%. Thus drain bed conductivity does not affect seepage fluxes considerably and can be considered of minor importance for model calibration.

Considering that conductivities generally vary over broad ranges within textural classes and parameter changes during model calibration could easily exceed 10%, substrate conductivities have a considerable effect on groundwater levels. In a closed catchment system seepage flux should equal the recharge flux and thus stay constant, regardless of the conductivity values specified. The catchment of the Schaugraben drain in the regional flow model is not fixed but results from the interaction of water fluxes and hydraulic parameters. Thus the Schaugraben catchment area (referred to gauging station P5) might change in size and shape depending on the individual parameter settings. Each change of conductivities or changes of the geological model would require a new definition of the catchment boundary.

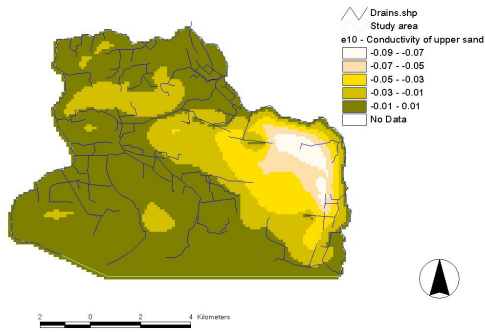


Figure 85: Sensitivity of groundwater level to saturated conductivity of upper sand

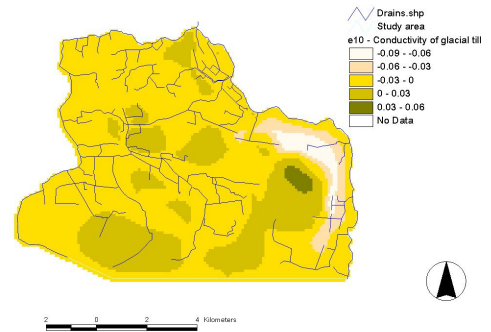


Figure 86: Sensitivity of groundwater level to saturated conductivity of glacial till

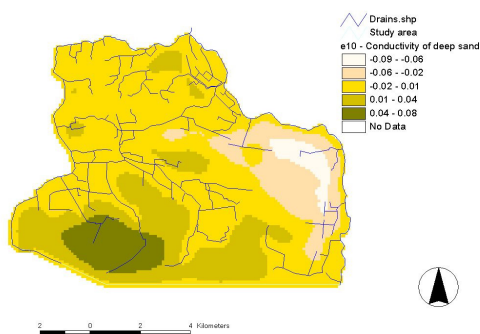


Figure 87: Sensitivity of groundwater level to saturated conductivity of deep sand

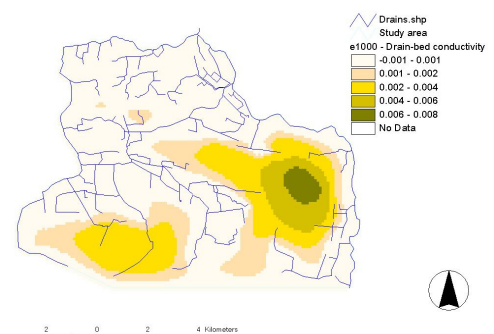


Figure 88: Sensitivity of groundwater level to drain-bed conductivity

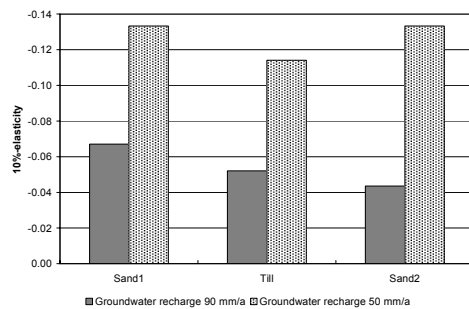


Figure 89: Sensitivity of seepage flux to substrate conductivity

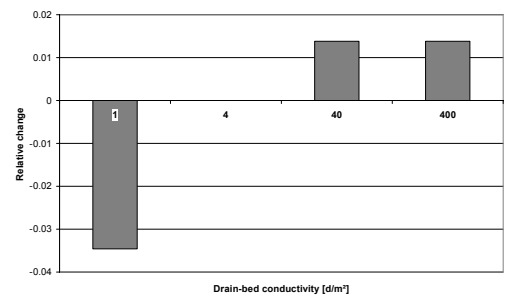


Figure 90: Relative change of seepage flux to flux to drained bed conductivity

5.5.2.2 Model calibration results

The final groundwater head distribution is given in Figure 91 and the corresponding plot of observed and calculated heads is given in Figure 92. Table 25 summarizes the calibration runs.

The groundwater surface and the P5 catchment are determined by the interaction of substrate distribution, channel system, substrate parameters and input fluxes. Considering all uncertainties of input data and observation data, a clear optimum simulation run satisfying all criteria is not given. In fact, multiple parameter sets were found, giving a reasonable representation of the flow system.

Seepage fluxes vary considerably according to parameter settings, and most simulations stay within the target range. Corresponding changes of head distribution and shape of the P5 catchment can be observed. Thus it was postulated as an additional criteria for model performance, that P5

catchment boundaries should lie completely within the model domain and not extend across constant head boundaries.

Observed groundwater heads are well represented by the model. The mean average error is about 0.61 m. The varying calibration runs do not suggest further possibilities of reducing the model error. The groundwater surface is largely determined by drain channel elevations. Drain channel elevations are compiled from topographical information and thus may differ locally from the real situation. Specific observation wells show large deviations throughout all calibration runs, indicating geological settings which are not represented in the hydrogeological model due to sparse borehole information. Both, uncertain drain elevations and geological information, limit the model fit to a model specific error.

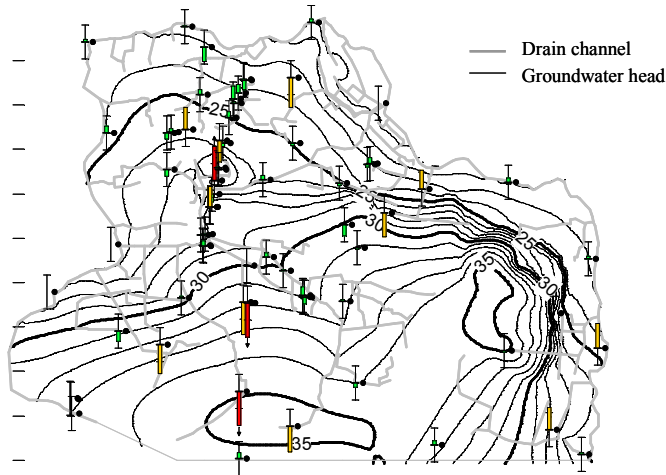


Figure 91: Simulated hydraulic head distribution (interval = 0.5m)

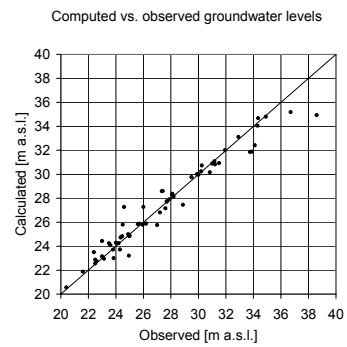


Figure 92: Observed and simulated groundwater heads

Table 25: Summary of regional flow model calibration

	ME [m]	MAE [m]	RMSE [m]	Seepage flux [m ³ /d]
Initial run	0.01	0.60	0.94	4548
Initial K _f [m/d]: Upper sand=6.0, Till=0.20, Lower Sand=6.0, Drainbed=4.0				
Range (Min-Max)	-0.36-0.34	0.56 - 0.84	0.83 – 1.18	3509 – 6006
Final run	-0.07	0.61	0.94	4116
Final K _f [m/d]: Upper sand=15.0, Till=0.20, Lower Sand=6.0, Drainbed=4.0				
ME = Mean error, MAE = Mean absolute error, RMSE = root mean squared error				

5.5.2.3 Delineation of the P5 catchment boundary

Pathlines of the MODPATH simulation are given in Figure 93. Watersheds are defined as locations of diverging flow directions. This information was used to define boundaries for the P5 catchment model. Boundaries of the model domain for subsequent simulations follow watersheds and flow paths. Pathline analysis shows that deep and shallow flow paths run parallel, so that clear catchment boundaries can be identified. Only north of gauging station P5 some deep groundwater flow paths cross the Schaugraben drain and leave the area on a subsurface flow path.

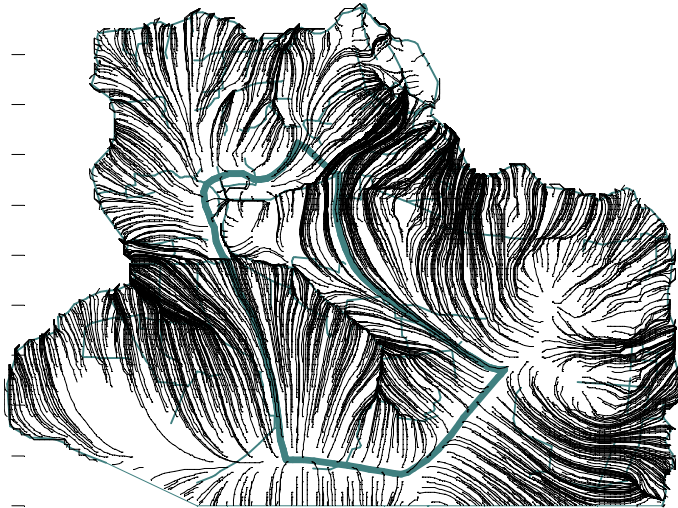


Figure 93: Pathlines of regional groundwater flow

In a previous study (Meissner, 2000) the Schaugraben catchment boundary was defined by surface topography and flow directions of the drain channels. In lowland areas, characterized by loose material, size and shape of the catchment do not depend on surface topography but are a result of the interactions between groundwater recharge, channel system and substrate. Consequently, topographical and groundwater catchment boundaries do not necessarily coincide. This is also the case for the old catchment boundary and the new boundary derived from the groundwater simulation. The latter is used in subsequent flow simulations, as this boundary is consistent with the given hydrogeological model and recharge simulation.

5.5.3 Modelling of groundwater nitrogen transport in the Schaugraben catchment P5

5.5.3.1 Results of the P5 catchment simulation

The results of the flow simulation are given as groundwater head distribution in Figure 94 and as water balance for the specific simulation runs in Table 26.

From the groundwater head distribution it can be seen that the upper reaches of the Schaugraben drain and its tributaries are not in contact with the groundwater surface, as the groundwater head gradient is not oriented towards the channels. The general flow direction is oriented in a northern direction. The Schaugraben drain receives most of the water from the areas south of the channel.

About 6% of the total input flux leaves the system over the downstream constant head boundary, the remaining 94% enter the channel system as seepage flux. About 3% of the input does not originate from recharge, but enters the model domain via the constant head boundary at the upstream model boundary. This flux compensates for incompatibilities of the catchment delineation with the natural flow system. The recharge flux of the “buffer area” simulation is distinctly lower than in the other simulations, due to the change in landuse. In the other simulations small differences can be found concerning the fluxes over constant head boundaries. They can be referred to small differences in the groundwater surface (and thus groundwater fluxes), resulting from the different spatial distribution of groundwater recharge.

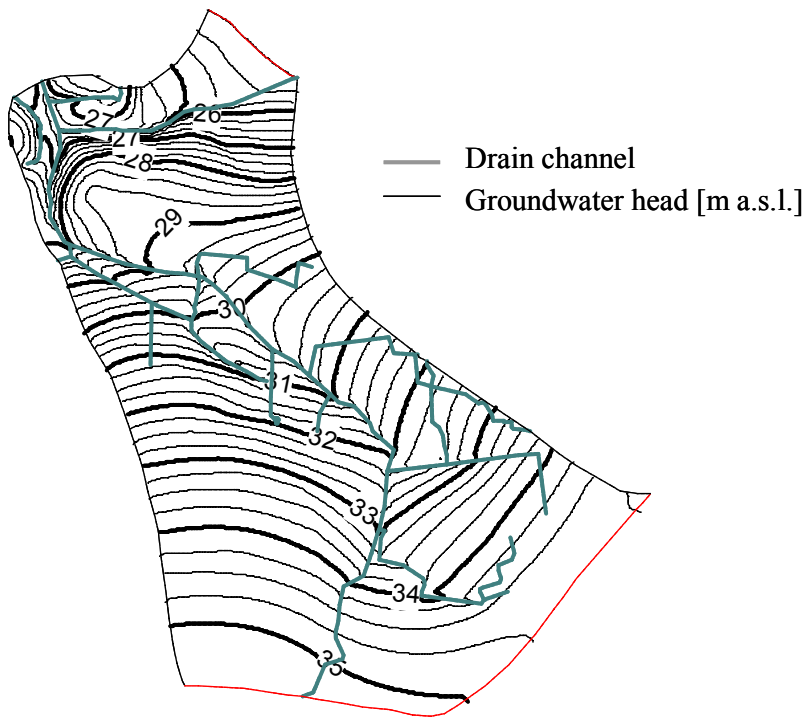


Figure 94: Calculated groundwater heads of the P5 catchment model

Table 26: Water balance of P5 catchment simulations

Simulation	Input [mm/a]		Output [mm/a]		Total [mm/a]	
	Recharge	Constant Head	Drain	Constant Head	In	Out
Distributed recharge	76 (97.2%)	2 (2.8%)	-74 (94.1%)	-5 (5.9%)	79	-79
Classified recharge	76 (97.7%)	2 (2.3%)	-74 (94.0%)	-5 (6.0%)	78	-78
Uniform recharge	76 (98.4%)	1 (1.6%)	-73 (94.0%)	-5 (6.0%)	77	-77
Buffer (100m)	71 (96.4%)	3 (3.6%)	-69 (93.8%)	-5 (6.0%)	73	-73
Model area	19.18	km ²				

The development of seepage concentrations (as average seepage concentration over all drain cells) of specific substances is shown in Figure 95 for conservative and Figure 96 for reactive transport, based on the “distributed input” simulation.

In the case of conservative transport, Nitrate concentrations increase approaching a maximum level, defined by the mean concentration of recharge water. Sulfate concentrations remain constant as initial concentrations are identical to recharge concentrations and rOM-concentrations show a slight increase, as the initial groundwater with low concentrations is mixed with recharge water of higher concentrations. The tracer and CO_3^{2-} were set to high initial groundwater concentrations and are not restored by recharge flux. They reflect the exchange of initial water with water entering the system from the recharge boundary.

In the reactive transport simulation, turnover processes are reflected in seepage water by considerably reduced nitrate concentrations with a maximum level of approximately 17 mg/l after 200 years, by an increase in sulfate concentrations due to pyrite oxidation, and by a less pronounced decrease in CO_3^{2-} due to production of inorganic carbon owing to degradation of organic matter.

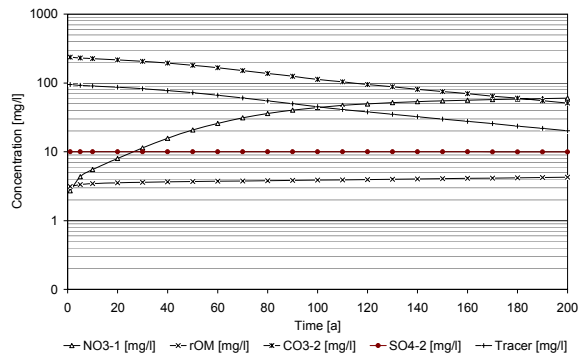


Figure 95: Development of mean seepage concentrations (conservative transport)

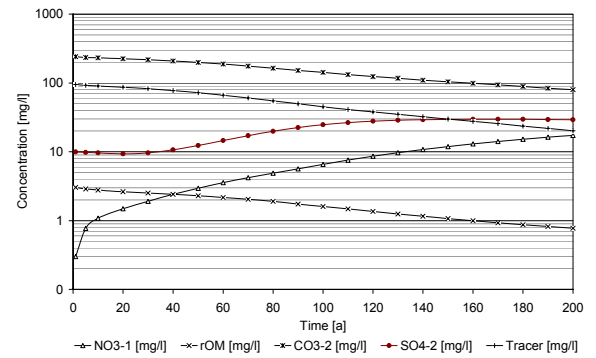


Figure 96: Development of mean seepage concentrations (reactive transport)

Figure 97 - Figure 100 present the development of nitrate concentrations in seepage water for the various simulations runs under conservative and reactive transport conditions.

Comparable to the artificial transect simulations, nitrate concentrations in seepage water increase following an S-shaped curve during conservative transport (Figure 97), according to the travel time distribution and the contribution of short and long flow paths to nitrate concentrations of seepage water. The maximum concentration is given by the average recharge concentration (70 mg/l), which is not completely reached during the simulation period of 200 years. It takes about 80 years, to get a nitrate concentration of 35 mg/l. The initial breakthrough to the aquifer system is characterized by a steep increase in nitrate concentrations, resulting from nitrate originating from areas in direct vicinity to the drain. The behaviour of nitrate breakthrough is well reflected in the first derivative of the breakthrough function (Figure 99), showing the change of nitrate concentrations per time. The initial breakthrough is characterized by a sharp peak, which is followed by a broad, second peak representing the sigmoidal increase in nitrate concentrations. The first peak can be referred to flow from neighbouring areas with low travel times, the second peak follows the travel time distribution and turnover in the remaining system. Reducing the spatial information of N-input from “distributed” to “classified” and “uniform” input, is clearly reflected in the breakthrough curves, although the differences of nitrate concentrations are not substantial. The “classified” and “uniform input” simulations behave more or less identical and approach the maximum level slower than the “distributed input” simulation, where concentrations increase faster due to the different arrangement of N-sources. The difference to the other two simulations reaches an approximately constant level throughout the simulation period. This gap can be expected to close again, if the simulation period was extended until the peak concentration is reached.

During reactive transport simulations, nitrate concentrations increase slowly at the beginning of the simulation period, with a growing increase until the end of the simulation (Figure 98). Seepage concentrations of nitrate during reactive transport simulations are considerable lower than in the conservative case and a nitrate concentration of 17 mg/l is not exceeded throughout the simulation. It is clearly to be seen, that corresponding to the conservative transport simulation, the “classified input” and “uniform input” simulations are again similar to each other (maximum nitrate concentration of 10 and 8 mg/l) and the increase in concentrations is slower than in the “distributed input” simulation (maximum nitrate concentration 17 mg/l). As shown in Figure 100, for the “distributed input” simulation, the rate of change in nitrate concentrations has exceeded a maximum and is again decreasing. This indicates, that future nitrate concentrations will approach a maximum as in the conservative transport simulations. The “classified” and “uniform input” simulations still show a growing increase in nitrate concentrations.

Application of a buffer area causes a reduction of nitrate concentrations compared to the “distributed input” simulation, which was taken as the un-buffered reference. The breakthrough curves run parallel to the corresponding curves of the reference simulation, but with lower concentrations. This can be observed for both, the conservative and the reactive case. The breakthrough curves and its derivatives do not indicate a special contribution of reactive processes (for example by considerably delay of breakthrough) and the lower concentrations can mainly be explained by the reduction of N-loads to the system.

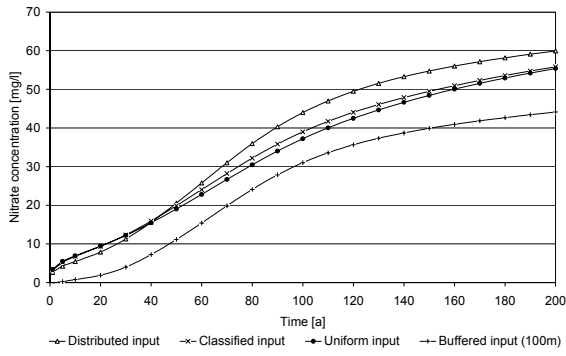


Figure 97: P5 catchment model runs – Nitrate concentrations of seepage water vs. time for conservative transport

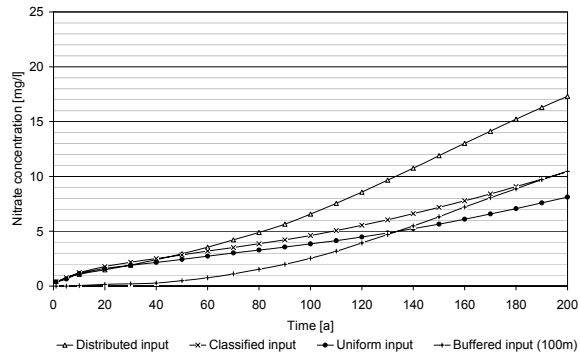


Figure 98: P5 catchment model runs – Nitrate concentrations in seepage water vs. time for reactive transport

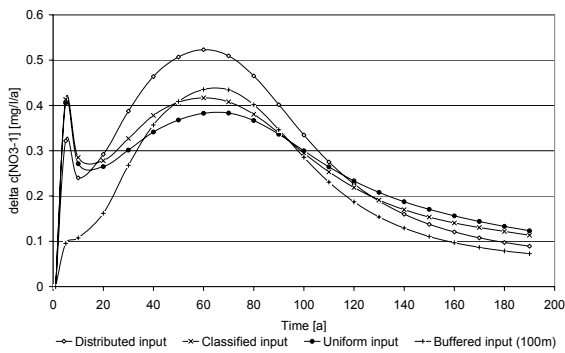


Figure 99: P5 catchment model runs – Change of Nitrate concentrations in seepage water vs. time for conservative transport

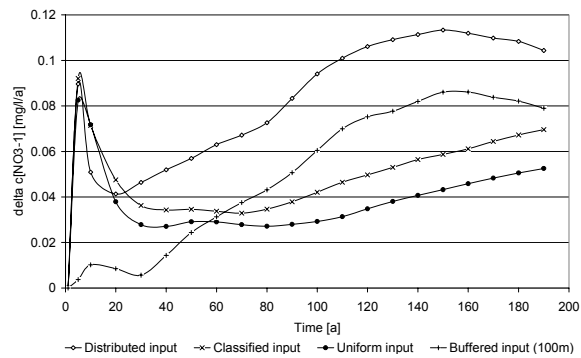


Figure 100: P5 catchment model runs – Change of nitrate concentrations in seepage water vs. time for reactive transport

As shown in Figure 101, seepage fluxes are not uniformly distributed in the channel system. High seepage fluxes can be observed in the central part of the channel system and at the outlet close to gauging station P5. In the same way, nitrate concentrations in seepage water and nitrate loads are spatially distributed in the channel system.

Assuming conservative transport, the distribution of nitrate loads reflects both, the distribution of seepage fluxes and of nitrate concentrations. The distribution of loads in the reactive transport simulation coincides with the distribution of nitrate concentrations.

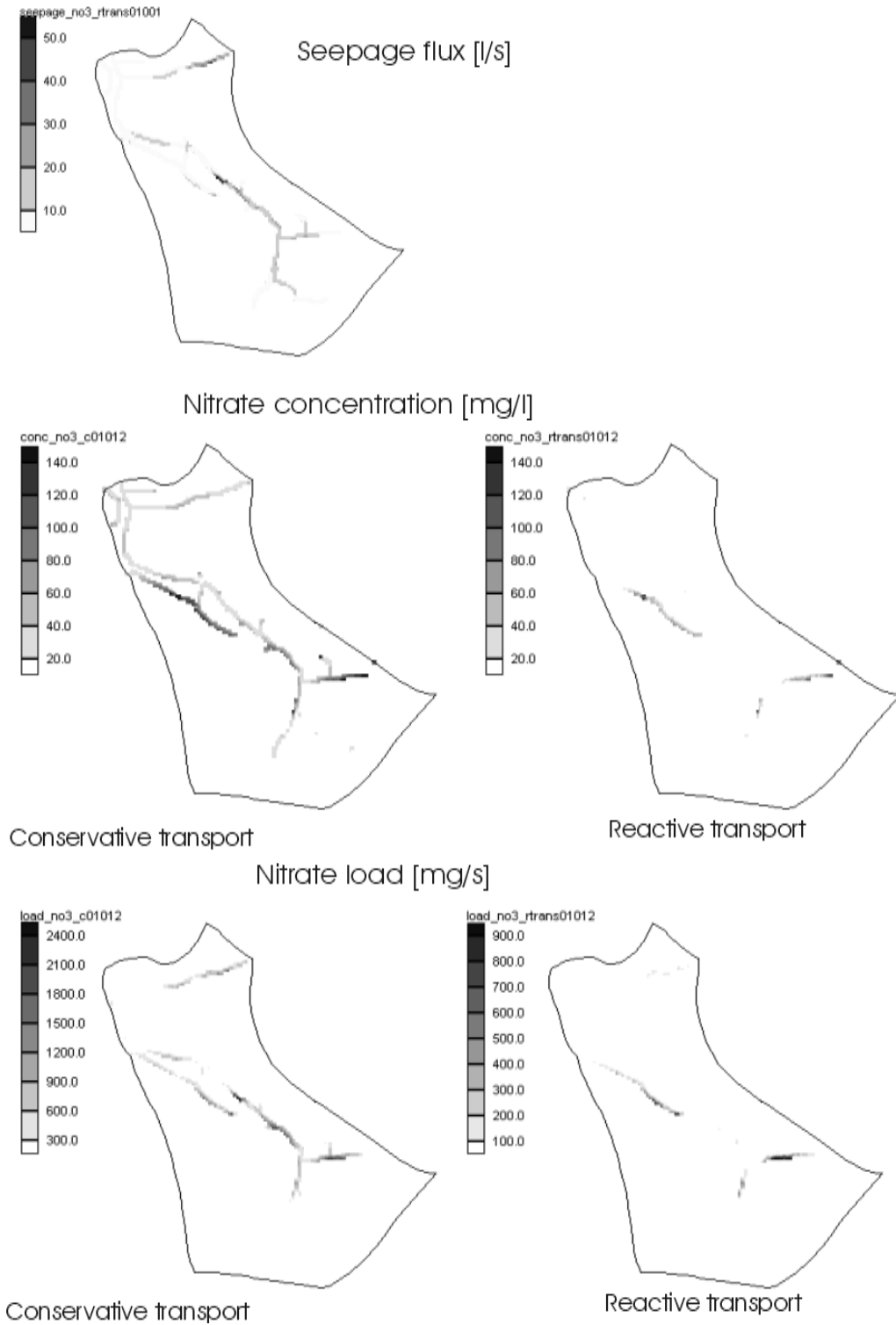


Figure 101: Seepage flux, nitrate concentrations and nitrate loads after 50 years

Nitrate (T=50a)

Conservative transport

Reactive transport

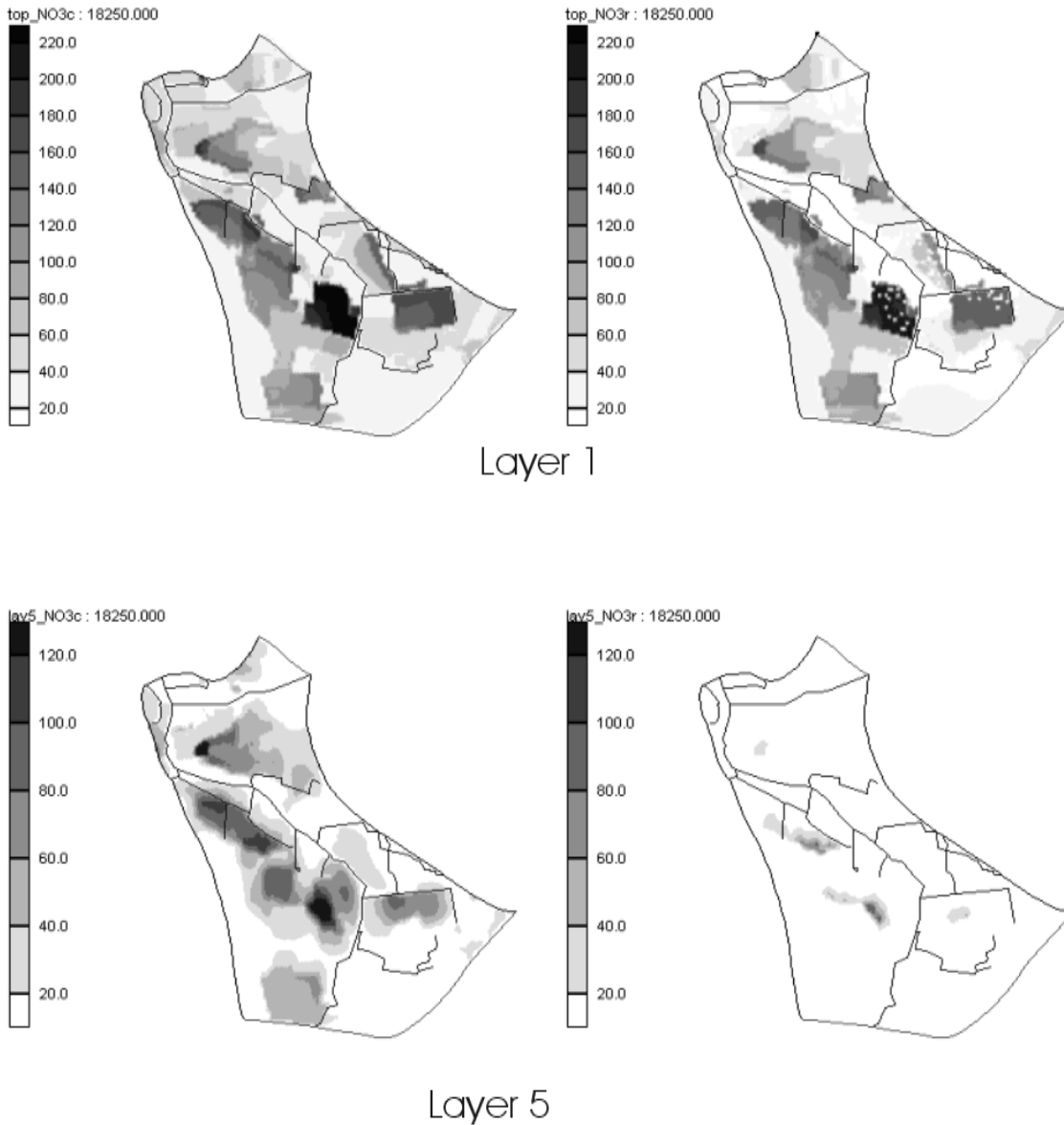


Figure 102: Distribution of Nitrate in upper and deep groundwater after 50 years

Figure 102 shows the spatial (horizontal) distribution of nitrate concentrations in the first (uppermost groundwater) and fifth model layer (deep groundwater) after 50 years, based on the “distributed input” simulation. The spatial distribution of nitrate concentrations in the uppermost groundwater layer is consistent with the spatial distribution of N-leaching from the soil, i.e. lower concentrations close to the drains and higher concentrations below arable land in greater distance from the drains. In the reactive transport simulation, nitrate is completely removed in a broad band along the drain channels. In these areas the content of SOM is considerably higher than in the rest of the modelling domain, allowing for an effective removal of nitrate.

Nitrate enters the deep groundwater locally, depending on the distribution of inputs as well as on the distribution of transport velocities. In the reactive transport simulation, the extent of contaminated areas is strongly reduced compared to conservative transport.

Nitrate (conservative transport)

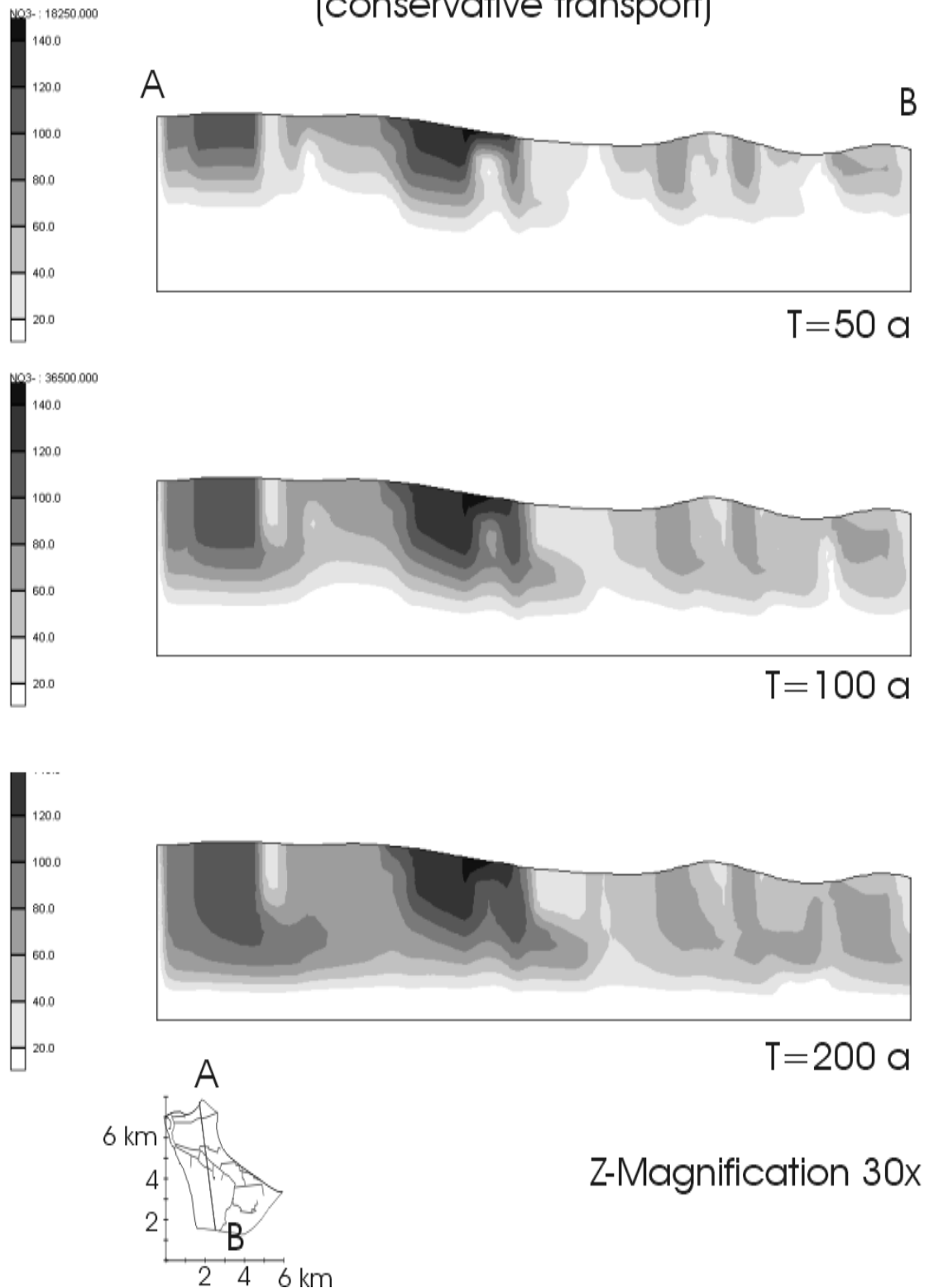


Figure 103: Distribution of nitrate along a cross-section of the model domain (conservative transport) after 50, 100 and 200 years.

Nitrate

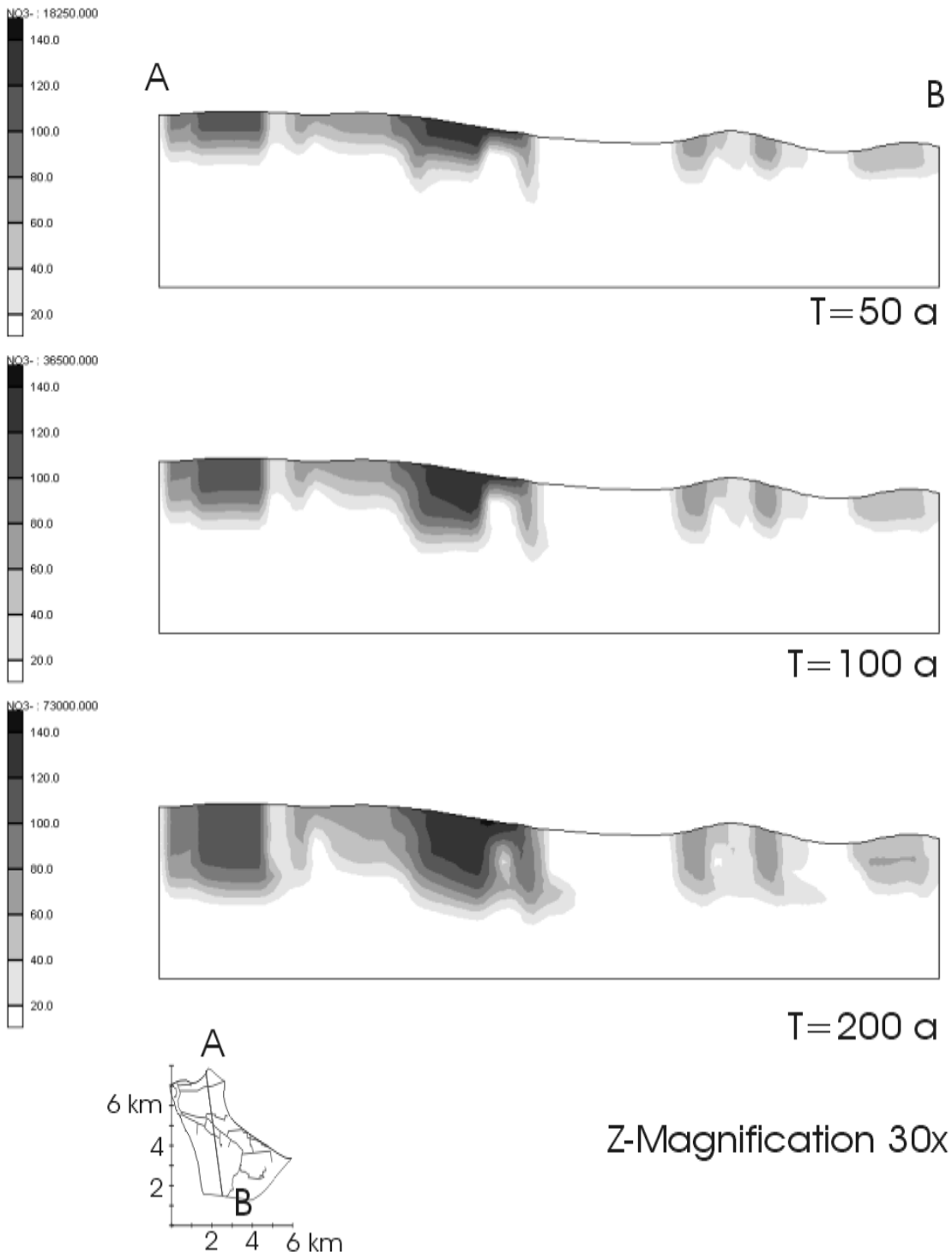
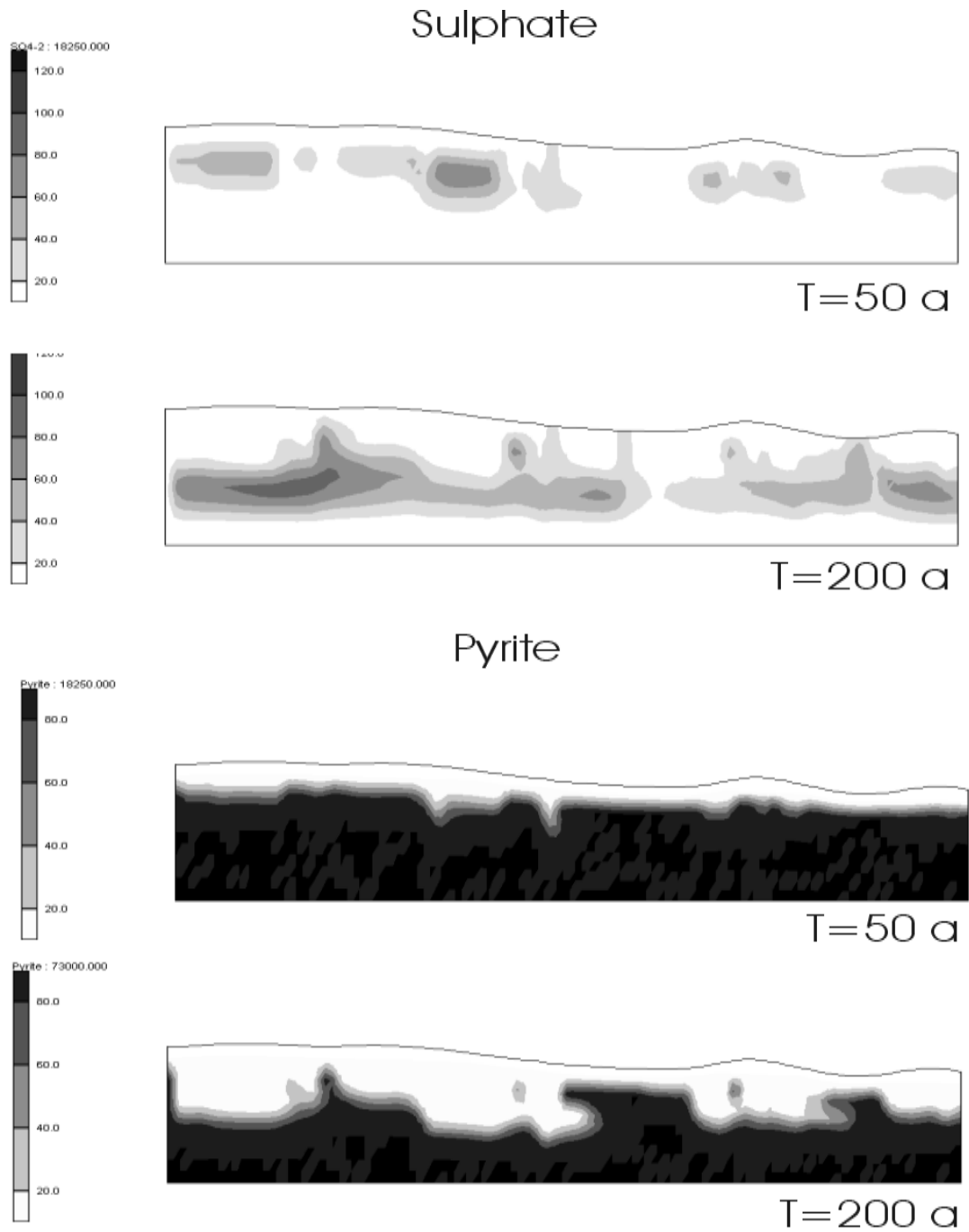
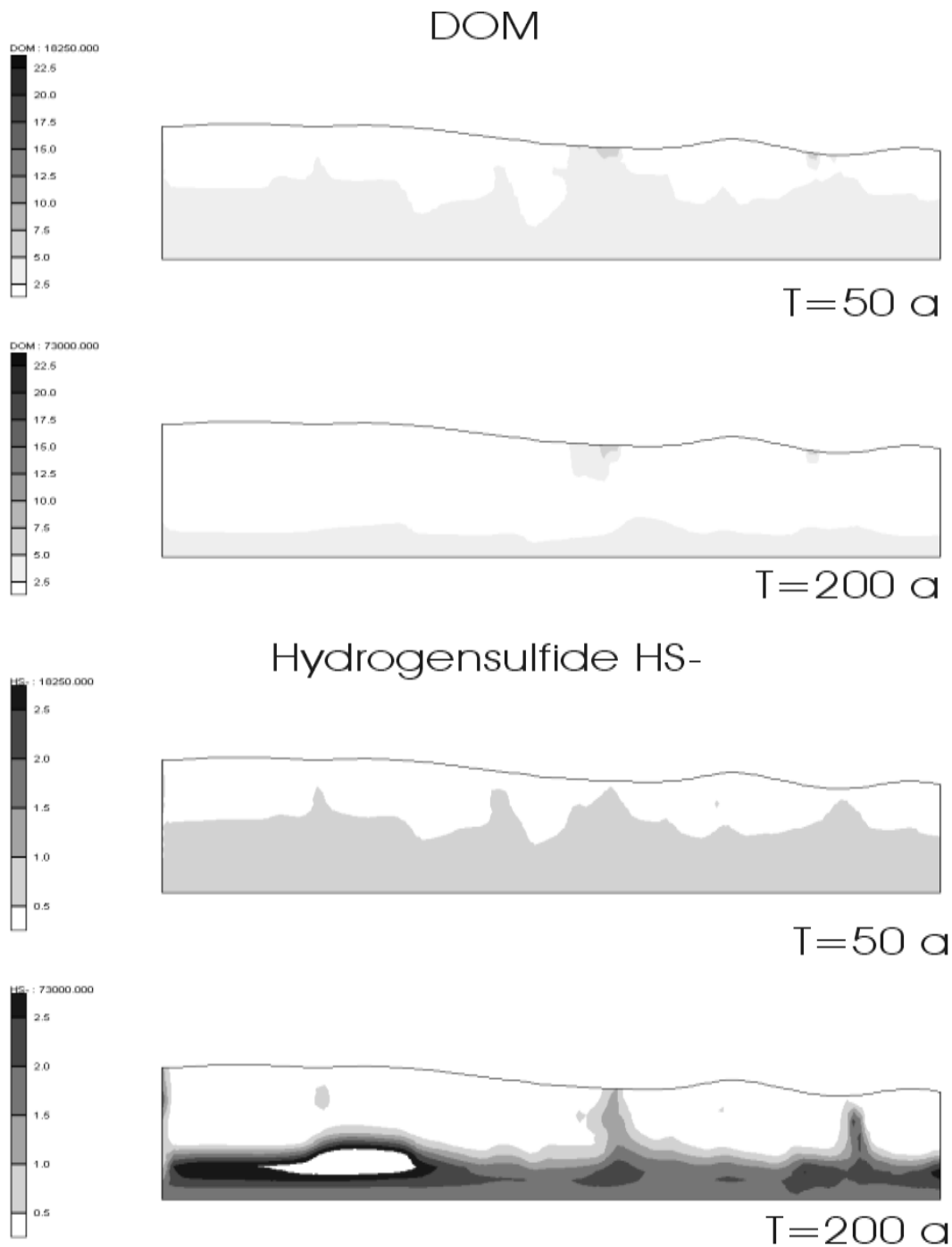


Figure 104: Distribution of nitrate along a cross-section of the model domain (reactive transport) after 50, 100 and 200 years.



Z-Magnification 30x

Figure 105: Distribution of sulfate and pyrite along a cross-section of the model domain after 50 and 200 years.



Z-Magnification 30x

Figure 106: Distribution of rOM and hydrogensulfide along a cross-section of the model domain after 50 and 200 years.

Figure 103 - Figure 106 demonstrate the distribution of solutes in vertical direction along a cross-section cutting the model domain. The depletion and production of the specific solutes following degradation of organic matter or pyrite oxidation is clearly reflected in the depletion of SOM and pyrite and production of sulphate. A desulfurication zone is found at the aquifer bottom, indicated by elevated hydrogensulfide concentrations. The propagation of nitrate and corresponding production or depletion of other substances is clearly heterogeneous. The reaction fronts are of irregular shape, characterized by zones of low progression and notable fingering into deeper parts,

depending on transport properties (conductivities, transport velocities) of the sediment.

5.5.3.2 Results of the subcatchment simulation

The hydraulic head distribution is given in Figure 107, the seepage concentrations for the reactive and conservative transport simulations are given in Figure 108 - Figure 111. The general features of nitrate breakthrough are similar to the preceding catchment scale simulations. The N-load from the soil is higher than in the catchment simulation (see Table 24). Therefore, seepage concentrations are higher as well. Differences in temporal development and absolute levels of seepage concentrations are due to the different arrangement of sources and sinks and transport characteristics of the submodel. The proportional effect of applying a buffer area is shown using different buffer width (0, 100 and 200m) for both, reactive and conservative transport. In contrast to the catchment scale simulations, concentrations of the “uniform input” are higher and increase faster than in the “classified input” simulation. This can be explained by the specific distribution of source areas within the model domain. A patch with considerable high N-leaching is located in the central part of the model domain, adjacent to the drain at the right margin. The drain at the upper margin is in contact with a grassland area, with low leaching of nitrate. In the “classified input” simulation, the loads are levelled out only for the landuse class. In the “uniform input” simulation, however, loads are levelled out over the total domain and N-emissions from the grassland are subsequently increased. The grassland area becomes an additional source area with low travel times, that was not active in the “classified input” simulation, whereas arable land is an active source of nitrate in both simulations.

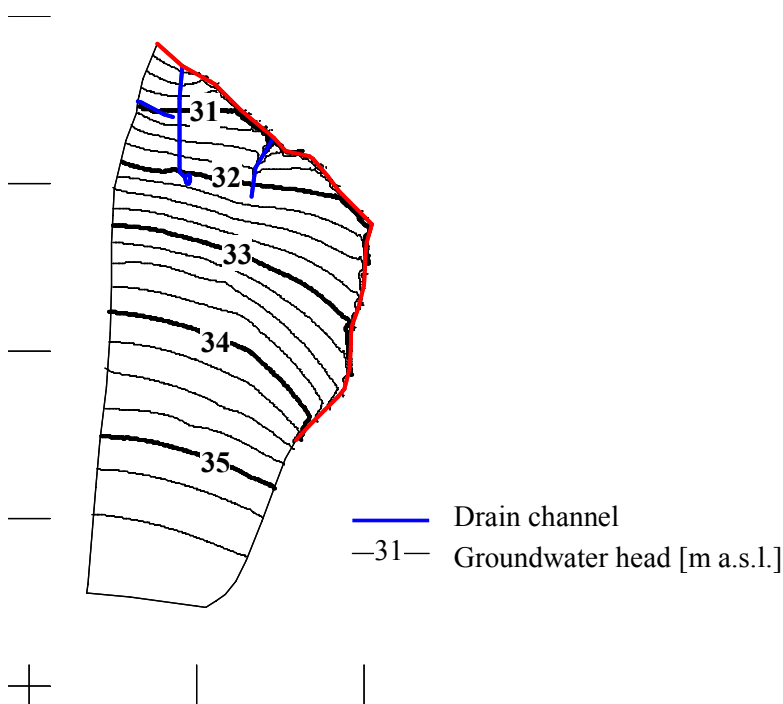


Figure 107: Simulated groundwater heads of the subcatchment model

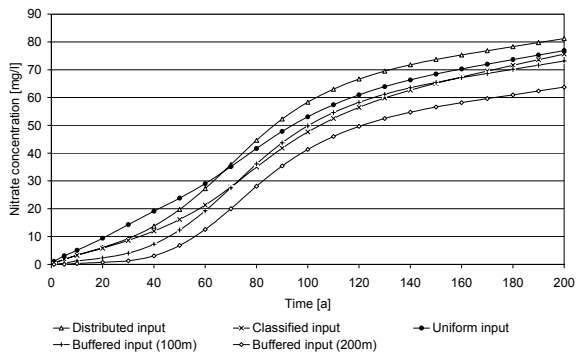


Figure 108: Subcatchment model runs – Mean nitrate concentrations in seepage water vs. time for conservative transport

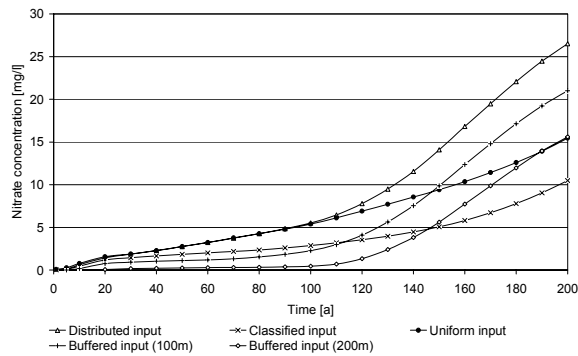


Figure 109: Subcatchment model runs – Mean nitrate concentrations in seepage water vs. time for reactive transport

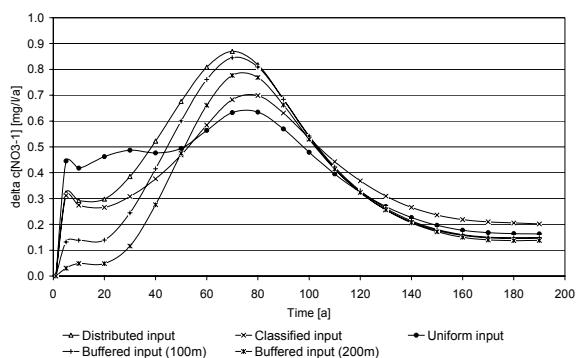


Figure 110: Subcatchment model runs – Change of mean nitrate concentrations in seepage water vs. time for conservative transport

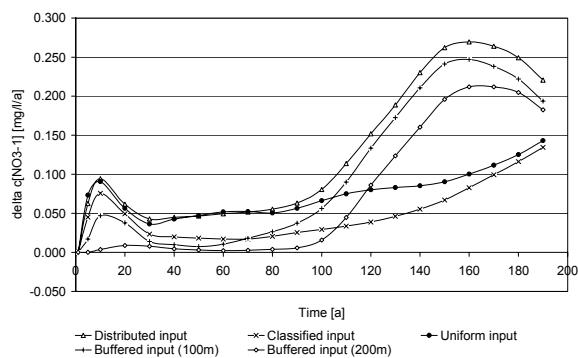


Figure 111: Subcatchment model runs – Change of mean nitrate concentrations in seepage water vs. time for reactive transport

5.5.3.3 Discussion

The preceding results of the groundwater simulations prove the model being capable of simulating spatial and chemical interactions related to nitrate transport in groundwater. The spatial distribution of nitrate within the sediment and the distribution of nitrate loads to the channel system are valuable information to determine “hot-spots” of nitrate pollution.

The role of spatial patterns on N-loads to the channel system was assessed by simplifying the spatial information from distributed to uniform input. Consequently, the distributed information is levelled out for landuse classes or the entire model domain causing a virtual reorganisation of source areas in relation to the distribution of near-stream areas with low travel times to surface waters and areas with higher travel times. This effect is mainly responsible for the different response observed in the single simulations. The differences are more clearly pronounced during reactive transport simulation runs than in the conservative transport runs. On the one hand, average seepage concentrations are an integrative measure over all drain cells. Thus, the spatial differentiation of seepage fluxes and concentrations is levelled out, when calculating average seepage data. On the other hand, total groundwater recharge and nitrate leaching are equal in all simulations and fix the upper threshold of possible seepage concentrations, forcing the breakthrough functions into a more or less similar shape. The influence of travel time distribution on the shape of the breakthrough curve seems to be higher than the influence of the spatial distribution of inputs. The advantage of simply reducing spatial information is that total recharge and N-loads remain constant. Otherwise, the effect of changed N-loads has to be taken into account for model interpretation as an additional factor influencing distribution and concentrations of nitrate in the system. For the same reason, input scenarios were defined on soil model outputs (distribution of recharge and N-leaching), rather than on soil model inputs (by rearrangement of

landuse patterns, management and soil properties). More pronounced effects can be expected if spatial patterns themselves are rearranged, while maintaining total loads and the patchiness of inputs. For example, a "classified input" simulation could also be based on the distribution of soil types. The investigation of spatial interactions does not need to confine on the redistribution of sources. Hydraulic or geochemical properties could be redistributed as well, e.g. by linking pools of pyrite and SOM or reaction parameters to the distribution of substrates.

The actual settings of the reaction scenario (distribution of reactive substances and reaction parameters) constitute a high reductive capacity of the system. Although a considerable reduction of nitrate concentrations can be observed compared to the conservative simulation, nitrate pollution is clearly reflected in seepage concentrations. From the beginning, nitrate concentrations are higher than 1mg/l and increase to final concentrations between 8 and 17 mg nitrate/l. The distribution of recharge loads also influences the removal of nitrate (see Figure 82 (Simulated mean annual N-leaching from the soil) and Figure 102 (Distribution of nitrate concentrations in upper groundwater)). Inputs concentrate on croplands, which are located in considerable distance from the channel system. Contaminated recharge water follows long flow paths, allowing for intensive contact and turnover with reactive substances. Close to the channel system, recharge water is more or less uncontaminated, as humic and gleyic soils under pasture have high soil denitrification capacities. If higher inputs of nitrate were located in direct vicinity of the drain channels, higher outputs into the channel system could be expected due to increased loads and short residence times in the aquifer.

Results of the buffer area simulation were comparable to the implementation of buffer areas in the artificial transect simulation. The reduction of seepage water concentrations can be referred to the decreased input of nitrate to the system. The buffer area does not enhance denitrification rates, as reactive pools remain unchanged. As in the transect simulation, the effect of plant N-uptake from groundwater was not considered. Plant N-uptake in the soil is implicitly considered in the model assuming that no nitrate is leached from the soil within the buffer areas. The contribution of a buffer area to nitrate removal (by denitrification) in a system with high reductive capacity may be marginal and should be evaluated carefully.

The temporal development of concentrations in seepage water and propagation of substances can be discussed in a general fashion only, as a discussion of absolute travel times for the specific catchment has to consider a variety of uncertainties. If conservative transport is considered, travel times and surface water response depend on the quality of the hydraulic model only. A standard porosity of 0.3 was used in transport simulations, but a value in the order of 0.15 would be reasonable as well. Decreasing porosity would proportionally increase transport velocity, and in this case the response would be accelerated by a factor of 2. This means, that a concentration of 35 mg/l could be achieved after 40 years and the maximum of 70 mg/l would be achieved well within the simulation period of 200 years. In the case of reactive transport, the size of reactive pools, turnover rates and the estimation of N-loads to the groundwater also determine the temporal development of nitrate breakthrough in ground- and surface water. According to the results of the artificial transect simulation, an increase in transport velocity by a modified porosity value would not only cause a faster model response. Additionally, the resulting seepage concentrations would be relatively higher, due to the reduced residence time within the sediment.

Observed nitrate concentrations in the Schaugraben drain channel (observed at gauging station P5) are 29 mg/l on average, ranging from 0 to 140 mg/l following distinct seasonal cycles, whereas observed seepage concentrations of nitrate lie between 1 and 17 mg/l. As only few seepage samples were available, observed seepage concentrations are possibly not representative. A direct comparison of surface water concentrations with simulated seepage concentrations is difficult, as the latter only present the base flow component of channel discharge and surface water processes also influence surface water concentrations. Additionally, the observation period is very short, compared to the simulation period and the previous history of inputs in the catchment is only poorly known. Thus observations can not be related to a specific time step of the simulation.

In the conservative transport simulations it takes about 70 years (with the given porosity of 0.3) to achieve an average nitrate concentration of 30 mg/l. As fertilizer levels were considerably higher before 1990, this level possibly may be reached faster in a real world situation. Assuming that input of excess N into the groundwater system has taken place for a period of 50 years, the simulated nitrate concentrations are within a reasonable range. However, experimental findings indicate

intensive reactive processes, thus the conservative transport scenario is not an adequate scenario for comparison to field data. In the reactive transport simulation, a seepage concentration of 3 mg/l is reached after 50 years, of 7 mg/l after 100 years and of 17 mg/l after 200 years. These concentrations lie in the order of observed seepage concentrations, but they are too low to explain observed surface water concentrations.

The model does not reflect intra-annual variations, as boundary conditions were kept constant throughout the simulation period. However, it is unlikely, that exfiltrating groundwater does considerably contribute to seasonal variations of surface water concentrations, as i) groundwater temperature cycles are not well pronounced or even not present (e.g. deep groundwater), ii) and seasonal patterns dissipate during groundwater transport by mixing and dispersive processes. Observed nitrate concentrations in groundwater wells of the study site do not show pronounced seasonal cycles of nitrate concentrations either.

Consequently, other sources have to be evaluated to explain concentrations up to 140 mg/l and a seasonal change of nitrate concentrations. According to Kunkel and Wendland (1998), it can be assumed that in areas with high aquifer denitrification capacity, nitrate concentrations observed in the discharge system originate mainly from direct flow components or drain flow. This assumption is supported by the well pronounced seasonal cycle of nitrate concentrations in surface water (see appendix A), indicating high inputs during winter. However, observed drain concentrations range between 9 and 165 mg NO₃⁻/l, which is in the order of simulated recharge concentrations (average concentration: 70 mg/l). Unfortunately, no discharge data were available for the various tile drains and total loads or average concentrations can not be estimated. A preliminary hydrograph separation indicated that direct runoff components accounts for less than 10% of channel discharge. A doubling of surface water concentrations from 30 mg/l to 60mg/l would require a drain flow concentration of 870 mg/l, assuming a 10% fraction of drain runoff. Thus, the given data do not completely explain surface water concentrations. According to Borges (2003, oral communications) a significant input of nitrogen into the channel system can also be attributed to other sources. In the study area, several fields are directly located at the Schaugraben drain and during fertilization considerably amounts of manure are directly brought into the channel system. The drain is also bordered by alder trees over considerable length. Leaf fall in autumn and subsequent mineralisation could also contribute to surface water concentrations. Putting all these sources together might well explain the observed nitrate concentrations and seasonal cycles.

Of course, it is also possible, that reactive processes are overestimated by the model. A reduction of reaction rate constants or contents of reactive substances would considerably raise seepage concentrations to levels more consistent with observed data. A seasonal cycle of nitrate concentrations in surface waters can also be caused by denitrification and plant N-uptake in the hyporrheic zone and the surface water system.

Putting it all together, surface water concentrations are the result of various interacting processes: i) low nitrate concentrations in seepage of groundwater, controlled by aquifer denitrification capacity, ii) intermittent contribution of direct flow components or drain flow with high nitrate concentrations, iii) seasonal denitrification and plant N-uptake in the surface water system iv) direct inputs into surface waters. Simulated seepage concentrations are not contradictory to observed surface water and seepage water concentrations. However, data on hand are not sufficient to quantify the relative contribution of these sources and processes.

A further extension of the model system to include the additional sources and processes (tile drains, hyporrheic zone and in-stream denitrification, plant uptake) would be necessary to calculate real surface water concentrations.

The results of the subcatchment simulations are consistent to the catchment simulation. Although individual behaviour can be observed, depending on the specific subcatchment characteristics (distribution of source areas and nitrate loads), the general characteristics of nitrate breakthrough are identical.

6 Discussion

6.1 Transport and turnover of nitrogen in lowland catchments

A model is only a simplified concept of reality and consequently a model can only represent processes and interactions which were considered a priori in the model definition. The following principles are inherent to the modelling system:

- Reactive pools of pyrite and organic matter define the total denitrification capacity of the aquifer. This denitrification capacity is not sustainable, as these pools are not renewable. The denitrification capacity expresses the potential for nitrate turnover and must not be mistaken for the denitrification rate, which expresses turnover per time increment.
- In soils a sustainable denitrification capacity is given by cycling of soil organic matter including primary production. The denitrification rate is limited, depending on the availability of degradable organic matter and the seasonal distribution of denitrifying conditions (temperature and anaerobic conditions).
- Soil organic matter adds a sustainable denitrification capacity to groundwater by leaching of dissolved organic matter and by close contact between soil organic matter and groundwater in semi-terrestrial locations.
- The reaction rates change over time depending on the availability and depletion of reactive substances. The total turnover is not only determined by reaction rates, but by contact time as well (contact time is reaction time).

In this study, model parameters are largely based on estimates from literature and may therefore not be representative for the specific study area. Uncertainty is inherent to the various input data and a further investment in field data assessment and monitoring can only partly overcome this problem for methodological reasons. Examples are the assessment of substrate distributions, vegetation nitrogen dynamics, and the definition of effective parameters. Consequently, model results for the Schaugraben catchment area are only valid with respect to these limitations. On the other hand, the simulations are based on realistic or reasonable estimates and assumptions, as far as can be judged from literature. Thus model results allow a general discussion of interactions between catchment characteristics and substance transport in the Schaugraben area and comparable catchments. The general results of the simulations related to N-transport can be summarized as follows:

- The response of ground- and surface water systems to N-loads is defined by distribution of flow paths and travel time characteristics, the spatial distribution of sources and sinks and the distribution of reactive sinks.
- Surface water concentrations can not be explained by the contribution of groundwater flow. Other sources and sinks of nitrate have to be taken into account, explaining the strong seasonal variations of nitrate concentrations observed in the surface water system. Possible mechanisms are drain flow, direct inputs by leaf fall and fertilisation, and surface water processes, which are not implemented in the model system.
- Seepage fluxes, nitrate concentrations in seepage water and nitrate loads vary spatially in the channel system. This allows to define hot spots, where contaminated groundwater enters the surface water system. Such areas can be of interest for targeted measures.
- Using different spatial information of N-emissions to groundwater was reflected in model results. Considerable differences were observed using aggregated spatial information compared to the distributed input simulations, due to reorganisation of source areas and their travel distance from the channel system. Spatial patterns within the catchment can only be evaluated, if the distribution of sources and sinks is represented in the model. A simplified input scenario, which does not resolve differences between individual patches, does not properly represent spatial features of groundwater or surface water contamination. It needs to be taken into account that the distribution of reactive substances in the groundwater was based on simple assumptions. Considering geochemical heterogeneity in the sediment will have considerable influence on model results.

6.2 Practical consequences for managing nitrogen pollution

The classical way of dealing with pollutants in the environment is the reduction of emissions. In the case of nitrogen pollution, a major source of nitrogen to catchments is application of nitrogen fertilizer on agricultural areas. A reduction of fertilizer application can be achieved by optimisation of management strategies, including reduced application of N-fertilizer, selection of fertilizer types and time of fertilizer application. Policy measures are another option to control excessive use of fertilizer or to bring forward new management strategies. However, not only the management of pollutants but also the management and manipulation of natural attenuation processes can be considered an important measure dealing with pollutions, as proposed by Zalewsky et al. (1997):

“... when human populations and aspirations are increasing, it is not enough to protect the water resources by reducing energy use and pollutant emissions – rather, it is necessary to enhance the buffering capacity of the catchment using an understanding of both, hydrological and ecological processes. In short, elimination of threats, without consideration of increased opportunities, cannot lead to the success.” (Zalewsky et al., 1997)

Natural attenuation processes have mostly been considered within the framework of risk assessment, focussing on the response of a natural system to a given pollution. Following the statement above, it has to be asked, i) if it is possible to utilise and manage denitrification capacity in lowland catchments and ii) if manipulation of natural attenuation can be a useful strategy to deal with nitrate pollution.

The denitrification capacity is determined by the chemical composition of the sediment and can not be altered artificially. To some extent, leaching of DOM from the soil may be changed by altered vegetation and soil water dynamics. Reaction rates can not be altered as well, as they depend on substrate characteristics and chemical constraints. Total denitrification may be enhanced by increasing contact time between nitrate and reactive pools. Therefore, it would be necessary to decrease hydraulic gradients and flow velocities or to promote anaerobic conditions in the area. The first could be achieved by reducing groundwater recharge through manipulation of the vegetation cover. The second option could be achieved by rewetting and restoration of wetlands. All these measures require (or are accompanied by) a change of vegetation cover and consequently, N-emissions will be altered as well. The effect of altered N-loads is possibly more important than the change in nitrogen turnover, which can be considered a by-product.

Natural attenuation of nitrate (denitrification) will cause a reduction of reactive pools and thus should not be considered an integral part of sustainable management strategies. However, this does not mean, that the measures indicated above are of no value for reduction of N-pollution.

Installation of buffer areas generally does not alter geochemical conditions of the subsoil. Solute transport in soil and groundwater is affected by buffer areas only as far as roots of the vegetation in the buffer area take up groundwater and solutes (DVWK, 1997). Due to the low relief in the area, surface runoff and erosion can be neglected as a source for nutrients entering surface waters. As discussed by Kofalk (1998), the effect of plant N-uptake for reduction of groundwater (or interflow) N-loads is highly variable and strongly depends on vegetation and vegetation dynamics. Evaluation of these effects was beyond the capacity of this study. Generally speaking, the main effect of buffer areas on N-transport in groundwater is based on the decrease in total N-load in the catchment. However, the areas close to surface waters are of considerable relevance for surface water pollution, due to the short travel times to the surface waters and the possibility of direct inputs of fertilizer. Especially in the Schaugraben area, there are many areas close to the channel system, which are intensively cultivated. Thus buffer areas may be an effective tool i) to reduce the total N-load to the catchment and ii) to keep N-loads away from areas with short travel times to the surface waters. Doing so, surface water response can be delayed for a certain period of time. Additionally, buffer areas may be useful tools for protection or restoration of areas with high denitrification potential, such as wetlands and organic soils.

The reduction of N-loads remains the main measure to protect ground- and surface waters, and optimisation of management strategies and targeted policies are needed. Distributed modelling of soil- and groundwater processes has to be considered as a tool to increase knowledge of flow paths, distribution of source and sink areas as well as of reactive sinks. This information can be used to target measures in areas with low denitrification capacity or high N-loads or to decide on

priority of measures for ground- and surface water protection.

It has to be kept in mind, however, that removal of nitrate is not independent of other geochemical processes and release of substances during denitrification reactions or in subsequent reactions (release and oxidation of iron(II), precipitation of iron oxides, desulfurication) are also of concern for water quality.

6.3 Characteristics of the modelling system

The development of a modelling approach that is capable of simulating nitrogen transport and turnover in soils and groundwater was a primary goal of this study. This was done by combined application of specific soil and groundwater models simulating water flow, solute transport and turnover. The modelling system allows the study of interactions between catchment characteristics and distribution of nitrate in the catchment system, including seepage into the surface water system. This is possible by combining distributed modelling of soil processes, 3-dimensional groundwater flow and full reactive transport, coupling nitrate turnover directly to reaction partners.

The main results extracted from the various model applications include i) distributed soil water and N-budgets, ii) distributed and average seepage fluxes and substance concentrations in the channel system and iii) two and three-dimensional evaluation of solute distributions, giving information on groundwater quality, hydrochemical aquifer zonation and propagation of hydrochemical zones in space and time, iv) travel time distributions.

The selection of the individual submodels aimed at a good representation of relevant nitrogen transport and turnover processes. At the same time, practical constraints had to be taken into account, such as the availability of the source code, the effort to transfer data between the models and costs of the models. The models used in this study are available as freeware and not bound to specific pre- and postprocessing software. The various sub-models are able to consider relevant processes and allow flexible model design. Application of loosely coupled models (i.e. by one-way transfer of model results) allows a fast and simple exchange of individual models, if the interfaces are well defined.

An improvement would be a modification of the soil water submodel. Application to lysimeter data showed, that the representation of soil water dynamics could be improved. This should be done primarily by a finer discretization of the soil column for water fluxes. In contrast, the complexity of the soil-nitrogen-model RISK-N is considered to be sufficient and allocation of accurate input data seems to be more important than model structure.

The key issue of the reaction-module is to link nitrate turnover stoichiometrically to the availability of reaction partners. Thus full reactive transport modelling is a prerequisite to solve this task. The complexity of the reaction system and the choice of reaction rate expressions are subject to the needs of the user and modifications are possible. Not all processes considered are needed to calculate nitrate turnover, some are used to define the general geochemical context. This is useful, as hydrochemical trends provide indirect measures of processes and give additional information for comparison of observed and simulated water quality.

The RT3D code requires programming of the reaction-module and recompilation after each modification. PHREEQC-based transport codes like PHT3D seem to be more flexible, as modifications can be made more easily and handling of equilibrium reactions is implemented as well. Alternatively, the TBC code can be used to implement reactive transport systems. It was not possible to test the performance of other transport codes and to compare them with the RT3D model. PHT3D was still under development. TBC does not offer an interface to MODFLOW. Concerning accuracy of the different transport codes, no considerable differences have to be expected, as transport equations and numerical restrictions are similar in all models.

An alternative modelling approach could be based on a single 3D-saturated/unsaturated flow model, which would consider vadose zone and groundwater flow and transport simultaneously and also allow a better representation of ground- and soilwater interactions (e.g. FEFLOW (Diersch, 1998)). Soil processes have to be considered by a separate soil-nitrogen-model as well, but vadose zone transport is already included. Thus a more common soil-nitrogen-model could be chosen, which can be based on elementary areas rather than on a model grid (e.g. Candy, WASMOD, etc.), as groundwater depth does not need to be considered. However, solution of the

non-linear Richards-equation for variably saturated flow is much more complex than solving a saturated flow problem. Considering reactive transport forces the entire system into time steps defined by the fastest process resolved. As a result, the computational demand is increased considerably. Another disadvantage of such an approach is that there are currently no codes available allowing integration of full reactive transport in variably saturated media. An increased demand for reactive transport modelling and the ongoing development of hard- and software facilitating the application of more complex and memory-demanding models, have stimulated the development of reactive groundwater transport codes in the last years. It can be expected, that technical development will furthermore stimulate development and application of new modelling approaches.

All groundwater simulations were carried out under steady-state conditions over decades and centuries. Theoretically, all modelling tools allow a time-variant simulation of nitrate transport, although the technical effort to simulate time-variant groundwater flow and transport using MODFLOW and RT3D is considerably high (MT3D and RT3D run under constant flow conditions only, thus new simulation runs have to be started for each stress period). The soil sub-model mRISK-N was run in transient mode with daily and monthly resolution, but results transferred to the groundwater model were aggregated to average data. Time variant modelling would be of special interest for simulation of intra-annual (seasonal) dynamics or for evaluation of long-term landuse-changes. In the latter case, however, temporal resolution would be based on years or even longer periods. Concerning the long residence times in the groundwater system, seasonal variations would only affect groundwater close to the surface. As a groundwater package is likely to undergo several temperature cycles as well as mixing with other groundwater packages, considerable seasonal variations in seepage concentrations do not need to be expected. Seasonal fluctuations of surface water concentrations are more likely a result of internal processes and the intermittent contribution of drainflow to surface water loads.

The model chain ends with seepage to surface waters, giving a potential contribution of groundwater flow (base flow) to nitrate contamination of surface waters. A representation of intermittent drain flow components as a second source of nitrate to surface waters is still needed to complete the representation of transport from the soil to the surface water system.

Such a calculation of drain flow requires i) a transient simulation to quantify annual flow rates and ii) an appropriate representation of chemical gradients from soil to groundwater in order to calculate accurate drain flow concentrations. Therefore, drain flow should be implemented in the soil model. Using the MODFLOW drain package would be inappropriate for this task, as cell-averaged groundwater concentrations are not equivalent to drain flow concentrations.

Seepage fluxes and concentrations could also be used as input data for the simulation of channel flow and surface water quality models. Hydraulic models coupling river systems to the MODFLOW groundwater model are already available (MODBRNCH, Swain and Wexler, 1996), whereas for coupling of surface water quality models appropriate interfaces still have to be developed. However, coupling of surface water models requires to consider the different spatial and temporal support of groundwater and surface water models, as surface water processes are again characterized by annual cycles and a finer spatial and temporal resolution than in the groundwater model is needed. Nitrogen turnover processes in the hyporheic zone can not be resolved by a groundwater model due to the limited spatial extent of the hyporheic zone. Such processes have to be considered in surface water quality models as well. Recent projects at the UFZ focus on Nitrogen turnover in the hyporheic zone and surface waters (Borges and Rode, 2002; Borges et al., 2003).

6.4 Transfer of the modelling approach and simulation results

The modelling approach can easily be applied in other lowland areas. The hydrological and chemical processes are in principle the same and the fully distributed approach allows a flexible adaption and parameterisation of the specific area under investigation. Due to the modular structure of the groundwater model and the flexible data transfer from the soil model, a wide range of hydrological settings and management situations can be considered. Problems will arise in areas with bedrock and a pronounced relief, as interflow components and surface runoff will become more important and other hydrological models are needed. The methodology as well as various software tools were developed and tested for the Schaugraben area and some experience could

be made. Thus application of tools and methodology in other areas will be much less extensive than for the Schaugraben area.

The main problem applying the models in other areas is the setup of an appropriate data base. As was shown, input data carry considerable uncertainty. Costs and time will constrain the effort put in field observations and data survey. The simulation of the Schaugraben area was largely based on public data, provided by geological and environmental authorities, e.g. climatic, (hydro-) geologic and topographic data. Public data should at least theoretically be available for other areas as well, probably with different density and quality. A crucial point is the survey of management data and plant parameters in order to calculate site-specific soil-N-budgets. Public data bases (e.g. statistics, fertilizer guidelines) can provide valuable information and estimates. These data can be improved by detailed and site specific surveys, as was done in the Schaugraben area.

Further simulations may concentrate on evaluation of management strategies or the effect of landuse changes in a reference area (e.g. Schaugraben area). The interactions between the reductive capacity (geochemical catchment properties), the travel time distribution (physical catchment properties) and the nitrogen load (management) are clearly defined in the model, though complex in detail. Thus the simulation results can be discussed at least qualitatively in other areas as well.

Transport simulations were carried out at the field scale (tracer experiment and artificial transect) and at the catchment scale (catchment and subcatchment simulations). Currently, there is a strong trend to simulate large catchment areas or river basins and to include water quality issues as well. In order to meet the requirements of the EU-WFD, the effect of (mostly small scale) measures shall be assessed on a river basin scale. There are also attempts to consider groundwater flow and reactive solute transport on a river basin scale. Thus the question is raised, if the modelling approach can be applied to larger areas as well.

Application of the modelling approach for large catchments is not a technical problem. However, transition to a larger scale is typically connected to a change in model support. Following Heuvelink (1998), the term "support" refers to size, shape and orientation of the model entities. The concept of support is related to the level of aggregation or sample volume, resolved by the model and defines the resolution and representation of real-world patterns in the model. The constraints set by the model support need to be considered in model setup and interpretation of model results. As shown, the behaviour of some rate expressions is not independent of grid resolution and numerical dispersion might cause unwanted distribution of substances. Consequently, it is generally considered good practice to test model results with different grid resolutions. However, a finer grid resolution does not necessarily mean a better representation of sedimentary and chemical structures, if field data do not allow finer interpolation. Another problem is that concentrations are always averaged over cell-size: Reaction parameters have to be considered as "effective parameters", if important structures are given at the sub-cell scale (e.g. humic layers) and simulated concentrations can not directly be compared to observed concentrations, as the observation scale (point data or integrative measures) is not equivalent to the model support.

One possibility to simulate river basins is to maintain a small scale model support and to extend a detailed data assessment to a larger area. Application of the various models is theoretically not confined by the size of an area, including even large river basins, if a small scale model support is maintained. However, severe practical constraints will be set by the computational capacity available and the effort of a detailed data assessment. Another possibility is to increase cell-sizes into the range of square-kilometers. In this case, the vertical and horizontal distribution of solutes can no longer be represented adequately and appropriate scale specific reaction approaches have to be applied, being capable of representing phaenomenological behaviour. Reaction parameters as well as reactive pools have to be assigned as effective values over grid-cell-size and methods to define such effective measures have to be developed. Also methods are needed to test model results on observed data.

As the modelling approach is based on coupling of various submodels, constraints of the possible model support are also set by the need to transfer meaningful data between the models. Model coupling requires spatial and temporal aggregation or disaggregation of model results, according to the specific characteristics of the models used, and important information may be lost.

6.5 Problems of model identification

The term model identification in this discussion refers to the problem of finding a set of model parameters giving the best fit to observed data. Typically, this involves model calibration to observed data as well as a validation to independent observation data, using the calibrated parameter set.

For complex modelling systems, it is useful to calibrate in the order water flow, solute transport and turnover and to separate for the various compartments (or submodels), if data allow doing so. However, there are various reasons impeding successful process or model identification, as shown in various simulations carried out in this study:

- Point observations (e.g. groundwater levels and concentrations) represent local conditions, which might not be reflected in input data. Thus point observations can not be related directly to model results at the specific locations.
- Processes can not clearly be separated using concentration data (e.g. seepage concentrations), as concentration data result from the interaction of substance loads and turnover processes in the preceding system compartments.
- A poor model fit can be caused by inaccurate model parameters as well as by uncertainties of input data. This is especially the case, if input data are spatially distributed (e.g. substrate distributions).
- Complex models are in fact a system of dependent and interacting processes, which have to be identified individually. The identification of individual processes (e.g. denitrification or mineralisation) requires extensive process studies, which are typically carried out as point observations or as laboratory studies. They can give estimates for actual model parameters only, but can not be considered representative at the catchment scale.
- Many processes or their interactions cause similar phenomenological behaviour and the system can be described by more than one parameter combination (parameter equifinality) (or by different action of processes, e.g. reaction velocity vs. substrate availability).
- Observation time series of not more than a few years are too short. Considering the high uncertainty of input data, only well pronounced trends can be considered significant. Substance outputs are considerably delayed to substance inputs, due to the slow catchment response. Thus long time-series of observation data over decades are needed to cover inputs and corresponding outputs as well as long-term trends.
- The water flow problem is constrained by water balance terms such as precipitation, discharge and water levels (groundwater surface). Each possible parameter combination has to satisfy the overall water balance and catchment water flow can be subjected to calibration. Transport and turnover, however, are much less defined and the simulation has to be based on input data and best parameter estimates.

To conclude this discussion, it can be said that a calibration or validation of such an integrated modelling approach is not possible. The best possible model fit for a specific area is limited by uncertainties of input data. Typical observation data on catchment scale do not identify the system, due to process interactions and non-representativeness. They provide valuable information, however, to assess plausibility of the simulation. Due to the slow catchment response to surface loads, long time series of observation data are needed. This seems to be a key issue for successful model identification.

6.6 Relation between modelling effort and progress in studying catchment processes

Integrated modelling of nitrogen transport and turnover in a catchment system is a complex task, involving expert knowledge from various disciplines. Although the models were kept as simple as possible, many data had to be processed for setup of a distributed simulation. Although many input data were taken from public sources, the effort put into data assessment and preprocessing was considerably high. Still, the data base can be improved by more detailed data or longer observation periods.

However, only a fully distributed modelling approach, integrating soil, vadose zone and

groundwater processes, provides the capability of studying nitrate transport in a lowland catchment system and to consider chemical and physical interactions. The simulations carried out gave a deep insight into spatial and temporal implications of nitrogen transport in lowland catchments. They also showed limitations as well as the high potential of such a modelling approach for studying nitrogen transport at the catchment scale. The possibility to integrate local observations into a spatial and temporal framework and to extrapolate processes for prognosis of future developments or scenario analysis can not be substituted by any sort of observation. Thus the work put into data assessment and processing is absolutely necessary and should be carried out carefully in order to provide the best possible data base.

Due to the complexity of the problem and the effort of data assessment and processing, such an integrated modelling project can strongly benefit, if it is connected to long-term interests. Then a mutual improvement of the modelling system and field data assessment is possible. On the one hand, model results help to improve and target monitoring strategies and to define process studies. On the other hand, the results of field data assessment may be used to improve the model data base and process representation. This procedure might lead to a step-wise reduction of uncertainty and improvement of the prognostic value. Such an approach might be of special interest for water suppliers and water authorities, as management and protection of ground- and surface waters has to consider economic interests as well as long-term developments of water quality.

6.7 Recommendations for model improvement and future research

As indicated above, further modifications and extensions of the modelling system are necessary. This includes the following topics:

- A better representation of soil water dynamics, using a finer discretisation of the soil column. This extension is expected to improve the simulation of intra-annual soil water dynamics and subsequently simulation of soil nitrogen dynamics.
- The implementation of a drain flow model to account for intermittent flow components, establishing a short cut of soil water and surface waters. This should be implemented in the soil model, as the groundwater model does not resolve small scale concentration gradients.
- Coupling of a surface water quality model, implementing hyporheic zone processes as well as in-stream processes, such as plant N-uptake, nitrification and denitrification.

The interaction between input of N to groundwater and output to the surface water system was based on simple simulation scenarios. Further studies should intensify investigation of model response to spatial distribution of source areas and reactive substances. Such simulations should consider model response i) to redistribution of N-inputs to groundwater maintaining patchiness, ii) to changes of landuse patterns and iii) distributed pools of pyrite and SOM (for example according to substrate distribution). Also of special interest is catchment response to changes in landuse and N-emissions or the analysis of different management strategies on a catchment scale.

A challenge for further simulations is to overcome problems of model parameterisation and input data assessment. Quality of input data, process representation and parameterisation largely determine the quality of simulation results.

The improvement of process representation and parameterisation of soil nitrogen processes requires extensive process investigations. For practical applications, transfer functions are urgently needed to estimate site specific rate constants from soil type, landuse and other readily available soil parameters (e.g. soil-pH, total C-content, etc.). Decreasing the uncertainty of input data addresses a variety of problems, such as quantification of atmospheric deposition, derivation of gross and net N-uptake rates, estimation of N-fixation, soil physical parameters, etc. As nitrogen turnover can be considered as a by-product of carbon turnover, further research should also focus on soil carbon dynamics to improve nitrogen modelling. Good examples are mineralisation and (heterotrophic) denitrification, which do not only depend on temperature and oxygen availability, but also on properties of soil organic matter.

A precondition for reactive groundwater transport modelling is to determine the amount and distribution of reactive substances in the aquifer. Sediment sampling is too cost-intensive to allow a dense sampling network. Groundwater samples, however, provide only indirect information, indicating presence or absence of reactive substances. This problem is related to the distribution of

substrates and hydraulic properties. Stochastic simulations may help to assess the effect of uncertain geological and geochemical information.

As for soil nitrogen modelling, further process studies are needed to understand nitrogen-related processes in groundwater and to determine rate constants and limiting factors. Various studies have focussed on the oxidation of pyrite by oxygen and nitrate. Here reactive transport modelling can be based on some estimates taken from literature. Very little, however, is known about dynamics of SOM and DOM in aquifers and their contribution to denitrification (or other turnover processes).

Another topic of research should focus on model support, scaling effects and corresponding derivation of effective model parameters. Scale dependend process models have to be developed, as well as methods for derivation of effective model parameters. A key problem for model application at various scales is the representation of relevant features or processes not resolved by model entities (e.g. representation of humic layers favouring denitrification processes).

7 References

- [AG Boden (1994)] AG Boden (1994): *Bodenkundliche Kartieranleitung*, 4th Edition, Hannover, Germany.
- [Artinger et al. (2000)] Artinger, R., Buckau, G., Geyer, S., Fritz, P., Wolf, M., Kim, J.I. (2000): Characterization of groundwater humic substances: influence of sedimentary organic carbon. *Applied Geochemistry*, *15*, 97-116.
- [Becker (1999)] Becker, K.-W. (1999): Nährstoffumsatz und -transport in der Dränzone landwirtschaftlich genutzter Böden - Beispiele: Stickstoff, Schwefel, Kalium. Ed.: Institut für Grundwasserwirtschaft, Technische Universität Dresden: Umsatz von Nährstoffen und Reaktionspartnern unterhalb des Wurzelraumes und im Grundwasser - Bedeutung für die Wasserbeschaffenheit. Volume 2, Dresden, Germany, 21-30.
- [Behrendt (1996)] Behrend, H. (1996): Quantifizierung der Nährstoffeinträge aus Flußgebieten des Landes Mecklenburg-Vorpommern. Research report, Institute of Inland Fisheries and Freshwater Ecology, Berlin, Germany.
- [Beven (2002)] Beven, K. (2002): The Future of Distributed Modelling - Special Issue. *Hydrological Processes*, *16*, 169-172.
- [Böhme and Russow (2002)] Böhme, F. and Russow, R. (2002): Formen der atmosphärischen N-Deposition und deren Berücksichtigung in Agrarökosystemen unter besonderer Berücksichtigung der ¹⁵N-Isotopenverdünnungsmethode (ITNI). In: Franko, U. (Ed.): *Stickstoff- ein Nährstoff aus dem Gleichgewicht: Ergebnisse aus dem Workshop "N-Deposition in Agrarökosystemen"* vom 2. bis 3. Mai 2002. UFZ-Bericht, 2002(16).
- [Borges and Rode (2002)] Borges, N., Rode, M. (2002): Entwicklung einer Methodik zur besseren Bestimmung von Denitrifikationsraten in Fließgewässersedimenten. In: Geller, W., Puncochar, P., Guhr, H., Tümpling jun., W. von, Medek, J., Smrt'ak, J., Feldmann, H., Uhlmann, O. (Eds): *Die Elbe - neue Horizonte des Flussgebietsmanagements*. 10. Magdeburger Gewässerschutzseminar, Conference proceedings. Leipzig, Germany, 49-50.
- [Borges et al. (2003)] Borges, N., Strauch, G., Rode, M. (2003): Nitrateintrag und -umsatz in kleinen Fließgewässern - Untersuchung stabiler Isotope im Oberflächenwasser. In: Manfred Dönike Gesellschaft e.V. (Ed.): *26. Jahrestagung der Arbeitsgemeinschaft Stabile Isotope* vom 6.-8. Oktober 2003. Conference transcript, Köln, Germany.
- [Böttcher et al. (1989)] Böttcher, J., Strebel, O., Duynisveld, W.H.M. (1989): Kinetik und Modellierung gekoppelter Stoffumsetzungen im Grundwasser eines Lockergesteins-Aquifers. *Geologisches Jahrbuch Reihe C*, *51*, 3-40.
- [Brye et al. (2001)] Brye, K.R., Norman, J.M., Bundy, L.G., Gower, S.T. (2001): Nitrogen and carbon leaching in agroecosystems and their role in denitrification potential. *Journal of Environmental Quality*, *30*, 58-70.
- [Buckau et al. (2000)] Buckau, G., Artinger, R., Geyer, S., Wolf, M., Fritz, P., Kim, J.I. (2000): Groundwater in-situ generation of aquatic humic and fulvic acids and the mineralization of sedimentary organic carbon. *Applied Geochemistry*, *15*, 819-832.
- [Chiang et al. (2002)] Chiang, W.H., Rausch, R., Schäfer, W. (2002): *Applied Groundwater-Modelling using Processing MODFLOW*, Study script, Summer-University Bremen (18.3.02.-22.3.02), Bremen, Germany.
- [Clement (1997)] Clement, T.P. (1997): *RT3D - A modular computer code for simulating reactive multispecies transport in 3-dimensional groundwater systems*, Richland, Washington, USA.
- [Diankov et al. (2003)] Diankov, Z., Welkovski, G., Marinov, D., Radoslavov, S., Nitcheva, O., Slavejkov, I., Petrov, K. (2003): Über die Anwendung einer Simulationsmethode zur Prognose der Verbreitung und Umwandlung von Nitratsubstanzen in Grundwasserströmungen. In: Institut für Grundwasserwirtschaft & Institut für Wasserchemie, Technische Universität Dresden (Ed.): *Diffuse input of chemicals into soil and groundwater - assessment and management*, Proceedings Institute

of Groundwater Management, 3, 275- 278.

[Diersch (1998)] Diersch, H.-J. G. (1998): FEFLOW - Finite element subsurface flow system. WASY GmbH, Berlin, Germany.

[DVWK (1996)] DVWK (1996): Ermittlung der Verdunstung von Land- und Wasserflächen. DVWK Merkblätter, 238.

[DVWK (1997)] DVWK (1997): Uferstreifen an Fließgewässern - Funktion, Gestaltung und Pflege. DVWK Merkblätter zur Wasserwirtschaft, 244.

[Dyck and Peschke (1995)] Dyck, S., Peschke, G. (1995): Grundlagen der Hydrogeologie. 3rd Edition, Berlin, Germany.

[European Communities (2000)] European Communities (2000): Directive 2000/60/EC of the European Parliament and of the Council of 23 October 2000 establishing a framework for Community action in the field of water policy. Official Journal of the European Communities, L 327/1, 1-73.

[FAO/ISRIC/ISSS (1998)] FAO/ISRIC/ISSS (1998): World Reference Base for Soil Resources. World Soil Resources Report No. 84, Rome, Italy.

[Faustzahlen für Landwirtschaft und Gartenbau (1993)] N.N. (1993): Faustzahlen für Landwirtschaft und Gartenbau, 12th edition, Münster-Hiltrup, Germany.

[Franko et al. (1995)] Franko, U., Oehlschlägel, B., Schenk, S. (1995): Modellierung von Bodenprozessen in Agrarlandschaften zur Untersuchung der Auswirkungen möglicher Klimaveränderungen. UFZ-Bericht, 1995(3).

[Frind et al. (1990)] Frind, E.O., Duynisveld, W.H.M., Strelbel, O., Boettcher, J. (1990): Modeling of Multicomponent Transport With Microbial Transformation in Groundwater: The Fuhrberg Case. Water Resources Research, 26(8), 1707-1719.

[Gelhar et al. (1992)] Gelhar, L.W., Welty, C., Rehfeld, K.R. (1992): A critical review of data on field scale dispersion in aquifers. Water Resources Research, 28(7), 1955-1974.

[Glugla (1969)] Glugla, G. (1969): Berechnungsverfahren zur Ermittlung des aktuellen Wassergehaltes und Gravitationswasserabflusses im Boden. Albrecht-Thaer-Archiv, 13(4), 371-376.

[GMS] US Department of Defense (1999): Groundwater Modelling System Version 3.0 - Reference Manual, Brigham Young University - Environmental Modelling Research Laboratory.

[Groenendijk and Kroes (1997)] Groenendijk, P., Kroes, J.G. (1997): Modelling the nitrogen and phosphorus leaching to groundwater and surface water: Animo 3.5, volume DLO-Winand Staring Centre Report 144, Wageningen, The Netherlands.

[Gusman and Marino (1999)] Gusman, A.J., Marino, M.A. (1999): Analytical Modeling of Nitrogen Dynamics in Soils and Ground Water. Journal of Irrigation and Drainage Engineering, 1999, 11/12, 330-337.

[Henning et al. (1999)] Henning, A.-K., Friedle, M., Rott, X. (1999): Untersuchungen zum Stickstoffumsatz im Zusammenhang mit subterrestrischer Enteisung und Entmanganung. In: Institut für Grundwasserwirtschaft, Technische Universität Dresden: Umsatz von Nährstoffen und Reaktionspartnern unterhalb des Wurzelraumes und im Grundwasser - Bedeutung für die Wasserbeschaffenheit. Volume 2, Dresden, Germany, 155-164.

[Herlitzius et al. (2003)] Herlitzius, J., Willms, M., Eulenstein, F., Macheleidt, W., Nestler, W. (2003): Nachhaltige Grundwasserbewirtschaftung an landwirtschaftlich genutzten Standorten am Beispiel der Elbaue bei Torgau. In: Institut für Grundwasserwirtschaft & Institut für Wasserchemie der TU Dresden: Diffuse input of chemicals into soil & groundwater - Assessment and management. Workshop 26.-28.02.2003. Proceedings Institute of Groundwater Management, 3, 235-248.

- [Heumann et al. (2002)] Heumann, S., Böttcher, J., Springob, G. (2002): N mineralization parameters of sandy arable soils. *Journal of Plant Nutrition and Soil Science*, *165*, 441-450.
- [Heuvelink (1998)] Heuvelink, G.B.M. (1998): Uncertainty analysis in environmental modelling under a change of spatial scale. *Nutrient Cycling in Agroecosystems*, *50*, 255-264.
- [Hörmann (1998)] Hörmann, G. (1998): Simpel - Speichermodelle zum Bodenwasserhaushalt. Kiel, 12.11.03, www.hydrology.uni-kiel.de/~schorsch/simpel/getrennt/dokumentation/simpel.pdf.
- [Hunter et al. (1998)] Hunter, K.S., Wang, Y., Van Capellen, P. (1998): Kinetic modeling of microbially-driven redox chemistry of subsurface environments: coupling transport, microbial metabolism and geochemistry. *Journal of Hydrology*, *209*, 53-80.
- [Huwe (1992)] Huwe, B. (1992): WHNSIM. A model to simulate the water, heat and nitrogen budget of agricultural fields. Program Documentation. Bayreuth, www.geo.uni-bayreuth.de/bodenphysik/lehre/Download/WHNSIM-doc.pdf.
- [Huwe and Totsche (1995)] Huwe, B., Totsche, K.U. (1995): Deterministic and stochastic modelling of water, heat and nitrogen dynamics on different scales with WHNSIM. *Journal of Contaminant Hydrology*, *20*, 265-284.
- [Isermann (2002)] Isermann, K. (2002): Atmosphärische N-Einträge als unabdingbare Bestandteile der N-Bilanzen von Agrarökosystemen sowie deren tolerierbaren bzw. unvermeidbaren gasförmigen N-Emissionen dargestellt am Beispiel Deutschlands. In: Franko, U.: Stickstoff - Ein Nährstoff aus dem Gleichgewicht: Ergebnisse aus dem Workshop "N-Deposition in Agrarökosystemen" vom 2. bis 3. Mai 2002. UFZ-Bericht, 2002(16).
- [Jordan and Weder (1995)] Jordan, H. and Weder, H.-J. (1995): Hydrogeologie: Grundlagen und Methoden; Regionale Hydrogeologie: Mecklenburg-Vorpommern, Brandenburg und Berlin, Sachsen-Anhalt, Sachsen, Thüringen. 2nd edition, Stuttgart, Germany.
- [Kainz and Hartmann (1997)] Kainz, W. & Hartmann, K.-J. (1997): Vorschlag zur Bereitstellung bodenkundlicher Kennwerte für mittel- und kleinmaßstäbige Bodenkarten auf der Basis von TGL 24300 Substraten. *Mitteilungen Geologie Sachsen-Anhalt*, *3*, 181-186.
- [Kalbitz and Geyer (2003)] Kalbitz, K., Geyer, S. (2003): Different effects of peat degradation on dissolved organic carbon and nitrogen. *Organic Geochemistry*, *33*, 319-326.
- [Kalbitz et al. (2000)] Kalbitz, K., Solinger, S., Park, J.-H., Michalzik, B., Matzner, E. (2000): Controls on the dynamics of dissolved organic matter in soils: a review. *Soil Science*, *165*(4), 277-304.
- [Kalbitz et al. (2003)] Kalbitz, K., Schwesig, D., Schmerwitz, J., Kaiser, K., Haumaier, L., Glaser, B., Ellerbrock, R., Leinweber, P. (2003): Changes in properties of soil-derived dissolved organic matter induced by biodegradation. *Soil Biology & Biogeochemistry*, *35*, 1129-1142.
- [Kamei and Ohmoto (2000)] Kamei, G., Ohmoto, H. (2000): The kinetics of reactions between pyrite and O₂-bearing water revealed from in situ monitoring of DO, Eh and pH in a closed system. *Geochimica et Cosmochimica Acta*, *64*(15), 2585-2601.
- [Kenkel (1999)] Kenkel, A. (1999): Wasser- und Stoffhaushalt im landwirtschaftlich genutzten Trinkwassereinzugsgebiet Gelliehausen (Gemeinde Gleichen). Dissertation. EcoRegio, 1.
- [Kersebaum (1995)] Kersebaum, K.C. (1995): Application of a simple management model to simulate water and nitrogen dynamics. *Ecological Modelling*, *81*, 145-156.
- [Kersebaum (1999)] Kersebaum, K.C. (1999): Übersicht über den Stand der Modellierung des Stickstoff-Kreislaufes in der ungesättigten Zone, Stand der Untersuchung zur Reaktionskinetik von Stickstoff im Boden. In: Institut für Grundwasserwirtschaft, Technische Universität Dresden: Umsatz von Nährstoffen und Reaktionspartnern unterhalb des Wurzelraumes und im Grundwasser - Bedeutung für die Wasserbeschaffenheit, Volume 2. Dresden, Germany, 175-185.
- [Kersebaum and Richter (1991)] Kersebaum, K.C., Richter, J. (1991): Modelling nitrogen dynamics in a plant-soil system with a simple model for advisory purposes. *Fertilizer Research*, *27*, 273-281.

[Kinzelbach and Rausch (1995)] Kinzelbach, W., Rausch, R. (1995): Grundwassermodellierung. Berlin, Germany.

[Kinzelbach et al. (1991)] Kinzelbach, W., Schäfer, W., Herzer, J. (1991): Numerical Modeling of Natural and Enhanced Denitrification Processes in Aquifers. *Water Resources Research*, 27(6), 1123-1135.

[Kofalk (1998)] Kofalk, S. (1998): Einfluss von Bodenvariabilität und Relief auf Wasserhaushalt und Stickstoffgehalte eines Grundmoränenstandortes. Dissertation. *Bodenökologie und Bodengenese*, 29, 166p.

[Kölle (1990)] Kölle, W. (1990): Nitratelimination im Aquifer- Reaktionspartner und Mechanismen. In: Walther, W. (Ed): Grundwasserbeschaffenheit in Niedersachsen - Diffuser Nitrateintrag. Fallstudien - Institut für Siedlungswasserwirtschaft, TU Braunschweig, 48, 129-145.

[Kölle (1999)] Kölle, W. (1990): Einfluß des Grundwasserleiters auf die Grundwasserbeschaffenheit aus der Sicht des Wasserchemikers, das Stoffdepot-Konzept. In: Institut für Grundwasserwirtschaft, Technische Universität Dresden: Umsatz von Nährstoffen und Reaktionspartnern unterhalb des Wurzelraumes und im Grundwasser - Bedeutung für die Wasserbeschaffenheit, Volume 2. Dresden, Germany, 69-83.

[Korom (1992)] Korom, S.F. (1992): Natural denitrification in the saturated zone: a review. *Water Resources Research*, 28(6), 1657-1668.

[Kunkel and Wendland (1998)] Kunkel, R., Wendland, F. (1998): Der Landschaftswasserhaushalt im Flußeinzugsgebiet der Elbe. *Schriften des Forschungszentrums Jülich, Reihe Umwelt, Volume 12*, Jülich, Germany.

[Kunkel and Wendland (1999)] Kunkel, R., Wendland, F. (1999): Das Weg-/Zeitverhalten des grundwasserbürtigen Abflusses im Elbeeinzugsgebiet. *Schriften des Forschungszentrums Jülich Reihe Umwelt, Volume 19*, Jülich, Germany.

[Landesanstalt für Landwirtschaft und Gartenbau (2002)] Landesanstalt für Landwirtschaft und Gartenbau Sachsen-Anhalt (2002): Richtwerte für eine gute fachliche Praxis beim Düngen im Rahmen einer ordnungsgemäßen Landbewirtschaftung, 4th Edition, Bernburg, Germany.

[Lichtner (1996)] Lichtner, P.C., Steefel, C.T., Oelkers, E.H. (1996): Reactive transport in porous media. *Reviews in Mineralogy*, 34.

[MacQuarrie and Sudicky (2001)] MacQuarrie, K.T.B., Sudicky, E.A. (2001): Multicomponent simulation of wastewater-derived nitrogen and carbon in shallow unconfined aquifers I. Model formulation and performance. *Journal of Contaminant Hydrology*, 47, 53-84.

[Marchetti et al. (1997)] Marchetti, R., Donatelli, M., Spallacci, P. (1997): Testing denitrification functions of dynamic crop models. *Journal of Environmental Quality*, 26, 394-401.

[Marschner and Kalbitz (2003)] Marschner, B., Kalbitz, K. (2003): Controls of bioavailability and biodegradability of dissolved organic matter in soils. *Geoderma*, 113, 211-235.

[Mayer (2000)] Mayer, K.U. (2000): MIN3P V1.1 User Guide. Unpublished, Waterloo, Canada.

[McDonald and Harbaugh (1988)] McDonald, M.G., Harbaugh, A.W. (1988): A modular three-dimensional finite-difference ground-water flow model. Washington, USA.

[Meissner (2000)] Meissner (2000, Ed.): Quantifizierung von diffusen Stoffausträgern aus der landwirtschaftlichen Flächennutzung in den Einzugsgebieten Oka und Elbe. *UFZ-Bericht*, 2000(13).

[Meissner et al. (1999)] Meissner, R., Seeger, J., Rupp, H. and Balla, H. (1999): Assessing the impact of agricultural land use changes on water quality. *Water Science Technology*, 40(2), 1-10.

[Merbach (2002)] Merbach, I. (2002): Die Nullparzellen des statischen Düngerversuches in Bad Lauchstädt als Indikator für atmosphärischen N-Eintrag. In: Franko, U.: Stickstoff - Ein Nährstoff aus dem Gleichgewicht: Ergebnisse aus dem Workshop "N-Deposition in Agrarökosystemen" vom 2. bis 3. Mai 2002. *UFZ Bericht*, 2002(16).

- [Miller and Donahue (1995)] Miller, R.W., Donahue, R.L. (1995): Soils in our environment. 7th Edition, Englewood Cliffs, New Jersey, USA.
- [Molénat and Gascuel-Oudoux (2002)] Molénat, J., Gascuel-Oudoux, C. (2002): Modelling flow and nitrate transport in groundwater for the prediction of water travel times and of consequences of land use evolution on water quality. *Hydrological Processes*, 16, 479-492.
- [Möller (unpublished)] Möller, D. (2002): Transport und Umsatz von Stickstoff in der Dränzone pleistozäner Tieflandböden, Unpublished internal report, UFZ. Falkenberg, Germany.
- [Nash and Sutcliffe (1970)] Nash, J.E., Sutcliffe, J.V. (1970): River flow forecasting through conceptual models. Part 1: a discussion of principles. *Journal of Hydrology*, 10, 282-290.
- [Neff and Asner (2001)] Neff, J.C., Asner, G.P. (2001): Dissolved organic carbon in terrestrial ecosystems: synthesis and a model. *Ecosystems*, 4, 29-48.
- [Oswald et al. (1999)] Oswald, T., Fohrmann, R., Overath, H. (1999): Standortabhängiger Stoffeintrag in das Grundwasser und dessen Einfluß auf den Stoffumsatz in quartären Porengrundwasserleitern Ostwestfalens und der Niederrheinischen Bucht unter besonderer Berücksichtigung des Stickstoffhaushaltes. In: Institut für Grundwasserwirtschaft, Technische Universität Dresden: Umsatz von Nährstoffen und Reaktionspartnern unterhalb des Wurzelraumes und im Grundwasser - Bedeutung für die Wasserbeschaffenheit, Volume 2, Dresden, Germany, 59-68.
- [Parkhurst and Appelo (1999)] Parkhurst, D.L., Appelo, C.A.J. (1999): User's guide to PHREEQC (version 2) - A computer program for speciation, batch-reaction, one-dimensional transport, and inverse geochemical calculations, Water-Resources Investigations Report 99-4259, Denver, Colorado, USA.
- [Pätsch et al. (2003)] Pätsch, M., Walther, W., Reinstorf, F., Weller, D. (2003): Research program and development of a suitable tool to minimize nitrogen emissions into groundwater of a pleistocene aquifer, northern low plain of Germany. In: Institut für Grundwasserwirtschaft & Institut für Wasserchemie, Technische Universität Dresden: Diffuse input of chemicals into soil and groundwater - assessment and management, Proceedings Institute of Groundwater Management, 3, 217-225.
- [Pollock (1994)] Pollock, D.W. (1994): User's Guide for MODPATH/MODPATH-PLOT, Version 3: A particle tracking post-processing package for MODFLOW, the U.S. Geological Survey finite-difference ground-water flow model. Reston, Virginia, USA.
- [Postma et al. (1991)] Postma, D., Boesen, C., Kristiansen, H., Larsen, F. (1991): Nitrate reduction in an unconfined sandy aquifer: water chemistry, reduction processes, and geochemical modeling. *Water Resources Research*, 27(8), 2027-2045.
- [Projektgruppe Elbe-Ökologie (1997)] Projektgruppe Elbe-Ökologie (1997): Darstellung und Bewertung von mesoskaligen Stickstoffmodellen. Berlin, Germany.
- [Prommer (2002)] Prommer, H. (2002): A reactive multicomponent transport model for saturated porous media - User's manual version 1.0. Edinburgh, 12.11.2003, www.pht3d.org/download/pht3d_manual_v1-0.pdf.
- [Reiche (1994)] Reiche, E.-W. (1994): Modelling water and nitrogen dynamics on catchment scale. *Ecological Modelling*, 75/76, 371-384.
- [Reiche (1991)] Reiche, E.W. (1991): Entwicklung, Validierung und Anwendung eines Modellsystems zur Beschreibung und flächenhaften Bilanzierung der Wasser- und Stickstoffdynamik in Böden. *Kieler Geographische Schriften*, 79.
- [Reichert (1998)] Reichert, P. (1998): AQUASIM 2.0 - User Manual. Computer program for the identification and simulation of aquatic systems. Dübendorf, Switzerland.
- [Reinstorf and Pätsch (1999)] Reinstorf, F., Pätsch, M. (1999): Übersicht über Modelle zum Nährstoff-Umsatz in der gesättigten Zone und im Grundwasser auf verschiedenen Skalenniveaus. In: Institut für Grundwasserwirtschaft - Technische Universität Dresden: Umsatz von Nährstoffen

und Reaktionspartnern unterhalb des Wurzelraumes und im Grundwasser - Bedeutung für die Wasserbeschaffenheit. Volume 2, Dresden, Germany, 187-200.

[Richards and Webster (1999)] Richards, J.E., Webster, C.P. (1999): Denitrification in the subsoil of the Broadbalk continuous Wheat Experiment. *Soil Biology & Biochemistry*, 31, 747-755.

[Rytter (2001)] Rytter, R.-M. (2001): Biomass production and allocation, including fine-root turnover, and annual N uptake in lysimeter-grown basket willows. *Forest Ecology and Management*, 140, 177-192.

[Schäfer et al. (1998)] Schäfer, D., Schäfer, W., Kinzelbach, W. (1998): Simulation of reactive processes related to biodegradation in aquifers 1. Structure of the three-dimensional reactive transport model. *Journal of Contaminant Hydrology*, 31, 167-186.

[Scheffer and Schachtschabel (1998)] Scheffer, F., Schachtschabel, P. (1998, Eds.): *Lehrbuch der Bodenkunde*, 14th Edition, Stuttgart, Germany.

[Schöniger (1998)] Schöniger, M. (1998): Regionale Studien zum Abflusvorgang im Untergrund unter Verwendung der Finiten-Elemente Methode. Habilitation. *Landschaftsökologie und Umweltbewertung*, 32.

[Schwartz (1999a)] Schwartz, R. (1999a): Bericht über bodenphysikalische Untersuchungen an 6 Profilen im Einzugsgebiet des Schaugrabens. Unpublished internal report, UFZ, Falkenberg, Germany.

[Schwartz (1999b)] Schwartz, R. (1999b): Ergänzungsbericht über bodenphysikalische Untersuchungen an 6 Profilen im Einzugsgebiet des Schaugrabens. Unpublished internal report, UFZ, Falkenberg, Germany.

[Sharpley and Williams (1990)] Sharpley, A.N., Williams, J.R. (1990): EPIC-Erosion Productivity Impact Calculator Vol. I - Model Documentation. USDA Technical bulletin No. 1768, Temple, Texas, USA.

[Siemens (2003)] Siemens, J. (2003): Controls of carbon, nitrogen and phosphorus fluxes in vadose zone and groundwater of protected watersheds in Münster (Germany). *Bodenökologie und Bodengenese*, 36.

[Sigg and Stumm (1996)] Sigg, L., Stumm, W. (1996): *Aquatische Chemie*. Stuttgart, Germany.

[Springob and Böttcher (1999)] Springob, G., Böttcher, J. (1999): Heterogenität von Verlagerungs- und Umsatzprozessen unterhalb des Wurzelraumes und Konsequenzen für deren Qualifizierung. In: Institut für Grundwasserwirtschaft - Technische Universität Dresden: Umsatz von Nährstoffen und Reaktionspartnern unterhalb des Wurzelraumes und im Grundwasser - Bedeutung für die Wasserbeschaffenheit. Volume 2, Dresden, Germany, 49-57.

[Swain and Wexler (1996)] Swain, E.D., Wexler, E.J. (1996): A coupled surface-water and ground-water flow model (MODBRNCH) for simulation of stream-aquifer interaction. *US Geological Survey Techniques of Water-Resources Investigations*, 6 (A6).

[TGL 24.300] TGL 24.300: Fachbereichsstandard: Aufnahme landwirtschaftlich genutzter Böden. Akademie der Landwirtschaftswissenschaften der DDR (Ed.), Eberswalde-Finow, 1976-85.

[Thomas and Büttner (1998)] Thomas, F.M., Büttner, G. (1998): Nutrient relations in healthy and damaged stands of mature oaks on clayey soils in northwestern Germany. *Forest Ecology and Management*, 108, 301-319.

[Van Capellen et al. (1996)] Van Capellen, P., Wang, Y. (1996): Cycling of iron and manganese in surface sediments: a general theory for the coupled transport and reaction of carbon, oxygen, nitrogen, sulfur, iron, and manganese. *American Journal of Science*, 296, 197-243.

[Van Dam et al. (1997)] Van Dam, J.C., Huygen, J., Wesseling, J.G., Feddes R.A., Kabat, P., van Walsum, P.E.V., Groenendijk, P., van Diepen, P., van Diepen, C.A. (1997): Theory of SWAP version 2.0: Simulation of water flow, solute transport and plant growth in the Soil-Water-Atmosphere-Plant environment. SC-DLO en WAU Report 71, Wageningen, The Netherlands.

- [Vanclouster et al. (1994)] Vanclouster, M., Viaene P., Diels, J., Christiaens, K. (1994): Wave v2.0: Mathematical model for simulating water and agrochemicals in the soil and vadose environment. Leuven, Belgium.
- [Vanderborght and Vereecken (2001)] Vanderborght, J. and Vereecken, H. (2001): Analysis of locally measured bromide breakthrough curves from a natural gradient tracer experiment at Krauthausen. *Journal of Contaminant Hydrology*, *48*, 23-43.
- [Verburg and Johnson (2001)] Verburg, P.S.J., Johnson, D.W. (2001): A spreadsheet-based biogeochemical model to simulate nutrient cycling processes in forest ecosystems. *Ecological Modelling*, *141*, 185-200.
- [Vereecken et al. (2000)] Vereecken, H., Döring, U., Hardelauf, H., Jaekel, U., Hashagen, U., Neuendorf, O., Schwarze, H., Seidemann, R. (2000): Analysis of solute transport in a heterogeneous aquifer: the Krauthausen field experiment. *Journal of Contaminant Hydrology*, *45*, 329-358.
- [Walther et al. (2001)] Walther, W., Becker, K.-W., Gliesche, C., Pätsch, M., Schalla, S. (2001): Zum Kenntnisstand über Umsetzung von Nährstoffen in der Dränzone und im Grundwasser und über deren Modellierung - 1. Teil: Chemische und biologische Umsetzungen. *Landnutzung und Landentwicklung*, *42*, 224-230.
- [Waterloo Hydrogeologic (2000)] Waterloo Hydrogeologic Inc. (2000): Visual Pest - Model-Independent Parameter Estimation. Software documentation. Waterloo, Canada.
- [Watmough and Dillon (2003)] Watmough, S.A., Dillon, P.J. (2003): Base cation and nitrogen budgets for seven forested catchments in central Ontario, 1983-1999. *Forest Ecology and Management*, *177*, 155-177.
- [Well et al. (2001)] Well, R., Höper, H., Mehranfar, O. (2001): Empirische Modelle zur Prognose der Denitrifikation im oberflächennahen Grundwasser. *Mitteilungen der Deutschen Bodenkundlichen Gesellschaft*, *96(2)*, 667-668.
- [Wendland and Kunkel (1999)] Wendland, F., Kunkel, R. (1999): Das Nitratabbauvermögen im Grundwasser des Elbeeinzugsgebietes. *Schriften des Forschungszentrums Jülich Reihe Umwelt*. Volume 13, Jülich, Germany.
- [Werner and Wodsak (1994)] Werner, W., Wodsak, H.-P. (1994): Stickstoff- und Phosphateintrag in die Fließgewässer Deutschlands unter besonderer Berücksichtigung des Eintragungsgeschehens im Lockergesteinsbereich der ehemaligen DDR. *Schriftenreihe Agrarspectrum*, *22*.
- [Widdowson et al. (1988)] Widdowson, M.A., Molz, F.J., Benefield, L.D. (1988): A Numerical Transport Model for Oxygen- and Nitrate-Based Respiration Linked to Substrate and Nutrient Availability in Porous Media. *Water Resources Research*, *24(9)*, 1553-1565.
- [Wriedt et al. (2001)] Wriedt, G., Blank, B., Meissner, R., Rode, M. (2001): Untersuchungen zum Stickstoffumsatz während der Boden- und Grundwasserpassage im pleistozänen Tiefland - Methoden und erste Ergebnisse. *Mitteilungen der Deutschen Bodenkundlichen Gesellschaft*, *96(1)*, 141-142.
- [Zalewski (2000)] Zalewski, M. (2000): Ecohydrology. The scientific background to use ecosystem properties as management tools towards sustainability of water resources. Guest Editorial. *Ecological Engineering*, *16*, 1-8.
- [Zalewsky et al. (1997)] Zalewsky, M., Janauer, G.A., Jolankai, G. (1997): Ecohydrology. A new paradigm for the sustainable use of aquatic resources. UNESCO IHP Technical Document in Hydrology, *7*, IHP-V Projects 2.3/2.4, UNESCO Paris, France.
- [Zheng (1990)] Zheng, C. (1990): MT3D - A modular three-dimensional transport model for simulation of advection, dispersion and chemical reactions of contaminants in groundwater systems. Ada, Oklahoma, USA.

Appendix

- A Overview of Lysimeter data and Schaugraben catchment data
- B mRISK-N model documentation
- C Formal description of the RT3D reaction-module

Appendix A - Overview of lysimeter data and Schaugraben catchment data

Table of Contents

LIST OF FIGURES	1
LIST OF TABLES	2
1 LYSIMETER DATA.....	3
1.1 RESULTS OF THE mRISK-N SENSITIVITY ANALYSIS BASED ON LYSIMETER DATA	3
1.2 SIMULATION OF SELECTED LYSIMETERS.....	7
2 FIELD DATA FROM THE SCHAUGRABEN CATCHMENT.....	9
2.1 CLIMATIC DATA	9
2.2 SOIL DATA.....	10
2.3 MANAGEMENT	14
2.4 DISTRIBUTION OF BOREHOLES, GROUNDWATER WELLS AND GAUGING STATIONS IN THE SCHAUGRABEN AREA	15
2.5 DISCHARGE AT GAUGING STATION P5	16
2.6 ANALYSIS OF SURFACE WATER SAMPLES AT GAUGING STATION P5 AND P2 AND SEEPAGE SAMPLES AT THE EXPERIMENTAL SITE.....	17
2.7 DISCHARGE AND NITRATE LOADS AT P5	17
2.8 CHEMICAL CHARACTERISATION OF GROUNDWATER SAMPLES AT THE EXPERIMENTAL SITE.....	18
2.9 CHEMICAL CHARACTERISATION OF GROUNDWATER AT OBSERVATION WELL 0063 AND 0068	19

List of Figures

Figure 1: Annual groundwater recharge and N-Leaching of Lysimeter 04.....	7
Figure 2: Cumulative annual groundwater recharge and N-Leaching of Lysimeter 04.....	8
Figure 3: Annual groundwater recharge and N-Leaching of Lysimeter 07.....	8
Figure 4: Cumulative annual groundwater recharge and N-Leaching of Lysimeter 07.....	8
Figure 5: Climatic record of the UFZ Lysimeter station in Falkenberg, 1982-2002 (P=Precipitation, ETP = Evapotranspiration, MAT = Mean annual temperature, MMT= Mean Monthly Temperature) 9	
Figure 6: Mean climatic data of UFZ Lysimeter station in Falkenberg (P=Precipitation, ETP = Evapotranspiration, MMT = Mean Monthly Temperature, DMT = Daily Mean Temperature).....	9
Figure 7: Soil units in the Schaugraben area and extrapolated soil units in the extended study area (Soil units based on TGL 2400, translated to WRB).....	10
Figure 8: Landuse distribution in the Schaugraben study area in 1996.....	14
Figure 9: Boreholes, groundwater wells and gauging stations in the Schaugraben area.....	15
Figure 10: Discharge measurements at gauging station P5 – continuous and weekly measurements since 1997.....	16
Figure 11: Mean composition of drain water at gauging station P5 and observation point P5 and of seepage water in seepage samplers SP2, SP3 and SP4.....	17
Figure 12: Monthly discharge and mean nitrate concentrations at gauging station P5, calculated from weekly measurements.....	18
Figure 13: Groundwater composition at the Schaugraben experimental site – Quartiles over all groundwater samples (in quartiles).....	19
Figure 14: Groundwater composition in wells 0063 and 0068, sampling 03.05.01.....	19

List of Tables

Table 1: Sensitivity of Lysimeter 03 (normalised10%-elasticity index).....	3
Table 2: Sensitivity of Lysimeter 04 (normalised10%-elasticity index).....	4
Table 3: Sensitivity of Lysimeter 05 (normalised10%-elasticity index).....	5
Table 4: Sensitivity of Lysimeter 07 (normalised10%-elasticity index).....	6
Table 5: Summary of the Lysimeter simulations – Mean values and standard deviation, based on the second calibration strategy (“optical fit”).....	7
Table 6: Soil units in the Schaugraben catchment area.....	10
Table 7: Soil physical parameters.....	11
Table 8: Reaction parameters set for specific soil units.....	13
Table 9: Characterisation of the discharge data set.....	16
Table 10: Annual runoff calculated from discharge data.....	17
Table 11: Characterisation of monthly discharge and N export at P5.....	18

1 Lysimeter data

1.1 Results of the mRISK-N sensitivity analysis based on lysimeter data

Results are given as normalised 10%-elasticity index for a change of the parameter by +10%. Parameters are:

PV = pore volume, FC = field capacity, RP = reduction point, WP = wilting point, Kf = saturated conductivity, LaiCap = Storage capacity of interception storage, InfCap = storage capacity of infiltration storage, InfDry = leaching constant of infiltration storage, Denit = denitrification rate constant, Min_r/s = rapid/slow mineralisation rate constant, GW_depth = groundwater depth

Numbers designate the corresponding soil horizon (1-3).

Table 1: Sensitivity of Lysimeter 03 (normalised 10%-elasticity index)

Observation	ETA	dS	Qout	Nloss	Min	Nit	Denit
Parameter	+10%	+10%	+10%	+10%	+10%	+10%	+10%
PV 1	0.000	0.000	0.000	0.054	0.000	0.000	-1.685
PV 2	0.000	0.000	0.000	0.007	0.000	0.000	-0.187
PV 3	0.000	0.000	0.000	0.133	0.000	0.000	-1.131
FC 1	0.236	-114.000	-1.127	-1.382	-0.174	0.067	0.527
FC 2	0.356	-170.000	-1.700	-1.762	0.000	0.000	0.115
FC 3	0.000	0.000	0.000	-0.079	0.000	0.000	1.164
RP 1	-0.176	0.000	0.797	0.693	0.180	0.215	0.724
RP 2	-0.230	0.000	1.042	0.415	0.000	0.000	-0.302
RP 3	0.000	0.000	0.000	0.000	0.000	0.000	0.000
WP 1	0.000	0.000	0.000	0.000	0.000	0.000	0.000
WP 2	0.000	0.000	0.000	0.000	0.000	0.000	0.000
WP 3	0.000	0.000	0.000	0.000	0.000	0.000	0.000
Kf 1	0.000	0.000	0.000	0.000	0.000	0.000	0.000
Kf 2	0.000	0.000	0.000	0.000	0.000	0.000	0.000
Kf 3	0.000	0.000	0.000	0.000	0.000	0.000	0.000
LaiCap	0.003	0.000	-0.014	0.005	0.000	0.000	0.016
InfCap	0.006	-6.000	-0.031	-0.033	-0.004	-0.001	-0.016
InfDry	0.011	0.000	-0.049	-0.014	0.000	0.000	0.011
Denit1	0.000	0.000	0.000	-0.013	0.000	0.000	0.417
Denit2	0.000	0.000	0.000	-0.004	0.000	0.000	0.104
Denit3	0.000	0.000	0.000	-0.052	0.000	0.000	0.434
Min_r	0.000	0.000	0.000	-0.356	0.102	0.030	-0.285
Min_s	0.000	0.000	0.000	-0.306	0.166	0.048	-0.231
GW-depth	0.000	0.000	0.000	0.009	0.000	0.000	0.906

Table 2: Sensitivity of Lysimeter 04 (normalised 10%-elasticity index)

Observation	ETA	dS	Qout	Nloss	Min	Nit	Denit
Parameter	+10%	+10%	+10%	+10%	+10%	+10%	+10%
PV 1	0.000	0.000	0.000	0.177	0.000	0.000	-3.588
PV 2	0.000	0.000	0.000	0.236	0.000	0.000	-1.343
PV 3	0.000	0.000	0.000	0.131	0.000	0.000	-0.234
FC 1	0.211	-1.716	-0.932	-0.444	-0.170	0.111	2.133
FC 2	0.285	-2.575	-1.267	-1.638	0.000	0.000	1.017
FC 3	0.000	0.000	0.000	-0.218	0.000	0.000	0.218
RP 1	-0.153	0.000	0.645	1.218	0.186	0.269	2.321
RP 2	-0.159	0.000	0.668	0.297	0.000	0.000	-0.024
RP 3	0.000	0.000	0.000	0.000	0.000	0.000	0.000
WP 1	0.000	0.000	0.000	0.000	0.000	0.000	0.000
WP 2	0.000	0.000	0.000	0.000	0.000	0.000	0.000
WP 3	0.000	0.000	0.000	0.000	0.000	0.000	0.000
Kf 1	0.000	0.000	0.000	0.000	0.000	0.000	0.000
Kf 2	0.000	0.000	0.000	0.000	0.000	0.000	0.000
Kf 3	0.000	0.000	0.000	0.000	0.000	0.000	0.000
LaiCap	0.000	0.000	0.000	0.000	0.000	0.000	0.001
LitCap	0.015	-0.112	-0.065	0.373	0.016	0.016	0.393
LitDry	0.007	0.000	-0.030	-0.021	0.004	0.003	-0.019
Kden 1	0.000	0.000	0.000	0.001	0.000	0.000	0.588
Kden 2	0.000	0.000	0.000	-0.050	0.000	0.000	0.325
Kden 3	0.000	0.000	0.000	-0.034	0.000	0.000	0.062
Kmin_r	0.000	0.000	0.000	0.069	0.106	0.030	0.058
Kmin_s	0.000	0.000	0.000	0.081	0.168	0.046	0.059
GW-depth	0.000	0.000	0.000	-0.248	0.000	0.000	0.117

Table 3: Sensitivity of Lysimeter 05 (normalised 10%-elasticity index)

Observation	ETA	dS	Qout	Nloss	Min	Nit	Denit
Parameter	+10%	+10%	+10%	+10%	+10%	+10%	+10%
PV 1	0.000	0.000	0.000	0.061	0.000	0.000	-1.375
PV 2	0.000	0.000	0.000	0.021	0.000	0.000	-0.351
PV 3	0.000	0.000	0.000	0.097	0.000	0.000	-1.288
FC 1	0.297	0.163	-1.002	-1.053	-0.192	0.021	0.650
FC 2	0.366	0.407	-1.231	-0.792	0.000	0.000	0.633
FC 3	0.000	0.000	0.000	-0.175	0.000	0.000	1.266
RP 1	-0.227	-3.415	0.734	1.262	0.189	0.322	0.958
RP 2	-0.295	-3.902	0.960	0.191	0.000	0.000	-0.343
RP 3	0.000	0.000	0.000	0.000	0.000	0.000	0.000
WP 1	0.000	0.000	0.000	0.000	0.000	0.000	0.000
WP 2	0.000	0.000	0.000	0.000	0.000	0.000	0.000
WP 3	0.000	0.000	0.000	0.000	0.000	0.000	0.000
Kf 1	0.000	0.000	0.000	0.000	0.000	0.000	0.000
Kf 2	0.000	0.000	0.000	0.000	0.000	0.000	0.000
Kf 3	0.000	0.000	0.000	0.000	0.000	0.000	0.000
LaiCap	0.000	0.000	-0.001	0.000	0.000	0.000	0.004
LitCap	0.013	0.407	-0.041	-0.063	-0.006	-0.005	-0.030
LitDry	0.001	0.000	-0.003	0.010	0.004	0.006	0.026
Kden 1	0.000	0.000	0.000	-0.015	0.000	0.000	0.338
Kden 2	0.000	0.000	0.000	-0.007	0.000	0.000	0.126
Kden 3	0.000	0.000	0.000	-0.037	0.000	0.000	0.499
Kmin_r	0.000	0.000	0.000	0.149	0.108	0.064	0.152
Kmin_s	0.000	0.000	0.000	0.220	0.170	0.100	0.208
GW-depth	0.000	0.000	0.000	-0.227	0.000	0.000	0.906

Table 4: Sensitivity of Lysimeter 07 (normalised 10%-elasticity index)

Observaiton	ETA	dS	Qout	Nloss	Min	Nit	Denit
Parameter	+10%	+10%	+10%	+10%	+10%	+10%	+10%
PV 1	0.002	-0.060	-0.009	0.009	-0.003	0.002	-0.557
PV 2	0.000	0.000	0.000	0.004	0.000	0.000	-0.084
PV 3	0.000	0.000	0.000	0.120	0.000	0.000	-3.287
FC 1	0.136	-1.291	-0.686	-1.050	-0.131	0.115	-0.167
FC 2	0.234	-2.072	-1.178	-1.122	0.000	0.000	0.195
FC 3	0.000	0.000	0.000	-0.174	0.000	0.000	3.092
RP 1	-0.146	-0.330	0.681	1.038	0.124	0.253	0.613
RP 2	-0.138	-0.120	0.654	0.166	0.000	0.000	-0.418
RP 3	0.000	0.000	0.000	0.000	0.000	0.000	0.000
WP 1	0.000	0.000	0.000	0.000	0.000	0.000	0.000
WP 2	0.000	0.000	0.000	0.000	0.000	0.000	0.000
WP 3	0.000	0.000	0.000	0.000	0.000	0.000	0.000
Kf 1	-0.001	0.090	0.008	-0.004	-0.002	-0.002	-0.028
Kf 2	0.000	0.000	0.000	0.000	0.000	0.000	0.000
Kf 3	0.000	0.000	0.000	0.000	0.000	0.000	0.000
LaiCap	0.000	0.000	0.000	-0.002	0.000	0.000	0.000
LitCap	0.002	-0.060	-0.010	-0.008	-0.005	-0.004	-0.028
LitDry	-0.004	0.000	0.020	0.028	-0.002	-0.002	0.000
Kden 1	0.000	0.000	0.000	0.000	0.000	0.000	0.084
Kden 2	0.000	0.000	0.000	-0.001	0.000	0.000	0.028
Kden 3	0.000	0.000	0.000	-0.030	0.000	0.000	0.836
Kmin_r	0.000	0.000	0.000	0.051	0.053	0.020	0.028
Kmin_s	0.000	0.000	0.000	0.152	0.147	0.056	0.139
GW-depth	0.000	0.000	0.000	-0.183	0.000	0.000	1.588

1.2 Simulation of selected lysimeters

Table 5: Summary of the Lysimeter simulations – Mean values and standard deviation, based on the second calibration strategy (“optical fit”)

	Lysimeter 03	Lysimeter 03	Lysimeter 04	Lysimeter 04	Lysimeter 05	Lysimeter 05	Lysimeter 07	Lysimeter 07	Lysimeter 53	Lysimeter 53
	μ	σ	μ	Σ	μ	σ	μ	σ	μ	Σ
Precipitation [mm/a]	553	110	553	110	553	110	553	110	553	110
Irrigation [mm/a]	0	0	0	0	12	22	12	23	109	61
Actual Evapotranspiration [mm/a]	453	60	445	59	440	58	468	63	527	44
Storage change [mm/a]	-3	18	-3	14	-2	6	-4	19	-2	6
Recharge [mm/a]	103	72	111	74	128	69	101	70	136	73
observed										
Mineral Fertilizer [kg N/ha]	180	0	180	0	0	0	0	0	142	23
Organic Fertilizer [kg N/ha]	0	0	0	0	68	78	68	78	57	92
Residue [kg N/ha]	80	0	80	0	155	129	159	140	0	0
Deposition [kg N/ha]	57	3	57	3	57	3	57	3	57	3
Volatilisation [kg N/ha]	18	0	18	0	14	16	14	16	26	18
Plant uptake [kg N/ha]	254	25	247	34	207	95	215	107	201	52
Mineralisation [kg N/ha]	78	7	77	7	153	20	179	21	35	4
Nitrification [kg N/ha]	161	6	149	5	160	31	162	30	136	27
Denitrification [kg N/ha]	1	0	7	2	1	1	0	0	36	21
N-Leaching [kg N/ha]	11	8	11	9	27	17	27	18	8	5
Observed										

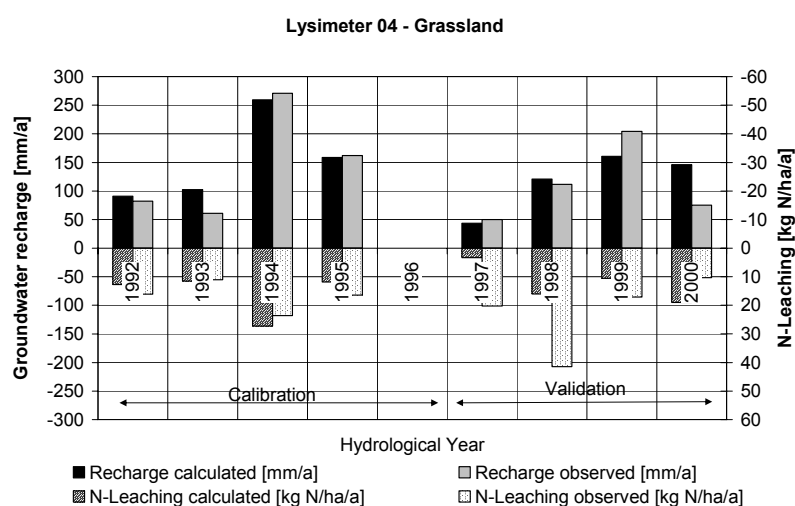


Figure 1: Annual groundwater recharge and N-Leaching of Lysimeter 04

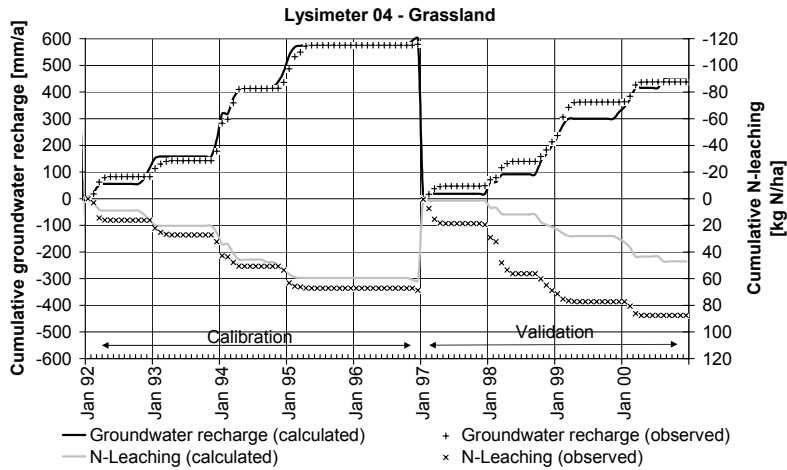


Figure 2: Cumulative annual groundwater recharge and N-Leaching of Lysimeter 04

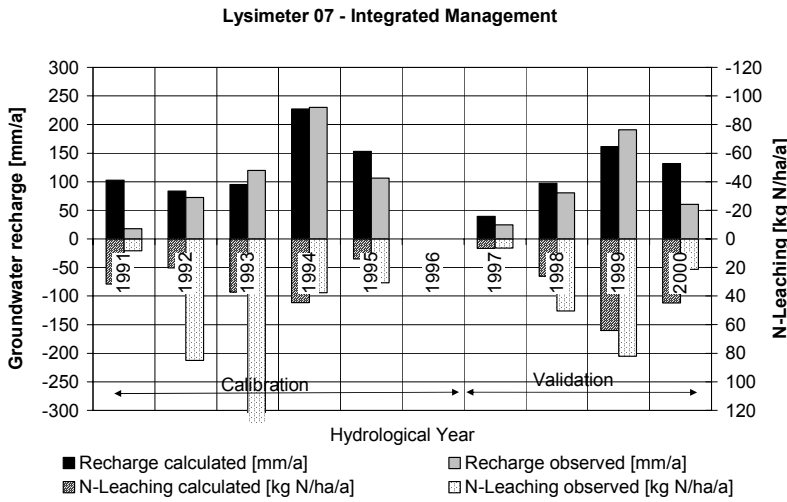


Figure 3: Annual groundwater recharge and N-Leaching of Lysimeter 07

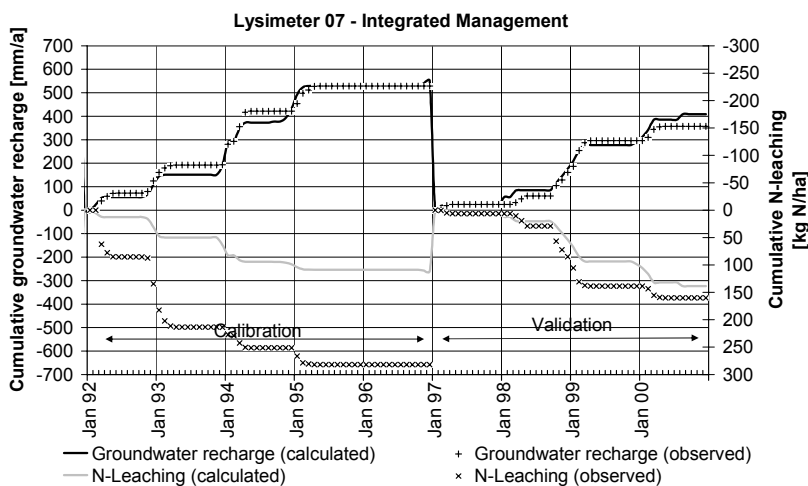


Figure 4: Cumulative annual groundwater recharge and N-Leaching of Lysimeter 07

2 Field data from the Schaugraben catchment

2.1 Climatic data

Climatic data have been taken from the UFZ Lysimeter station in Falkenberg (app.15 km northeast of the study area). Missing data have been completed with data from the DWD climatic station in Seehausen (app. 15 km north of the study area, 5 km east of Falkenberg). The climatic record includes precipitation, air temperature, wind speed, global radiation, humidity, and duration of sunshine on a daily basis since 1982.

Mean annual precipitation is 548 mm/a. Potential evapotranspiration has been calculated according to Penman-Wendling (DVWK, 1996), mean evapotranspiration is 574 mm/a. Mean annual temperature is 9.0°C, ranging from mean monthly temperatures of 0.8°C in January to 18.1 °C in Juli.

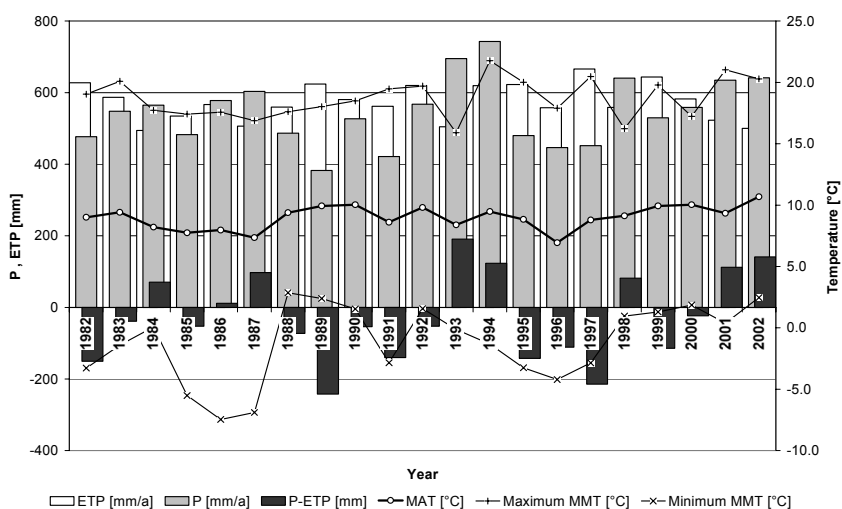


Figure 5: Climatic record of the UFZ Lysimeter station in Falkenberg, 1982-2002 (P=Precipitation, ETP = Evapotranspiration, MAT = Mean annual temperature, MMT= Mean Monthly Temperature)

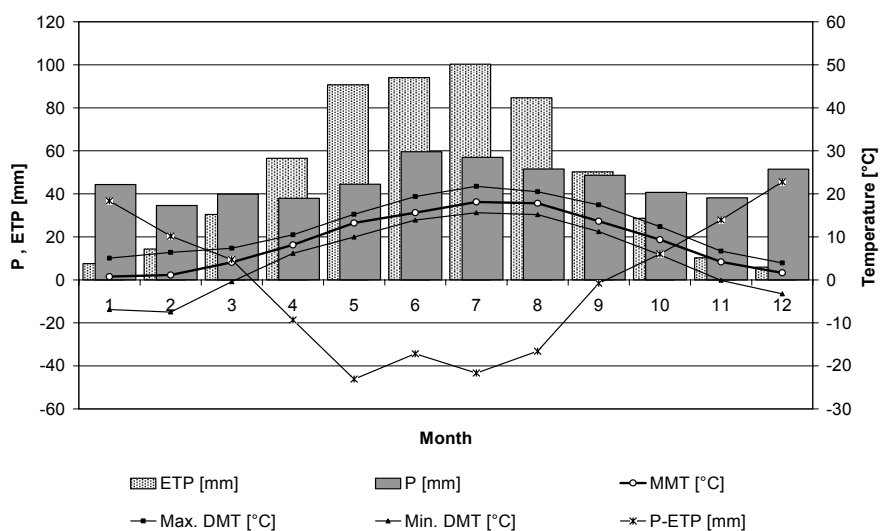


Figure 6: Mean climatic data of UFZ Lysimeter station in Falkenberg (P=Precipitation, ETP = Evapotranspiration, MMT = Mean Monthly Temperature, DMT = Daily Mean Temperature)

2.2 Soil data

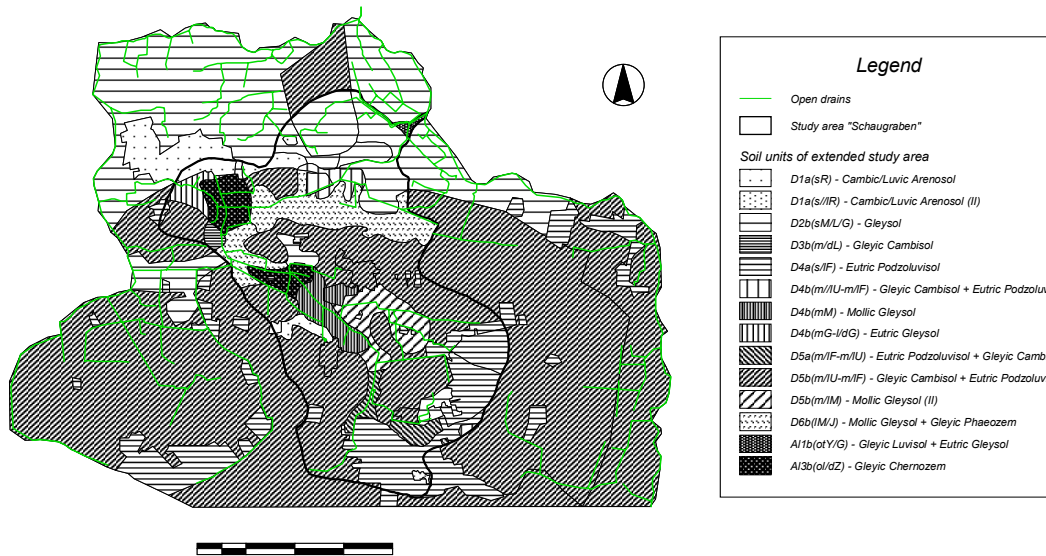


Figure 7: Soil units in the Schaugraben area and extrapolated soil units in the extended study area (Soil units based on TGL 2400, translated to WRB)

Table 6: Soil units in the Schaugraben catchment area

Soil characterisation according to TGL 24.300	TGL soil type	Water regime	Translation to WRB
D1a(sR)	Rosterde	Free drainage	Cambic/Luvis Arenosol
D1a(s/IR)	Rosterde	Free drainage	Cambic/Luvis Arenosol
D2b(sM/L/G)	Gley	Groundwater	Gleysol
D3b(m/dL)	Braungley	Groundwater	Gleyic Cambisol
D4a(s/IF)	Fahlerde	Free drainage	Eutric Podzoluvisol
D4a(m/IU-m/IF)	Braunstaugley	Water logging	Gleyic Cambisol
	Fahlerde	Free drainage	Eutric Podzoluvisol
D4a(mM)	Humusgley	Free drainage	Mollic Gleysol
D4a(mG-l/dG)	Grundgley	Free drainage	Eutric Gleysol
D5a(m/IF-m/IU)	Fahlerde	Free drainage	Eutric Podzoluvisol
	Braunstaugley	Water logging	Gleyic Cambisol
D5b(m/IU-m/IF)	Fahlerde	Groundwater	Eutric Podzoluvisol
	Braunstaugley	Water logging	Gleyic Cambisol
D5b(m/IM)	Humusgley	Groundwater	Mollic Gleysol
D6b(IM/J)	Humusgley	Groundwater	Mollic Gleysol
	Schwarzstaugley		Gleyic Phaeozem
Al1b(otY/G)	Halbamphigley	Groundwater	Gleyic Luvisol
	Grundgley		Eutric Gleysol
Al3b(ol/dZ)	Schwarzgley	Groundwater	Gleyic Chernozem

Table 7: Soil physical parameters

Horizon	Thickness [m]	PV [%]	FC [%]	WP [%]	IWC [%]	RP [%]	c [m/d]	Textur	AWC [%]
D1a(sR)									
1	0.4	0.365	0.2	0.06	0.16	0.12	1.40	s	0.14
2	1.1	0.365	0.2	0.06	0.16	0.12	1.60	s	0.14
3	0.5	0.365	0.2	0.06	0.16	0.12	1.60	s	0.14
D1a(s/IR)									
1	0.3	0.365	0.2	0.06	0.16	0.12	1.40	s	0.14
2	1.2	0.38	0.26	0.10	0.21	0.156	0.26	s	0.16
3	0.5	0.4	0.31	0.14	0.25	0.186	0.26	l	0.17
D2b(sM/L/G)									
1	0.3	0.365	0.2	0.06	0.16	0.12	1.40	s	0.14
2	1.2	0.365	0.2	0.06	0.16	0.12	1.60	s	0.14
3	0.5	0.365	0.2	0.06	0.16	0.12	1.60	s	0.14
D3b(m/dL)									
1	0.3	0.36	0.23	0.06	0.18	0.138	0.68	m	0.17
2	1.2	0.36	0.2	0.06	0.16	0.12	1.40	d	0.14
3	0.5	0.36	0.2	0.06	0.16	0.12	1.40	d	0.14
D4a(s/IF)									
1	0.3	0.365	0.2	0.06	0.16	0.12	1.40	s	0.14
2	1.2	0.4	0.31	0.14	0.25	0.186	0.26	l	0.17
3	0.5	0.4	0.31	0.14	0.25	0.186	0.26	l	0.17
D4a(m/IU-m/IF)									
1	0.3	0.36	0.23	0.06	0.18	0.138	0.68	m	0.17
2	1.2	0.36	0.27	0.10	0.22	0.162	0.26	m	0.17
3	0.5	0.4	0.31	0.14	0.248	0.186	0.26	l	0.17
D4a(mM)									
1	0.3	0.36	0.23	0.06	0.184	0.138	0.68	m	0.17
2	1.2	0.36	0.23	0.06	0.184	0.138	0.68	m	0.17
3	0.5	0.36	0.23	0.06	0.184	0.138	0.68	m	0.17
D4a(mG-l/dG)									
1	0.3	0.36	0.23	0.06	0.184	0.138	0.68	m	0.17
2	1.2	0.36	0.23	0.06	0.184	0.138	0.68	m	0.17
3	0.5	0.36	0.2	0.06	0.16	0.12	1.6	d	0.14

D5a(m/IF-m/IU)									
1	0.3	0.36	0.23	0.06	0.184	0.138	0.68	m	0.17
2	1.2	0.4	0.31	0.14	0.248	0.186	0.26	l	0.17
3	0.5	0.4	0.31	0.14	0.248	0.186	0.26	l	0.17
D5b(m/IU-m/IF)									
1	0.3	0.36	0.23	0.06	0.184	0.138	0.68	m	0.17
2	1.2	0.38	0.27	0.06	0.216	0.162	0.26	m	0.21
3	0.5	0.4	0.31	0.14	0.248	0.186	0.26	l	0.17
D5b(m/LM)									
1	0.3	0.36	0.23	0.06	0.184	0.138	0.68	m	0.17
2	1.2	0.4	0.31	0.14	0.248	0.186	0.26	l	0.17
3	0.5	0.4	0.31	0.14	0.248	0.186	0.26	l	0.17
D6b(lM/J)									
1	0.3	0.4	0.31	0.14	0.248	0.186	0.23	l	0.17
2	1.2	0.4	0.31	0.14	0.248	0.186	0.26	l	0.17
3	0.5	0.4	0.31	0.14	0.248	0.186	0.26	l	0.17
Al1b(otY/G)									
1	0.3	0.46	0.41	0.26	0.328	0.246	0.1	ot	0.15
2	1.2	0.46	0.41	0.26	0.328	0.246	0.12	ot	0.15
3	0.5	0.46	0.41	0.26	0.328	0.246	0.12	ot	0.15
Al3b(ol/dZ)									
1	0.3	0.4	0.31	0.14	0.248	0.186	0.23	ol	0.17
2	1.2	0.36	0.2	0.06	0.16	0.12	1.6	d	0.14
3	0.5	0.36	0.2	0.06	0.16	0.12	1.6	d	0.14
For all soils:									
Interception storage capacity					0.002		[m/LAI]		
Infiltration storage drying factor					3		[-]		
Infiltration storage capacity					0.005		[m]		

Table 8: Reaction parameters set for specific soil units

Soil	k_{den} (URZ) [1/day]	k_{den} (LRZ) [1/day]	k_{den} (IVZ) [1/day]
D1a(sR)	0.0001	0.0001	0.0001
D1a(s//IR)	0.0001	0.0001	0.0001
D2b(sM/L/G)	0.002	0.001	0.0001
D3b(m/dL)	0.002	0.001	0.0001
D4a(s/IF)	0.0001	0.0001	0.0001
D4a(m//IU-m/IF)	0.001	0.001	0.0001
D4a(mM)	0.004	0.002	0.0001
D4a(mG-l/dG)	0.002	0.001	0.0001
D5a(m/IF-m/IU)	0.0001	0.0001	0.0001
D5b(m/IU-m/IF)	0.0001	0.0001	0.0001
D5b(m/IM)	0.004	0.002	0.0001
D6b(IM/J)	0.004	0.002	0.0001
A11b(otY/G)	0.002	0.001	0.0001
A13b(ol/dZ)	0.004	0.002	0.0001
For all soils:			
k_{min} (rapid)	0.01064	[1/d]	
k_{min} (slow)	0.0045	[1/d]	

2.3 Management

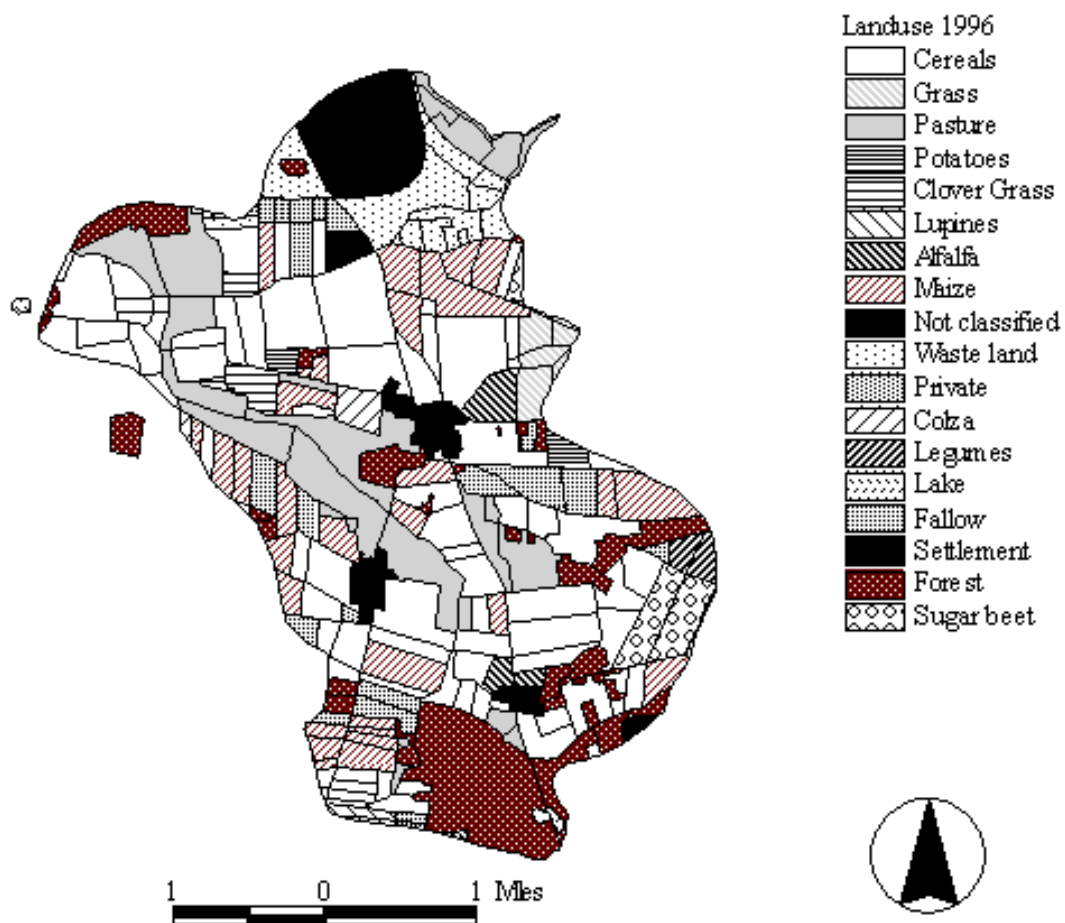


Figure 8: Landuse distribution in the Schaugraben study area in 1996

2.4 Distribution of boreholes, groundwater wells and gauging stations in the Schaugraben area

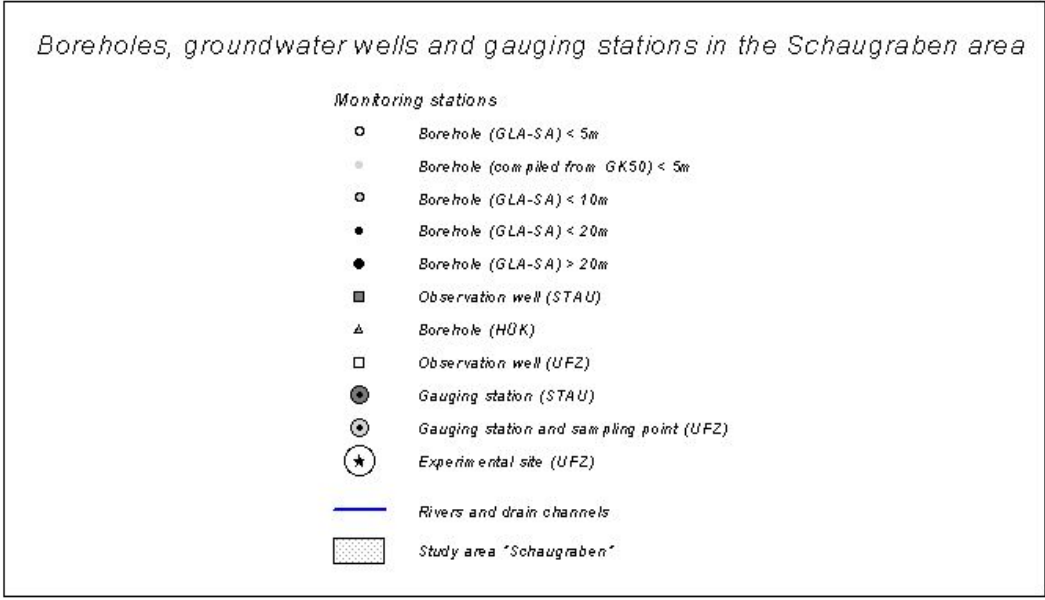
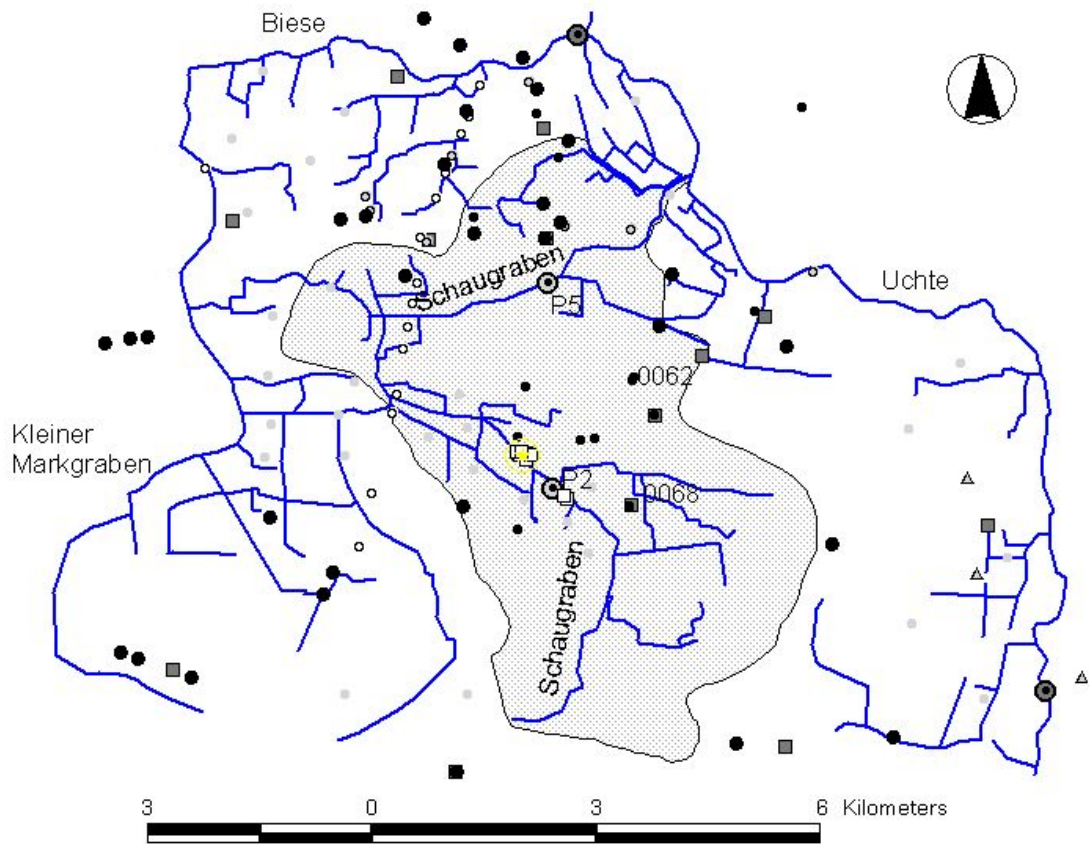


Figure 9: Boreholes, groundwater wells and gauging stations in the Schaugraben area.

2.5 Discharge at gauging station P5

The gauging station P5 is the main gauge of the Schaugraben drain. It was installed in 1996 and has been used for continuous discharge monitoring and daily water sampling. Parallel, a weekly sampling and discharge measurement has been conducted. Data have been collected from 1997-1999 and from 2000 to 2002.

Discharge measurements of the gauging station P5 are discontinuous and longer gaps occur due to sensor failure. Weekly and continuous observations differ considerably and do not coincide. Thus substance loads and total discharge strongly depend on the data set used for calculation. Due to various technical problems with the data logger and sensor equipment the weekly measurements are considered the more reliable data base.

Evaluation of flow components showed that direct runoff accounts for 4% of total runoff, whereas fast and slow baseflow account for 94%. A chemical hydrograph separation based on concentrations of sulfate, chloride and silica suggested more or less equal contribution of fast and slow baseflow. Due to the short observation period, these data can give a rough orientation only.

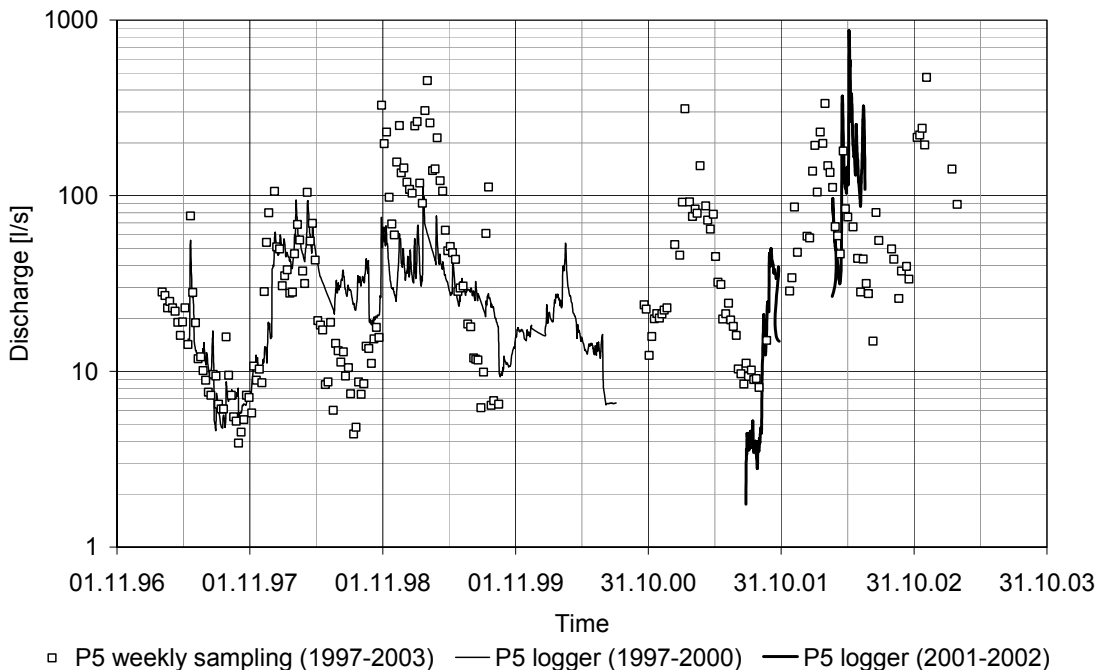


Figure 10: Discharge measurements at gauging station P5 – continuous and weekly measurements since 1997

Table 9: Characterisation of the discharge data set

	Discharge (weekly sampling) [l/s]
Mean discharge	62.4
Minimum	3.9
Maximum	470.9
25%-Quantil	12.0
Median	28.5
75%- Quantil	78.9

Table 10: Annual runoff calculated from discharge data

Year	Runoff [mm]	Month observed
1997	24 ¹⁾	10 (Mar-Dec)
1998	68	12
1999	160 ¹⁾	9 (Jan-Sep)
2000	80	3 (Oct-Dec)
2001	72 ¹⁾	11 (-Oct)
2002	117	12
Average ²⁾	87 [mm]	55 [l/s]

¹⁾ Corrected for 12 months, ²⁾ without 2000

2.6 Analysis of surface water samples at gauging station P5 and P2 and seepage samples at the experimental site

Surface water samples analyzed for NO_3^- , NH_4^+ , NO_2^- , DOC, SO_4^{2-} , Cl⁻, TIC, Si. The following figure shows the chemical composition of drain water at gauging stations P5 and P2 and in seepage samplers at the experimental site.

Schaugraben drain (P2,P5) and seepage water (SP2 - SP4)

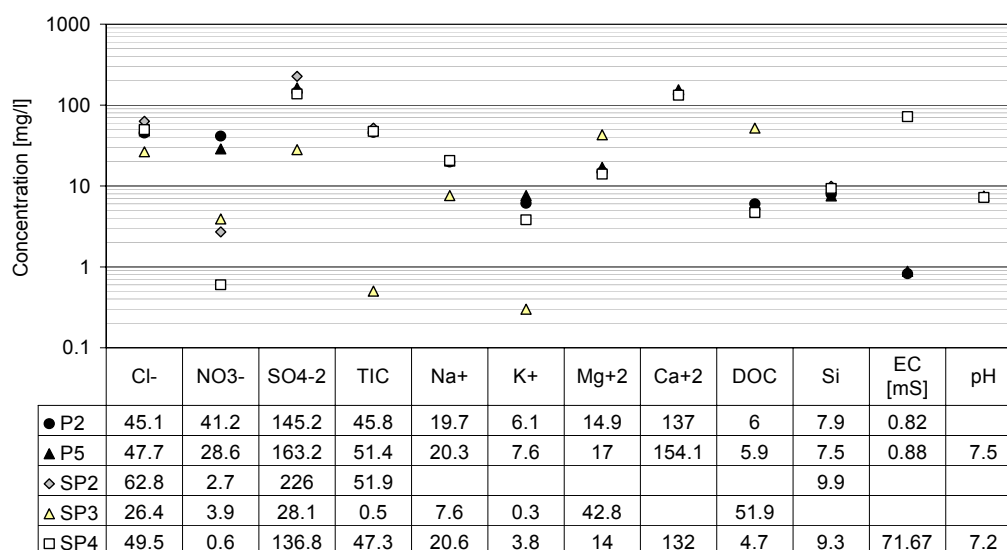


Figure 11: Mean composition of drain water at gauging station P5 and observation point P2 and of seepage water in seepage samplers SP2, SP3 and SP4

2.7 Discharge and Nitrate loads at P5

Total discharge and loads have been calculated from the weekly sampling series interpolating time specific samples by a step-wise function for both, discharge and solute concentrations. In figure xx monthly discharge and mean monthly nitrate concentrations are given. It can clearly be seen that nitrate concentrations follow a seasonal cycle with small concentrations during summer, where runoff is low and enhanced denitrification takes place in soils and hyporheic zones, and higher concentrations in winter, with low denitrification and higher runoff rates. Possibly, the sources of

water and nitrogen may also change between summer and winter.

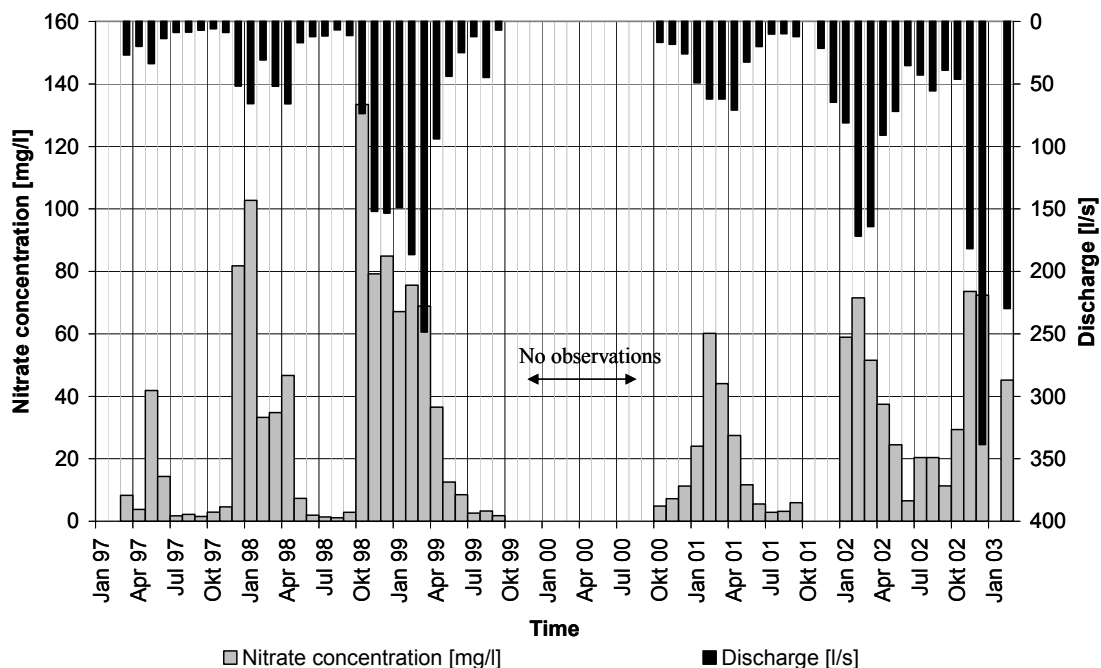


Figure 12: Monthly discharge and mean nitrate concentrations at gauging station P5, calculated from weekly measurements

Table 27: Characterisation of monthly discharge and N export at P5

	Discharge [l/s]	N-Load [mg/s]	Nitrate concentration [mg/l]
Mean discharge	61.2	728	29
Minimum	0.0	0	0
Maximum	338.7	5536	133
25%-Quantile	12.1	7.2	3
Median	37.2	92.6	14
75%- Quantile	71.2	792.1	46

2.8 Chemical characterisation of groundwater samples at the experimental site

Several observation wells have been installed at the experimental site. Filter depths are between 2 and 3m below surface. Groundwater levels were observed weekly, groundwater samples were taken irregularly over a period from 2000 to 2002. The samples were analyzed for NO_3^- , NH_4^+ , NO_2^- , SO_4^{2-} , Cl^- , K^+ , Na^+ , Mg^{2+} , Ca^{2+} , DOC, Si. Substance concentrations indicate high spatial heterogeneity. Nitrate could be found in some wells, whereas it is lacking in other wells. It is highly possibly, that nitrate is leached to groundwater locally following preferential flow paths or according to irregular distribution of nitrate sources, such as excrements of grazing cattle. A summary of observed concentrations is given in the following figure.

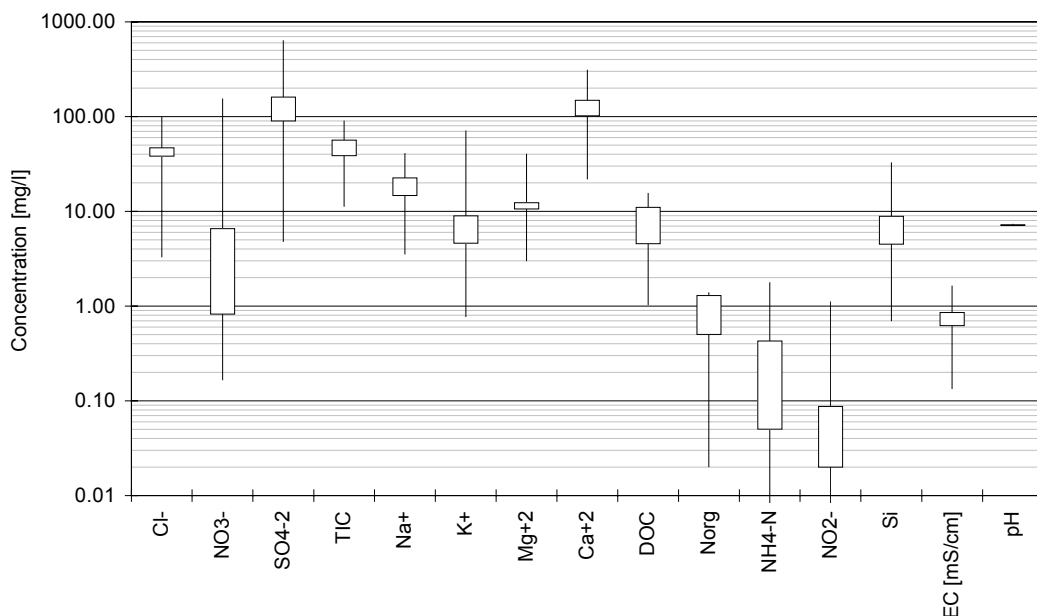


Figure 13: Groundwater composition at the Schaugraben experimental site – Quartiles over all groundwater samples (in quartiles)

2.9 Chemical characterisation of groundwater at observation well 0063 and 0068

The groundwater wells 0063 and 0068 are part of the official groundwater level observation network and allow sampling of deeper groundwater. They have been sampled once in order to get an idea about groundwater chemistry in the main aquifer system. Whereas in well 0063 high concentrations of nitrate are present, no nitrate was found in well 0068. However, concentrations in sulphate are considerably increased in contrast to well 0063, indicating presence of pyrite and substantial autotrophic denitrification.

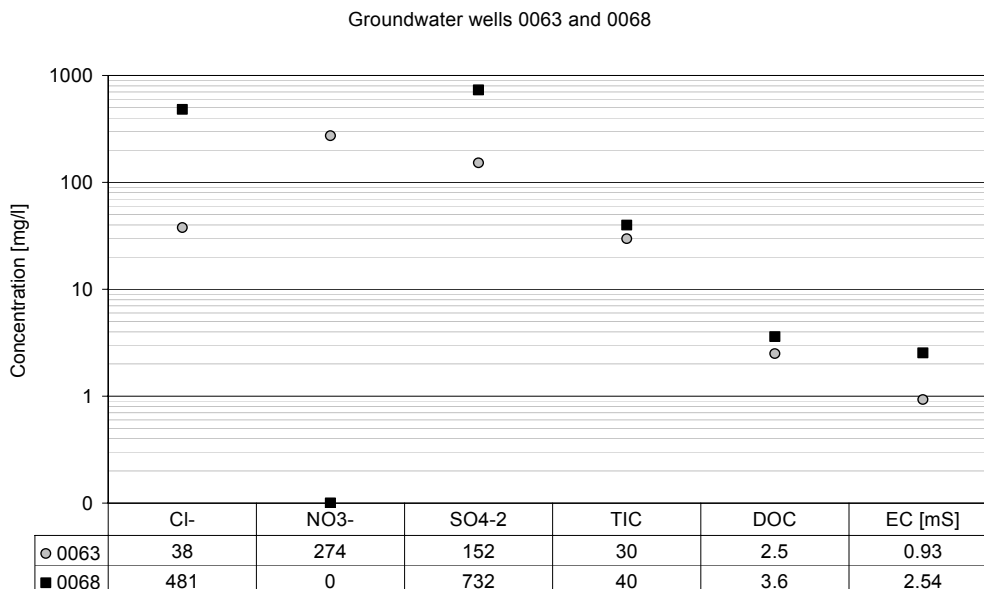


Figure 14: Groundwater composition in wells 0063 and 0068, sampling 03.05.01

Appendix B - Documentation of the modified RISK-N (mRISK-N) - Model

© 2003 Gunter Wriedt, UFZ-Umweltforschungszentrum Leipzig-Halle GmbH, Brückstr. 3a, 39114 Magdeburg, gunter.wriedt@ufz.de

Table of contents

1	INTRODUCTION	2
2	MODEL EQUATIONS	2
2.1	SOIL WATER BALANCE MODEL	2
2.1.1	<i>General structure</i>	2
2.1.2	<i>Units</i>	2
2.1.3	<i>Interception storage</i>	3
2.1.4	<i>Infiltration storage model.....</i>	3
2.1.5	<i>Soil water storage model.....</i>	4
2.2	SOIL TEMPERATURE	5
2.3	SOIL NITROGEN MODEL	6
2.3.1	<i>General structure</i>	6
2.3.2	<i>N-balance of upper root zone.....</i>	6
2.3.3	<i>N-balance lower root zone</i>	9
2.3.4	<i>N-balance intermediate vadose zone.....</i>	10
2.3.5	<i>Denitrification model</i>	11
2.3.6	<i>Nitrate fluxes from soil zones</i>	11
3	REFERENCES	13

1 Introduction

The code presented here as mRISK-N (modified RISK-N) combines the analytical soil nitrogen model RISK-N, published by Gusman & Marino 1999 and a simple soil water model based on a capacity storage approach, following the SIMPEL-model (Hörmann, 1998).

Input data are stored in a variety of input files containing climatic data, a soil profile database and a management database. The superfile allows the definition of multiple simulations defined by a unique combination of soil profile, management scenario and groundwater depth using a simulation list. This allows the definition of sensitivity studies, scenario simulations and distributed regional simulations.

The temporal discretisation follows the stress period concept as used in MODFLOW. During each stress period, all boundary fluxes are considered constant. For the soil water model and the soil nitrogen model, the temporal discretisation can be defined independently. This allows the soil model to be run with daily climatic data, whereas the soil nitrogen model can be run with monthly or seasonal resolution. Soil water balance data are aggregated according to the resolution of the soil nitrogen model.

2 Model equations

2.1 Soil water balance model

2.1.1 General structure

The soil water model is characterized by a series of storages, controlling water flow and evapotranspiration in the soil column. The interception and infiltration storage control the amount of excess precipitation entering the soil column. The soil column itself is divided into three compartments: upper root zone (URZ), lower root zone (LRZ) and intermediate vadose zone (IVZ), following the discretisation of the soil nitrogen model. The lower boundary of the soil column is the groundwater table. The model structure is given in Figure .

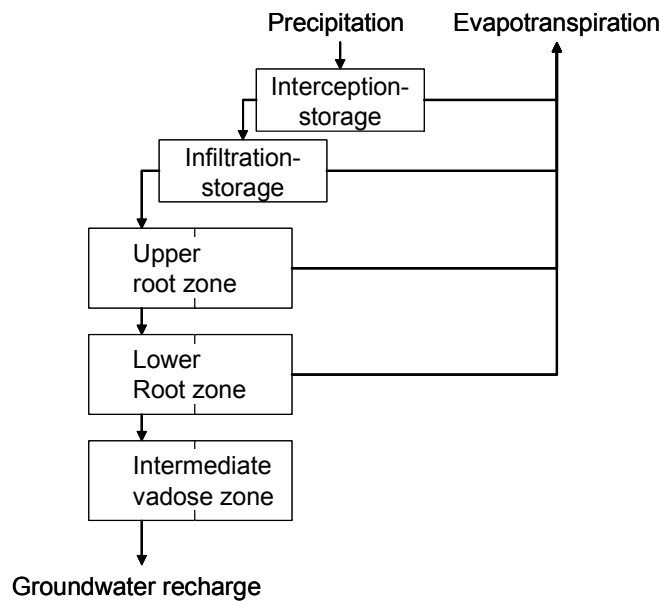


Figure 1: Structure of the soil water submodel

The soil water balance is calculated explicitly in time steps of one-day duration. Climatic input data have to be provided as daily data.

2.1.2 Units

All soil water contents are given in [m]. Fluxes are considered as absolute fluxes for the given time step interval and also given in [m]. These units are not explicitly specified in the following equations.

2.1.3 Interception storage

Leaf interception was calculated using a simple overflow storage.

The interception storage capacity is defined as a function of the leaf area index LAI as:

$$S_{Leaf} = S_{LAI}^{Min} + LAI \cdot C_{LAI} \quad (1)$$

with S_{leaf} =interception storage capacity, C_{LAI} =specific storage capacity [m/LAI], S_{LAI}^{min} = minimum storage capacity

Potential evaporation from the interception storage is confined by interception storage capacity and potential evapotranspiration:

$$ETp_{LAI} = Min(S_{Leaf}, ETp) \quad (2)$$

with ETp_{LAI} = potential evapotranspiration from interception storage, ETp = potential evapotranspiration

Precipitation not consumed by evaporation is transferred to the next storage

$$P_{Surplus}^{LAI} = Max(0, P - ETp_{LAI}) \quad (3)$$

with $P_{surplus}^{LAI}$ = excess precipitation, P =Precipitation

The remaining evapotranspiration is given by the equation:

$$ETa_{LAI}^{Surplus} = ETp - ETp_{LAI} - Min(0, P - ETp_{LAI}) \quad (4)$$

with $ETa_{LAI}^{surplus}$ = excess evapotranspiration

Actual evaporation from leaf interception is calculated as difference between potential evapotranspiration and remaining evapotranspiration:

$$ETa_{LAI} = ETp - ETa_{surplus} \quad (5)$$

with ETa_{LAI} = actual evapotranspiration from interception storage

2.1.4 Infiltration storage model

The maximum evapotranspiration from the infiltration storage is defined as:

$$ETp_{Inf}^{Max} = Min \left(ETp_{LAI}^{Surplus}, Min \left(C_{Inf}, \frac{S_{Inf}^0 + P_{LAI}^{Surplus}}{k_{Inf}} \right) \right) \quad (6)$$

with ETp_{Inf}^{Max} = Maximum evapotranspiration from infiltration storage, C_{Inf} = infiltration storage capacity, k_{inf} = storage coefficient, S_{inf}^0 = initial water content

The new storage water content is calculated according to:

$$S'_{Inf} = Min \left(C_{Inf}, Max \left(0, S_{Inf}^0 + P_{LAI}^{Surplus} - ETp_{Inf}^{Max} \right) \right) \quad (7)$$

with S_{inf}' = new storage water content

Excess water percolating into the soil column is then given by:

$$P_{Inf}^{Surplus} = Max \left(0, S_{Inf}^0 + P_{LAI}^{Surplus} - ETp_{Inf}^{Max} - S'_{Inf} \right) \quad (8)$$

with $P_{inf}^{surplus}$ = excess water infiltrating into soil column

And the remaining potential evapotranspiration available for subsequent storages is:

$$ETp_{Inf}^{Surplus} = ETp_{LAI}^{Surplus} - ETa_{Inf}^{Max} - \text{Min}(0, S_{Inf}^0 + P_{LAI}^{Surplus} - ETp_{Inf}^{Max}) \quad (9)$$

with $ETp_{Inf}^{surplus}$ = excess evapotranspiration

2.1.5 Soil water storage model

Soil water balance for each soil compartment (URZ, LRZ, IVZ) is calculated according to Hörmann (1998). The linear storage equation, however, was substituted by the formulation used in the EPIC-model (Sharpley, Williams (1990).

The actual soil water content is defined by the initial soil water content and the amount of water flow across the upper boundary:

$$S^{1a} = S^0 + P^{Surplus} \quad (10)$$

with S^{1a} = new soil water storage, S^0 = initial soil water storage, $P^{surplus}$ = excess water leached from preceding storage

If the soil water content exceeds the reduction point RP, actual evapotranspiration is equal to potential evapotranspiration. Else the evapotranspiration is confined by the ratio of soil water content to reduction point and a root factor.

$$ETa = \begin{cases} ETp & \text{if } S^* > RP \\ \text{Min}\left(ETp \cdot \left(\frac{S^{1a}}{RP} - 1\right), ETp \cdot f_{Rootfraction}\right) & \text{else} \end{cases} \quad (11)$$

with ETa = actual evapotranspiration, RP = reduction point, f = rootfraction [-]

The actual soil water content is corrected for evapotranspiration according to:

$$S^{1b} = S^{1a} - ETa \quad (12)$$

with S^{1b} = soil water storage corrected for ETa

It is assumed that only soil water exceeding field capacity does percolate into deeper layers. Then depletion of the soil water storage is calculated according to:

$$\frac{dS}{dt} = -k \cdot (S - FC) \quad (13)$$

with S = soil water storage, FC = Field capacity, k = storage coefficient [d^{-1}]

whose solution is given by

$$S_i = (S^{1b} - FC) \cdot e^{-k\Delta t} \quad \text{with} \quad \frac{1}{k} = \left(\frac{PV - FC}{Kf}\right) \quad (14)$$

where S_i = new soil storage, S^{1b} = initial soil storage, dt = time increment [d], PV = pore volume, FC = field capacity, K_f = saturated hydraulic conductivity [$m d^{-1}$]

The amount of leaching water is given as the difference between final and preceding soil storage water content:

$$P_i^{Surplus} = S^{1b} - S_i \quad (15)$$

with $P_i^{surplus}$ = percolation

Groundwater recharge is the excess water leaching from the last soil storage. The intermediate vadose zone is located below the root zone, thus no plant roots are present and evapotranspiration becomes from this storage becomes zero.

2.2 Soil temperature

Due to the simple structure of the model, soil temperatures can not be calculated using a heat transport model. The soil temperature model is a straightforward approach, based on the assumption that soil temperatures are confined by damped daily air temperatures in the top soil and by mean annual temperatures or a damped annual cycle in deeper soil layers, depending on the depth of the lower boundary.

The upper root zone temperature is calculated as the average temperature of the preceding 3 days.

$$T_{URZ}(i) = \sum_{d=i}^{i-3} T_{Air}(d) \quad (16)$$

with T_{URZ} = temperature of upper root zone [$^{\circ}\text{C}$], T_{Air} = air temperature [$^{\circ}\text{C}$], i =day index

Soil temperature in deeper layers was considered to be confined by the mean annual temperature. If the soil column does not extend into greater depth, an annual cycle was applied as the average temperature of the preceding two months. The threshold was set arbitrarily to a depth of 3m.

$$T_{IVZ}(i) = \begin{cases} MAT & z > 3m \\ \sum_{d=i}^{i-60} T_{Air}(d) & z < 3m \end{cases} \quad (17)$$

with T_{URZ} = temperature of upper root zone [$^{\circ}\text{C}$], T_{IVZ} = temperature of lower root zone [$^{\circ}\text{C}$], T_{Air} = air temperature [$^{\circ}\text{C}$], MAT = Mean annual temperature [$^{\circ}\text{C}$], i =day index, z = lower depth of IVZ [m]

Temperature of the lower root zone was calculated as a depth-weighted average between URZ- and IVZ temperature.

2.3 Soil nitrogen model

2.3.1 General structure

The soil column is divided into three layers, upper root zone, lower root zone and intermediate vadose zone, which extends to the groundwater surface. Model structure and relevant processes are shown in Figure .

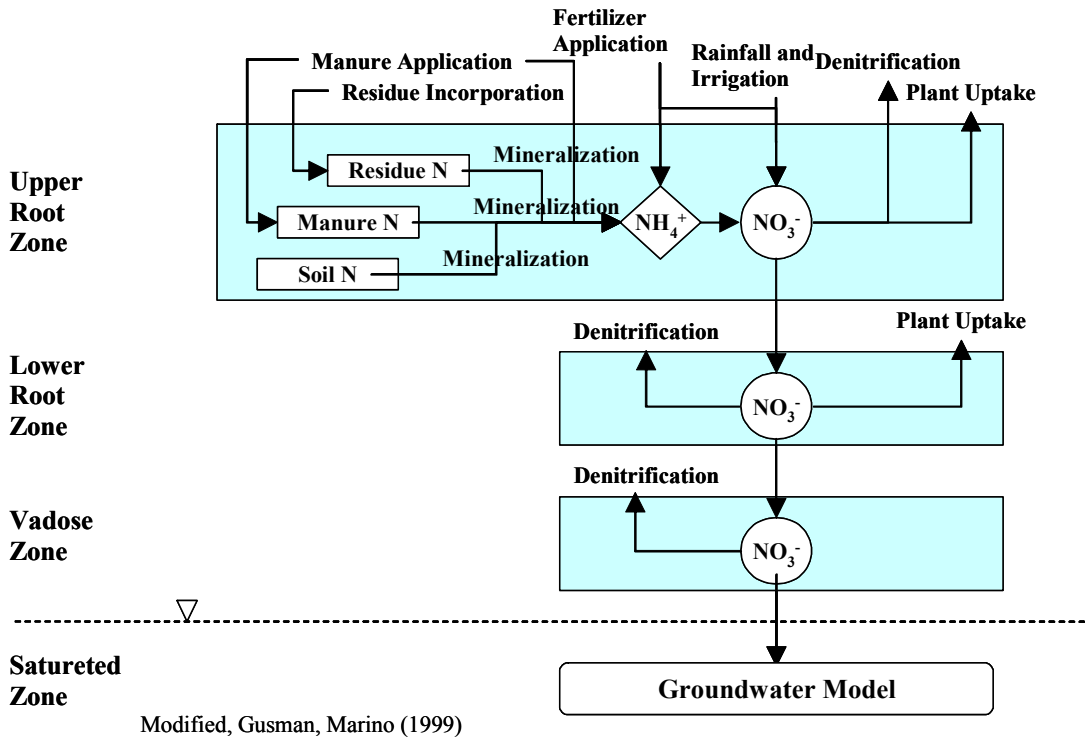


Figure 2: Structure of the soil nitrogen submodel RISK-N

2.3.2 N-balance of upper root zone

Nitrogen mineralisation

The equations to determine mineralisation rates of rapid and slow organic N pools are taken from Kersebaum and Richter (1991). They have been transformed in order to apply different effective mineralisation rate constants.

Rapid mineralisation rate

$$k_{mr}(T, \theta) = k_r^{35} \cdot e^{\frac{9800}{35+273}} \cdot e^{\frac{-9800}{T+273}} \cdot F_{wm} \quad (18)$$

Slow mineralisation rate

$$k_{ms}(T, \theta) = k_s^{35} \cdot e^{\frac{8400}{35+273}} \cdot e^{\frac{-8400}{T+273}} \cdot F_{wm} \quad (19)$$

with $k_{ms/mr}$ = rate of slow/rapid mineralisation, $k_{r/s}^{35}$ = rate constant for rapid/slow mineralisation at 35°C [d⁻¹], T = temperature [°C], θ = soil water content [-], F_{wm} = water content factor

The soil water content factor defines an optimum mineralisation for soil water contents around field capacity, according to Cabon et al. (1991)

$$F_{wm} = \begin{cases} \frac{\theta}{FC} & \theta < FC \\ \frac{FC}{\theta} & FC < \theta \end{cases} \quad (20)$$

where F_{wm} = soil water content factor, θ = soil water content [-], FC = Field capacity [-]

The rapid mineralisation of organic N is described according to Gusman & Marino (1999) by the equation

$$C_r(t) = \left[C_r(t_0) + \frac{(F_{man}^r M_{Man} + F_{Res}^r M_{Res})}{H_{ur}} \right] e^{-k_{mr}(t-t_0)} = C_r^* e^{-k_{mr}(t-t_0)} \quad (21)$$

where $C_r(t)$ = rapidly mineralizing N concentration in URZ [g N/m³], t = time since N application [d], k_{mr} = rate coefficient for net mineralisation [d⁻¹], $C_r(t_0)$ = initial rapidly mineralizing N concentration in URZ [g N/m³], F_{man}^r = rapidly mineralizing fraction of manure N (0.25), M_{man} = total manure N applied [g N/m²], F_{res}^r = rapidly mineralizing fraction of residue N (0.5), M_{res} = mass of residue added to the soil [g N/m²], H_{ur} = depth of URZ [m]

Mineralisation M_r of rapid organic matter can be solved according to equation

$$M_r(t) = \left[C_r(t_0) + \frac{(F_{man}^r M_{Man} + F_{Res}^r M_{Res})}{H_{ur}} \right] e^{-k_{mr}(t-t_0)} - \left[C_r(t_0) + \frac{(F_{man}^r M_{Man} + F_{Res}^r M_{Res})}{H_{ur}} \right] \quad (22)$$

which can be rearranged to

$$M_r(t) = -(1 - e^{-k_{mr}(t-t_0)}) \cdot C_r^* \quad (23)$$

where $M_r(t)$ = total rapid mineralisation in time interval [t,t₀]

Slow mineralisation of organic N is solved analogously with equivalent equations.

A resident fraction of slowly mineralizing N not taking part in turnover is considered as a constant value, and thus the total content of slowly mineralizing nitrogen C_s^{tot} is given by

$$C_s^{Tot}(t) = C_s(t) + C_s^{Soil} \quad (24)$$

where $C_s(t)$ = content of slowly mineralizing N and C_s^{soil} = content of resident N in the soil.

Ammonium Mass Balance

A linear sorption isotherm is used to describe the relation between adsorbed and solution Ammonium-N according to the equation

$$C_{as} = K_d \cdot C_{al} \quad (25)$$

where K_d = distribution coefficient [m³ soil solution / g soil], C_{as} = ammonium concentration in adsorbed phase [g NH₄-N / g soil], C_{al} = ammonium concentration in soil solution [g NH₄-N / m³ soil solution]

The ammonium-N concentration of the soil solution is described according to Gusman & Marino (1999) by the mass balance equation

$$C_{al}(t) = e^{-(k_n/R_{ur})(t-t_0)} C_{al}(t_0) + \left(\frac{1}{\theta_{ur}} R_{ur}\right) \int_{t_0}^t e^{-(k_n/R_{ur})(t-\tau)} \left[k_{mr} C_r(\tau) + k_{ms} C_s(\tau) + \frac{q_{ur} C_{a0}(\tau)}{H_{ur}} \right] d\tau \quad (26)$$

and the retardation factor

$$R_{ur} = 1 + \frac{\rho_{soil} K_d}{\theta_{ur}} \quad (27)$$

where C_{al} =concentration of ammonium N in soil solution [g NH₄-N/m³ soil solution], θ_{ur} = volumetric water content in URZ [m³ soil solution/m³ soil], k_n = first order nitrification rate constant [d⁻¹], ρ_{soil} =soil bulk density in URZ [g/m³ soil], $C_{a0}(\tau)$ =ammonium concentration at soil surface [g NH₄-N/m³ soil solution], τ =dummy variable for integration

Fertilizer application and deposition is considered according to equation

$$q_{ur} C_{a0}(t) = [M_a + Dep_a^{dry} \Delta t_0] \delta(t - t_0) + (p - r) C_{ap} \quad (28)$$

where C_{ap} = ammonium concentration in precipitation [g NH₄-N/m³ solution] , Dep_a^{dry} = constant rate of dry deposition [g NH₄-N/m²/d], Δt_0 =duration of the previous season

The following substitutions have been made:

$$A = [M_a + Dep_a^{dry} \Delta t_0] \delta(t - t_0) = [M_a + Dep_a^{dry} \Delta t_0] \quad (29)$$

$$B = (p - r) C_{ap} \quad (30)$$

$$\rho = k_n / R_{ur} \quad (31)$$

The solution of equation 31 is then given by

$$C_{al}(t) = e^{-\rho(t-t_0)} \left[C_{al}(t_0) - \left(\frac{1}{\theta_{ur}} R_{ur}\right) k_{mr} C_r^* \frac{1}{\rho - k_{mr}} - \left(\frac{1}{\theta_{ur}} R_{ur}\right) k_{ms} C_s^* \frac{1}{\rho - k_{ms}} + \left(\frac{1}{\theta_{ur}} R_{ur}\right) \frac{A}{H_{ur}} - \left(\frac{1}{\theta_{ur}} R_{ur}\right) \frac{B}{H_{ur}} \frac{1}{\rho} \right]^{B_0} + \left[\left(\frac{1}{\theta_{ur}} R_{ur}\right) k_{mr} C_r^* \frac{1}{\rho - k_{mr}} \right]^{C_0} e^{-k_{mr}(t-t_0)} + \left[\left(\frac{1}{\theta_{ur}} R_{ur}\right) k_{ms} C_s^* \frac{1}{\rho - k_{ms}} \right]^{D_0} e^{-k_{ms}(t-t_0)} + \left[\left(\frac{1}{\theta_{ur}} R_{ur}\right) \frac{B}{H_{ur}} \frac{1}{\rho} \right]^{E_0} \quad (32)$$

which can be simplified into the equation

$$C_{al}(t) = B_0 e^{-\rho(t-t_0)} + C_0 e^{-k_{mr}(t-t_0)} + D_0 e^{-k_{ms}(t-t_0)} + E_0 \quad (33)$$

Nitrate mass balance

The nitrate mass balance of the upper root zone is described by Gusman & Marino (1999) by the equation

$$C_n^{ur}(t) = e^{-\alpha_n(t-t_0)} C_n^{ur}(t_0) + \int_{t_0}^t e^{-\alpha_n(t-\tau)} \left[k_n C_{al}(\tau) + \frac{q_{ur} C_{n0}(\tau) - U_{ur}}{\theta_{ur} H_{ur}} \right] d\tau \quad (34)$$

and

$$\alpha_n = \frac{q_{ur}^*}{\theta_{ur} H_{ur}} + k_{den} \quad (35)$$

where $C_{ur}^n(t_0)$ =initial nitrate concentration in URZ [g NO₃-N/m³ soil solution], $C_{al}(\tau)$ =ammonium concentration from equation (33) [g NH₄-N / m³ soil solution], $C_{n0}(t)$ = nitrate concentration at soil surface [g NO₃-N / m³ soil solution], k_{dur} =first order denitrification rate constant in URZ [d⁻¹], U_{ur} = plant uptake in URZ [g NO₃-N / m² soil/d], q_{ur}^* = water flux from URZ [m/d]

Substituting

$$q_{ur} C_{n0}(\tau) = M_n \delta(\tau - t_0) + i C_{ni} \quad (36)$$

where M_n = Mass of fertilizer nitrate applied [g NO₃-N/m²], i = irrigation rate [m/d], C_{ni} =nitrate concentration in irrigation water [g NO₃-N/m³]

and applying equation 34 from the ammonium mass balance

$$C_{al}(t) = B_0 e^{-\rho(t-t_0)} + C_0 e^{-k_{mr}(t-t_0)} + D_0 e^{-k_{ms}(t-t_0)} + E_0 \quad (37)$$

yields

$$C_n^{ur}(t) = \left[C_n^{ur}(t_0) - k_n B_0 \frac{1}{\alpha - \rho} - k_n C_0 \frac{1}{\alpha - k_{mr}} - k_n D_0 \frac{1}{\alpha - k_{ms}} \right]_{A_1} e^{-\alpha_n(t-t_0)} \\ + \left[k_n B_0 \frac{1}{\alpha - \rho} \right]_{B_1} e^{-\rho(t-t_0)} + \left[k_n C_0 \frac{1}{\alpha - k_{mr}} \right]_{C_1} e^{-k_{mr}(t-t_0)} + \left[k_n D_0 \frac{1}{\alpha - k_{ms}} \right]_{D_1} e^{-k_{ms}(t-t_0)} \\ + \left[k_n E_0 \frac{1}{\alpha} + \frac{i C_{ni}}{\theta_{ur} H_{ur}} \frac{1}{\alpha} - \frac{U_{ur}}{\theta_{ur} H_{ur}} \frac{1}{\alpha} \right]_{E_1} \quad (38)$$

which can be written as a simplified formulation as

$$C_n^{ur}(t) = A_1 e^{-\alpha_n(t-t_0)} + B_1 e^{-\rho(t-t_0)} + C_1 e^{-k_{mr}(t-t_0)} + D_1 e^{-k_{ms}(t-t_0)} + E_1 \quad (39)$$

2.3.3 N-balance lower root zone

The nitrate mass balance of the lower root zone is described by Gusman & Marino (1999) using the equation

$$C_n^{lr}(t) = e^{-\beta_n(t-t_0)} C_n^{lr}(t_0) + \int_{t_0}^t e^{-\beta_n(t-\tau)} \left[\frac{q_{ur}^* C_n^{ur}(\tau) - U_{lr}}{\theta_{lr} H_{lr}} \right] d\tau \quad (40)$$

with

$$\beta_n = \frac{q_{lr}^*}{\theta_{lr} H_{lr}} + k_{den} \quad (41)$$

where $C_{lr}^n(t)$ = nitrate concentration in LRZ [g NO₃-N/m³ soil solution], $C_{lr}^n(t_0)$ =initial nitrate concentration in LRZ [g NO₃-N/m³ soil solution], C_{ur}^n = nitrate concentration in URZ [g NO₃-N/m³ soil solution], q_{lr}^* = water flux from the LRZ [m/d], θ_{lr} = volumetric water content in LRZ [m³ soil solution/m³ soil], $k_{d,lr}$ =first order denitrification rate constant in LRZ [d⁻¹], U_{lr} = plant uptake in LRZ [g NO₃-N /m² soil/d]

and from the upper root zone nitrate mass balance (equation 39):

$$C_n^{ur}(\tau) = A_1 e^{-\alpha_n(\tau-t_0)} + B_1 e^{-\rho(\tau-t_0)} + C_1 e^{-k_{mr}(\tau-t_0)} + D_1 e^{-k_{ms}(\tau-t_0)} + E_1 \quad (42)$$

Solving the equation yields

$$C_n^{lr}(t) = \left[C_{lr}^n(t_0) - \frac{q_{ur}^* A_1}{\theta_{lr} H_{lr}} \frac{1}{\beta - \alpha} - \frac{q_{ur}^* B_1}{\theta_{lr} H_{lr}} \frac{1}{\beta - \rho} \right] e^{-\beta_n(t-t_0)} \\ + \left[\frac{q_{ur}^* C_1}{\theta_{lr} H_{lr}} \frac{1}{\beta - k_{mr}} - \frac{q_{ur}^* D_1}{\theta_{lr} H_{lr}} \frac{1}{\beta - k_{ms}} - \frac{q_{ur}^* E_1}{\theta_{lr} H_{lr}} \frac{1}{\beta} + \frac{U_{lr}}{\theta_{lr} H_{lr}} \frac{1}{\beta} \right]_{A_2} e^{-\beta_n(t-t_0)} \\ + \left[\frac{q_{ur}^* A_1}{\theta_{lr} H_{lr}} \frac{1}{\beta - \alpha} \right]_{B_2} e^{-\alpha_n(t-t_0)} + \left[\frac{q_{ur}^* B_1}{\theta_{lr} H_{lr}} \frac{1}{\beta - \rho} \right]_{C_2} e^{-\rho(t-t_0)} + \left[\frac{q_{ur}^* C_1}{\theta_{lr} H_{lr}} \frac{1}{\beta - k_{mr}} \right]_{D_2} e^{-k_{mr}(t-t_0)} \quad (43) \\ + \left[\frac{q_{ur}^* D_1}{\theta_{lr} H_{lr}} \frac{1}{\beta - k_{ms}} \right]_{E_2} e^{-k_{ms}(\tau-t_0)} + \left[\frac{q_{ur}^* E_1}{\theta_{lr} H_{lr}} \frac{1}{\beta} - \frac{U_{lr}}{\theta_{lr} H_{lr}} \frac{1}{\beta} \right]_{F_2}$$

which is simplified into the equation

$$C_n^{lr}(t) = A_2 e^{-\beta_n(t-t_0)} + B_2 e^{-\alpha_n(t-t_0)} + C_2 e^{-\rho(t-t_0)} + D_2 e^{-k_{mr}(t-t_0)} + E_2 e^{-k_{ms}(\tau-t_0)} + F_2 \quad (44)$$

2.3.4 N-balance intermediate vadose zone

The nitrate mass balance of the intermediate vadose zone is described by Gusman & Marino (1999) using the equation

$$C_n^v(t) = e^{-\gamma_n(t-t_0)} C_n^v(t_0) + \int_{t_0}^t e^{-\gamma_n(t-\tau)} \left[\frac{q_{lr}^* C_{lr}^n(\tau)}{\theta_v H_v} \right] d\tau \quad (45)$$

with

$$\gamma_n = \frac{q_v^*}{\theta_v H_v} + k_{den} \quad (46)$$

where $C_n^v(t)$ = nitrate concentration in IVZ [g NO₃-N/m³ soil solution], $C_n^v(t_0)$ =initial nitrate concentration in IVZ [g NO₃-N/m³ soil solution], C_{lr}^n = nitrate concentration in LRZ [g NO₃-N/m³ soil solution], q_v^* = water flux from the IVZ [m/d], θ_v = volumetric water content in LRZ [m³ soil solution/m³ soil], k_{den} =first order denitrification rate constant in LRZ [d⁻¹]

and from the lower root zone nitrate mass balance (equation 44)

$$C_n^{lr}(\tau) = A_2 e^{-\beta_n(\tau-t_0)} + B_2 e^{-\alpha_n(\tau-t_0)} + C_2 e^{-\rho(\tau-t_0)} + D_2 e^{-k_{mr}(\tau-t_0)} + E_2 e^{-k_{ms}(\tau-t_0)} + F_2 \quad (47)$$

Solving the equation yields

$$\begin{aligned}
C_n^v(t) = & \left[C_n^v(t_0) - \frac{q_{lr}^* A_2}{\theta_v H_v} \frac{1}{\gamma - \beta} - \frac{q_{lr}^* B_2}{\theta_v H_v} \frac{1}{\gamma - \alpha} - \frac{q_{lr}^* C_2}{\theta_v H_v} \frac{1}{\gamma - \rho} \right. \\
& \left. - \frac{q_{lr}^* D_2}{\theta_v H_v} \frac{1}{\gamma - k_{mr}} - \frac{q_{lr}^* E_2}{\theta_v H_v} \frac{1}{\gamma - k_{ms}} - \frac{q_{lr}^* F_2}{\theta_v H_v} \frac{1}{\gamma} \right]_{A_3} e^{-\gamma_n(t-t_0)} \\
& + \left[\frac{q_{lr}^* A_2}{\theta_v H_v} \frac{1}{\gamma - \beta} \right]_{B_3} e^{-\beta_n(t-t_0)} + \left[\frac{q_{lr}^* B_2}{\theta_v H_v} \frac{1}{\gamma - \alpha} \right]_{C_3} e^{-\alpha_n(t-t_0)} + \left[\frac{q_{lr}^* C_2}{\theta_v H_v} \frac{1}{\gamma - \rho} \right]_{D_3} e^{-\rho(t-t_0)} \\
& + \left[\frac{q_{lr}^* D_2}{\theta_v H_v} \frac{1}{\gamma - k_{mr}} \right]_{E_3} e^{-k_{mr}(t-t_0)} + \left[\frac{q_{lr}^* E_2}{\theta_v H_v} \frac{1}{\gamma - k_{ms}} \right]_{F_3} e^{-k_{ms}(t-t_0)} + \left[\frac{q_{lr}^* F_2}{\theta_v H_v} \frac{1}{\gamma} \right]_{G_3}
\end{aligned} \quad (48)$$

which is written in simplified form as

$$C_n^v(t) = A_3 e^{-\gamma_n(t-t_0)} + B_3 e^{-\beta_n(t-t_0)} + C_3 e^{-\alpha_n(t-t_0)} + D_3 e^{-\rho(t-t_0)} + E_3 e^{-k_{mr}(t-t_0)} + F_3 e^{-k_{ms}(t-t_0)} + G_3 \quad (49)$$

2.3.5 Denitrification model

The seasonal denitrification rate coefficients are calculated according to the CropSyst model, as described in Marchetti et al. (1997):

$$k_d = k_{15} \cdot F_{wd} \cdot F_t \quad (50)$$

where k_{15} = first order denitrification rate coefficient referred to 15°C [d^{-1}], k_d = effective denitrification rate coefficient [d^{-1}], F_{wd} = soil water content factor [-], F_t = soil temperature factor [-]

The soil water content factor is defined by the equation

$$F_{wd} = \exp(0.304 + 2.94(\theta_{sat} - \theta) - 47(\theta_{sat} - \theta)^2) \quad (51)$$

where θ = volumetric soil water content [m^3 solution/ m^3 soil]

The soil temperature factor was defined different from Gusman and Marino (1999) by an approximation of the Van't Hoff equation for temperatures $> 4^\circ C$ and a linear decrease to zero between 0 and $4^\circ C$:

$$F_t = \begin{cases} 0.001 & T < 0^\circ C \\ 0.44 \cdot \frac{T}{4} & 0^\circ < T < 4^\circ C \\ 2.1^{(T-15)/10} & T > 4^\circ C \end{cases} \quad (52)$$

where T = temperature [$^\circ C$]

2.3.6 Nitrate fluxes from soil zones

The nitrate mass flux from one compartment to another during a time period $[t, t_0]$ can be calculated according to Gusman & Marino using the equation

$$C_n^i[t, t_0] = \int_{t_0}^t q_i^* C_n^i(\tau) d\tau \quad (53)$$

C_n^i = nitrate flux from zone i in time interval $[t, t_0]$ [g NO_3-N], C_n^i = nitrate concentration in zone i [g NO_3-N/m^3 soil solution], q_i^* = flux from zone i , $i=\{URZ, LRZ, IVZ\}$

Upper root zone

For the URZ equation (53) can be written as

$$C_n^{ur}[t, t_0] = \int_{t_0}^t q_{ur}^* C_n^{ur}(\tau) d\tau \quad (54)$$

with

$$C_n^{ur}(\tau) = A_1 e^{-\alpha_n(\tau-t_0)} + B_1 e^{-\rho(\tau-t_0)} + C_1 e^{-k_{mr}(\tau-t_0)} + D_1 e^{-k_{ms}(\tau-t_0)} + E_1 \quad (55)$$

The solution is given by the equation

$$C_n^{ur}[t, t_0] = q_{ur}^* \left(\begin{array}{l} \frac{A_1}{\alpha} e^{-\alpha_n(t_0-t)} + \frac{B_1}{\rho} e^{-\rho(t_0-t)} + \frac{C_1}{k_{mr}} e^{-k_{mr}(t_0-t)} + \frac{D_1}{k_{ms}} e^{-k_{ms}(t_0-t)} \\ - \frac{A_1}{\alpha} - \frac{B_1}{\rho} - \frac{C_1}{k_{mr}} - \frac{D_1}{k_{ms}} + E_1(t-t_0) \end{array} \right) \quad (56)$$

Lower root zone

For the URZ equation (53) can be written as

$$C_n^{lr}[t, t_0] = \int_{t_0}^t q_{lr}^* C_n^{lr}(\tau) d\tau \quad (57)$$

with

$$C_n^{lr}(\tau) = A_2 e^{-\beta_n(\tau-t_0)} + B_2 e^{-\alpha_n(\tau-t_0)} + C_2 e^{-\rho(\tau-t_0)} + D_2 e^{-k_{mr}(\tau-t_0)} + E_2 e^{-k_{ms}(\tau-t_0)} + F_2 \quad (58)$$

The solution is given by the equation

$$C_n^{ur}[t, t_0] = q_{ur}^* \left(\begin{array}{l} \frac{A_2}{\beta} e^{-\alpha_n(t_0-t)} + \frac{B_2}{\alpha} e^{-\alpha_n(t_0-t)} + \frac{C_2}{\rho} e^{-\rho(t_0-t)} + \frac{D_2}{k_{mr}} e^{-k_{mr}(t_0-t)} + \frac{E_2}{k_{ms}} e^{-k_{ms}(t_0-t)} \\ - q_{ur}^* \left(\frac{A_2}{\beta} + \frac{B_2}{\alpha} + \frac{C_2}{\rho} + \frac{D_2}{k_{mr}} + \frac{E_2}{k_{ms}} \right) + q_{ur}^*(F_2(t-t_0)) \end{array} \right) \quad (59)$$

Intermediate vadose zone

For the IVZ equation (53) can be written as

$$C_n^r[t, t_0] = \int_{t_0}^t q_{ur}^* C_n^{ur}(\tau) d\tau \quad (60)$$

with

$$C_n^v(\tau) = A_3 e^{-\gamma_n(\tau-t_0)} + B_3 e^{-\beta_n(\tau-t_0)} + C_3 e^{-\alpha_n(\tau-t_0)} + D_3 e^{-\rho(\tau-t_0)} + E_3 e^{-k_{mr}(\tau-t_0)} + F_3 e^{-k_{ms}(\tau-t_0)} + G_3 \quad (61)$$

The solution is given by the equation

$$C_n^v[t, t_0] = q_v^* \left(\frac{A_3}{\gamma} e^{-\alpha_n(t_0-t)} + \frac{B_3}{\beta} e^{-\alpha_n(t_0-t)} + \frac{C_3}{\alpha} e^{-\alpha_n(t_0-t)} + \frac{D_3}{\rho} e^{-\rho(t_0-t)} + \frac{E_3}{k_{mr}} e^{-k_{mr}(t_0-t)} + \frac{F_3}{k_{ms}} e^{-k_{ms}(t_0-t)} \right) - q_{ur}^* \left(\frac{A_3}{\gamma} + \frac{B_3}{\beta} + \frac{C_3}{\alpha} + \frac{D_3}{\rho} + \frac{E_3}{k_{mr}} + \frac{F_3}{k_{ms}} \right) + q_{ur}^* (G_3(t-t_0))$$

(62)

3 References

- Gusman, A.J., Marino, M.A. (1999): Analytical Modelling of Nitrogen Dynamics in Soils and Groundwater. *Journal of Irrigation and Drainage Engineering* 1999(11/12), 330-337.
- Hörmann, G. (1998): Simpel-Speichermodule zum Bodenwasserhaushalt. Dokumentation zu Simpel 2, <http://www.pz-oekosys.uni-kiel.de/~schorsch/simpel/index.htm>.
- Sharpley, A.N., Williams, J.R. (1990): EPIC-Erosion Productivity Impact Calculator Vol. I - Model Documentation, USDA Technical bulletin No. 1768, Temple, TX

Appendix C - Formal Description of A Reaction Module for Calculation of Nitrogen Turnover in Groundwater Systems

© 2003, Gunter Wriedt, UFZ Umweltforschungszentrum Leipzig-Halle GmbH, Department Hydrologische Modellierung, Brückstr. 3a, 39114 Magdeburg, gunter.wriedt@ufz.de

Table of Contents

1	INTRODUCTION	1
2	UNITS.....	1
3	REACTION EQUATION SYSTEM.....	2
4	DEFINITION OF REACTION RATES.....	5
5	DEFINITION OF TOTAL COMPONENT CONCENTRATIONS	7
6	DEFINITION OF MOBILE COMPONENT CONCENTRATIONS.....	7
7	DERIVATION OF REACTION RATES FOR MOBILE COMPONENTS.....	8
8	CALCULATION OF SECONDARY SPECIES CONCENTRATIONS	9
9	REFERENCES	11

1 Introduction

This documentation presents the formal description of a reaction module for simulation of nitrogen transport and turnover of nitrogen compounds in groundwater systems. The reaction module was developed as a user-defined reaction module for the RT3D code (Clement 1997). The implementation of the reaction system using total component concentrations defined in a canonical matrix follows approaches presented in Lichtner et al. (1996). This approach was chosen as the use of total components facilitates the implementation of equilibrium reactions into the reaction system and numerical errors (e.g. round-off of species concentrations) are reduced.

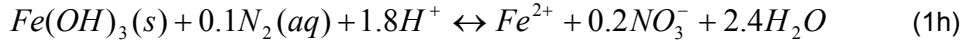
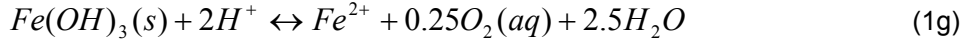
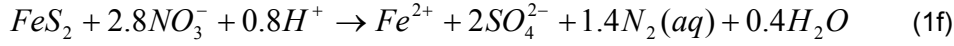
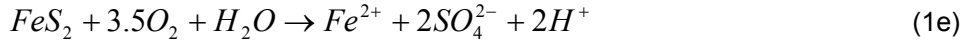
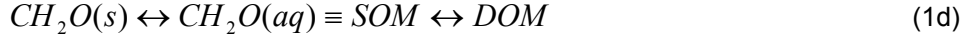
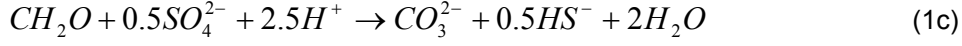
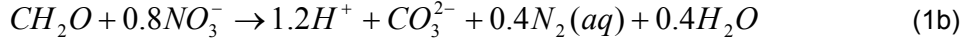
The definition of rate expressions and corresponding reaction parameters are not included in this documentation. The reaction module allows implementation of almost any type of kinetic rate expressions, which may be chosen or modified according to the special needs of the user.

2 Units

All concentrations are given in [Moles L⁻³]. Reaction rates are defined as [Moles L⁻³ T⁻¹]

3 Reaction equation system

The reaction equation system is described by the following reaction equations. The reaction stoichiometry is referred to the unit electron donator.



CH₂O is dissolved organic matter (DOM) and CH₂O(s) is sedimentary organic matter (SOM). Reaction 1d is no chemical reaction in a strict sense but describes the transfer between reactive organic matter (as DOM) and a stable pool of sedimentary organic matter.

In general form the reaction equations can be written as:

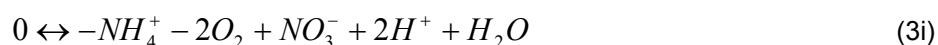
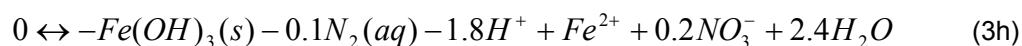
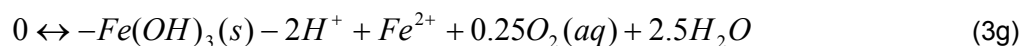
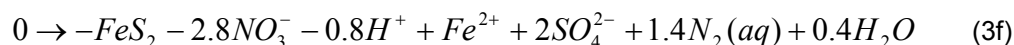
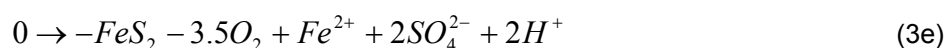
$$0 \leftrightarrow \sum_{i=1}^K v_{ir} \cdot A_i, (r = 1, \dots, N_r) \quad (2)$$

with v_{ir} =stoichiometric coefficient of species i in reaction r , A_i =Activity of species i , N_r =Number of reactions, r =reaction index, K =number of species, i =species index,

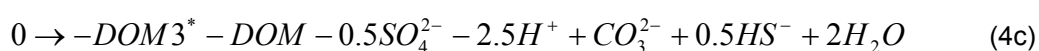
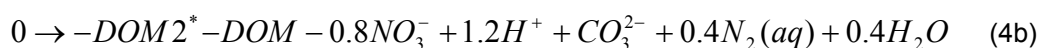
The reaction system will be based mainly on kinetic rate expressions rather than equilibrium reactions. Thus it is sufficient to use concentrations instead of activities. This will be different for calculation of pH and carbonate speciation and will be discussed later.

The reaction system is re-written as:





The reaction equation system is transferred into a canonical stoichiometry matrix. Therefore it is necessary, to define a set of components or primary species, from which the remaining species or secondary species can be composed of. Components undergoing alternative reaction pathways are considered as primary components and the single reactions are related to a secondary dummy species, which is considered as a mineral (immobile) phase. The example for the DOM-transformation shows how the reaction equation is rewritten introducing the dummy species:



Minerals undergoing parallel reaction pathways (Ferrihydrite and Pyrite) are treated in the same way.

The canonical matrix of the reaction equation system is written as:

		Primary components, only mobile species											
N/ N _c	Comp- onents / Species	H ⁺	O ₂ (aq)	NO ₃ ⁻	NH ₄ ⁺ (aq)	N ₂ (aq)	SO ₄ ²⁻	HS ⁻	Fe ²⁺	Ca ²⁺	CO ₃ ²⁻	DOM	H ₂ O
1	H ⁺	1											
2	O ₂ (aq)		1										
3	NO ₃ ⁻			1									
4	NH ₄ ⁺				1								
4	N ₂ (aq)					1							
6	SO ₄ ²⁻						1						
7	HS ⁻							1					
8	Fe ⁺²								1				
9	Ca ⁺²									1			
10	CO ₃ ²⁻										1		
10	DOM											1	
11	FeS ₂												
12	Fe(OH) ₃												
13	H ₂ O												1
14	DOM(1)	2	-1								1	-1	
15	DOM(2)	1.2		-0.8		0.4					1	-1	0.4
16	DOM(3)	-2.5					-0.5	0.5			1	-1	2
17	SOM											1	
18	FeS ₂ (1)	2	-3.5				2		1				
19	FeS ₂ (2)	-0.8		-2.8		1.4	2		1				0.4
20	Fe(OH) ₃ (1)	-2	0.25						1				2.5
21	Fe(OH) ₃ (2)	-1.8		0.2		0.1			1				2.4
22	NH ₄ 1	2	-2	1	-1								1
23	CaCO ₃									1	1		
24	HCO ₃ ⁻	1									1		
25	H ₂ CO ₃	2									1		
26	OH ⁻	-1											1

The immobile primary components SOM, FeS₂, Fe(OH)₃ and CaCO₃ have been omitted in the canonical matrix for lack of space. They are related to their corresponding secondary species SOM, FeS₂(1), FeS₂(2), Fe(OH)₃(1), Fe(OH)₃(2), CaCO₃ by a stoichiometric factor of -1.

4 Definition of reaction rates

The reaction rates of the secondary species are defined below. They will be considered as elementary rates.

$$I_{14} = \frac{\partial[DOM]}{\partial t} = R_{DOM}^1 \quad (5a)$$

$$I_{15} = \frac{\partial[DOM]}{\partial t} = R_{DOM}^2 \quad (5b)$$

$$I_{16} = \frac{\partial[DOM]}{\partial t} = R_{DOM}^3 \quad (5c)$$

$$I_{17} = \frac{\partial[SOM]}{\partial t} = R_{SOM} \quad (5d)$$

$$I_{18} = \frac{\partial[FeS_2]}{\partial t} = R_{FeS_2}^1 \quad (5e)$$

$$I_{19} = \frac{\partial[FeS_2]}{\partial t} = R_{FeS_2}^2 \quad (5f)$$

$$I_{20} = \frac{\partial[Fe(OH)_3]}{\partial t} = R_{Fe(OH)_3}^1 \quad (5g)$$

$$I_{21} = \frac{\partial[Fe(OH)_3]}{\partial t} = R_{Fe(OH)_3}^2 \quad (5h)$$

$$I_{22} = \frac{\partial[NH_4^+]}{\partial t} = R_{Nitrification} \quad (5i)$$

$$I_{23} = \frac{\partial[CaCO_3]}{\partial t} = R_{Calcite} \quad (5j)$$

$$I_{24} = \frac{\partial[HCO_3^-]}{\partial t} = R_{Bicarbonate} \quad (5k)$$

$$I_{25} = \frac{\partial[H_2CO_3]}{\partial t} = R_{CarbonicAcid} \quad (5l)$$

$$I_{26} = \frac{\partial[OH^-]}{\partial t} = R_{Hydroxide} \quad (5m)$$

The total reaction rate for a component which undergoes alternative reactions is given by the sum of the partial reaction rates:

$$I_{DOM} = \frac{\partial[DOM]}{\partial t} = I_{14} + I_{15} + I_{16} - I_{17} = R_{DOM}^{Tot} \quad (6a)$$

$$I_{FeS_2} = \frac{\partial[FeS_2]}{\partial t} = I_{18} + I_{19} = R_{Pyrite}^{Tot} \quad (6b)$$

$$I_{Fe(OH)_3} = \frac{\partial[Fe(OH)_3]}{\partial t} = I_{20} + I_{21} = R_{Ferrihydrite}^{Tot} \quad (6c)$$

The elementary reaction rates can be defined by kinetic rate expressions. This is beyond the scope of this formal description and will be discussed separately.

With the aid of the canonical matrix, the reaction rates of the components (primary species) can be expressed as:

$$R_j = - \sum_{i=N_c+1}^N v_{ij} \cdot I_i \quad (7)$$

with R_j = Reaction rate of component j , v_{ij} = stoichiometric coefficient, I_i =Reaction rate of secondary species i , N_c =Number of components, N =Number of species (incl. primary components)

The component reaction rates for the mobile components are then written as:

$$R_{H^+} = -2 \cdot I_{14} - 1.2 \cdot I_{15} + 2.5 \cdot I_{16} - 2 \cdot I_{18} + 0.8 \cdot I_{19} + 2 \cdot I_{20} + 1.8 \cdot I_{21} - 2 \cdot I_{22} - I_{24} - 2 \cdot I_{25} + I_{26} \quad (8a)$$

$$R_{O_2} = -I_{14} + 3.5 \cdot I_{18} - 0.25 \cdot I_{20} + 2 \cdot I_{22} \quad (8b)$$

$$R_{NO_3^-} = 0.8 \cdot I_{15} + 2.8 \cdot I_{19} - 0.2 \cdot I_{21} - 1 \cdot I_{22} \quad (8c)$$

$$R_{NH_4^+} = I_{22} \quad (8d)$$

$$R_{N_2} = -0.4 \cdot I_{15} - 1.4 \cdot I_{19} + 0.1 \cdot I_{21} \quad (8e)$$

$$R_{SO_4^{2-}} = 0.5 \cdot I_{16} - 2 \cdot I_{18} - 2 \cdot I_{19} \quad (8f)$$

$$R_{HS^-} = -0.5 \cdot I_{16} \quad (8g)$$

$$R_{Fe^{2+}} = -I_{18} - I_{19} - I_{20} - I_{21} \quad (8h)$$

$$R_{Ca^{2+}} = -I_{23} \quad (8i)$$

$$R_{CO_3^{2-}} = -I_{14} - I_{15} - I_{16} - I_{23} - I_{24} - I_{25} \quad (8j)$$

$$R_{DOM} = I_{14} + I_{15} + I_{16} - I_{17} \quad (8k)$$

$$R_{H_2O} = -0.4 \cdot I_{15} - 2 \cdot I_{16} - 0.4 \cdot I_{19} - 2.5 \cdot I_{20} - 2.4 \cdot I_{21} - I_{22} - I_{26} \quad (8l)$$

and for mineral components as:

$$R_{Pyrite} = I_{18} + I_{19} \quad (9a)$$

$$R_{Ferrihydrite} = I_{20} + I_{21} \quad (9b)$$

$$R_{Calcite} = I_{23} \quad (9c)$$

$$R_{SOM} = I_{17} \quad (9d)$$

Mineral components are calculated explicitly, whereas mobile species are calculated based on

total concentrations.

5 Definition of total component concentrations

The number of species can be expressed as in Equation (10):

$$N_{\text{sec}} = N_{\text{aq}} + N_{\text{g}} + N_{\text{min}} \quad (10)$$

with N_{sec} = number of secondary species, N_{aq} =number of aqueous species, N_{g} =number of gaseous species, N_{min} =number of mineral species

The total component concentrations are given by the sum over all secondary species:

$$[j]_{\text{Tot}} = [j] + \sum_{i=1}^{N_{\text{sec}}} v_{ij} \cdot [i] \quad (11)$$

with $[j]_{\text{Tot}}$ =Total concentration of component j, $[i]$ =Concentration of secondary species i, v_{ij} = stoichiometric coefficient

The total component concentrations of all mobile primary components can be written as:

$$\begin{aligned} [H]_{\text{TOT}} &= [H^+] + 2 \cdot [DOM1] + 1.2 \cdot [DOM2] - 2.5 \cdot [DOM3] \\ &+ 2 \cdot [FeS_2 1] - 0.8 \cdot [FeS_2 2] - 2 \cdot [Fe(OH)_3 1] - 1.8 \cdot [Fe(OH)_3 2] \\ &+ 2 \cdot [NH_4^+ 1] + [HCO_3^-] + 2 \cdot [H_2CO_3] - [OH^-] \end{aligned} \quad (12a)$$

$$[O_2]_{\text{TOT}} = [O_2(aq)] - [DOM1] - 3.5 \cdot [FeS_2 1] + 0.25 \cdot [Fe(OH)_3 1] - 2 \cdot [NH_4^+ 1] \quad (12b)$$

$$[NO_3]_{\text{TOT}} = [NO_3^-] - 0.8 \cdot [DOM2] - 2.8 \cdot [FeS_2 2] + 0.2 \cdot [Fe(OH)_3 2] + [NH_4^+ 1] \quad (12c)$$

$$[NH_4]_{\text{TOT}} = [NH_4^+] - [NH_4^+ 1] \quad (12d)$$

$$[N_2]_{\text{TOT}} = [N_2] + 0.4 \cdot [DOM2] + 1.4 \cdot [FeS_2 2] - 0.1 \cdot [Fe(OH)_3 2] \quad (12e)$$

$$[SO_4]_{\text{TOT}} = [SO_4] - 0.5 \cdot [DOM3] + 2 \cdot [FeS_2 1] + 2 \cdot [FeS_2 2] \quad (12f)$$

$$[HS]_{\text{TOT}} = [HS^-] + 0.5 \cdot [DOM3] \quad (12g)$$

$$[Fe]_{\text{TOT}} = [Fe^{2+}] + [FeS_2 1] + [FeS_2 2] + [Fe(OH)_3 1] + [Fe(OH)_3 2] \quad (12h)$$

$$[Ca]_{\text{TOT}} = [Ca^{2+}] + [CaCO_3] \quad (12i)$$

$$[CO_3]_{\text{TOT}} = [CO_3^-] + [DOM1] + [DOM2] + [DOM3] + [HCO_3^-] + [H_2CO_3] \quad (12j)$$

$$[DOM]_{\text{TOT}} = [DOM] - [DOM1] - [DOM2] - [DOM3] + [SOM] \quad (12k)$$

6 Definition of mobile component concentrations

For transport calculations, only the mobile part of the total components needs to be considered, and a mobile component concentration is defined as difference between total component concentrations and the sum over all immobile secondary species (minerals):

$$u(j) = [j]_{TOT} - \sum_{i=\min} v_{ij} \cdot [\min]_i \quad (13)$$

with $u(j)$ =mobile component concentration, $[\min]_i$ = Concentration of immobile secondary species i , i =immobile (mineral) secondary species index

Applying equation 13, yields a new set of mobile component concentrations:

$$u(H) = [H^+] + 2 \cdot [NH_4^+] + [HCO_3^-] + 2 \cdot [H_2CO_3] - [OH^-] \quad (14a)$$

$$u(O_2) = [O_2(aq)] - 2 \cdot [NH_4^+] \quad (14b)$$

$$u(NO_3) = [NO_3^-] + [NH_4^+] \quad (14c)$$

$$u(NH_4) = [NH_4^+] \quad (14d)$$

$$u(N_2) = [N_2] \quad (14e)$$

$$u(SO_4) = [SO_4] \quad (14f)$$

$$u(HS) = [HS^-] \quad (14g)$$

$$u(Fe) = [Fe^{2+}] \quad (14h)$$

$$u(Ca) = [Ca^{2+}] \quad (14i)$$

$$u(CO_3) = [CO_3^-] + [HCO_3^-] + [H_2CO_3] \quad (14j)$$

$$u(DOM) = [DOM] \quad (14k)$$

7 Derivation of reaction rates for mobile components

The reaction rates for the mobile components are given by:

$$\hat{L}u(j) = - \sum_{i=\min} v_{ij} \cdot R_i \quad (15)$$

wit $Lu(j)$ = reaction rate of mobile component j , v_{ij} =stoichiometric coefficient, R_i =Reaction rate of component i , i =immobile (mineral) component index

This yields the following Source/Sink-Terms for the mobile components:

$$\begin{aligned} \hat{L}u(H) = & -2 \cdot R_{DOM1} - 1.2 \cdot R_{DOM2} + 2.5 \cdot R_{DOM3} - 2 \cdot R_{Pyrite1} + \\ & 0.8 \cdot R_{Pyrite2} + 2 \cdot R_{Ferrihydrite1} + 1.8 \cdot R_{Ferrihydrite2} - 2 \cdot R_{Nitrification} \end{aligned} \quad (16a)$$

$$\hat{L}u(O_2) = R_{DOM1} + 3.5 \cdot R_{Pyrite1} - 0.25 \cdot R_{Ferrihydrite1} + 2 \cdot R_{Nitrification} \quad (16b)$$

$$\hat{L}u(NO_3) = 0.8 \cdot R_{DOM2} + 2.8 \cdot R_{Pyrite2} - 0.2 \cdot R_{Ferrihydrite2} - R_{Nitrification} \quad (16c)$$

$$\hat{L}u(NH_4) = R_{Nitrification} \quad (16d)$$

$$\hat{L}u(N_2) = -0.4 \cdot R_{DOM2} - 1.4 \cdot R_{Pyrite2} + 0.1 \cdot R_{Ferrihydrite2} \quad (16e)$$

$$\hat{L}u(SO_4) = 0.5 \cdot R_{DOM3} - 2 \cdot R_{Pyrite1} - 2 \cdot R_{Pyrite2} \quad (16f)$$

$$\hat{L}u(HS) = -0.5 \cdot R_{DOM3} \quad (16g)$$

$$\hat{L}u(Fe) = -R_{Pyrite1} - R_{Pyrite2} - R_{Ferrihydrite1} - R_{Ferrihydrite2} \quad (16h)$$

$$\hat{L}u(Ca) = -R_{Calcite} \quad (16i)$$

$$\hat{L}u(CO_3) = -R_{DOM1} - R_{DOM2} - R_{DOM3} - R_{Calcite} \quad (16j)$$

$$\hat{L}u(DOM) = R_{DOM}^{Tot} = -R_{SOM} + R_{DOM1} + R_{DOM2} + R_{DOM3} \quad (16k)$$

The equivalent formulation for mineral phases yields:

$$\hat{L}u(Pyrite) = R_{Pyrite} \quad (17a)$$

$$\hat{L}u(Ferrihydrite) = R_{Ferrihydrite} \quad (17b)$$

$$\hat{L}u(Calcite) = R_{Calcite} \quad (17c)$$

$$\hat{L}u(SOM) = R_{SOM} \quad (17d)$$

8 Calculation of secondary species concentrations

The reaction system does not explicitly calculate pH. This information can be calculated from component concentrations.

Dissolution of calcite can be considered as a kinetic process instead of equilibrium reactions. However, in both cases carbonate concentrations are needed. They also have to be resolved from component concentrations applying the law of mass action. The law of mass action yields the following equilibrium reactions for carbonate, carbonic acid and for dissoziation:

$$K_{HCO_3^-} = \frac{[H^+] \cdot [CO_3^{2-}]}{[HCO_3^-]} \Rightarrow [HCO_3^-] = \frac{[H^+] \cdot [CO_3^{2-}]}{K_{HCO_3^-}} \quad (18)$$

$$K_{H_2CO_3} = \frac{[H^+]^2 \cdot [CO_3^{2-}]}{[H_2CO_3]} \Rightarrow [H_2CO_3] = \frac{[H^+]^2 \cdot [CO_3^{2-}]}{K_{H_2CO_3}} \quad (19)$$

$$K_{H_2O} = [H^+] \cdot [OH^-] \Rightarrow [OH^-] = \frac{K_{H_2O}}{[H^+]} \quad (20)$$

The mobile component concentration of carbonate is given by

$$u(CO_3) = [CO_3^{2-}] + [HCO_3^-] + [H_2CO_3] \quad (21)$$

The species concentrations are substituted by the corresponding equilibrium expressions and the equation is solved for $[CO_3^{2-}]$:

$$\begin{aligned} \Leftrightarrow u(CO_3) &= [CO_3^{2-}] + \frac{[H^+] \cdot [CO_3^{2-}]}{K_{HCO_3^-}} + \frac{[H^+]^2 \cdot [CO_3^{2-}]}{K_{H_2CO_3}} \\ \Leftrightarrow u(CO_3) &= [CO_3^{2-}] \cdot \left(1 + \frac{[H^+]}{K_{HCO_3^-}} + \frac{[H^+]^2}{K_{H_2CO_3}} \right) \\ \Leftrightarrow [CO_3^{2-}] &= \frac{u(CO_3^{2-})}{\left(1 + \frac{[H^+]}{K_{HCO_3^-}} + \frac{[H^+]^2}{K_{H_2CO_3}} \right)} = f_1(H^+) \end{aligned} \quad (22)$$

The mobile component concentration of hydrogen and ammonium are given by

$$u(H) = [H^+] + 2 \cdot [NH_4^+] + [HCO_3^-] + 2 \cdot [H_2CO_3] - [OH^-] \quad (23)$$

$$u(NH_4) = [NH_4^+] \quad (24)$$

The species concentrations are substituted by the corresponding equilibrium expressions and the equation is also solved for $[CO_3^{2-}]$:

$$\begin{aligned} \Leftrightarrow u(H) &= [H^+] + 2 \cdot [NH_4^+] + \frac{[H^+] \cdot [CO_3^{2-}]}{K_{HCO_3^-}} + 2 \cdot \frac{[H^+]^2 \cdot [CO_3^{2-}]}{K_{H_2CO_3}} - \frac{K_{H_2O}}{[H^+]} \\ \Leftrightarrow u(H) - 2 \cdot [NH_4^+] &= [H^+] + [CO_3^{2-}] \cdot \left(\frac{[H^+]}{K_{HCO_3^-}} + 2 \cdot \frac{[H^+]^2}{K_{H_2CO_3}} \right) - \frac{K_{H_2O}}{[H^+]} \\ \Leftrightarrow [CO_3^{2-}] &= \frac{u(H) - 2 \cdot [NH_4^+] - [H^+] + \frac{K_{H_2O}}{[H^+]}}{\left(\frac{[H^+]}{K_{HCO_3^-}} + 2 \cdot \frac{[H^+]^2}{K_{H_2CO_3}} \right)} = f_2(H^+) \end{aligned} \quad (25)$$

This yields two equations solving carbonate concentration as a function of H^+ . Setting $f_1(H^+)$ equal to $f_2(H^+)$, $[H^+]$ can be obtained by solving for zero.

$$f_1(H^+) = f_2(H^+) \Rightarrow 0 = f_1(H^+) - f_2(H^+) = F(H^+) \quad (26)$$

Equation (26) is a quadratic equation, which can be solved by numerical solution schemes providing $[H^+]$ and pH. Carbonate speciation is then solved by applying $[H^+]$ to the mass action equations.

For a correct calculation of $[H^+]$, carbonate speciation and pH, activities have to be considered rather than concentrations. This can be done by applying the Debye-Hückel-equation or other calculation methods.

9 References

- Clement, T.P. (1997): A modular Computer Code for Simulating Reactive Multispecies Transport in 3-Dimensional Groundwater Systems, Richland, WA.
- Lichtner, P.C., Steefel, C., Oelkers, E.H. (Eds.) (1996): Reactive Transport in Porous Media. Reviews in Mineralogy, Volume 34, Washington.
- Sigg, L., Stumm, W. (1996): Aquatische Chemie, Stuttgart.

Curriculum vitae

Dipl.-Geogr. Gunter Wriedt

Verdener Strasse 27
27751 Delmenhorst

Personal data

Date and place of birth 15.02.1974 in Papenburg

Work experience

Since 10/2003	UFZ Umweltforschungszentrum Leipzig-Halle GmbH, Magdeburg, Scientist. Development of an adaptive flood forecasting model for the White Elster.
04/2000-09/2003	UFZ Umweltforschungszentrum Leipzig-Halle GmbH, Magdeburg, Scientist/PhD-student. Modelling of nitrogen transport in lowland catchments
11/1998-12/1998	DFD Deutsches Fernerkundungsdatenzentrum, Oberpfaffenhofen. Internship, GIS-application
07/1998-09/1998	Planteforsk Holt Forskingssenter, Tromsø (N). Pedological research for master's thesis
08/1997-10/1997	FADR Foundation for Agricultural Development Research, Moskau (RUS). Internship, pedological expedition
10/1996-07/1997	Institute of plant nutrition and soil science, University of Kiel, student assistant.
08/1996-09/1996	BFL Büro für Landschaftsentwicklung GmbH, Eckernförde, Internship

University education

10/2001-5/2004	Doctoral candidate at the University of Potsdam, Institute of Geoecology
12/1999	Diploma in Geography Diploma Thesis: „Aspekte der Geoökologie subpolarer Böden – Eisendynamik und Wasserhaushalt am Beispiel zweier Pseudogleye im Tverrelvdalen (Finmark)“
10/1994-12/1999	Study of Geography, Christian-Albrechts-Universität (CAU) in Kiel, specialisation in Soil Science, Chemistry and Zoology

Service

10/1993-12/1994	Alternative service, Jugendbildungsstätte Theodor Wuppermann e.V. in Juist
-----------------	--

School education

17.05.93	Abitur, Gymnasium Papenburg
1980-1993	Primary school and Gymnasium in Papenburg

Eidesstattliche Erklärung

Hiermit erkläre ich an Eides statt, dass ich die vorgelegte Dissertation mit dem Titel „Modelling of nitrogen transport and turnover during soil and groundwater passage in a lowland catchment of Northern Germany“ selbständig und ohne unerlaubte Hilfe angefertigt habe und dass ich die die Arbeit noch keinem anderen Fachbereich bzw. noch keiner anderen Fakultät vorgelegt habe. Ich erkläre ebenso, dass die Arbeit ausschliesslich mit den angegebenen Mitteln angefertigt wurde.

Delmenhorst, den 8.2.2004

Gunter Wriedt